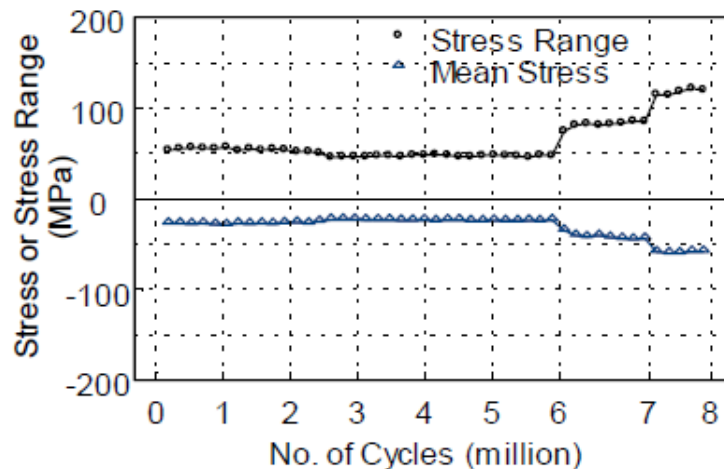




Division of Research
& Innovation

Effects of Fabrication Procedures and Weld Melt-Through on Fatigue Resistance of Orthotropic Steel Deck Welds

Final Report



Effect of Fabrication Procedures and Weld Melt-Through on Fatigue Resistance of Orthotropic Steel Deck Welds

Final Report

Report No. CA08-0607

December 2008

Prepared By:

Department of Structural Engineering
University of California, San Diego
La Jolla, CA 92093

Prepared For:

California Department of Transportation
Engineering Services Center
1801 30th Street
Sacramento, CA 95816

California Department of Transportation
Division of Research and Innovation, MS-83
1227 O Street
Sacramento, CA 95814

DISCLAIMER STATEMENT

This document is disseminated in the interest of information exchange. The contents of this report reflect the views of the authors who are responsible for the facts and accuracy of the data presented herein. The contents do not necessarily reflect the official views or policies of the State of California or the Federal Highway Administration. This publication does not constitute a standard, specification or regulation. This report does not constitute an endorsement by the Department of any product described herein.

STATE OF CALIFORNIA DEPARTMENT OF TRANSPORTATION
TECHNICAL REPORT DOCUMENTATION PAGE
 TR0003 (REV. 10/98)

1. REPORT NUMBER CA08-0607		2. GOVERNMENT ASSOCIATION NUMBER		3. RECIPIENT'S CATALOG NUMBER	
4. TITLE AND SUBTITLE Effects of Fabrication Procedures and Weld Melt-Through on Fatigue Resistance of Orthotropic Steel Deck Welds				5. REPORT DATE December, 2008	
7. AUTHOR(S) Hyoung-Bo Sim, Chia-Ming Uang				6. PERFORMING ORGANIZATION CODE	
9. PERFORMING ORGANIZATION NAME AND ADDRESS Department of Structural Engineering University of California, San Diego La Jolla, CA 92093-0085				8. PERFORMING ORGANIZATION REPORT NO. SSRP-07/13	
12. SPONSORING AGENCY AND ADDRESS California Department of Transportation Engineering Services Center 1801 30 th Street Sacramento, CA 95816 California Department of Transportation Division of Research and Innovation, MS-83 1227 O Street Sacramento, CA 95814				10. WORK UNIT NUMBER	
				11. CONTRACT OR GRANT NUMBER DRI Research Task No. 0607 Contract No. 59A0442	
15. SUPPLEMENTAL NOTES This report may also be referenced as report SSRP-07/13 published by the UCSD.				13. TYPE OF REPORT AND PERIOD COVERED Final Report	
				14. SPONSORING AGENCY CODE 913	
16. ABSTRACT <p>A common practice for the fabrication of orthotropic bridge deck in the US involves using 80% partial-joint-penetration groove welds (PJP) to join closed ribs to a deck plate. Avoiding weld melt-through with the thin rib plate may be difficult to achieve in practice because a tight fit may not always be achievable. When weld melt-through occurs, which is difficult to inspect inside the ribs, it is not clear how the geometric discontinuities would affect the fatigue resistance. Furthermore, a distortion control plan, which involves heat straightening or even pre-cambering, is also used for the fabricated orthotropic deck in order to meet the flatness requirement. It is unclear how repeated heating along the PJP weld line would affect the fatigue resistance.</p> <p>Six 2-span, full-scale orthotropic steel deck specimens (10 m long by 3 m wide) were fabricated and tested in order to study the effects of both weld melt-through and distortion control measures on the fatigue resistance of the deck-to-rib PJP welded joint. Three of the specimens were only heat straightened, and the other three were pre-cambered to minimize the need for subsequent heat straightening. For the two distortion control schemes one of the three weld conditions [80% PJP weld, 100% PJP weld with evident continuous weld melt-through, and alternating the above two weld conditions every 1 m] was used for each specimen. Up to 8 million cycles of loading, which simulated the expected maximum stress range corresponding to axle loads of 3×HS15 with 15% impact, were applied at the mid-length of each span and were out of phase to simulate the effect of a moving truck. The load level and boundary conditions were modified slightly based on the observed cracks that occurred in the diaphragm cutouts in the first specimen.</p> <p>Based on the loading scheme applied and the test results of the remaining five specimens, it was observed that three specimens experienced cracking at the rib-to-deck PJP welds at seven loaded locations. It was thought initially that weld melt-through which creates geometric discontinuities at the weld root was the main concern. But only one of the seven cracks initiated from the weld root inside the closed rib, and all the other six cracks initiated from the weld toe outside the closed rib. Based on the loading pattern applied, therefore, it appears that these welds are more vulnerable to cracks initiating from the weld toe, not weld root. Of the only one crack that developed at the weld root, the crack initiated from a location transitioning from 80% PJP weld to 100% PJP weld. This type of geometric discontinuity may be representative of the effect of weld melt-through in actual production of orthotropic steel decks. Two of the five specimens did not experience PJP weld cracks, and were the ones that were effectively pre-cambered; a third panel was insufficiently pre-cambered and the resulting distortion and heat straightening were the same as required for the un-cambered panels. Therefore, effective pre-cambering is beneficial to mitigate the crack potential in rib-to-deck PJP welds.</p>					
17. KEY WORDS Orthotropic steel deck, closed rib, weld melt-through, heat straightening, pre-cambering, fatigue test			18. DISTRIBUTION STATEMENT No restrictions. This document is available to the public through the National Technical Information Service, Springfield, VA 22161		
19. SECURITY CLASSIFICATION (of this report) Unclassified		20. NUMBER OF PAGES 189 Pages		21. PRICE	



**STRUCTURAL SYSTEMS
RESEARCH PROJECT**

Report No.
SSRP-07/13
FINAL

**EFFECTS OF FABRICATION PROCEDURES
AND WELD MELT-THROUGH ON FATIGUE
RESISTANCE OF ORTHOTROPIC STEEL
DECK WELDS**

by

**HYOUNG-BO SIM
CHIA-MING UANG**

Final Report Submitted to the California Department of
Transportation (Caltrans) Under Contract No. 59A0442

August 2007

Department of Structural Engineering
University of California, San Diego
La Jolla, California 92093-0085

University of California, San Diego
Department of Structural Engineering
Structural Systems Research Project

Report No. SSRP-07/13

FINAL

**Effects of Fabrication Procedures and Weld Melt-Through on
Fatigue Resistance of Orthotropic Steel Deck Welds**

by

Hyoung-Bo Sim

Graduate Student Researcher

Chia-Ming Uang

Professor of Structural Engineering

Final Report to Submitted to the California Department of Transportation
(Caltrans) Under Contract No. 59A0442

Department of Structural Engineering
University of California, San Diego
La Jolla, California 92093-0085

August 2007

1. Report No. FHWA/CA/ES-2007/13		2. Government Accession No.		3. Recipient's Catalog No.	
4. Title and Subtitle Effects of Fabrication Procedures and Weld Melt-Through on Fatigue Resistance of Orthotropic Steel Deck Welds				5. Report Date August 2007	
				6. Performing Organization Code	
7. Author(s) Hyoung-Bo Sim Chia-Ming Uang				8. Performing Organization Report No. SSRP 07/13	
9. Performing Organization Name and Address Division of Structural Engineering School of Engineering University of California, San Diego La Jolla, California 92093-0085				10. Work Unit No. (TRAIS)	
				11. Contract or Grant No. 59A0442	
12. Sponsoring Agency Name and Address California Department of Transportation Engineering Service Center 1801 30 th St., West Building MS-9 Sacramento, California 95807				13. Type of Report and Period Covered Final Report, July 2004 – September 2006	
				14. Sponsoring Agency Code	
15. Supplementary Notes Prepared in cooperation with the State of California Department of Transportation.					
16. Abstract <p>A common practice for the fabrication of orthotropic bridge deck in the US involves using 80% partial-joint-penetration groove welds (PJP) to join closed ribs to a deck plate. Avoiding weld melt-through with the thin rib plate may be difficult to achieve in practice because a tight fit may not always be achievable. When weld melt-through occurs, which is difficult to inspect inside the ribs, it is not clear how the geometric discontinuities would affect the fatigue resistance. Furthermore, a distortion control plan, which involves heat straightening or even pre-cambering, is also used for the fabricated orthotropic deck in order to meet the flatness requirement. It is unclear how repeated heating along the PJP weld line would affect the fatigue resistance.</p> <p>Six 2-span, full-scale orthotropic steel deck specimens (10 m long by 3 m wide) were fabricated and tested in order to study the effects of both weld melt-through and distortion control measures on the fatigue resistance of the deck-to-rib PJP welded joint. Three of the specimens were only heat straightened, and the other three were pre-cambered to minimize the need for subsequent heat straightening. For the two distortion control schemes one of the three weld conditions [80% PJP weld, 100% PJP weld with evident continuous weld melt-through, and alternating the above two weld conditions every 1 m] was used for each specimen. Up to 8 million cycles of loading, which simulated the expected maximum stress range corresponding to axle loads of 3×HS15 with 15% impact, were applied at the mid-length of each span and were out of phase to simulate the effect of a moving truck. The load level and boundary conditions were modified slightly based on the observed cracks that occurred in the diaphragm cutouts in the first specimen.</p> <p>Based on the loading scheme applied and the test results of the remaining five specimens, it was observed that three specimens experienced cracking at the rib-to-deck PJP welds at seven loaded locations. It was thought initially that weld melt-through which creates geometric discontinuities at the weld root was the main concern. But only one of the seven cracks initiated from the weld root inside the closed rib, and all the other six cracks initiated from the weld toe outside the closed rib. Based on the loading pattern applied, therefore, it appears that these welds are more vulnerable to cracks initiating from the weld toe, not weld root. Of the only one crack that developed at the weld root, the crack initiated from a location transitioning from 80% PJP weld to 100% PJP weld. This type of geometric discontinuity may be representative of the effect of weld melt-through in actual production of orthotropic steel decks.</p> <p>Two of the five specimens did not experience PJP weld cracks, and were the ones that were effectively pre-cambered; a third panel was insufficiently pre-cambered and the resulting distortion and heat straightening were the same as required for the un-cambered panels. Therefore, effective pre-cambering is beneficial to mitigate the crack potential in rib-to-deck PJP welds.</p>					
17. Key Words Orthotropic steel deck, closed rib, weld melt-through, heat straightening, pre-cambering, fatigue test				18. Distribution Statement No restrictions	
19. Security Classification (of this report) Unclassified		20. Security Classification (of this page) Unclassified		21. No. of Pages 182	22. Price

DISCLAIMER

The contents of this report reflect the views of the authors who are responsible for the facts and the accuracy of the data presented herein. The contents do not necessarily reflect the official views or policies of the State of California. This report does not constitute a standard, specification or regulation.

ACKNOWLEDGEMENTS

Funding for this research was provided by the California Department of Transportation under Contract No. 59A0442. We would like to thank Dr. C. Sikorsky (project manager), Mr. B. Boal, Dr. M. Wahbeh, Dr. E. Thimmhardy, and Dr. L. Duan of the California Department of Transportation. Professor John Fisher from Lehigh University served as an independent consultant for this project.

The testing was conducted in the Charles Lee Powell Structures Laboratories at the University of California, San Diego. Assistance from Dr. T. Hanji, Messrs. Jong-Kook Hong and James Newell throughout the testing is much appreciated.

ABSTRACT

A common practice for the fabrication of orthotropic bridge deck in the US involves using 80% partial-joint-penetration groove welds (PJP) to join closed ribs to a deck plate. Avoiding weld melt-through with the thin rib plate may be difficult to achieve in practice because a tight fit may not always be achievable. When weld melt-through occurs, which is difficult to inspect inside the ribs, it is not clear how the geometric discontinuities would affect the fatigue resistance. Furthermore, a distortion control plan, which involves heat straightening or even pre-cambering, is also used for the fabricated orthotropic deck in order to meet the flatness requirement. It is unclear how repeated heating along the PJP weld line would affect the fatigue resistance.

Six 2-span, full-scale orthotropic steel deck specimens (10 m long by 3 m wide) were fabricated and tested in order to study the effects of both weld melt-through and distortion control measures on the fatigue resistance of the deck-to-rib PJP welded joint. Three of the specimens were only heat straightened, and the other three were pre-cambered to minimize the need for subsequent heat straightening. For the two distortion control schemes one of the three weld conditions [80% PJP weld, 100% PJP weld with evident continuous weld melt-through, and alternating the above two weld conditions every 1 m] was used for each specimen. Up to 8 million cycles of loading, which simulated the expected maximum stress range corresponding to axle loads of 3×HS15 with 15% impact, were applied at the mid-length of each span and were out of phase to simulate the effect of a moving truck. The load level and boundary conditions were modified slightly based on the observed cracks that occurred in the diaphragm cutouts in the first specimen.

Based on the loading scheme applied and the test results of the remaining five specimens, it was observed that three specimens experienced cracking at the rib-to-deck PJP welds at seven loaded locations. It was thought initially that weld melt-through which creates geometric discontinuities at the weld root was the main concern. But only one of the seven cracks initiated from the weld root inside the closed rib, and all the other six cracks initiated from the weld toe outside the closed rib. Based on the loading pattern applied, therefore, it appears that these welds are more vulnerable to cracks initiating

from the weld toe, not weld root. Of the only one that developed at the weld root, the crack initiated from a location transitioning from 80% PJP weld to 100% PJP weld. This type of geometric discontinuity may be representative of the effect of weld melt-through in actual production of orthotropic steel decks.

Two of the five specimens did not experience PJP weld cracks, and were the ones that were effectively pre-cambered; a third panel was insufficiently pre-cambered and the resulting distortion and heat straightening were the same as required for the un-cambered panels. Therefore, effective pre-cambering is beneficial to mitigate the crack potential in rib-to-deck PJP welds.

TABLE OF CONTENTS

DISCLAIMER	i
ACKNOWLEDGEMENTS	ii
ABSTRACT	iii
TABLE OF CONTENTS	v
LIST OF TABLES	vii
LIST OF FIGURES	viii
LIST OF FIGURES	viii
LIST OF SYMBOLS	xiv
1. INTRODUCTION	1
1.1 Background	1
1.2 Objectives	7
2. TESTING PROGRAM	8
2.1 Panel Fabrication	8
2.1.1 General	8
2.1.2 Rib-to-Deck Plate PJP Welded Joint	8
2.1.3 Distortion Controls (Pre-Cambering and Heat Straightening).....	11
2.1.4 Distortion Measurements	16
2.1.5 Intersection of Closed Rib to Diaphragms.....	24
2.2 Material Properties.....	26
2.3 Test Setup.....	28
2.4 Loading	32
2.5 Instrumentation	34
2.5.1 General.....	34
2.5.2 Strain Gages in Deck Plate near Rib-to-Deck Welds	34
2.5.3 Strain Gages in Ribs near Rib-to-Deck Welds	37
2.5.4 Strain Gages in Ribs, Diaphragms, and Bulkheads at Supports	45
3. FINITE ELEMENT ANALYSIS	50
3.1 Introduction.....	50
3.2 Predicted Global Behavior	50
3.3 Predicted Stresses for Model 1	60
3.3.1 Stress Contour on Ribs at Support Diaphragms	60

3.3.2	Principal Stress Distribution on Bulkhead and Diaphragm Plates.....	64
3.3.3	Stress Distribution on Ribs near Rib-to-Deck Joints	67
3.4	Predicted Stresses for Model 2	70
3.4.1	Stress Contour on Ribs at Support Diaphragms	70
3.4.2	Principal Stress Distribution on Bulkhead and Diaphragm Plates.....	74
3.4.3	Stress Distribution on Ribs near Rib-to-Deck Welded Joints.....	77
4.	SPECIMEN 1 TEST RESULTS	80
4.1	Testing Program.....	80
4.2	Fatigue Cracks in Ribs at End Support Diaphragms	82
4.3	Measured Response	90
4.3.1	Rib Stress Distribution near the Rib-to-Deck Welds.....	90
4.3.2	Stress Distribution on Bulkheads and Diaphragms	94
4.3.3	Stress Comparisons between Predicted and Measured Responses	99
4.4	Modifications for Testing of Specimens 2 to 6.....	100
5.	SPECIMENS 2 TO 6 TEST RESULTS	103
5.1	Testing Program.....	103
5.2	Measured Response near the Rib-to-Deck PJP Welds	105
5.2.1	Deck Plate Stress Distribution	105
5.2.2	Rib Stress Distribution near Rib-to-Deck Welds.....	117
5.2.3	Fatigue Cracks near Rib-to-Deck Welds	141
5.3	Measured Response at Support Diaphragms	146
5.3.1	Stress Distribution in Ribs, Diaphragms, and Bulkheads	146
5.3.2	Fatigue Cracks Observed in Ribs below Bulkhead and Diaphragm Cutout.....	157
5.4	Comparison of Test Results	161
5.4.1	Effect of Heat Straightening on Fatigue Resistance of Rib-to-Deck Welds	161
5.4.2	Effect of Weld Melt-Through on Fatigue Resistance of Rib-to-Deck Welds	161
6.	SUMMARY AND CONCLUSIONS	163
6.1	Summary	163
6.2	Conclusions.....	164
	REFERENCES	166

LIST OF TABLES

Table 2.1 Designation of Specimens	11
Table 2.2 Pre-cambering Measures.....	16
Table 2.3 Measured Value of d	26
Table 2.4 Mechanical Properties.....	27
Table 2.5 Chemical Analysis (from Certified Mill Test Report).....	27
Table 2.6 Test Matrix.....	29
Table 4.1 Specimen 1: Stress Range and Mean Stresses in Ribs near Rib-to-Deck Welds	91
Table 4.2 Specimen 1: Stress Range and Mean Stresses on Bulkheads and Diaphragms	95
Table 4.3 Specimen 1: Comparison between predicted and Measured Responses	99
Table 5.1 Specimen 4: Stress Range and Mean Stress in Deck Plate near the PJP Welds	106
Table 5.2 Specimen 5: Stress Range and Mean Stress in Deck Plate near the PJP Welds	107
Table 5.3 Specimen 6: Stress Range and Mean Stress in Deck Plate near the PJP Welds	108
Table 5.4 Specimen 2: Stress Range and Mean Stress in Ribs near the PJP Welds.....	118
Table 5.5 Specimen 3: Stress Range and Mean Stress in Ribs near the PJP Welds.....	119
Table 5.6 Specimen 4: Stress Range and Mean Stress in Ribs near the PJP Welds.....	120
Table 5.7 Specimen 5: Stress Range and Mean Stress in Ribs near the PJP Welds.....	121
Table 5.8 Specimen 6: Stress Range and Mean Stress in Ribs near the PJP Welds.....	122
Table 5.9 Specimen 2: Stress Range and Mean Stress at Support Diaphragms	147
Table 5.10 Specimen 3: Stress Range and Mean Stress at Support Diaphragms	147
Table 5.11 Specimen 4: Stress Range and Mean Stress at Support Diaphragms	148
Table 5.12 Specimen 5: Stress Range and Mean Stress at Support Diaphragms	148
Table 5.13 Specimen 4: Crack Length Below Rib-to-Bulkhead Connection (mm).....	157
Table 5.14 Number of Cracks and Crack Types at Loading Locations.....	162

LIST OF FIGURES

Figure 1.1 Typical Cross Section of Orthotropic Box Girder.....	2
Figure 1.2 Fatigue Cracks on Orthotropic Steel Deck (Machida et al. 2003)	3
Figure 1.3 Cross Sectional Dimensions (Wolchuk 2004).....	4
Figure 1.4 Diaphragm Cutout Details of New Carquinez Bridge (Wolchuk 2004)	5
Figure 1.5 Typical PJP Welds at Rib-to-Deck Plate Joint.....	7
Figure 2.1 Plan and Side View of Test Panel	8
Figure 2.2 Cross Section between Support Diaphragms	9
Figure 2.3 Cross Section at Support Diaphragms.....	9
Figure 2.4 Details at Diaphragm Cutout.....	9
Figure 2.5 Submerged Arc Welding Operation	10
Figure 2.6 View of Weld Melt-through Inside of Rib	11
Figure 2.7 Heat Straightening Operation	12
Figure 2.8 Heat-Straightened Locations	14
Figure 2.9 Pre-Cambering.....	15
Figure 2.10 Pre-Cambering Scheme.....	15
Figure 2.11 Location of Distortion Measurements	17
Figure 2.12 Specimen 1: Distortion Measurements.....	18
Figure 2.13 Specimen 2: Distortion Measurements.....	19
Figure 2.14 Specimen 3: Distortion Measurements.....	20
Figure 2.15 Specimen 4: Distortion Measurements.....	21
Figure 2.16 Specimen 5: Distortion Measurements.....	22
Figure 2.17 Specimen 6: Distortion Measurements.....	23
Figure 2.18 Deck Distortion in the Longitudinal Direction.....	24
Figure 2.19 Deck Distortion in the Transverse Direction.....	24
Figure 2.20 Intersection of Rib with Diaphragms	25
Figure 2.21 HRB Hardness Test (Specimen 5).....	28
Figure 2.22 End View of Test Setup.....	30
Figure 2.23 Elevation of Test Setup	30
Figure 2.24 East Test Setup (Specimens 2 and 3)	31
Figure 2.25 West Test Setup (Specimens 1, 4, 5, and 6)	31

Figure 2.26 Specimen 1: Loading Scheme	33
Figure 2.27 Specimens 2 to 6: Loading Scheme.....	33
Figure 2.28 Specimen 1: Uni-axial Strain Gages in Deck Plate near Rib-to-Deck Welds	35
Figure 2.29 Specimen 2: Uni-axial Strain Gages in Deck Plate near Rib-to-Deck Welds	35
Figure 2.30 Specimen 3: Uni-axial Strain Gages in Bottom of Deck Plate near Rib-to-Deck Welds.....	36
Figure 2.31 Specimen 4: Strain Gage Rosettes in Bottom of Deck Plate near Rib-to-Deck Welds	36
Figure 2.32 Specimen 5: Uni-axial Strain Gages in Deck Plate Near Rib-to-Deck Welds	36
Figure 2.33 Specimen 6: Uni-axial Strain Gages in Deck Plate near Rib-to-Deck Welds	37
Figure 2.34 Specimen 1: Strain Gages in Outer Surface of Rib R2 near Rib-to-Deck Welds	38
Figure 2.35 Specimen 1: Strain Gages in Rib R3 near Rib-to-Deck Welds.....	38
Figure 2.36 Specimen 2: Strain Gages in Outer Surface of Rib R2 near Rib-to-Deck Welds	39
Figure 2.37 Specimen 2: Strain Gages in Outer Surface of Rib R3 near Rib-to-Deck Welds	39
Figure 2.38 Specimen 2: Strain Gages in Outer Surface of Rib R4 near Rib-to-Deck Welds	40
Figure 2.39 Specimen 3: Strain Gages in Outer Surface of Rib R2 near Rib-to-Deck Welds	40
Figure 2.40 Specimen 3: Strain Gages in Outer Surface of Rib R3 near Rib-to-Deck Welds	41
Figure 2.41 Specimen 4: Strain Gages in Outer Surface of Rib R2 near Rib-to-Deck Welds	41
Figure 2.42 Specimen 4: Strain Gages in Outer Surface of Rib R3 near Rib-to-Deck Welds	42
Figure 2.43 Specimen 4: Strain Gages in Inner Surface of Rib R3 near Rib-to-Deck Welds	42

Figure 2.44 Specimen 5: Strain Gages in Outer Surface of Rib R2 near Rib-to-Deck Welds	43
Figure 2.45 Specimen 5: Strain Gages in Inner Surface of Rib R2 near Rib-to-Deck Welds	43
Figure 2.46 Specimen 6: Strain Gages in Outer Surface of Rib R2 near Rib-to-Deck Welds	44
Figure 2.47 Specimen 6: Strain Gages in Outer Surface of Rib R3 Near Rib-to-Deck Welds	44
Figure 2.48 Strain Gage Instrumentation Inside of Ribs	45
Figure 2.49 Specimen 1: Gages in Bulkheads and Diaphragms at Supports.....	46
Figure 2.50 Specimen 2: Gages in Ribs, Bulkheads and Diaphragms at Supports	47
Figure 2.51 Specimen 3: Gages in Ribs, Bulkheads and Diaphragms at Supports	48
Figure 2.52 Specimen 4: Gages in Ribs at Supports.....	49
Figure 2.53 Specimen 5: Gages in Ribs at Supports.....	49
Figure 3.1 ABAQUS Modeling.....	50
Figure 3.2 Model 1: Plan View and Loading Steps	52
Figure 3.3 Model 2: Plan View and Loading Steps	53
Figure 3.4 Model 1: Deformed Shape (Amplification Factor = 50).....	54
Figure 3.5 Model 2: Deformed Shape (Amplification Factor = 50).....	55
Figure 3.6 Model 1: Deformed Shape at Cross Section 1 (Amplification Factor = 50)...	56
Figure 3.7 Model 1: Deformed Shape at Cross Section 2 (Amplification Factor = 50)...	57
Figure 3.8 Model 1: Deformed Shape at Cross Section 3 through Load Steps 1, 2, and 3	58
Figure 3.9 Model 2: Deformed Shape at Cross Section 1 (Amplification Factor = 50)...	58
Figure 3.10 Model 2: Deformed Shape at Cross Section 2 (Amplification Factor = 50). 59	
Figure 3.11 Model 2: Deformed Shape at Cross Section 3 through Load Steps 1, 2, and 3	60
Figure 3.12 Model 1: Location of Detail A	61
Figure 3.13 Model 1: Stress Contour Inside the Rib of Detail A (MPa)	62
Figure 3.14 Model 1: Stress Contour Outside the Rib of Detail A (MPa).....	63
Figure 3.15 Model 1: Principal Stress Contour or Tensor at Detail A (MPa)	65

Figure 3.16 Designation of Rib-to-Deck Joints	68
Figure 3.17 Location and Direction of Stresses in Deck Plate and Ribs	68
Figure 3.18 Model 1: Predicted Stresses in Ribs at Joint 1	69
Figure 3.19 Model 1: Predicted Stresses in Deck Plate at Joint 1	69
Figure 3.20 Model 1: Predicted Stresses in Ribs at Joint 2	69
Figure 3.21 Model 1: Predicted Stresses in Deck Plate at Joint 2	70
Figure 3.22 Model 2: Location of Detail B.....	71
Figure 3.23 Model 2: Stress Contour Inside the Rib of Detail B (MPa)	72
Figure 3.24 Model 2: Stress Contour Outside the Rib of Detail B (MPa).....	73
Figure 3.25 Model 2: Principal Stress Contour or Tensor at Detail B (MPa)	75
Figure 3.26 Model 2: Predicted Stresses in Deck Plate at Joint 1	78
Figure 3.27 Model 2: Predicted Stresses in Ribs at Joint 1	78
Figure 3.28 Model 2: Predicted Stresses in Deck Plate at Joint 2	78
Figure 3.29 Model 2: Predicted Stresses in Ribs at Joint 2	79
Figure 4.1 Specimen 1: Plan View with Rib and Diaphragm Designations.....	81
Figure 4.2 Specimen 1: Test Setup and Diaphragm Locations.....	81
Figure 4.3 Specimen 1: Typical Applied Load and Measured Deflection Time History .	82
Figure 4.4 Specimen 1: Crack Pattern on the Rib below bulkhead and diaphragm cutout	83
Figure 4.5 Specimen 1: Fatigue Crack at D1-R2-East.....	84
Figure 4.6 Specimen 1: Fatigue Crack at D1-R2-West	85
Figure 4.7 Specimen 1: Fatigue Crack at D1-R3-East.....	86
Figure 4.8 Specimen 1: Fatigue Crack at D1-R3-West	87
Figure 4.9 Specimen 1: Fatigue Crack at D3-R2-East.....	88
Figure 4.10 Specimen 1: Fatigue Crack at D3-R3-West	89
Figure 4.11 Specimen 1: Stress Range and Mean Stresses in Rib R2	92
Figure 4.12 Specimen 1: Stress Range and Mean Stresses in Rib R3 near Rib-to-Deck Welds	93
Figure 4.13 Specimen 1: Stress Range and Mean Stresses on Bulkhead	96
Figure 4.14 Specimen 1: Stress Range and Mean Stresses on Diaphragms	97
Figure 4.15 Specimen 1: Comparison between Predicted and Measured responses	100

Figure 4.16 Model Configuration and Predicted Rib Stresses at Cutout Location (MPa)	101
.....	
Figure 4.17 Boundary Condition Modifications.....	102
Figure 5.1 Specimens 2 to 6: Plan View with Rib and Diaphragm Designations	104
Figure 5.2 Specimens 2 to 6: Typical Applied Load and Measured Deflection Time History.....	105
Figure 5.3 Specimen 4: Stress Range and Mean Stress in Deck Plate near the PJP Welds	
.....	109
Figure 5.4 Specimen 5: Stress Range and Mean Stress in Deck Plate near the PJP Welds	
.....	111
Figure 5.5 Specimen 6: Stress Range and Mean Stress in Deck Plate near the PJP Welds	
.....	115
Figure 5.6 Specimen 2: Stress Range and Mean Stress in Rib R2 near the PJP Welds .	123
Figure 5.7 Specimen 2: Stress Range and Mean Stress in Rib R3 near the PJP Welds .	124
Figure 5.8 Specimen 2: Stress Range and Mean Stress in Rib R4 near the PJP Welds .	125
Figure 5.9 Specimen 3: Stress Range and Mean Stress in Rib R2 near the PJP Welds .	126
Figure 5.10 Specimen 3: Stress Range and Mean Stress in Rib R3 near the PJP Welds	127
Figure 5.11 Specimen 4: Stress Range and Mean Stress in Rib R2 near the PJP Welds	129
Figure 5.12 Specimen 4: Stress Range and Mean Stress in Rib R3 near the PJP Welds	130
Figure 5.13 Specimen 5: Stress Range and Mean Stress in Rib R2 near the PJP Welds	133
Figure 5.14 Specimen 6: Stress Range and Mean Stress in Rib R2 near the PJP Welds	138
Figure 5.15 Specimen 6: Stress Range and Mean Stress in Rib R3 near the PJP Welds	140
Figure 5.16 Four Cutting Locations with Designations (C1 to C4).....	142
Figure 5.17 Sliced Pieces.....	142
Figure 5.18 Typical Crack Pattern at Rib-to-Deck PJP Welds.....	143
Figure 5.19 Specimen 2: Depth of Crack Initiating from Rib-to-Deck PJP Welds.....	143
Figure 5.20 Specimen 2: Indication of Linear Crack at Rib-to-Deck PJP Weld	144
Figure 5.21 Specimen 3: Crack Depth at Rib-to-Deck PJP Welds (Location C1)	144
Figure 5.22 Specimen 6: Crack Depth at Rib-to-Deck PJP Welds.....	145
Figure 5.23 Specimen 2: Stress Range and Mean Stress in Ribs at Supports	149
Figure 5.24 Specimen 2: Stress Range and Mean Stress in Bulkheads and Diaphragms	150

Figure 5.25 Specimen 3: Stress Range and Mean Stress in Ribs at Supports	152
Figure 5.26 Specimen 3: Stress Range and Mean Stress in Bulkheads and Diaphragms	153
Figure 5.27 Specimen 4: Stress Range and Mean Stress in Ribs at Supports	154
Figure 5.28 Specimen 5: Stress Range and Mean Stress in Ribs at Supports	156
Figure 5.29 Specimen 5: Observed Crack Pattern at End Supports (at 8 M cycles)	158
Figure 5.30 Cross Section through the Crack at End Support	159
Figure 5.31 Specimen 4: Cracks at Rib-to-Bulkhead Welded Joint (D1-R2-East)	160

LIST OF SYMBOLS

C1	Cutting location 1
C2	Cutting location 2
C3	Cutting location 3
C4	Cutting location 4
CJP	Complete Joint Penetration
D1	Diaphragm 1
D2	Diaphragm 2
D3	Diaphragm 3
E	Modulus of elasticity
MT	Magnetic particle test
P	Applied load
PJP	Partial Joint Penetration
R1	Rib 1
R2	Rib 2
R3	Rib 3
R4	Rib 4
S_m	Mean stress
S_r	Stress range
UT	Ultrasonic test
a	Larger of the spacing of the rib walls
d	Distance from the top of the free cutout to the bottom of the bulkhead
h'	Length of the inclined portion of the rib wall
$t_{d,eff}$	Effective thickness of the deck plate
t_r	Thickness of the rib wall

1. INTRODUCTION

1.1 Background

Modern orthotropic steel bridge decks were developed in Europe over five decades ago. In an effort to create a bridge with limited resources available during World War II, European bridge engineers developed lightweight steel bridge decks that feature not only economical but also excellent structural characteristics. An orthotropic steel deck typically consists of thin steel plate stiffened by a series of closely spaced longitudinal ribs and transverse floor beams supporting the deck plate (see Figure 1.1). The longitudinal ribs are welded to the underside of the deck plate in a parallel pattern perpendicular to the floor beams, thus the deck becomes much more rigid in the longitudinal direction than the transverse direction. As the structural behavior is different in the longitudinal and transverse directions, the system is orthogonal-anisotropic and is called orthotropic for short (Troitsky 1987).

Longitudinal ribs welded to the deck plate can be either open ribs or closed ribs. Open ribs which have small torsional stiffness are usually made from flat bars, inverted T-sections, bulb shapes, angles, or channels. For closed ribs with much larger torsional stiffness than the open ribs, semicircular, triangular, boxed, or trapezoidal shapes are often used, and among which the trapezoidal rib section is most commonly used. Advantages to the deck system with open ribs may lie in the simplicity for fabrication and ease of maintenance due to availability of getting access to both sides of the rib-to-deck welds. Disadvantages to the open rib deck system are that the wheel-load distribution capacity in the transverse direction is relatively small, and the deck is heavier compared to the closed ribs deck system due to close spacing of floor beams. The deck system stiffened by closed ribs has more efficiency for transverse distribution of the wheel load than the open rib system due to high torsional and flexural stiffness (Troitsky 1987). In addition, the deck with closed ribs uses less welding than is necessary with open ribs due to wide spacing of floor beams. Nevertheless, closed ribs can be welded to the deck plate from one side (i.e., outside) only, thus making weld inspection impossible after welding due to a lack of access to the inside of the closed ribs.

Despite their light weight and other excellent structural characteristics, orthotropic steel deck bridges have recently experienced a variety of fatigue problems resulting from high cyclic stresses in conjunction with poor welding details (Kaczinski et al. 1997, Bocchieri et al. 1998).

In Japan, a detailed investigation of the occurrence of fatigue cracks of orthotropic steel bridges in urban cities was reported by Machida et al. (2003). Figure 1.2 shows typical crack patterns. In addition to the crack at the rib-to-diaphragm junction, crack at the rib-to-deck welded joint is also a concern. The latter joints are prone to fatigue cracking because they are subjected to wheel load directly; stress concentration occurs both in the weld toe due to local plate bending and bearing stresses and in the weld root due to the characteristic deformation made of the joint from wheel load (Machida et al. 2003). Unfortunately, inspection and repair of the back side of this weld (i.e., weld root) for closed ribs is not practical due to lack of access. Cracks like type 1a in Figure 1.2(c) will not be discovered until the crack propagates thorough the entire thickness of the plate and shows sign in wearing surface.

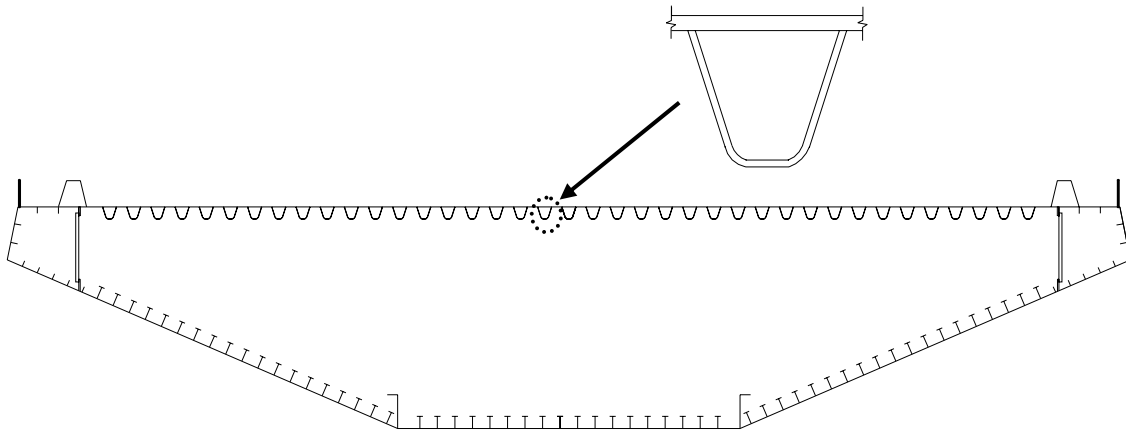


Figure 1.1 Typical Cross Section of Orthotropic Box Girder

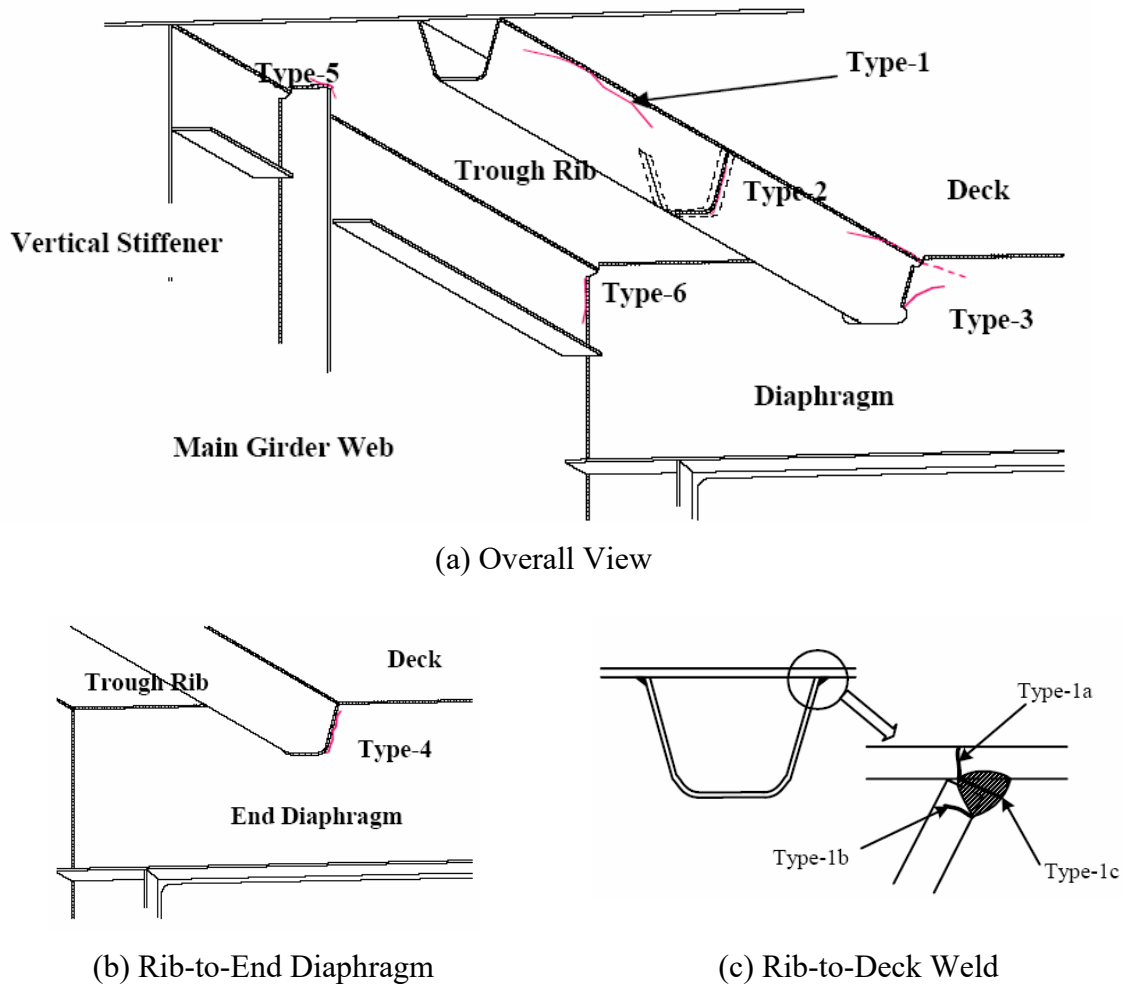


Figure 1.2 Fatigue Cracks on Orthotropic Steel Deck (Machida et al. 2003)

In the United States, fatigue cracking is classified as either load-induced cracking or distortion-induced cracking (AASHTO 2007). Load-induced fatigue cracking results from the fluctuation of the nominal primary stresses, which can be computed using standard first-order design calculations. Permissible values of stress range are obtained from S-N curves for various detail categories. On the other hand, distortion-induced fatigue cracking results from the imposition of deformations producing secondary stresses, which are very difficult to quantify for routine design. No calculation of stresses is required; instead, the design only needs to satisfy a set of prescriptive detailing requirements in the AASHTO Specification.

Taking the rib-to-deck detail in Figure 1.2 as an example, AASHTO Specification provides the following prescriptive requirements:

- (1) The deck plate thickness shall not be less than 14.0 mm or 4 percent of the larger spacing of rib webs.
- (2) The thickness of closed ribs shall not be less than 6.0 mm.
- (3) The thickness of the rib shall be limited by satisfying the following dimensioning requirement:

$$\frac{t_r \cdot a^3}{t_{d,eff}^3 \cdot h'} \leq 400 \quad (1.1)$$

See Figure 1.3 for symbols. This requirement is intended to minimize the local out-of-plane flexural stress in the rib web at the junction with the deck plate.

- (4) Eighty percent partial penetration welds between the webs of a closed rib and the deck plate should be permitted.

For the detail of diaphragm cutout at the intersection with the rib, prescriptive rules are also specified in the AASHTO Specification. A typical example of this detail is shown in Figure 1.4. According to the Commentary of Article 9.8.3.7.4 of the AASHTO Specification, secondary stresses at the rib-floorbeam interaction can be minimized if an internal diaphragm (bulkhead) is placed inside of the rib in the plane of the floorbeam web. The designer has the option of either terminating the internal diaphragm below the top of the free cutout, in which case the diaphragm should extend at least 25 mm below the top of the free cutout and must have a fatigue resistant welded connection (e.g., complete joint penetration groove weld) to the rib wall, or extending the diaphragm to the bottom of the rib and welding all around.

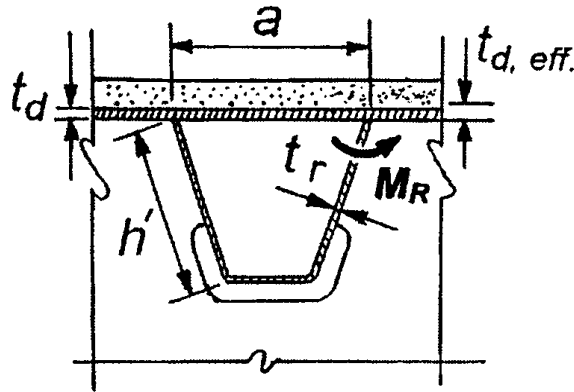
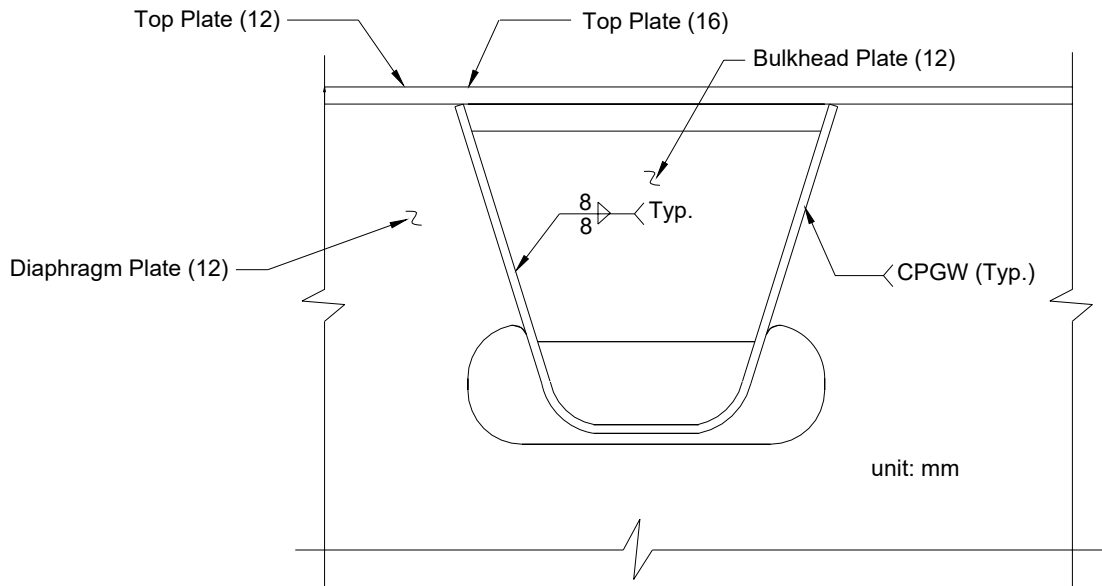
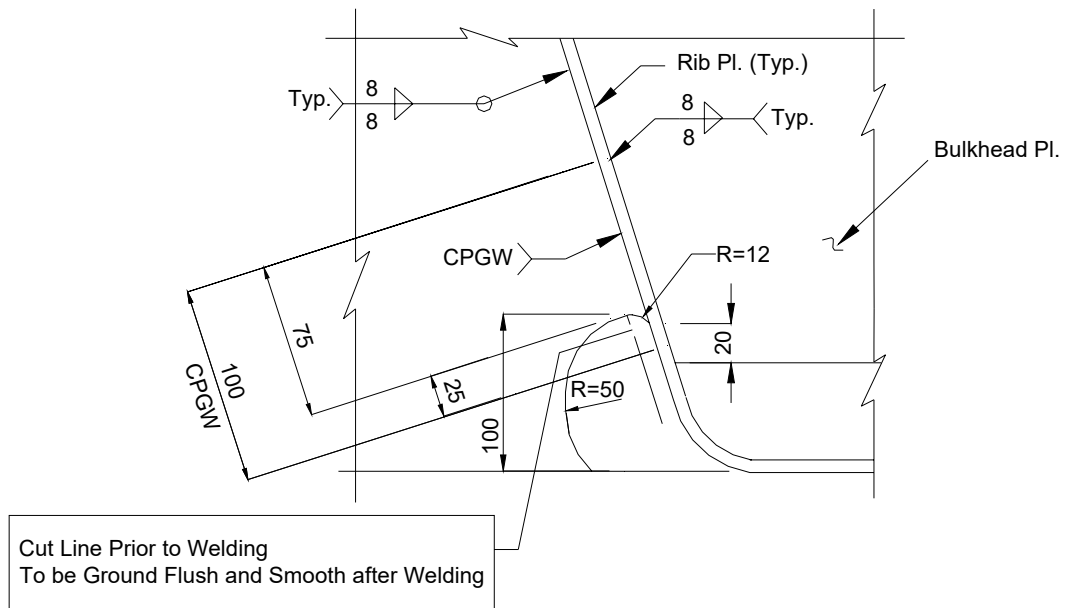


Figure 1.3 Cross Sectional Dimensions (Wolchuk 2004)



(a) Details at Rib-to-Diaphragm Intersections of New Carquinez Bridge



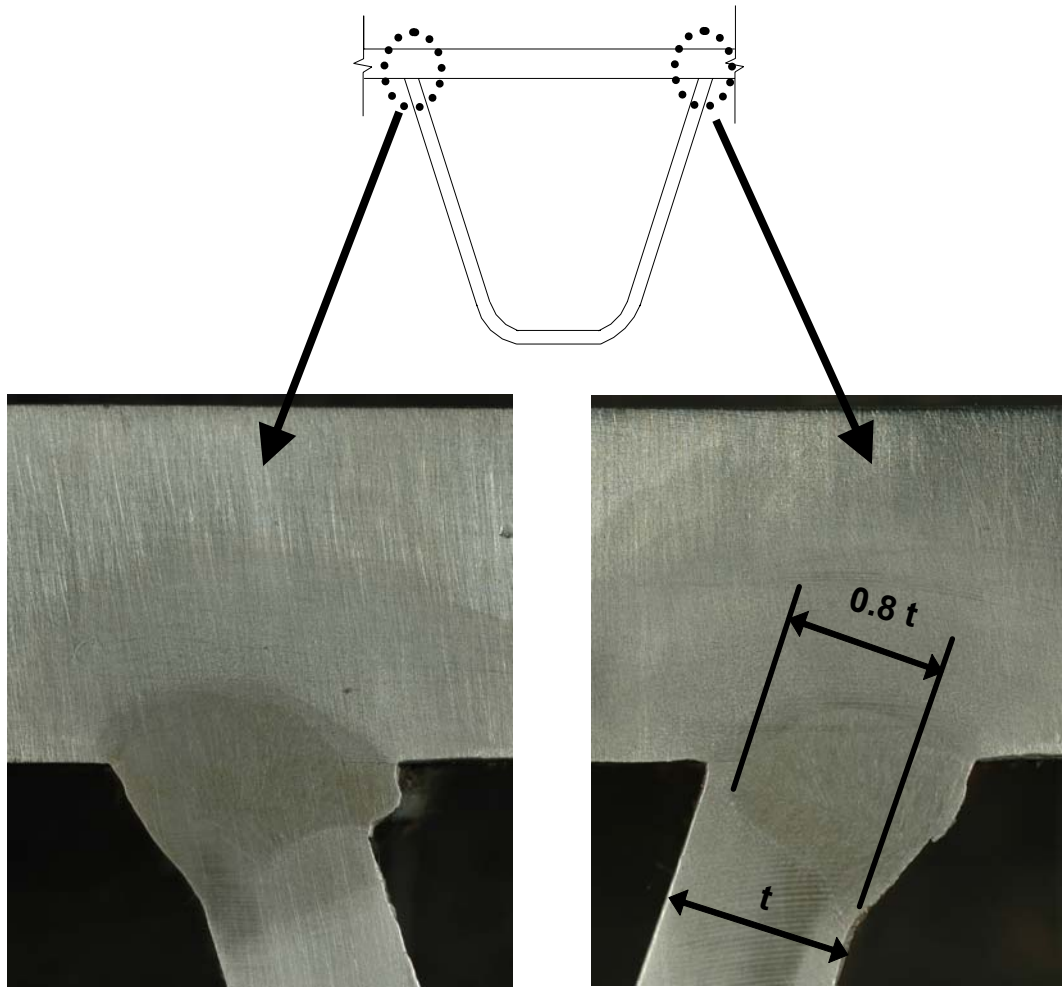
(b) Cutout Detail

Figure 1.4 Diaphragm Cutout Details of New Carquinez Bridge (Wolchuk 2004)

The weld details in use at rib-to-deck joints vary in different countries. In Japan, fillet welds are used for these closed rib-to-deck plate joints, and Japan Road Association Specification requires at least a weld penetration of 75% of the rib thickness (Ya et al.

2007). In the United States, Article 9.8.3.7.2 of the AASHTO Specification code specifies 80% partial penetration groove welds. The Commentary states that partial penetration welds are generally used for connecting closed ribs with thickness greater than 6.35 mm (1/4 in) to deck plates. Such welds, which require careful choice of automatic welding processes and a tight fit, are less susceptible to fatigue failure than full penetration groove welds requiring backup bars. In practice, however, the amount of penetration into the joint components is difficult to control, and the actual weld size achieved varies due to many parameters, including power source, material, and fit-up tolerances. Because of the thin thickness (say, 8 mm) of the rib plate, weld melt-through to the back side of this weld is also difficult to avoid. Some are of the opinion that this weld melt-through might affect the fatigue resistance at these welded joints. Figure 1.5 shows two weld details of 80% PJP without weld melt-through and with weld melt-through.

As an orthotropic steel deck is fabricated from thin steel plates and closed ribs joined together by extensive welding, thermal distortion would result. To satisfy the flatness requirement of the deck plate, heat straightening is commonly used. Some are of the opinions that heat straightening, especially used repeatedly, may affect the fatigue resistance of the PJP weld. Pre-cambering prior to welding is also common in practice to minimize the need for heat straightening (Masahiro et al. 2006).



(a) with Weld Melt-Through

(b) without Weld Melt-Through

Figure 1.5 Typical PJP Welds at Rib-to-Deck Plate Joint

1.2 Objectives

The main objective of this study was to evaluate through full-scale testing the effects of the following two factors on the fatigue resistance of closed rib-to-deck PJP welds:

- (1) weld melt-through, and
- (2) distortion control measures including pre-cambering

2. TESTING PROGRAM

2.1 Panel Fabrication

2.1.1 General

Six full-scale deck panels, 10 m long and 3 m wide, were fabricated by Oregon Iron Works, Inc. Figure 2.1 shows plan and side view of the test panel. The deck consists of 8 mm thick 4 ribs and a 16 mm thick deck plate, and the deck is supported by three equally spaced support diaphragms as a two span continuous unit. The thickness of the diaphragm plate is 16 mm. An 8 mm thick bulkhead (internal diaphragm) was installed inside each closed rib at the support diaphragms. The cross sections of the deck are shown in Figures 2.2 and 2.3. Details at diaphragm cutout are shown in Figure 2.4.

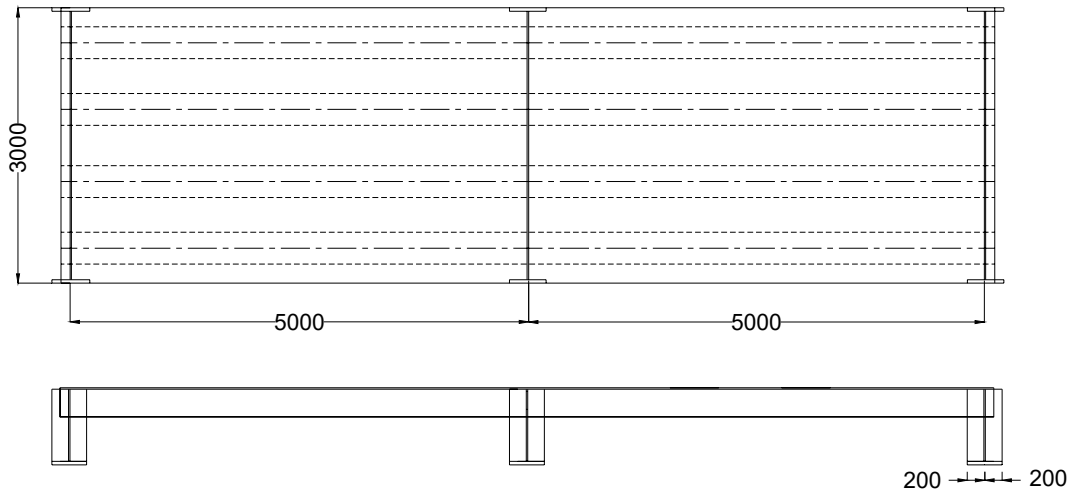


Figure 2.1 Plan and Side View of Test Panel

2.1.2 Rib-to-Deck Plate PJP Welded Joint

The test panel contains three conditions of rib-to-deck weld details in order to provide a comparison of their fatigue resistance. The weld conditions are: (a) 80% PJP groove weld without weld melt-through; (b) 100% PJP groove weld with evident continuous weld melt-through; (c) 80% or 100% PJP with intermittent weld melt-through every 1 m (i.e., alternating between the weld conditions (a) and (b) every 1 m).

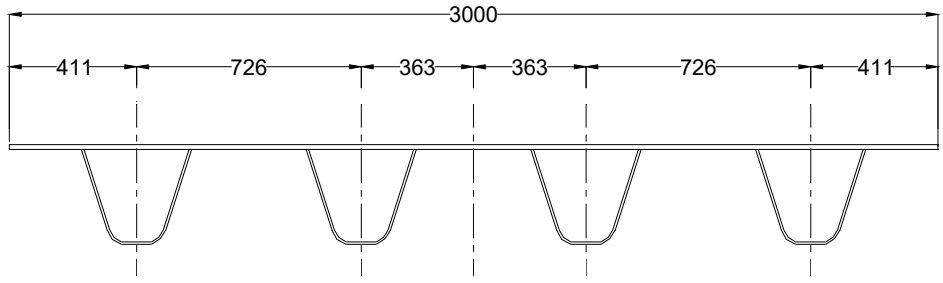


Figure 2.2 Cross Section between Support Diaphragms

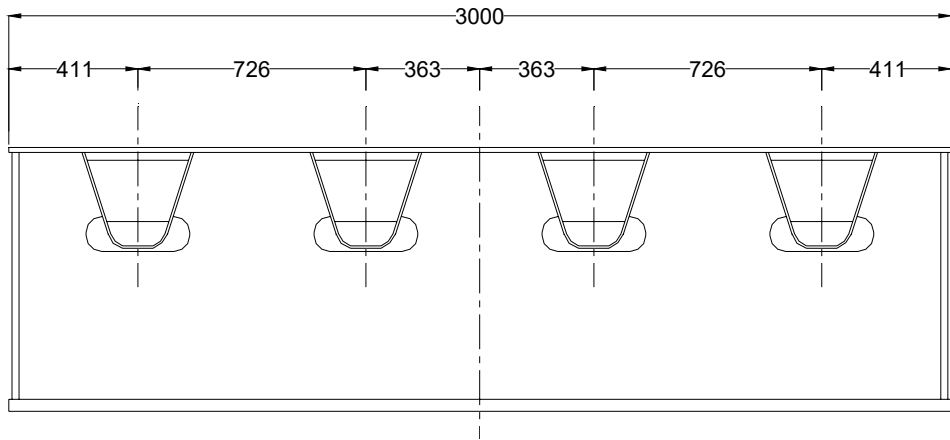


Figure 2.3 Cross Section at Support Diaphragms

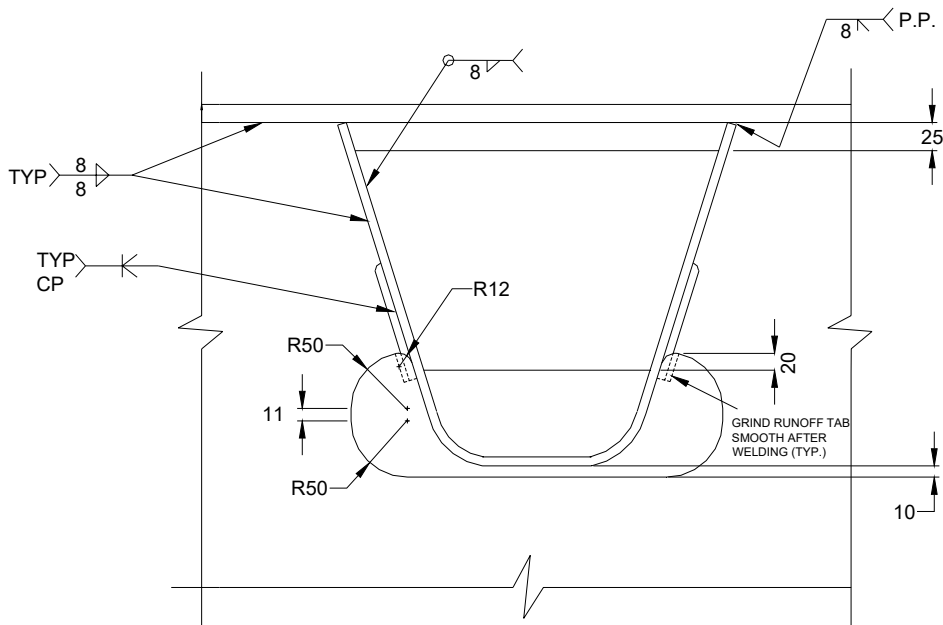


Figure 2.4 Details at Diaphragm Cutout

In order to achieve the desired weld conditions, a continuous 5 m long mock-up was welded with acceptable results. For specimen fabrication, the ribs were fit to the deck plate with a maximum allowable gap of 3 thousandths of an inch, and tack welded to the deck plate with 13 mm tack welds. The tack welds were ground down prior to rib-to-deck plate welding to minimize the tack weld profile. A rib was welded to the deck plate at a time using a Panjaris type gantry Submerged Arc Welding (SAW) with two single electrode heads to weld both sides of a rib simultaneously. The weld reinforcement was minimized to between 2 and 3 mm. Figure 2.5 shows a SAW welding operation used to connect the ribs to the deck plate. An evident view of the weld melt-through backside of the weld is shown in Figure 2.6.

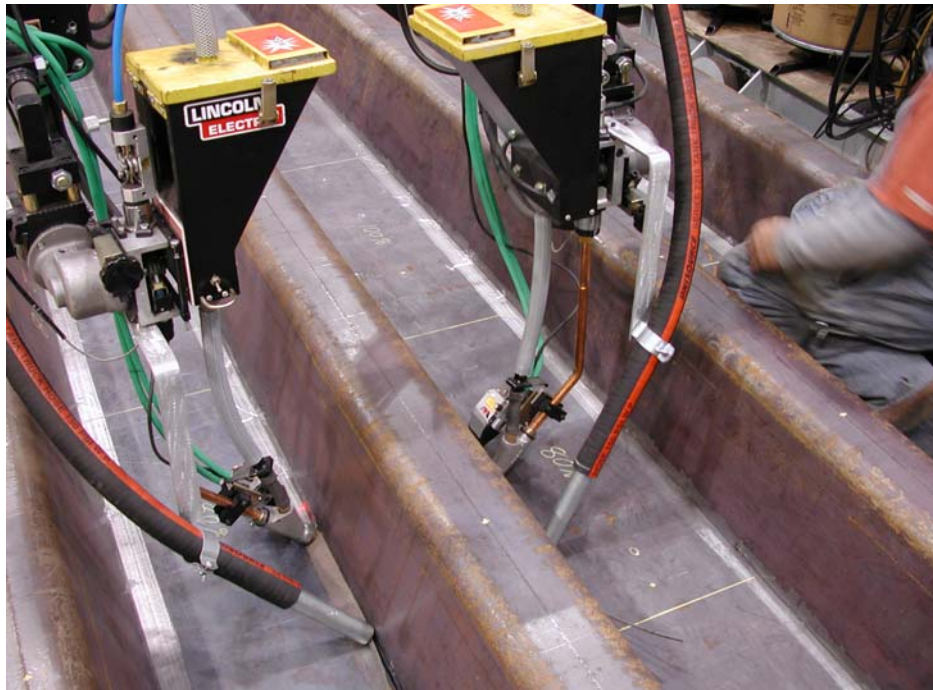


Figure 2.5 Submerged Arc Welding Operation



Figure 2.6 View of Weld Melt-through Inside of Rib

2.1.3 Distortion Controls (Pre-Cambering and Heat Straightening)

The specified deck plate flatness requirement was that the peak-to-peak tolerance in the longitudinal direction was 5 mm, and the peak-to-peak tolerance in the transverse direction was 3 mm. The distortion control plan included heat straightening. Three out of six panels were also pre-cambered in order to minimize the amount of required heat straightening. Designation of the test specimens is shown in Table 2.1.

Table 2.1 Designation of Specimens

	without Pre-camber	with Pre-camber
80 % PJP without Weld Melt-through	Specimen 1	Specimen 4
100 % PJP with Continuous Weld Melt-through	Specimen 2	Specimen 5
Intermittent Weld Melt-through Every 1 m	Specimen 3	Specimen 6

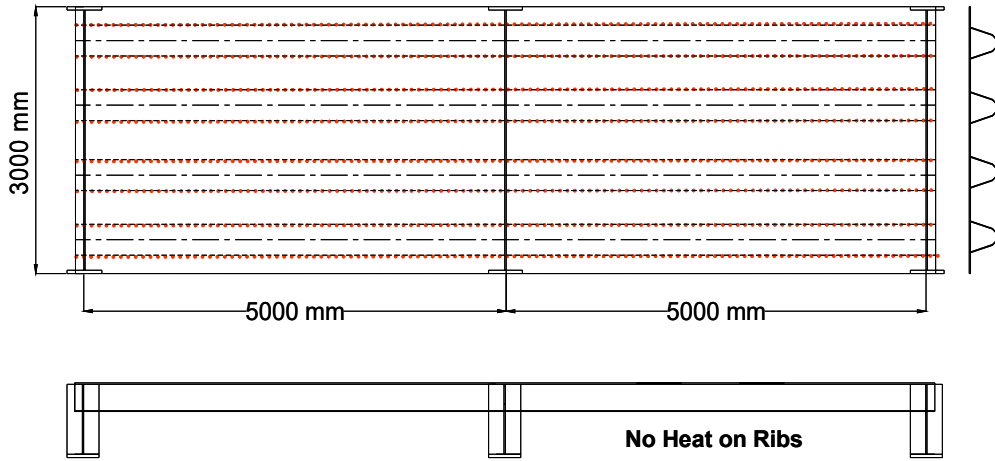
Figure 2.7 shows a view of the heat straightening operation from the top of the deck plate. Heating for a target temperature of approximately 450 °F with a travel speed of 280 mm per minute was applied from top of the deck plate to the longitudinal rib-to-

deck welds to control the distortion in the transverse (i.e., width) direction, and the bottom parts of the ribs were heated to control the distortion in the longitudinal direction. Heat straightened locations for the specimens are shown in Figure 2.8.

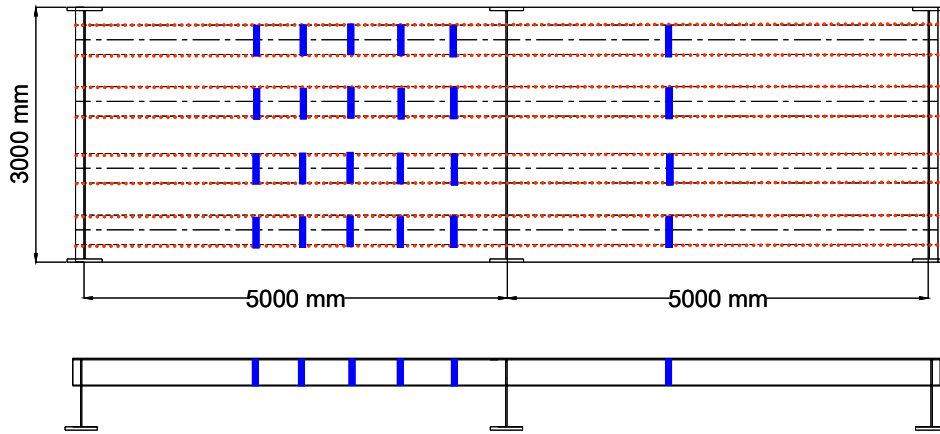
For the other three panels (Specimens 4, 5, and 6), the amount of pre-cambering was determined from the welding distortion pattern observed from the other 3 specimens that were not pre-cambered. Depending on the measured distortion level after welding, the pre-cambered panels were also heat straightened to satisfy the plate flatness requirement. Pre-cambering involved placing shim plates at each end of the panel, clamping down the sides, and weighting down the center. A view of pre-cambering is shown in Figure 2.9. Since the first pre-cambered panel (Specimen 6) did not produce a significant difference in as welded distortion compared with the same weld condition panel (Specimen 3), additional shims and heavier weight were used for the next two panels (Specimens 4 and 5) [see Figure 2.10 and Table 2.2]. Support diaphragms were installed until deck plates satisfied the flatness requirement.



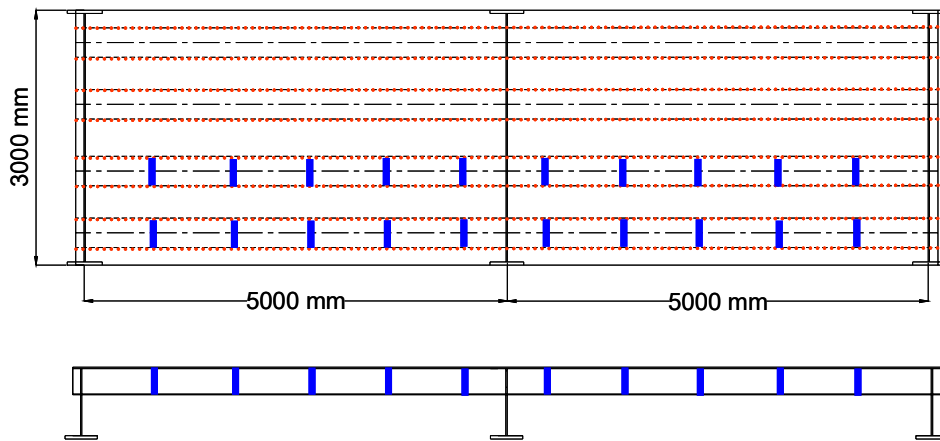
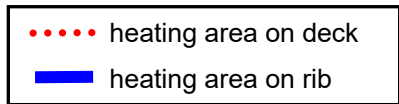
Figure 2.7 Heat Straightening Operation



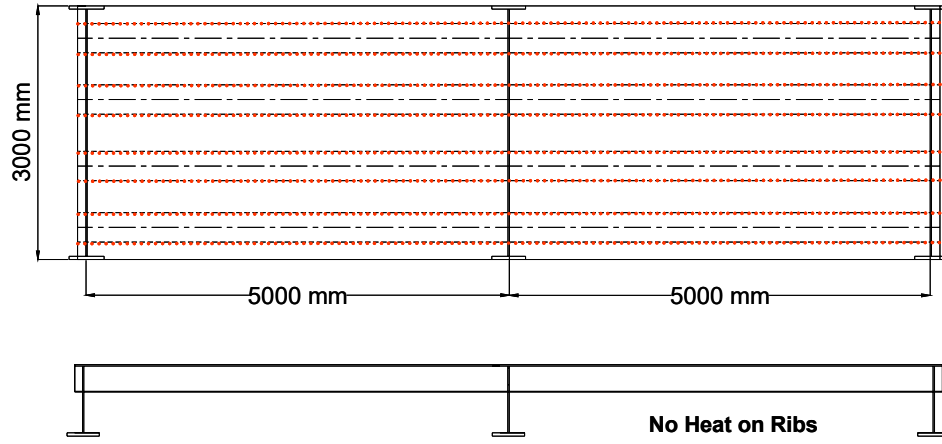
(a) Specimen 1



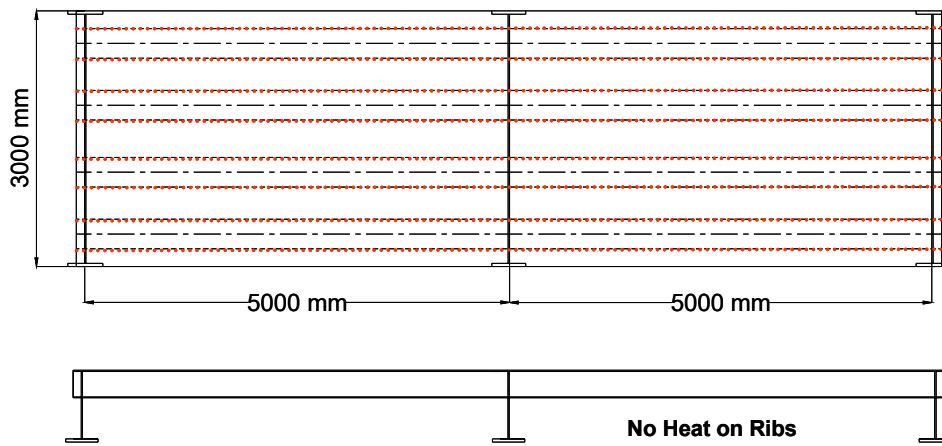
(b) Specimen 2



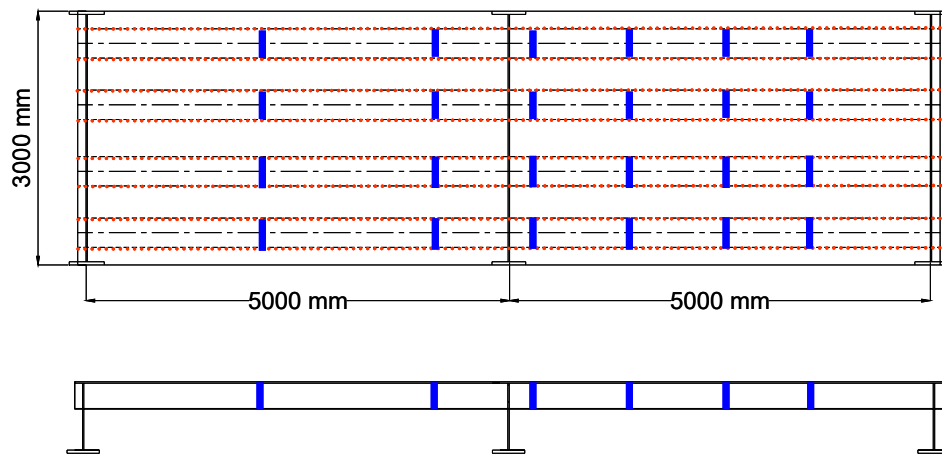
(c) Specimen 3



(d) Specimen 4



(e) Specimen 5



(f) Specimen 6

Figure 2.8 Heat-Straightened Locations



Figure 2.9 Pre-Cambering

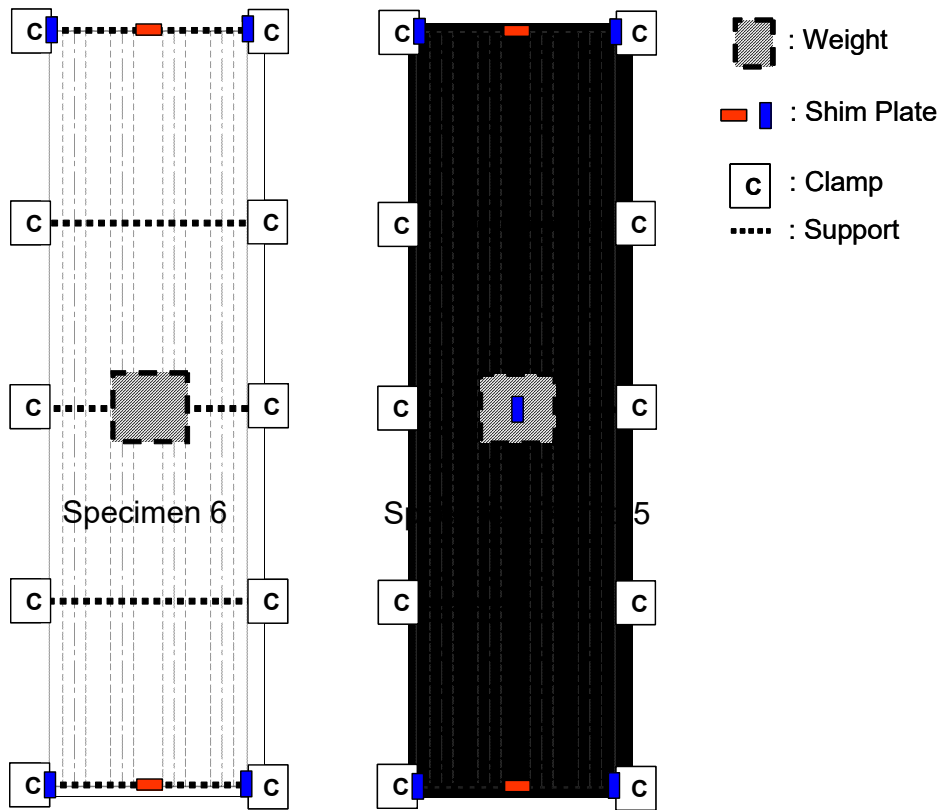




Figure 2.10 Pre-Cambering Scheme

Table 2.2 Pre-cambering Measures

	Weight (lb)	Shim height (mm) 	Shim height (mm) 
Specimen 4	42,000	20	10
Specimen 5	38,000	50	25
Specimen 6	7,300	22	10

2.1.4 Distortion Measurements

Distortion measurements on the panels were performed with the Laser Tracker system. Measurements were taken from 9 locations across the width of the panel and at the center of each rib, center of the space between adjacent two ribs, and at each edge of the panel. These measurements were taken at 600 mm spacing along the length of the panel. Figure 2.11 shows the locations of the measurement points. Figures 2.12 to 2.17 show plots of distortion measurements for each of the six specimens. From the measurements, it was shown that the maximum height deviation of the deck plate was approximately 20 mm. Plots of the deck distortions for comparison of six specimens are shown in Figures 2.18 and 2.19. From the plots, it was found that the two effectively pre-cambered specimens (Specimens 4 and 5) had less welding distortion than the other specimens. No strain measurements of the components were taken during fabrication.

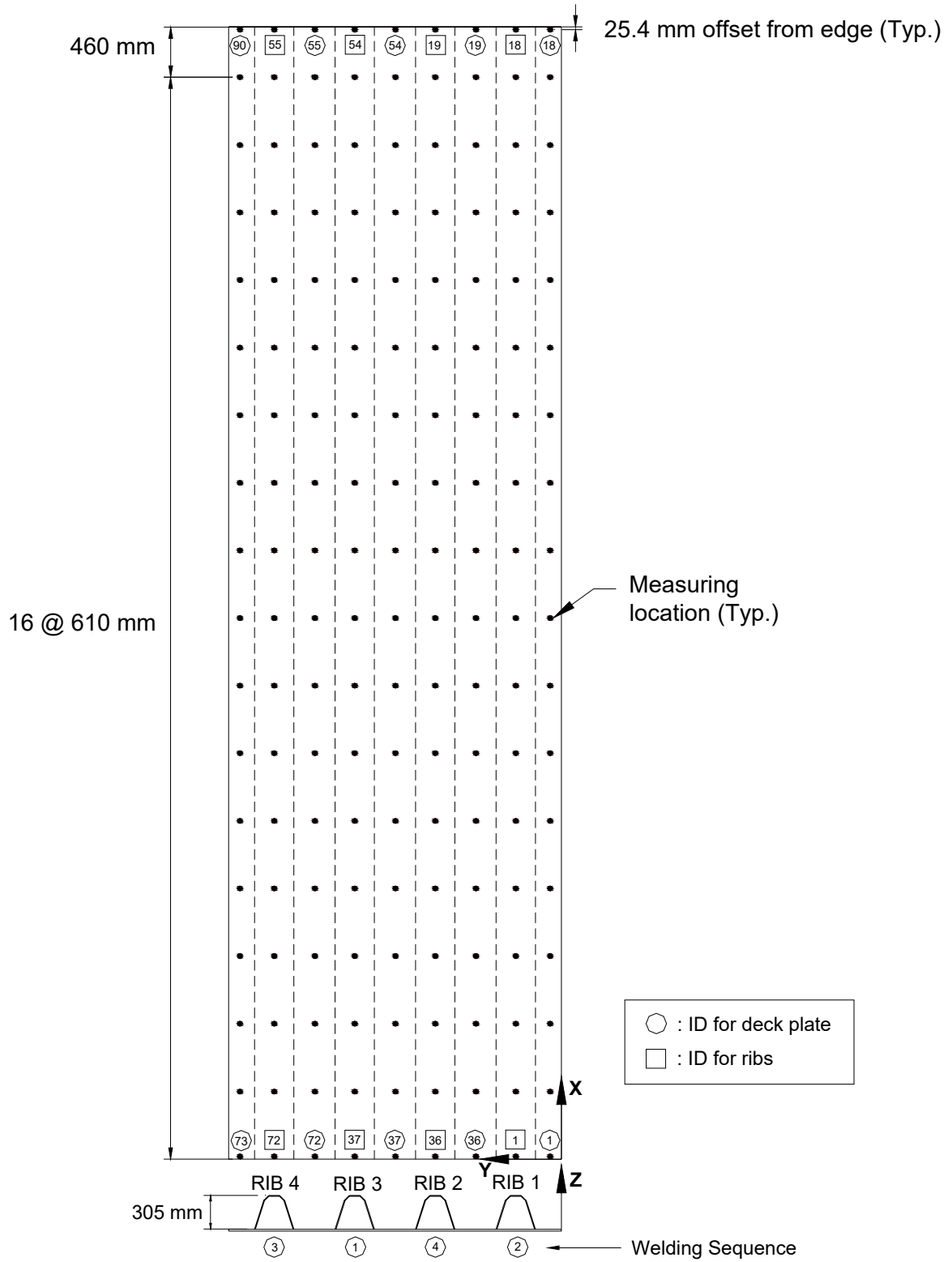
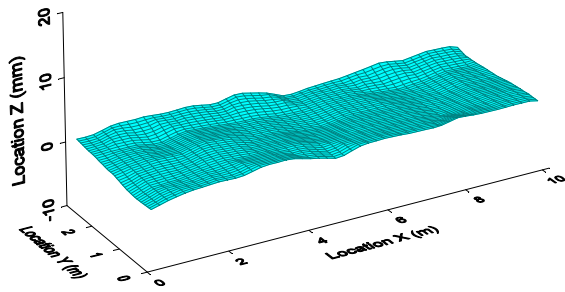
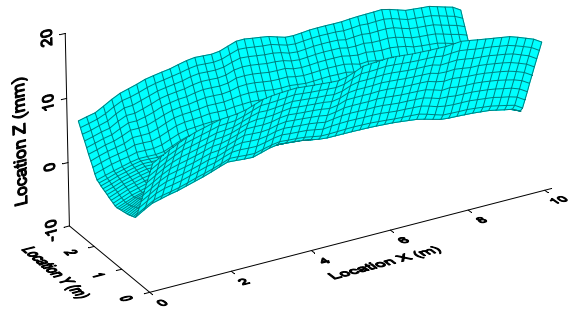


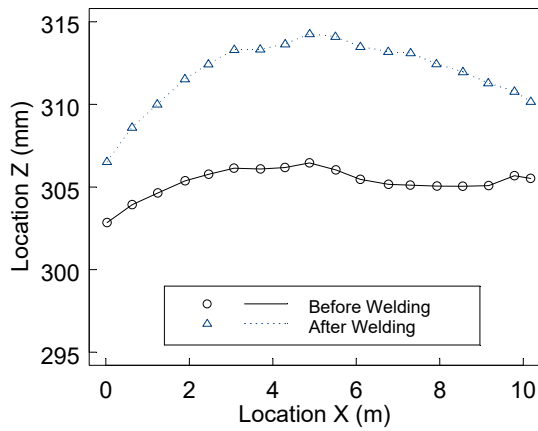
Figure 2.11 Location of Distortion Measurements



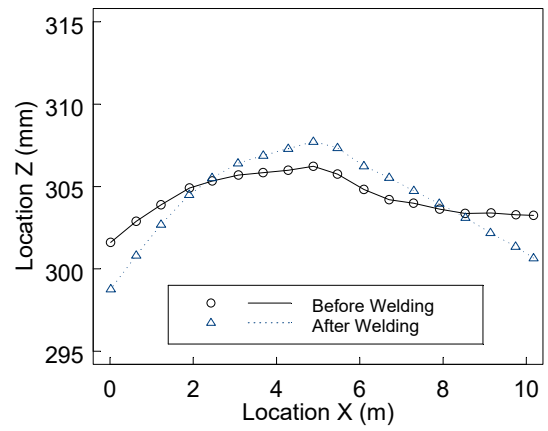
(a) Deck Plate before Welding



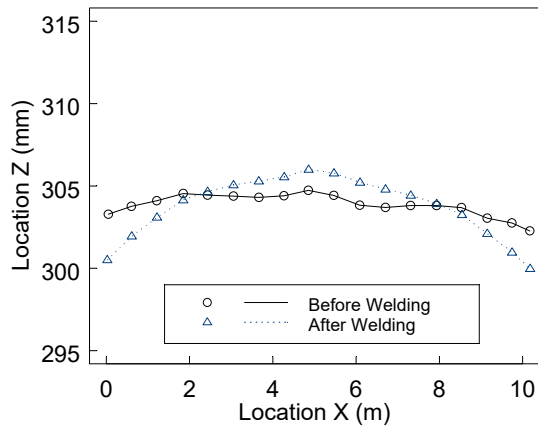
(b) Deck Plate after Welding



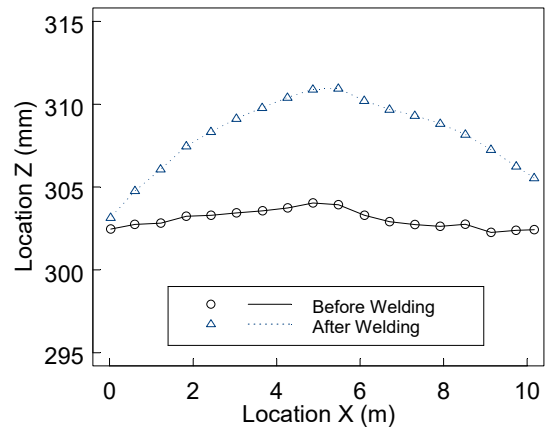
(c) RIB 1 (Reading ID: 1 – 18)



(d) RIB 2 (Reading ID: 19 – 36)

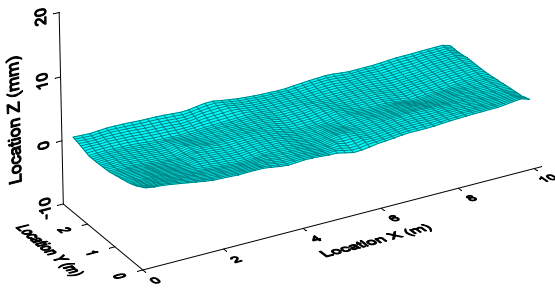


(e) RIB 3 (Reading ID: 37 – 54)

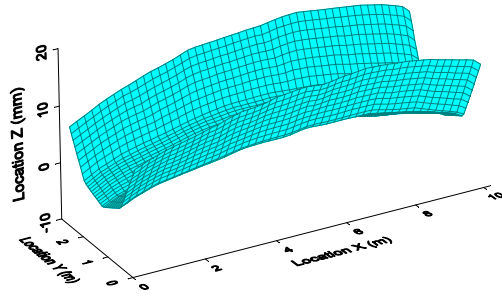


(f) RIB 4 (Reading ID: 55 – 72)

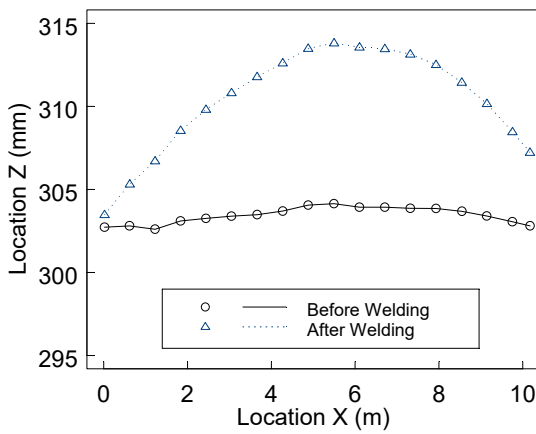
Figure 2.12 Specimen 1: Distortion Measurements



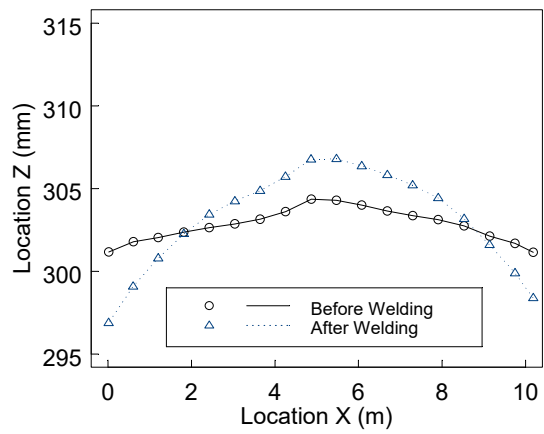
(a) Deck Plate before Welding



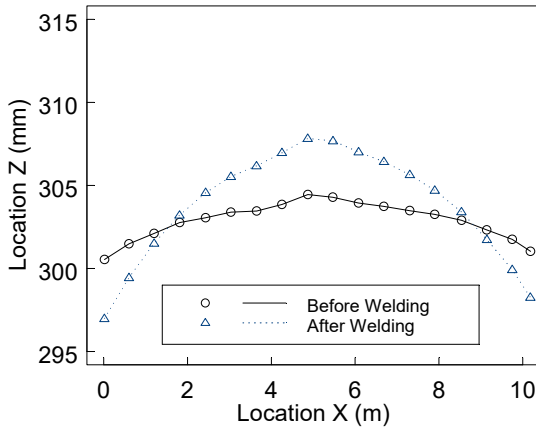
(b) Deck Plate after Welding



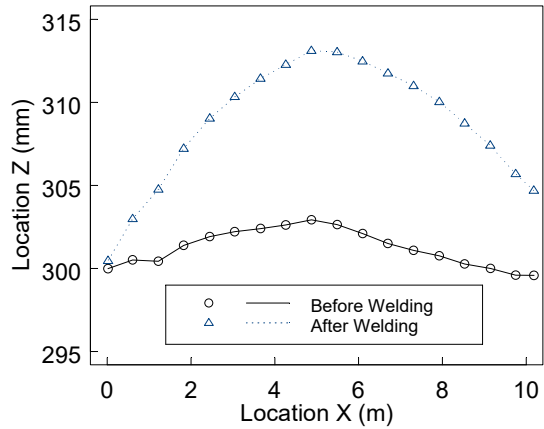
(c) RIB 1 (Reading ID: 1 – 18)



(d) RIB 2 (Reading ID: 19 – 36)

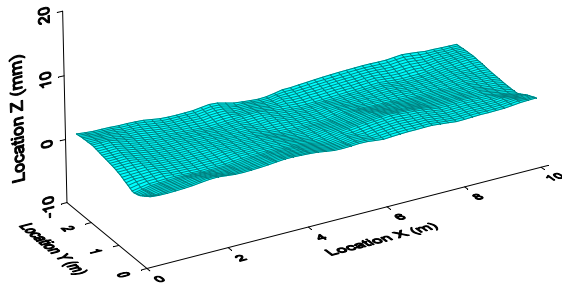


(e) RIB 3 (Reading ID: 37 – 54)

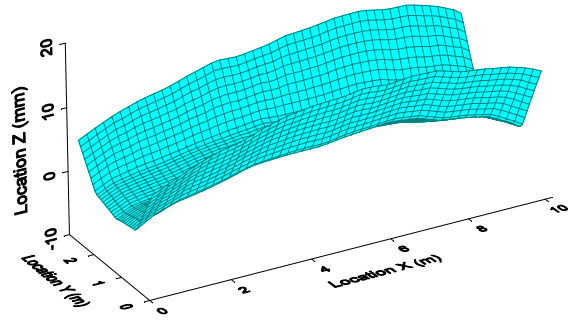


(f) RIB 4 (Reading ID: 55 – 72)

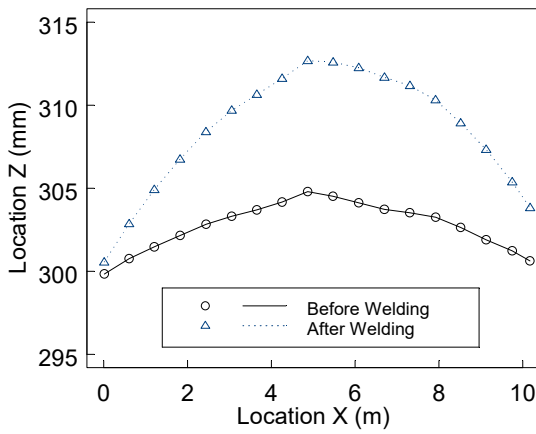
Figure 2.13 Specimen 2: Distortion Measurements



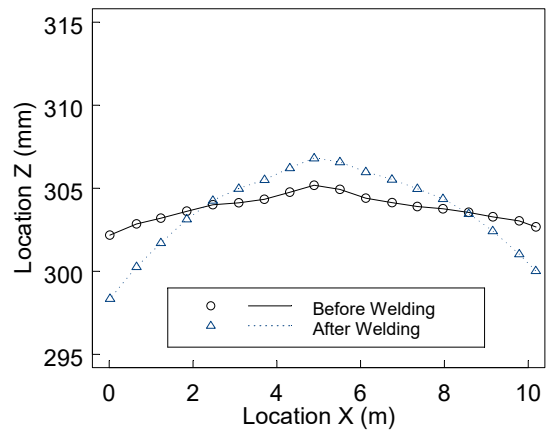
(a) Deck Plate before Welding



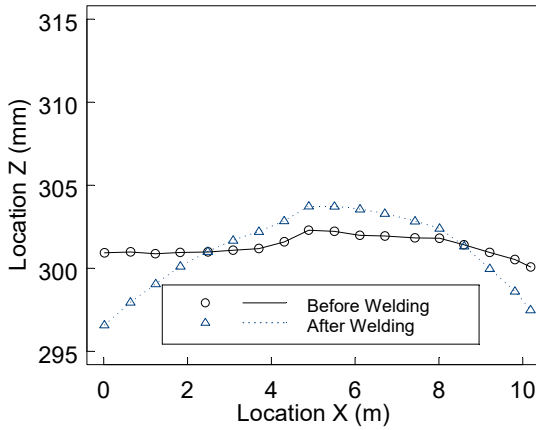
(b) Deck Plate after Welding



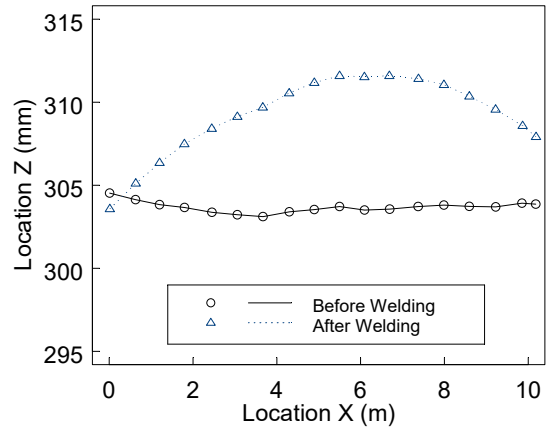
(c) RIB 1 (Reading ID: 1 – 18)



(d) RIB 2 (Reading ID: 19 – 36)

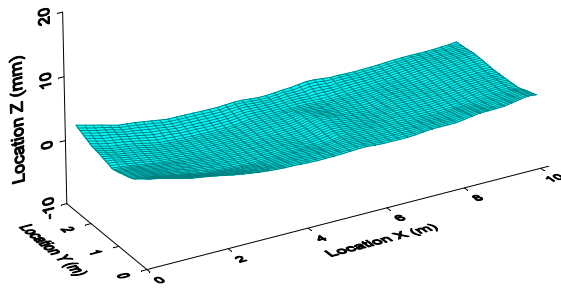


(e) RIB 3 (Reading ID: 37 – 54)

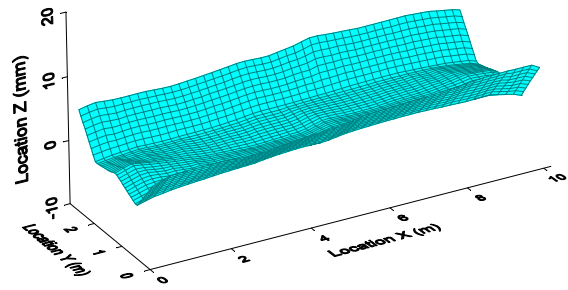


(f) RIB 4 (Reading ID: 55 – 72)

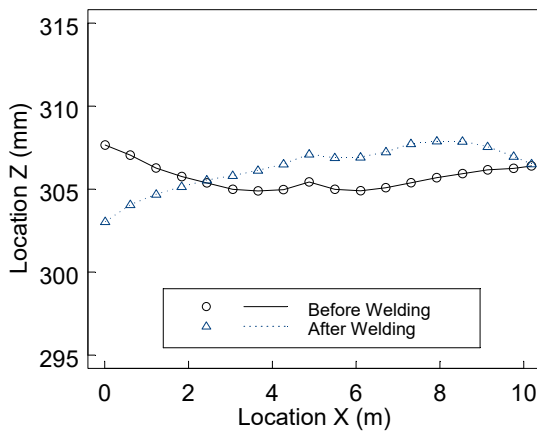
Figure 2.14 Specimen 3: Distortion Measurements



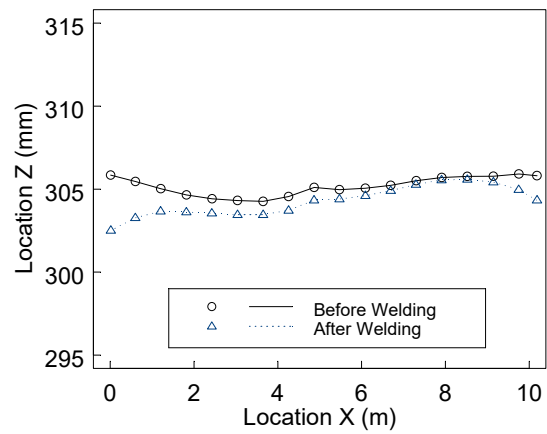
(a) Deck Plate before Welding



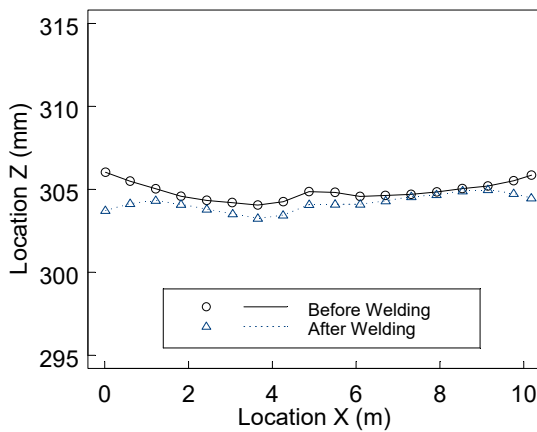
(b) Deck Plate after Welding



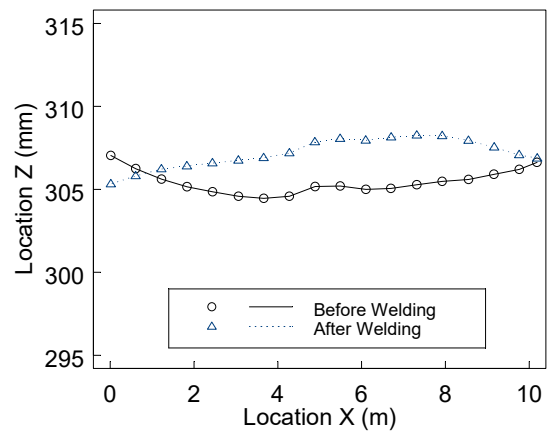
(c) RIB 1 (Reading ID: 1 – 18)



(d) RIB 2 (Reading ID: 19 – 36)

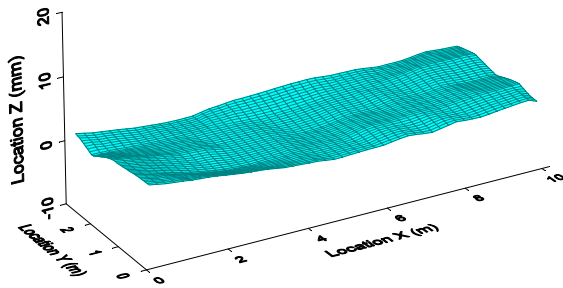


(e) RIB 3 (Reading ID: 37 – 54)

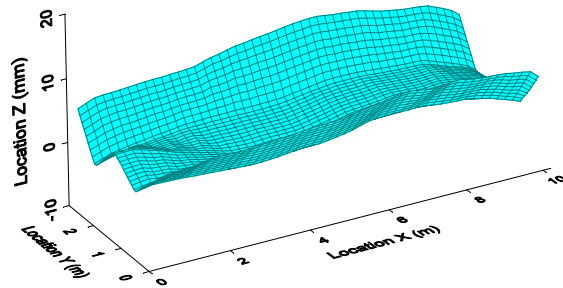


(f) RIB 4 (Reading ID: 55 – 72)

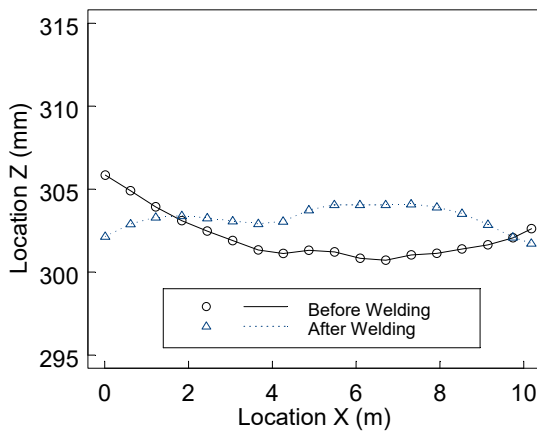
Figure 2.15 Specimen 4: Distortion Measurements



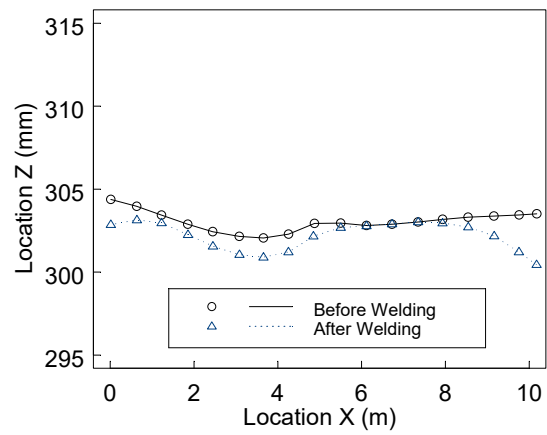
(a) Deck Plate before Welding



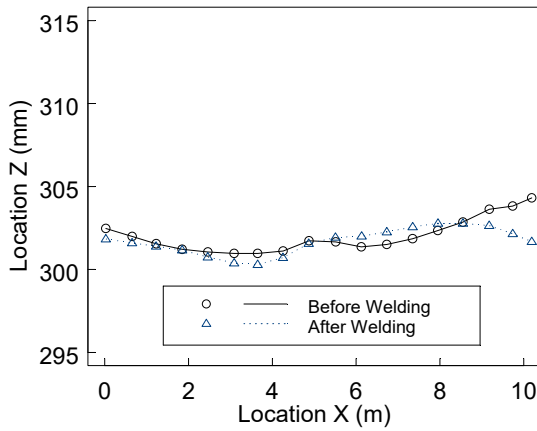
(b) Deck Plate after Welding



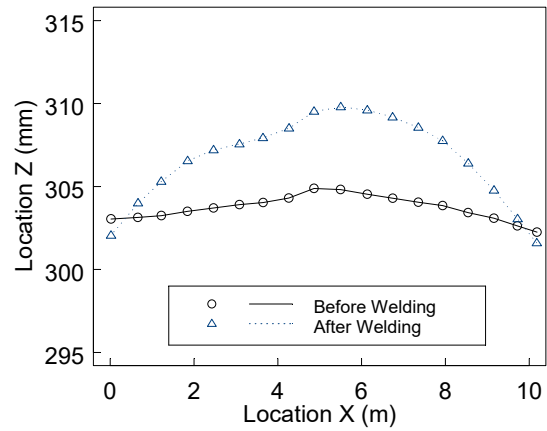
(c) RIB 1 (Reading ID: 1 – 18)



(d) RIB 2 (Reading ID: 19 – 36)

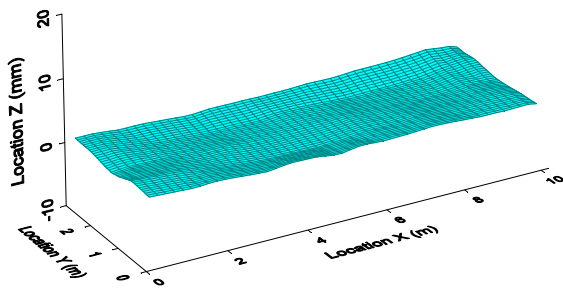


(e) RIB 3 (Reading ID: 37 – 54)

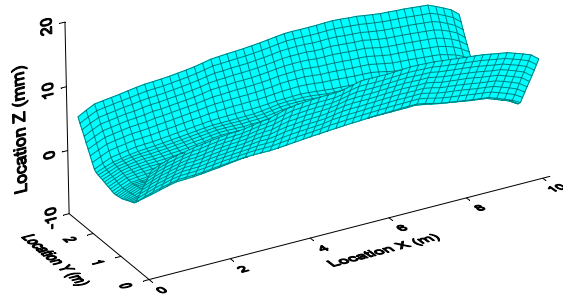


(f) RIB 4 (Reading ID: 55 – 72)

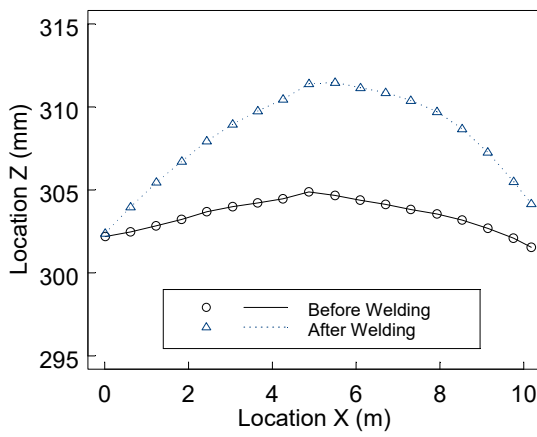
Figure 2.16 Specimen 5: Distortion Measurements



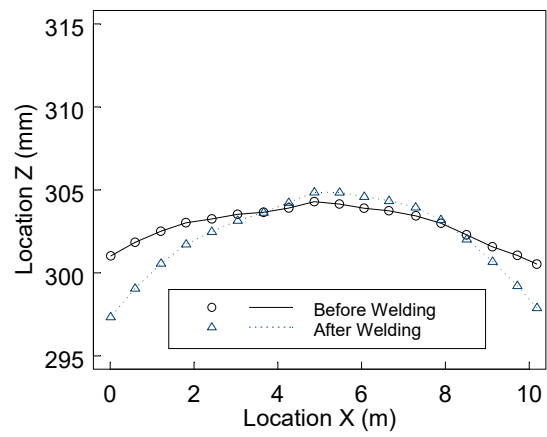
(a) Deck Plate before Welding



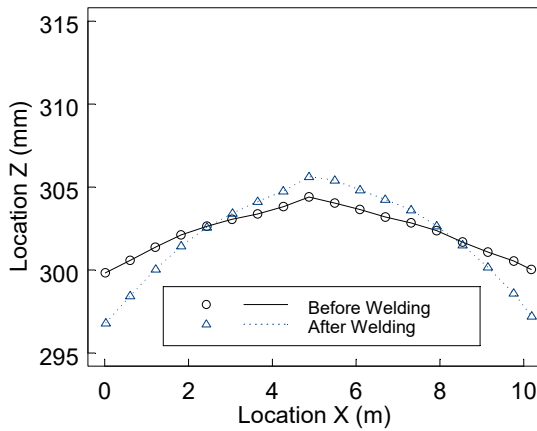
(b) Deck Plate after Welding



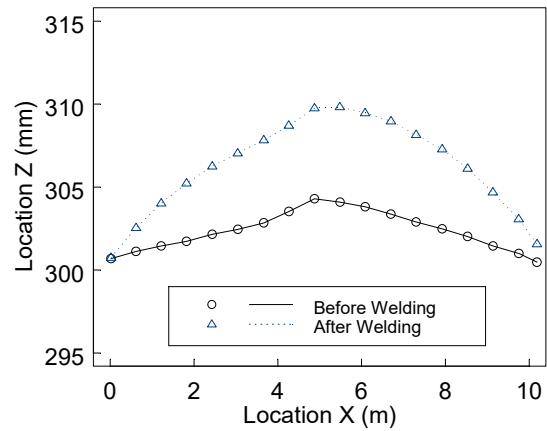
(c) RIB 1 (Reading ID: 1 – 18)



(d) RIB 2 (Reading ID: 19 – 36)

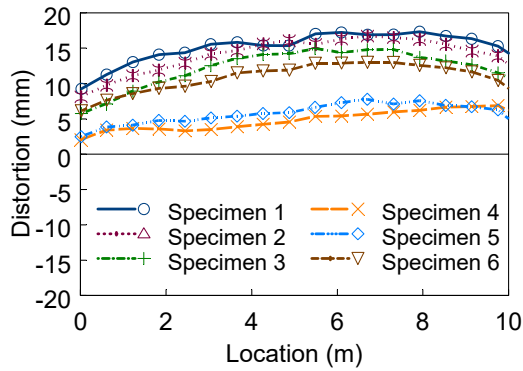


(e) RIB 3 (Reading ID: 37 – 54)

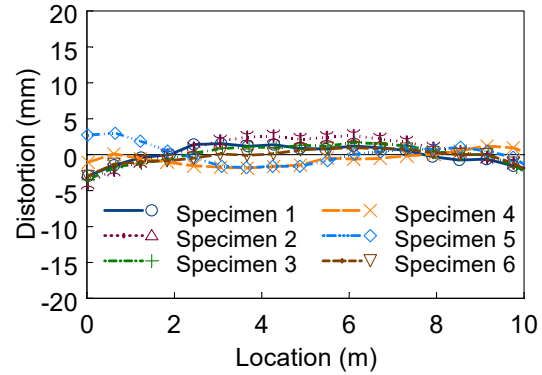


(f) RIB 4 (Reading ID: 55 – 72)

Figure 2.17 Specimen 6: Distortion Measurements

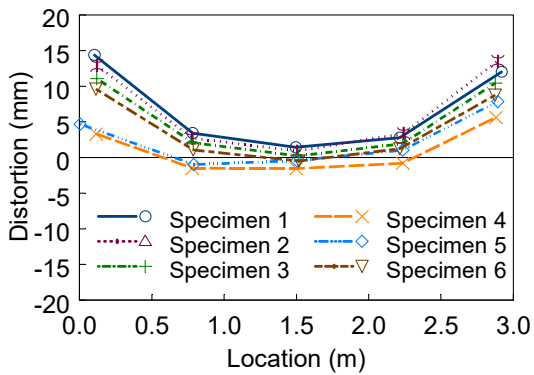


(a) Edge

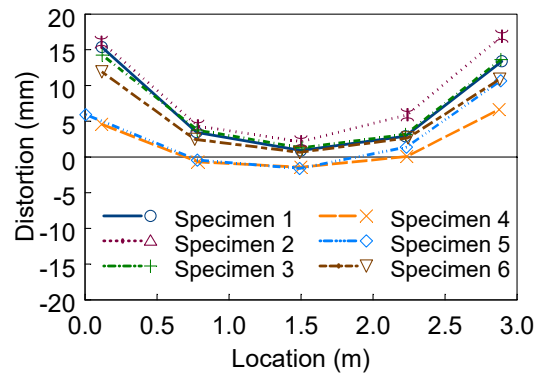


(b) Center

Figure 2.18 Deck Distortion in the Longitudinal Direction



(a) Midspan

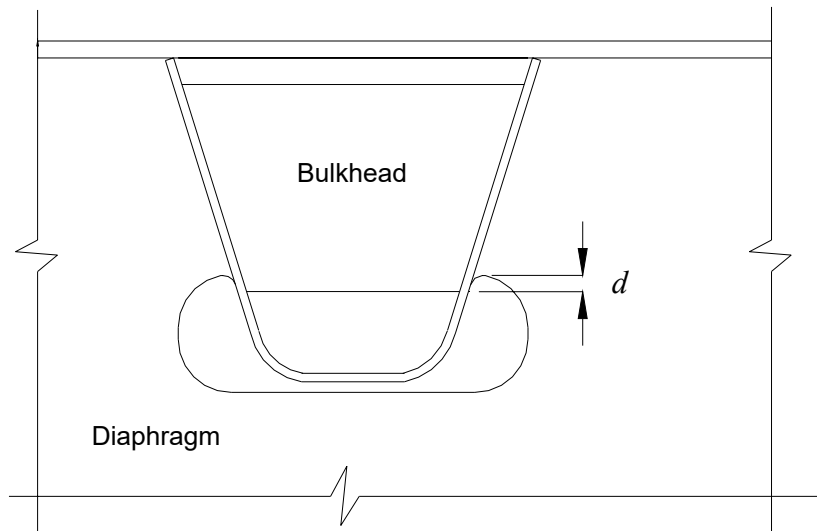


(b) Interior Support Diaphragm

Figure 2.19 Deck Distortion in the Transverse Direction

2.1.5 Intersection of Closed Rib to Diaphragms

As explained in Section 1.1, the AASHTO Specification requires at least a distance of 25 mm from the top of the free cutout to the bottom of the bulkhead plate [see dimension d in Figure 2.20(a)]. Figure 2.20(b) and (c) shows the photo views of the corresponding detail of one fabricated specimen (Specimen 1). The specified d in the design drawing was 20 mm, which was slightly less than the required 25 mm (see Figure 2.4). The measured values of d are summarized in Table 2.3. As shown in the table, the measured d values were less than the required 25 mm.



(a) Designation of distance "d"



(b) Left Side



(c) Right Side

Figure 2.20 Intersection of Rib with Diaphragms

Table 2.3 Measured Value of d

Diaphragm No.	Rib No.		d (mm)
D1	R1	East	13
		West	14
	R2	East	13
		West	11
	R3	East	13
		West	11
	R4	East	13
		West	11
D3	R1	East	13
		West	11
	R2	East	12
		West	10
	R3	East	12
		West	11
	R4	East	14
		West	14

2.2 Material Properties

ASTM A709-03A Grade 50 steel was used for the panels. After fatigue testing, tensile coupons were cut from the rib and deck plate in each of the panels for material testing. The coupon test results are summarized in Table 2.4. Chemical analysis result from certified mill test report is summarized in Table 2.5. HRB hardness tests for all specimens were conducted with pieces from the region of rib-to-deck weld joint, and a typical test result is shown in Figure 2.21.

Table 2.4 Mechanical Properties

Specimens	Components	Yield Strength (MPa)	Tensile Strength (MPa)	Elongation (%)
1	Rib Plate	405	519	33
	Deck Plate	392	493	33
2	Rib Plate	359	462	32
	Deck Plate	400	532	41
3	Rib Plate	405	473	37
	Deck Plate	367	459	44
4	Rib Plate	429	474	38
	Deck Plate	403	488	43
5	Rib Plate	412	486	37
	Deck Plate	405	522	42
6	Rib Plate	394	477	40
	Deck Plate	416	471	36

Table 2.5 Chemical Analysis (from Certified Mill Test Report)

Element	Deck Plate	Rib Plate
C	0.14 – 0.16	0.14 – 0.16
Mn	0.87 – 0.91	0.90 – 0.91
P	0.009 – 0.016	0.009 – 0.011
S	0.010 – 0.014	0.002 – 0.004
Si	0.27 – 0.29	0.27 – 0.28
Cu	0.01	0.01 – 0.02
Ni	0.05	0.01
V	0.013 – 0.015	0.022
Cb	0.014 – 0.022	0.014 – 0.017
Al	0.027 – 0.034	0.036 – 0.037
Cr	0.01 – 0.02	0.01
Mo	0.00	0.00

specimen was supported by three concrete blocks, 0.9 m high from the floor. In order to accommodate flexible support conditions, a half-circular rod (diameter = 13 mm) was inserted below the base plate of the end supports for testing of Specimens 2 to 6. The specimen was loaded using hydraulic actuators at midspan. The loads from each actuator at midspan were uniformly distributed through a spreader beam to the loading pads simulating 250 mm×510 mm tire contact area of a wheel recommended in the AASHTO LRFD code. A 6.4 mm thick neoprene rubber pad with the same hardness as the tires was placed under the spreader beam to ensure that the load is uniformly distributed over the contact area.

Table 2.6 Test Matrix

Weld Condition	Without Pre-Camber	With Pre-Camber
I	Specimen 1	Specimen 4
II	Specimen 2	Specimen 5
III	Specimen 3	Specimen 6

Weld Condition I: 80 % PJP without Weld Melt-Through

Weld Condition II: 100 % PJP with Evident Continuous Weld Melt-Through

Weld Condition III: Alternating Weld Conditions I and II Every 1 m

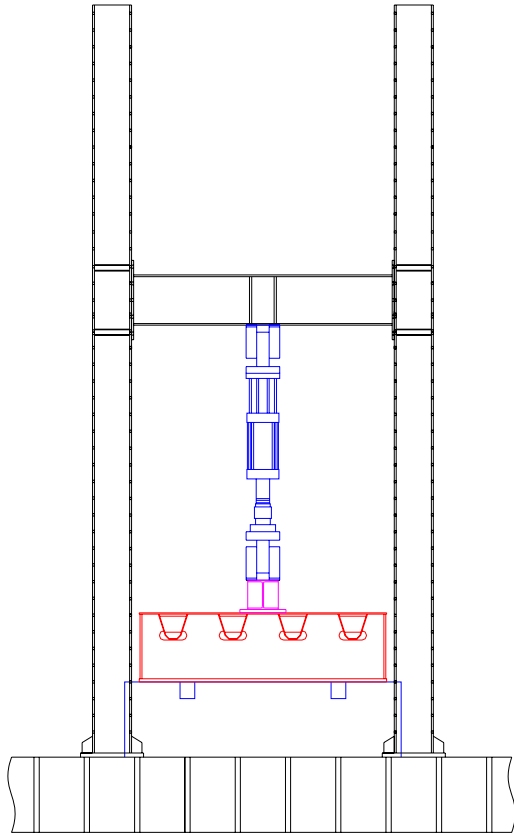


Figure 2.22 End View of Test Setup

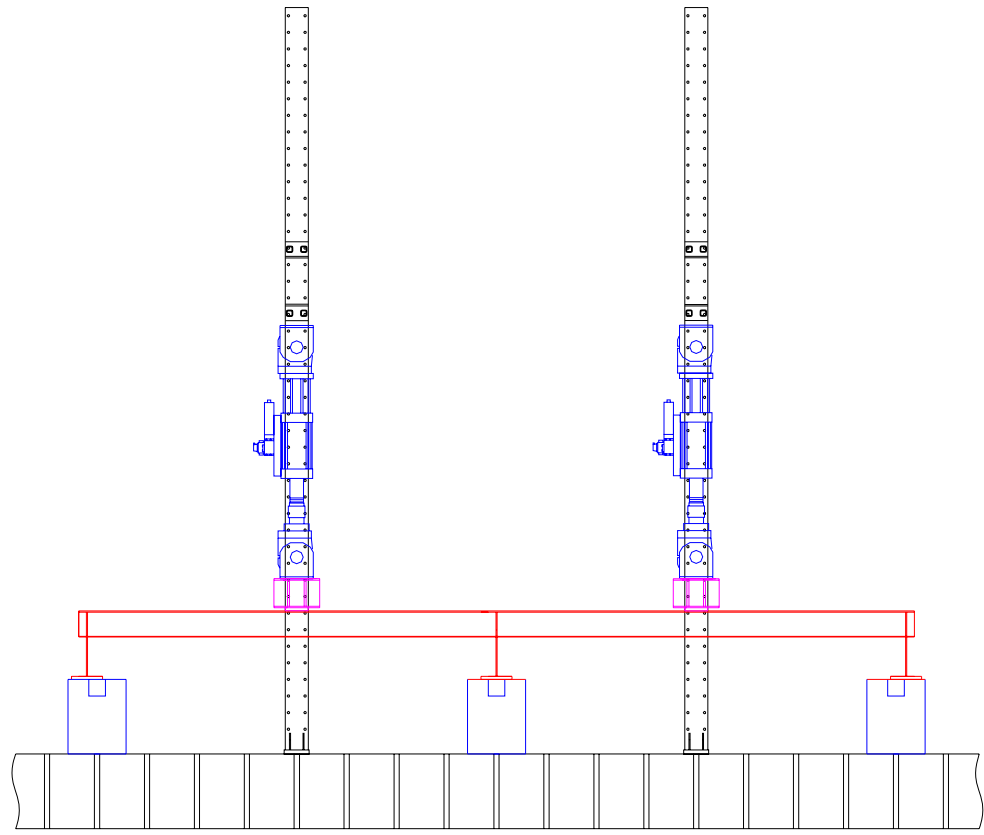


Figure 2.23 Elevation of Test Setup



Figure 2.24 East Test Setup (Specimens 2 and 3)



Figure 2.25 West Test Setup (Specimens 1, 4, 5, and 6)

2.4 Loading

The 2007 AASHTO LRFD Specification specifies a design truck HS 20. For fatigue design, a factor of 0.75 is used for the HS20, meaning implicitly HS15 truck. The load of each axle for HS15 is 108.75 kN (0.75×145 kN), and the spacing between the 108.75 kN axles is specified as 9000 mm. A half of each axle was considered for loading scheme because the width of the test specimen could not accommodate a full axle load of truck. A single axle load was centered at midspan using hydraulic actuators for testing of Specimens 2 to 6. The loads from actuators at midspan were out-of-phase to simulate the effect of a truck passage. The AASHTO Specification uses $2 \times (\text{HS15} + 15\% \text{ Impact})$ for calculating the maximum stress range. Testing at Lehigh University (Tsakopoulos 1999) reported that fatigue cracking under the single axle loads away from the diaphragm was not observed at the rib-to-deck connection. Based on the field measurements on orthotropic decks, it was also demonstrated that the specified load of $2 \times (\text{HS15} + 15\% \text{ Impact})$ was not conservative for certain deck elements such as the rib-to-diaphragm connections and other elements such as expansion joints. For the rib-to-deck connection, it was close to a factor of 2. Based on the above information, an axle load of $3 \times (\text{HS15} + 15\% \text{ Impact})$ was used (Fisher 2005). The magnitude of the loading on the single axle was 188 kN based on three times HS15 plus 15% impact (i.e., $3 \times 108.75 \text{ kN} \times 1.15 \times \frac{1}{2}$ (a half axle) = 188 kN). Testing of the first specimen (Specimen 1) was carried out at a full axle load, 380 kN, on the dual axles (tandem configuration) centered at midspan. Figure 2.26 shows a loading scheme used for testing of Specimen 1, and Figure 2.27 for testing of Specimens 2 through 6.

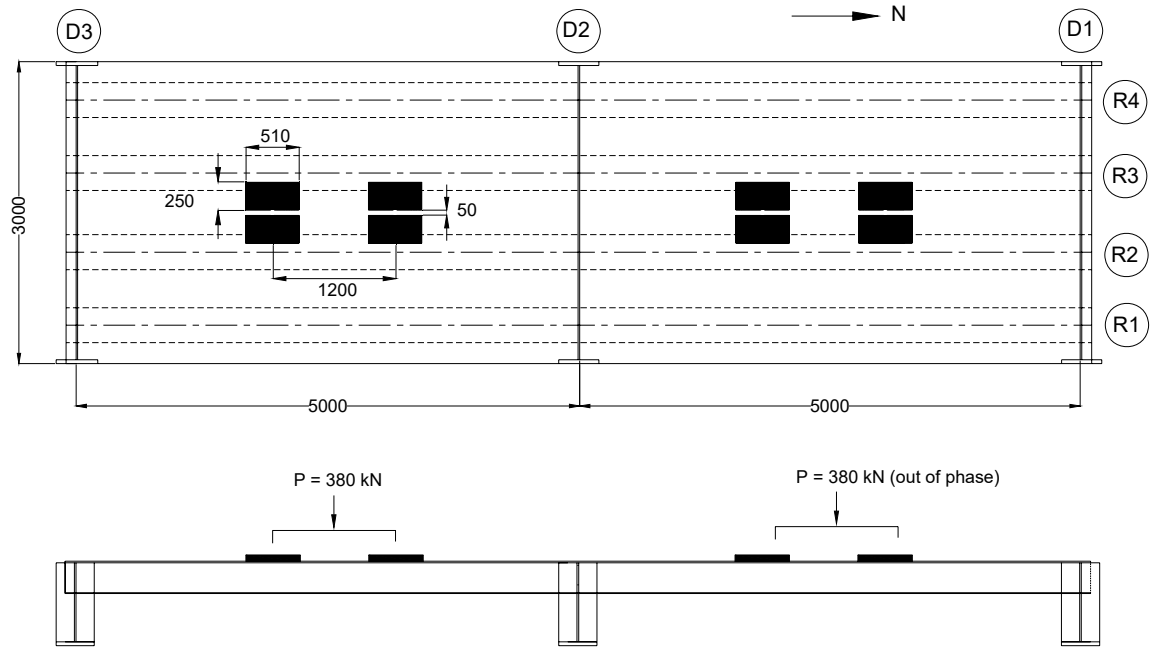


Figure 2.26 Specimen 1: Loading Scheme

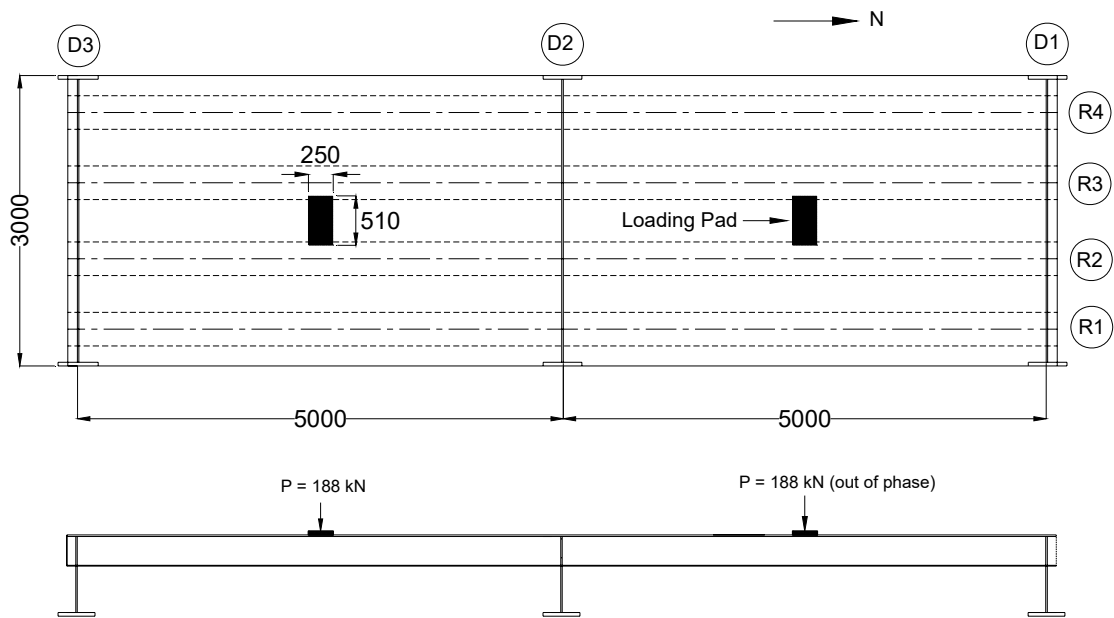


Figure 2.27 Specimens 2 to 6: Loading Scheme

2.5 Instrumentation

2.5.1 General

The test specimens were instrumented with strain gages at fatigue sensitive connection details and displacement transducers at midspan. Either uni-axial strain gages or strain gage rosettes were used for monitoring local distribution of cyclic stresses at details of rib-to-deck welds and diaphragms. The strain gage locations for Specimens 2 to 6, which vary slightly from one specimen to the other, were determined from both the finite element analysis and test results of Specimen 1.

2.5.2 Strain Gages in Deck Plate near Rib-to-Deck Welds

Figures 2.28 to 2.33 show the locations of strain gages placed on the deck plate to measure the transverse strains, perpendicular to the rib-to-deck welds. Most strain gages were placed on the bottom of the deck plate. Some strain gages, labeled in parentheses in the figures, were placed on the top of the deck plate. The strain gages on the bottom of the deck plate were positioned 10 mm or 25 mm away from the weld toe. As shown in the figures, both uni-axial strain gages and component 1 of strain gage rosettes were oriented in the transverse (or width) direction, perpendicular to the rib-to-deck welds, and component 2 was oriented in the longitudinal direction, parallel to the rib-to-deck weld. The strain gages in Specimen 1 were placed at quarter points of the north span in the longitudinal direction. The strain gages in Specimens 3 to 6 were placed under the loading pads with a spacing of 130 mm in the longitudinal direction.

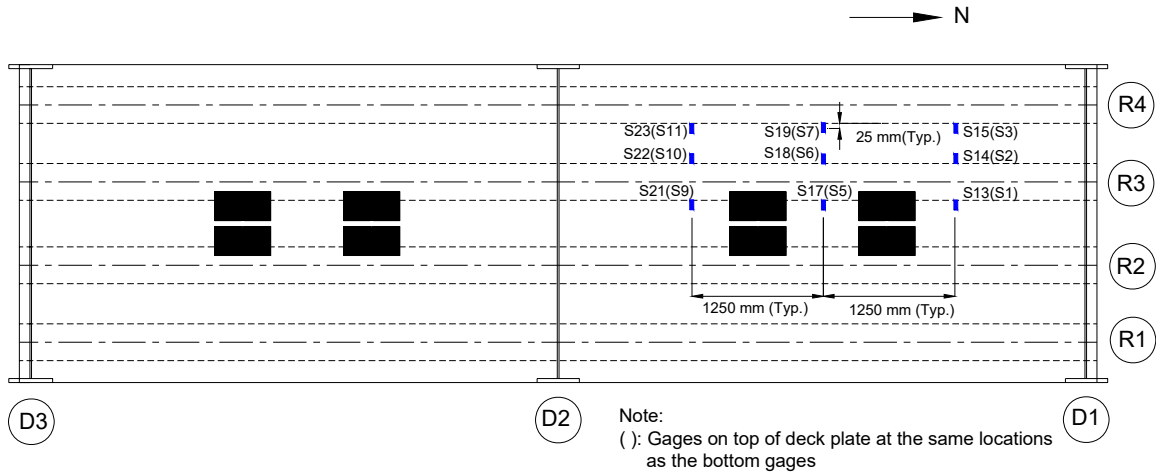


Figure 2.28 Specimen 1: Uni-axial Strain Gages in Deck Plate near Rib-to-Deck Welds

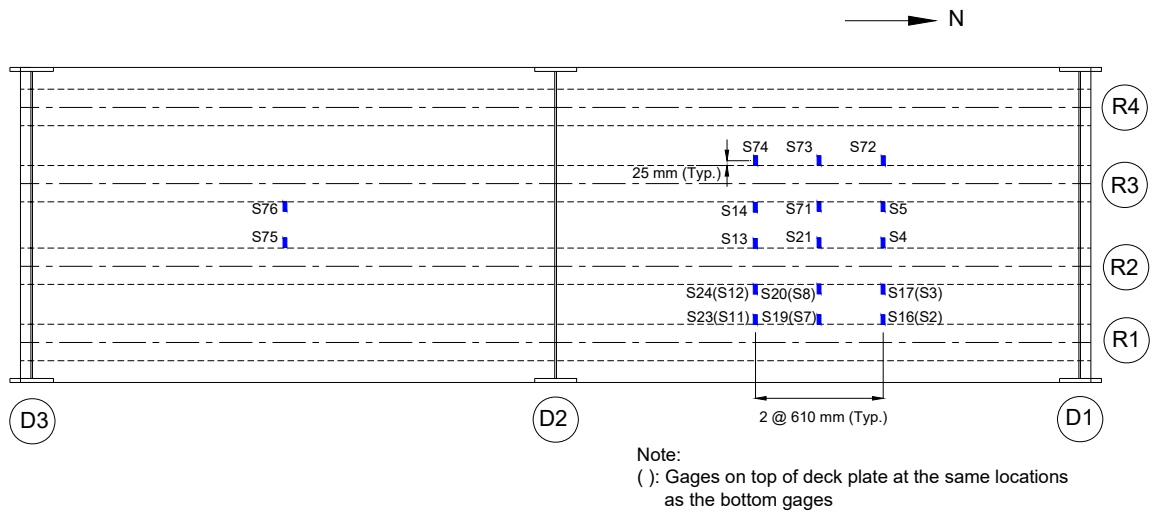


Figure 2.29 Specimen 2: Uni-axial Strain Gages in Deck Plate near Rib-to-Deck Welds

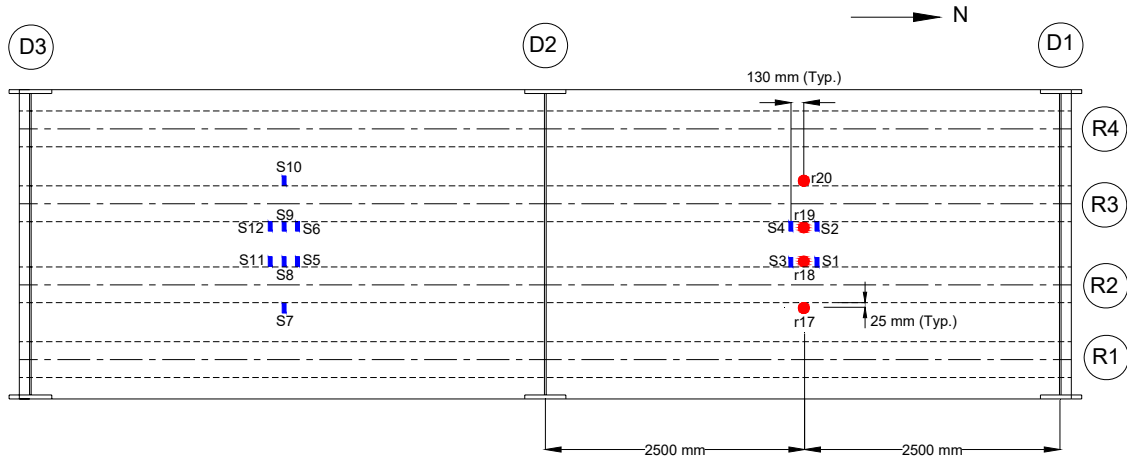


Figure 2.30 Specimen 3: Uni-axial Strain Gages in Bottom of Deck Plate near Rib-to-Deck Welds

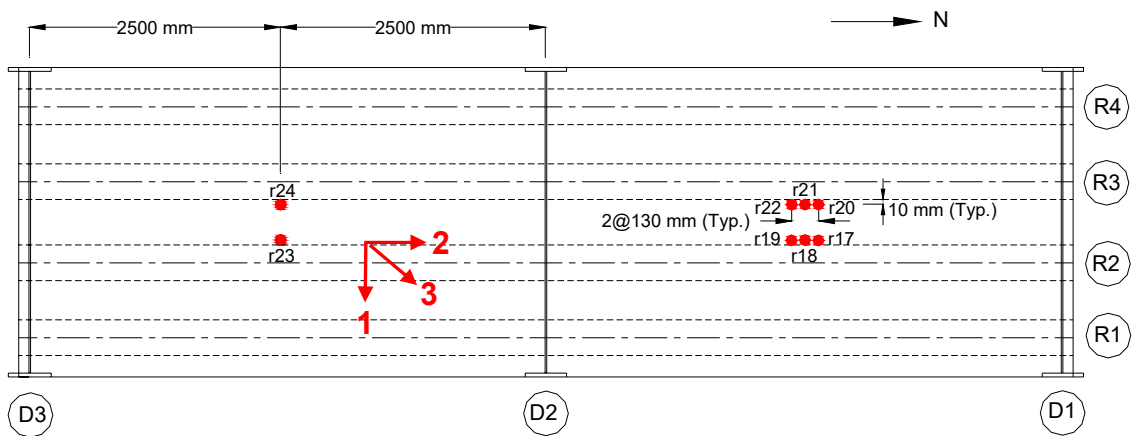


Figure 2.31 Specimen 4: Strain Gage Rosettes in Bottom of Deck Plate near Rib-to-Deck Welds

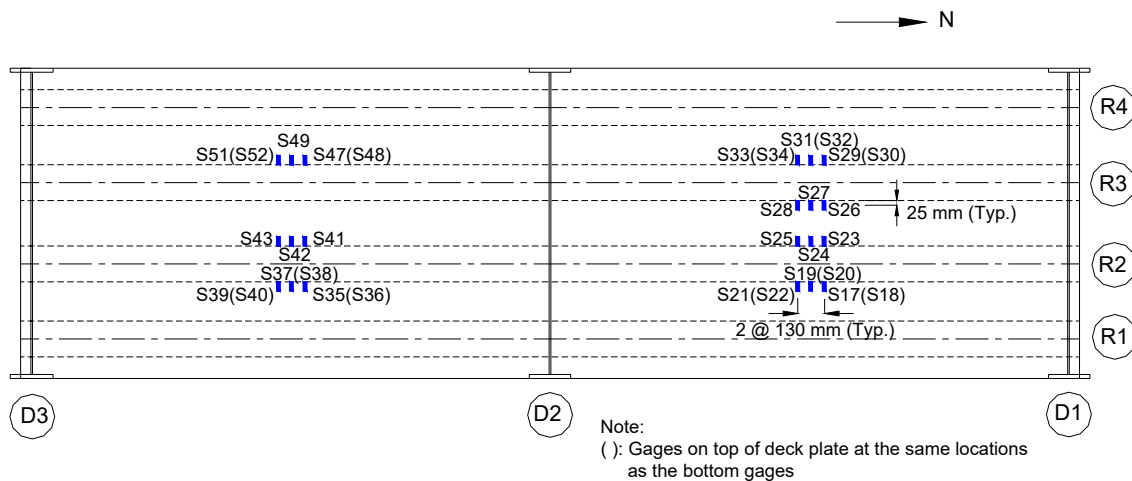


Figure 2.32 Specimen 5: Uni-axial Strain Gages in Deck Plate Near Rib-to-Deck Welds

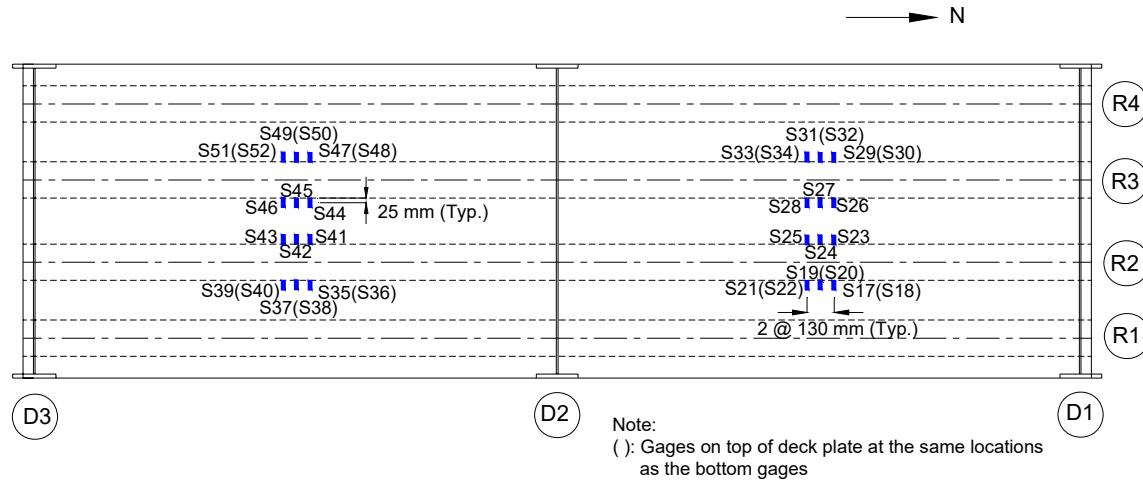


Figure 2.33 Specimen 6: Uni-axial Strain Gages in Deck Plate near Rib-to-Deck Welds

2.5.3 Strain Gages in Ribs near Rib-to-Deck Welds

Both uni-axial strain gages and strain gage rosettes were installed on the rib walls adjacent to the rib-to-deck welds near the loading locations to measure the local strains. Figures 2.34 to 2.47 show layouts of the gages installed on the rib walls for specimens. Most of the strain gages were installed on the interior two ribs, Ribs R2 and R3. For some locations in Specimens 1, 4, and 5, back-to-back strain gage rosettes were placed on both sides of rib walls. Strain gages on the inner surface of rib walls were installed prior to rib-to-deck welding in order to get access to inside of the closed ribs (see Figure 2.48). These strain gages inside were placed 38 mm away from the bottom of deck plate to avoid excessive heat exposure during welding operation. The outer surface gages on rib walls were positioned between 15 mm and 38 mm away from the bottom of the deck plate. As shown in Figures 2.34 and 2.36, component 1 of strain gage rosettes and uni-axial strain gages were oriented in the transverse direction, perpendicular to the rib-to-deck weld. Component 2 of strain gage rosettes was oriented in the longitudinal direction, parallel to the rib-to-deck weld.

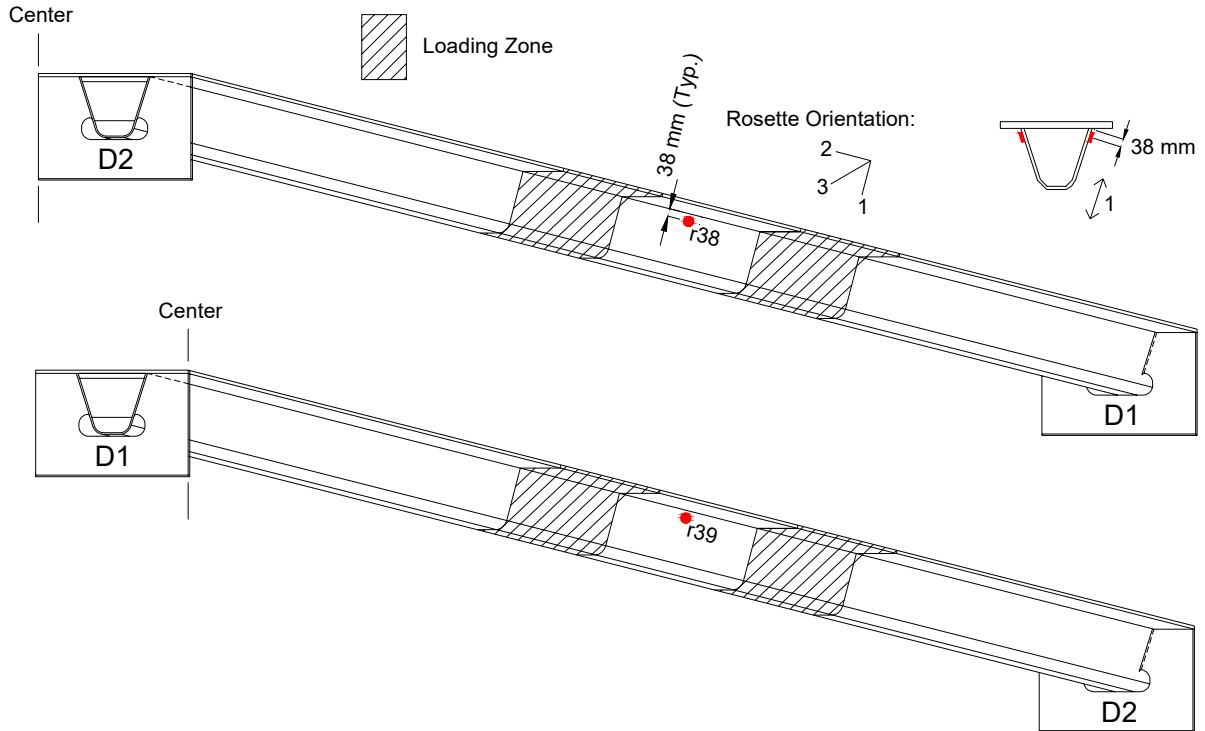


Figure 2.34 Specimen 1: Strain Gages in Outer Surface of Rib R2 near Rib-to-Deck Welds

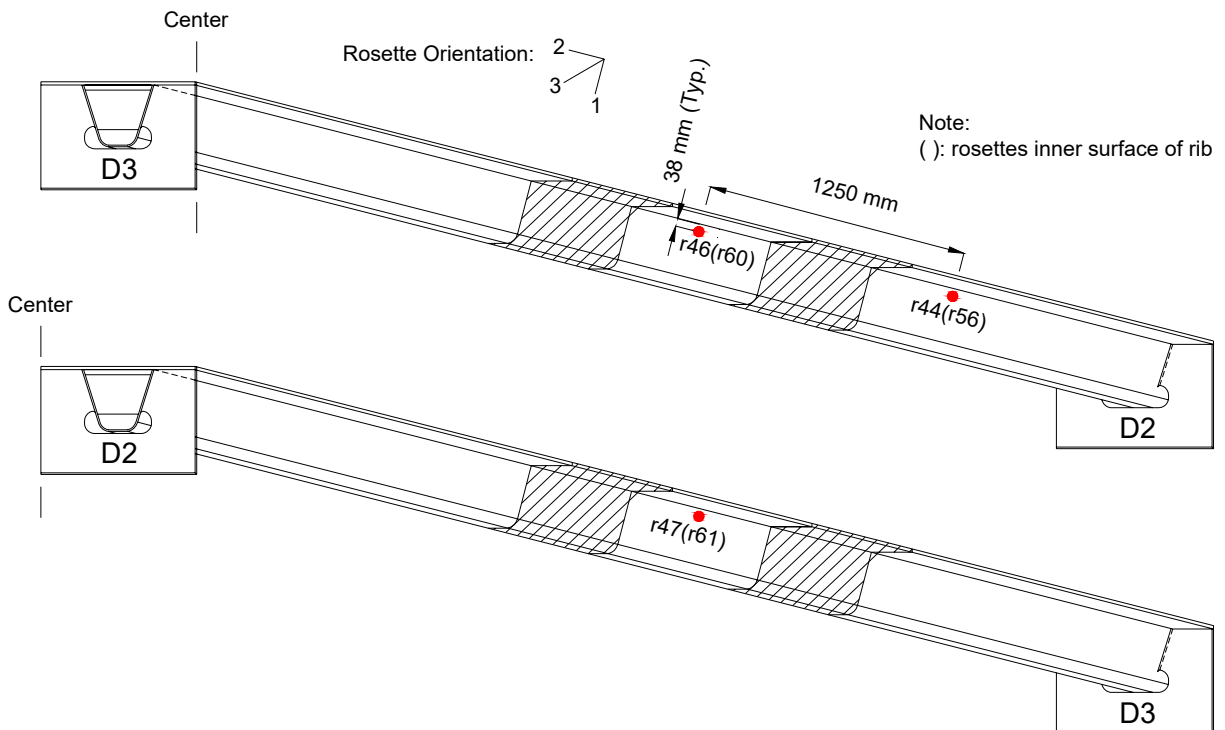


Figure 2.35 Specimen 1: Strain Gages in Rib R3 near Rib-to-Deck Welds

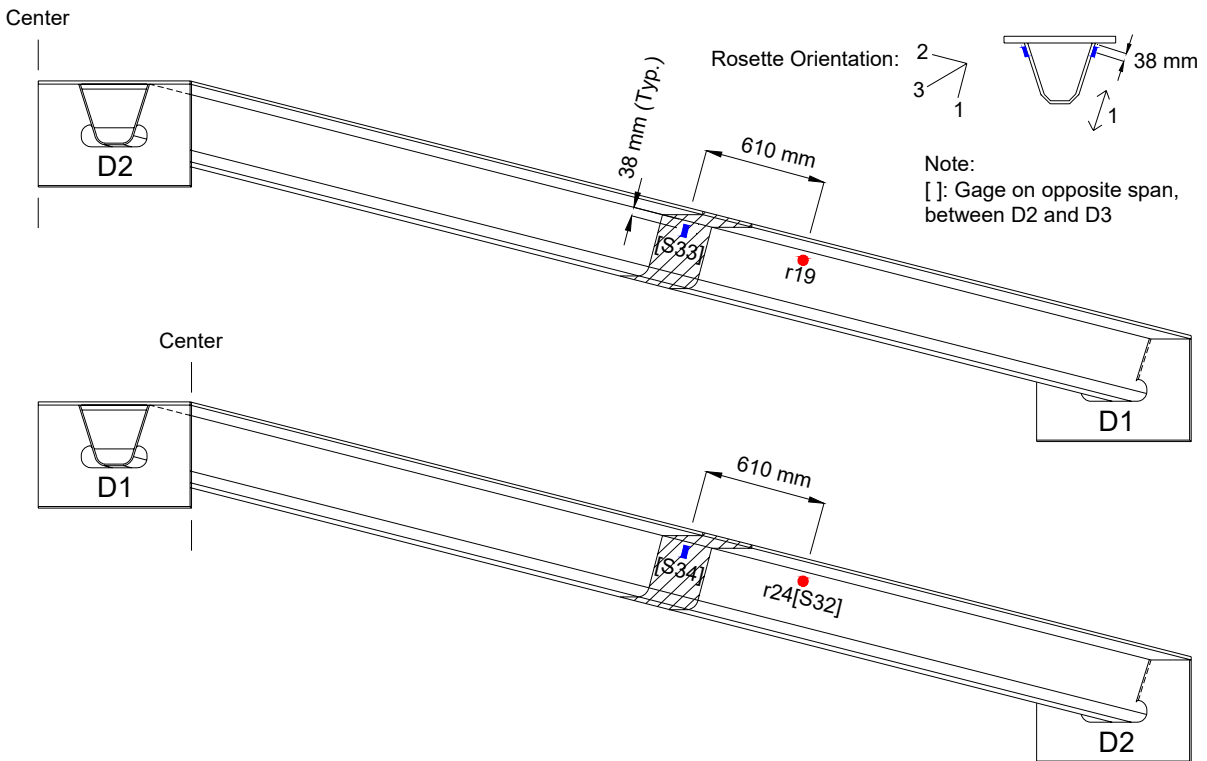


Figure 2.36 Specimen 2: Strain Gages in Outer Surface of Rib R2 near Rib-to-Deck Welds

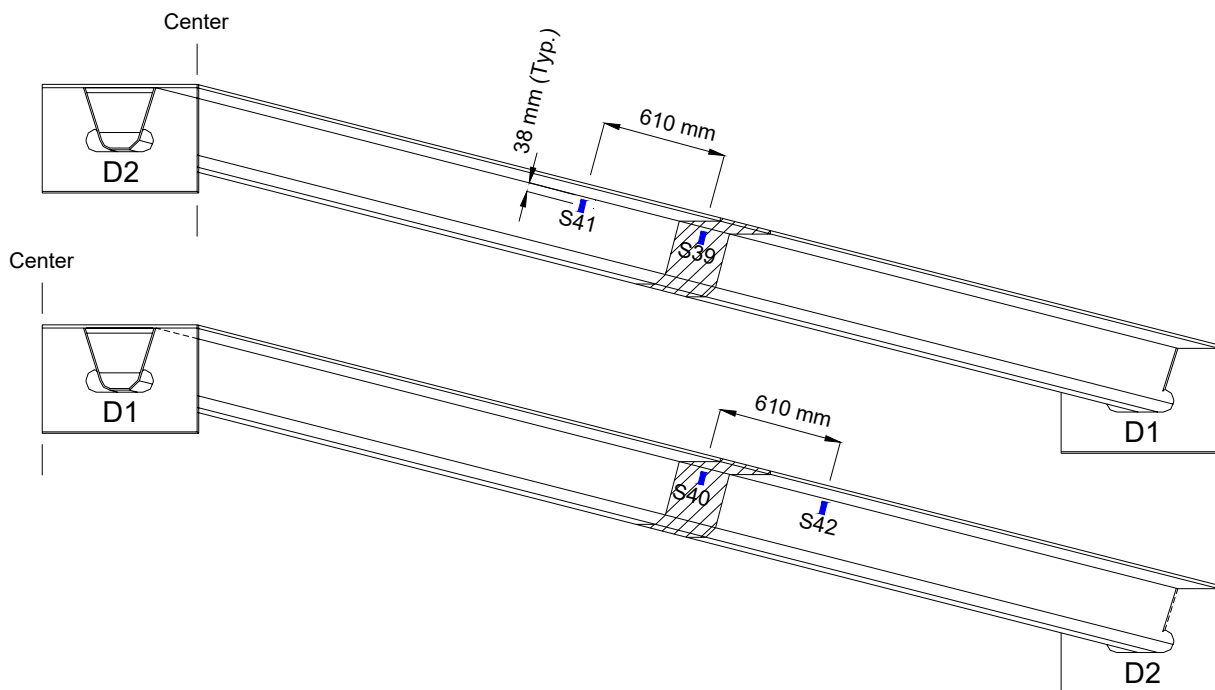


Figure 2.37 Specimen 2: Strain Gages in Outer Surface of Rib R3 near Rib-to-Deck Welds

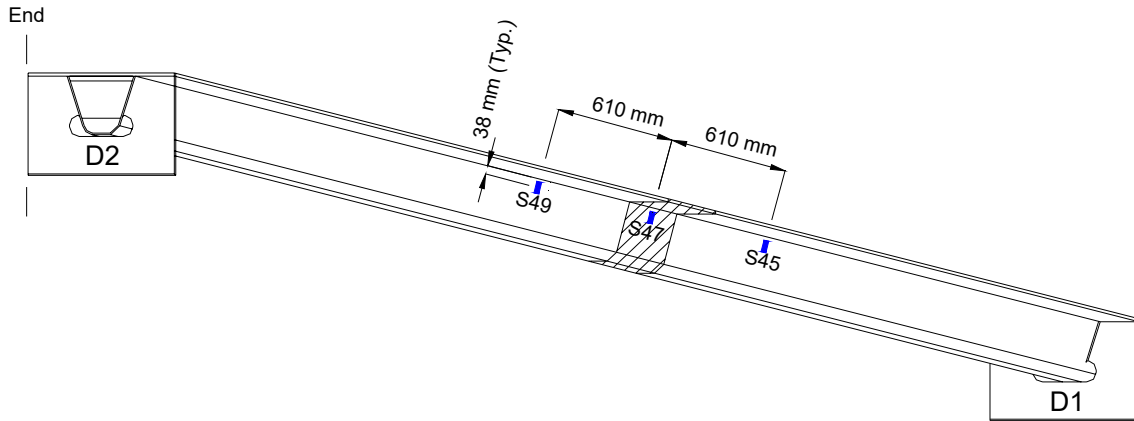


Figure 2.38 Specimen 2: Strain Gages in Outer Surface of Rib R4 near Rib-to-Deck Welds

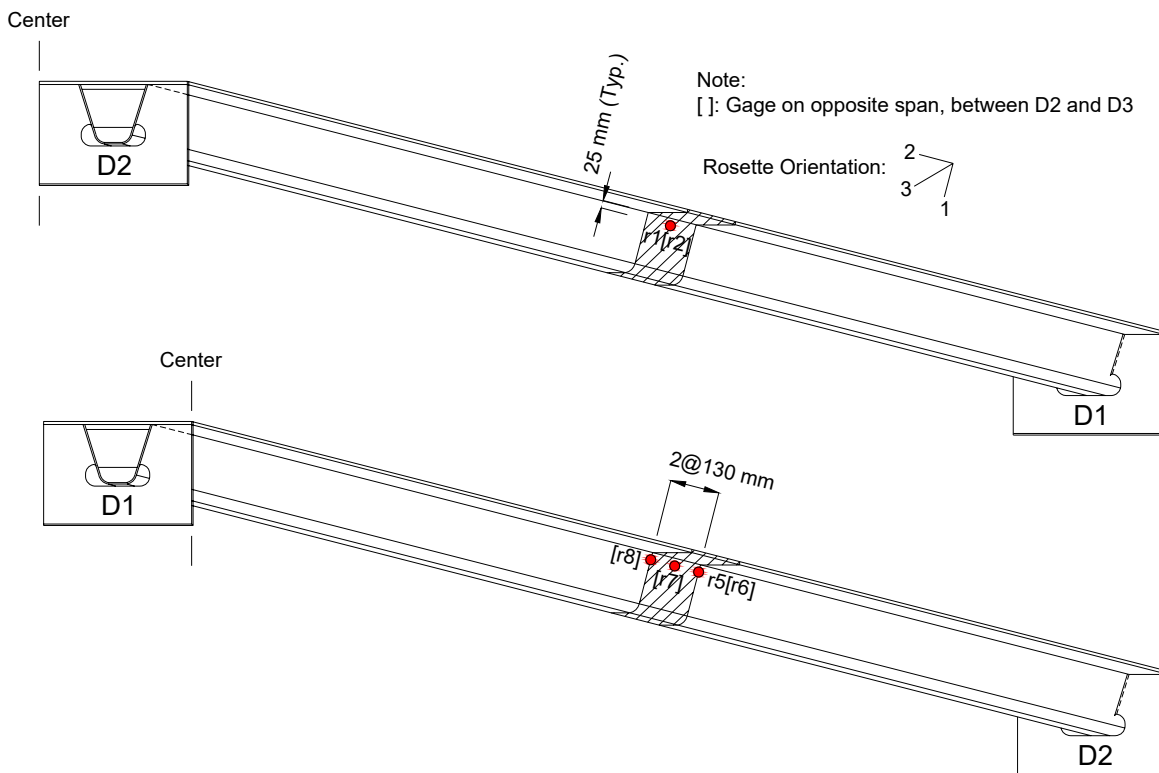


Figure 2.39 Specimen 3: Strain Gages in Outer Surface of Rib R2 near Rib-to-Deck Welds

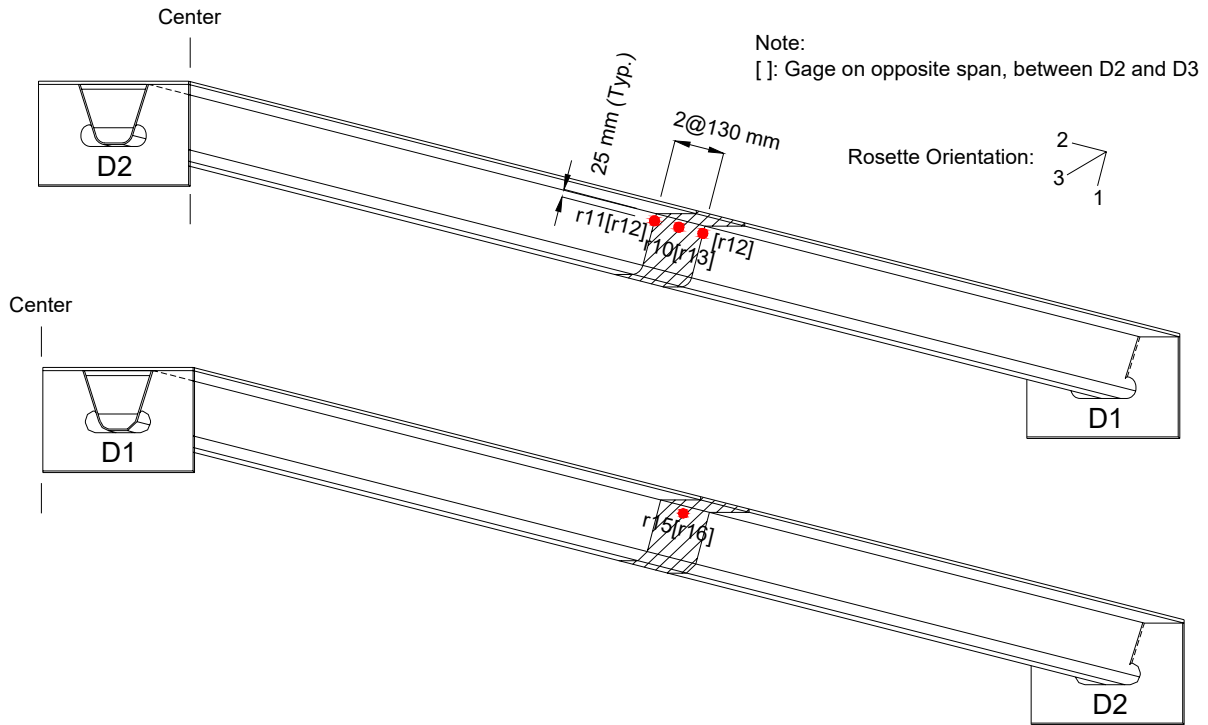


Figure 2.40 Specimen 3: Strain Gages in Outer Surface of Rib R3 near Rib-to-Deck Welds

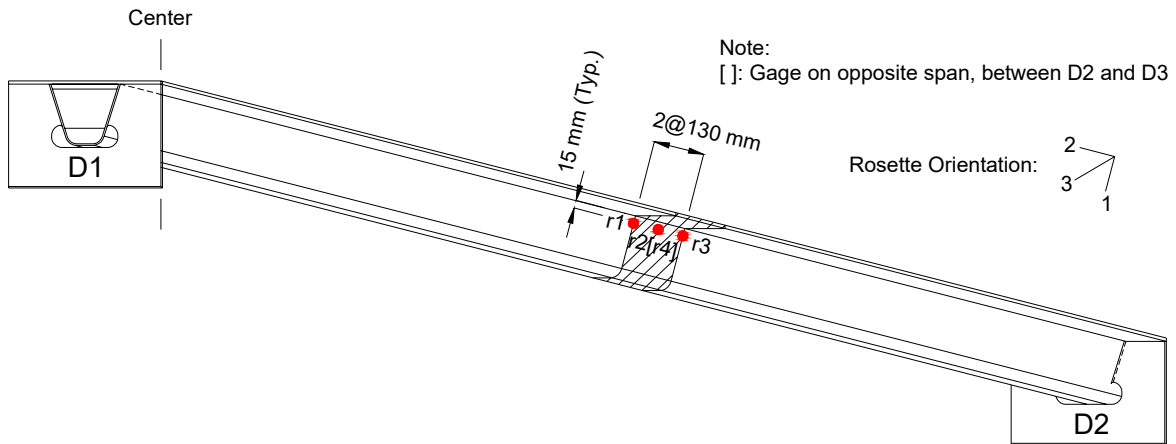


Figure 2.41 Specimen 4: Strain Gages in Outer Surface of Rib R2 near Rib-to-Deck Welds

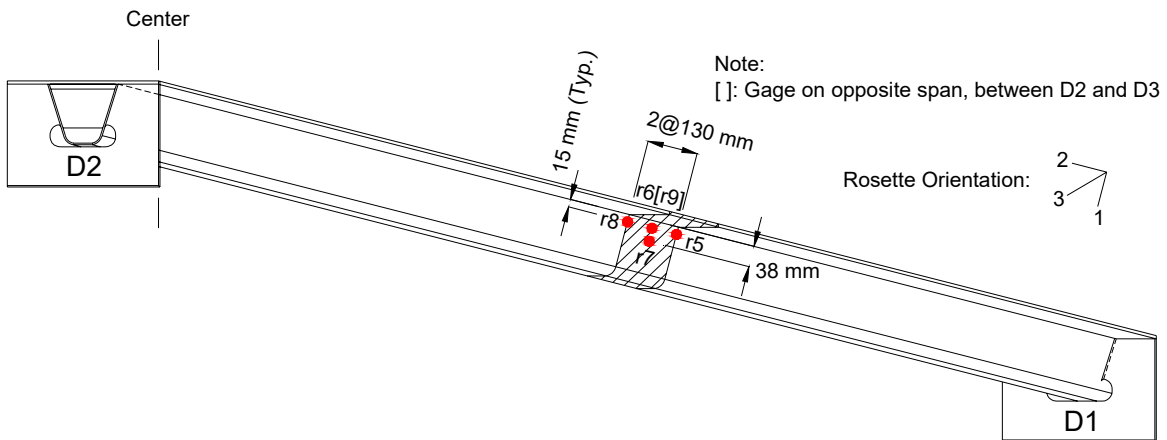


Figure 2.42 Specimen 4: Strain Gages in Outer Surface of Rib R3 near Rib-to-Deck Welds

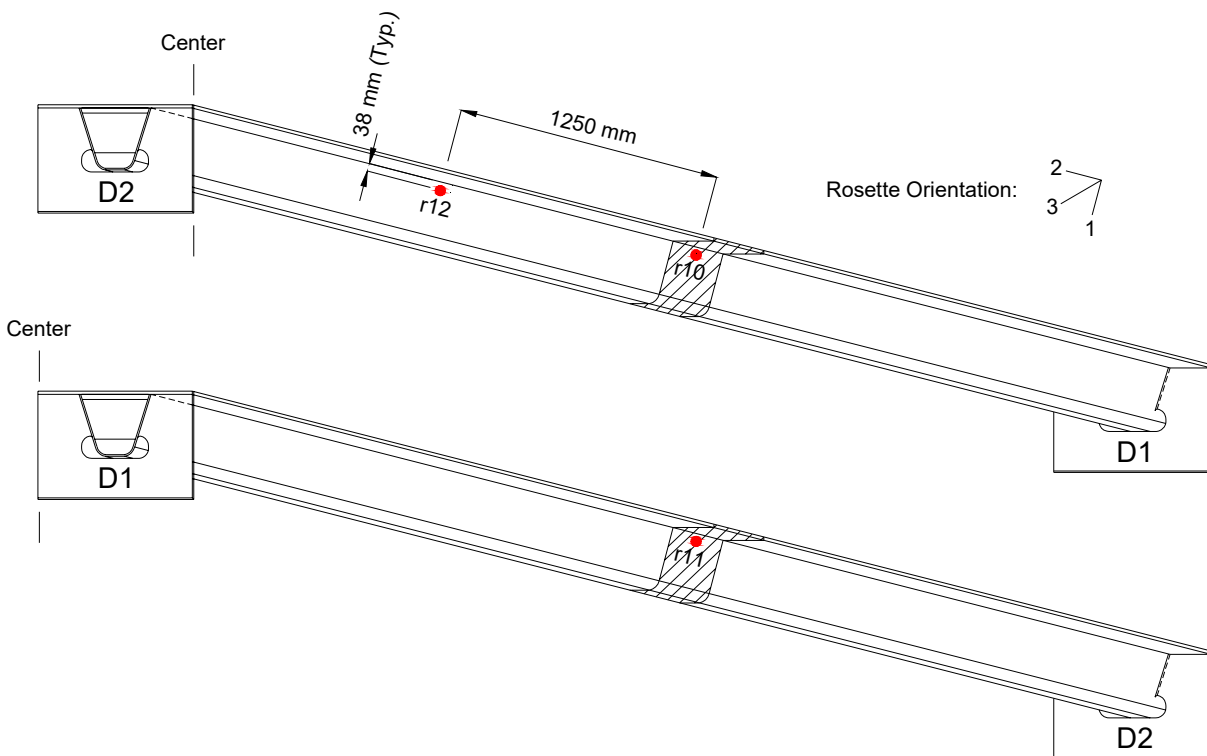


Figure 2.43 Specimen 4: Strain Gages in Inner Surface of Rib R3 near Rib-to-Deck Welds

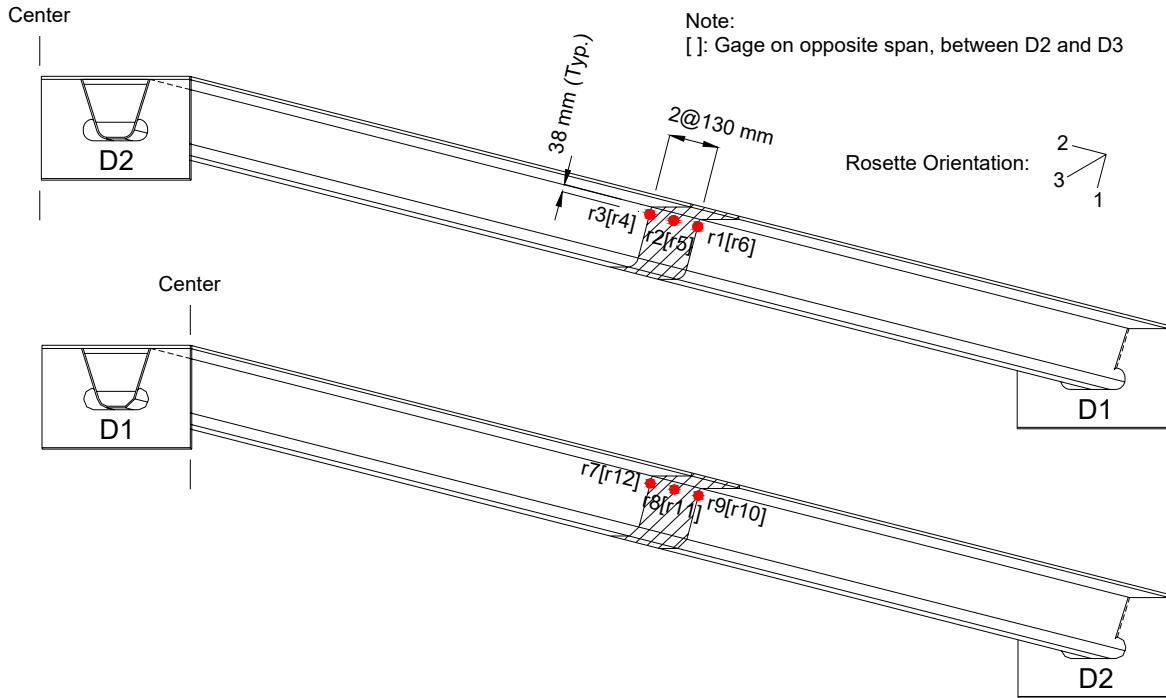


Figure 2.44 Specimen 5: Strain Gages in Outer Surface of Rib R2 near Rib-to-Deck Welds

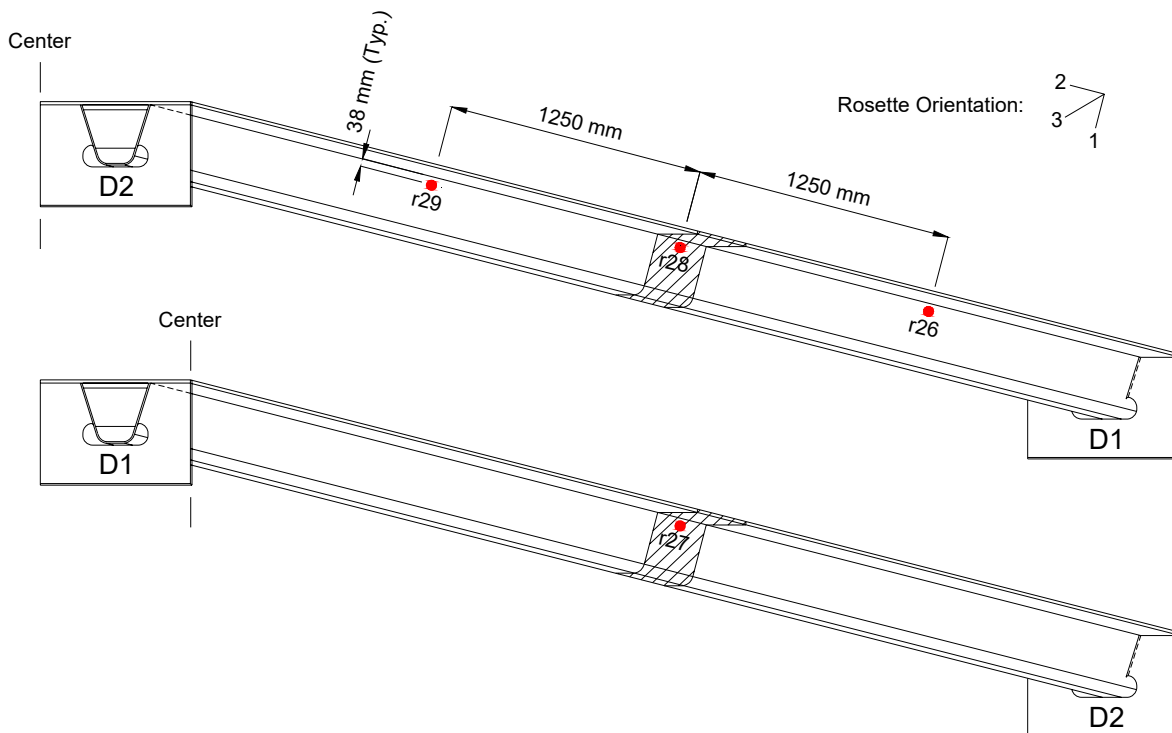


Figure 2.45 Specimen 5: Strain Gages in Inner Surface of Rib R2 near Rib-to-Deck Welds

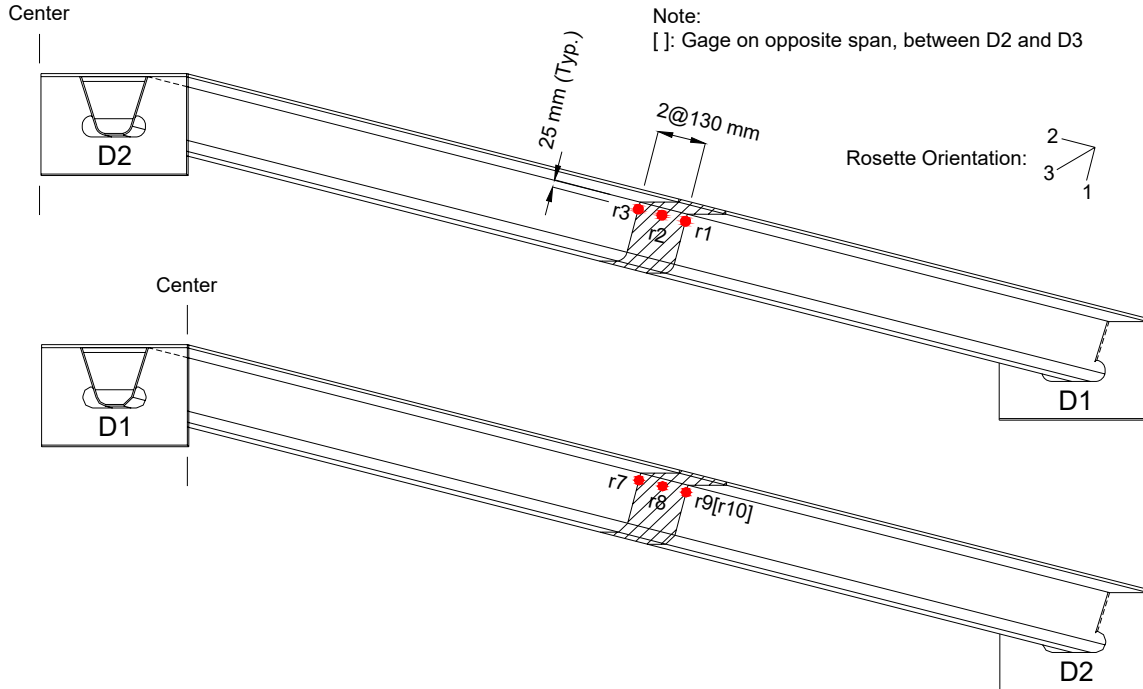


Figure 2.46 Specimen 6: Strain Gages in Outer Surface of Rib R2 near Rib-to-Deck Welds

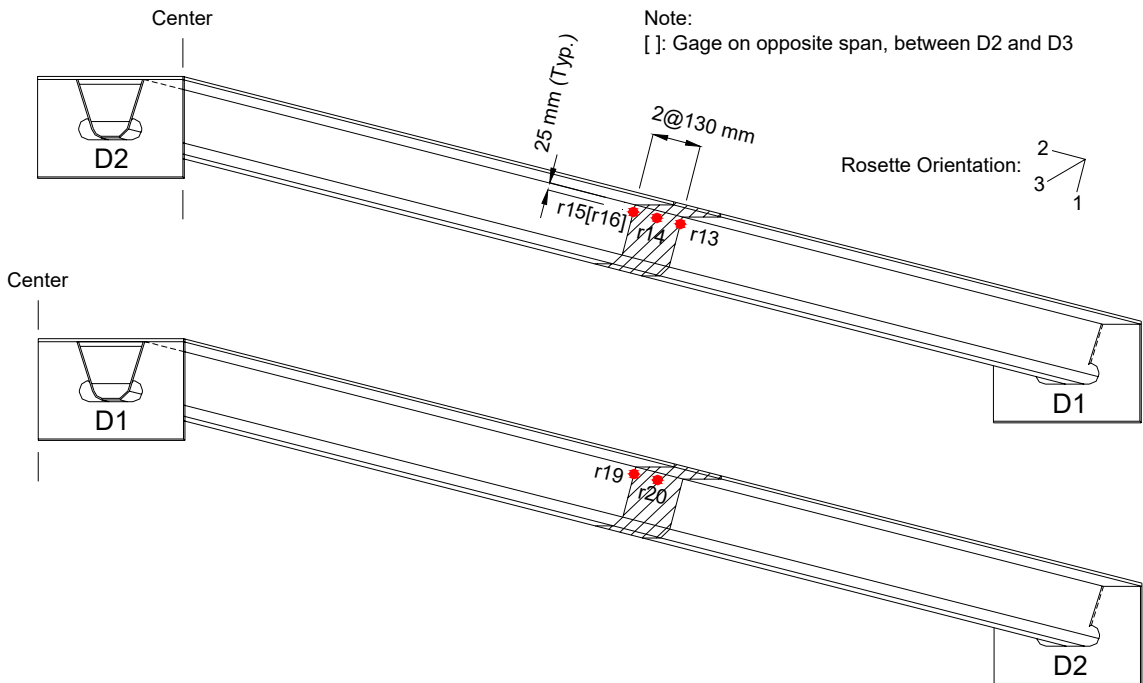


Figure 2.47 Specimen 6: Strain Gages in Outer Surface of Rib R3 Near Rib-to-Deck Welds



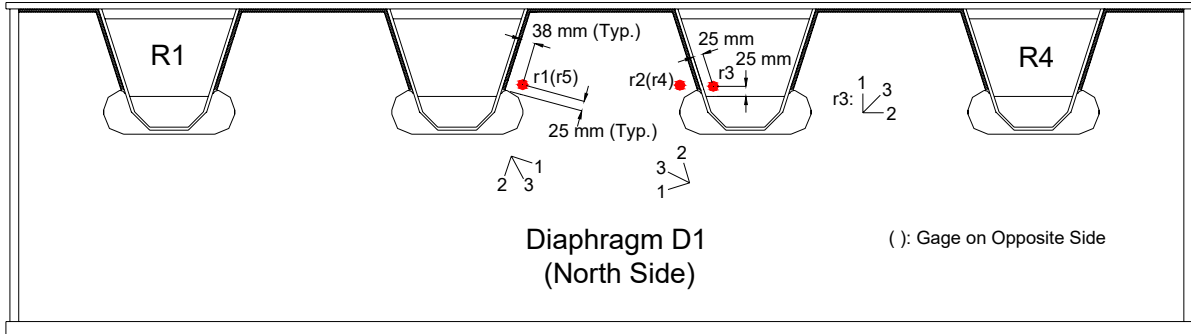
Figure 2.48 Strain Gage Instrumentation Inside of Ribs

2.5.4 Strain Gages in Ribs, Diaphragms, and Bulkheads at Supports

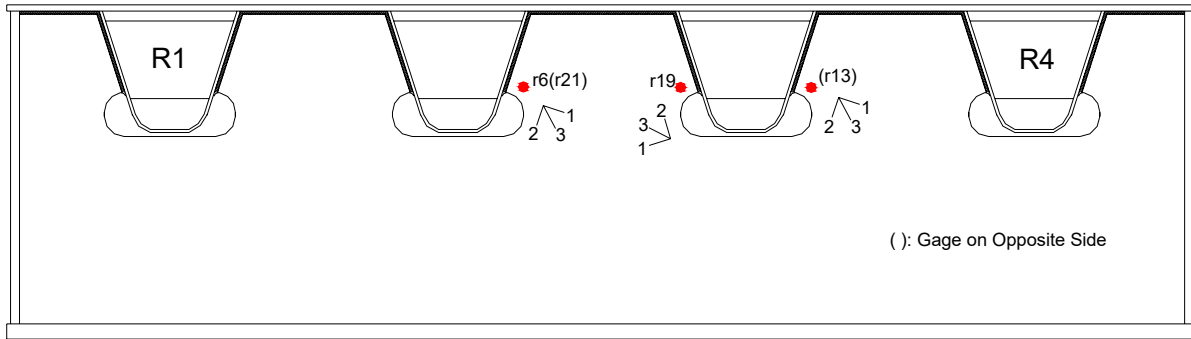
Figures 2.49 to 2.53 show the location and orientation of the strain gages placed in ribs, bulkheads, and diaphragms at supports. Strain gages in ribs were installed to measure the strains below the weld toe termination of the bulkhead plate and diaphragm plate terminations. For Specimen 4, back-to-back uni-axial strain gages were placed on both sides of the rib (see Figure 2.52). The strain gages inside the ribs were positioned either 10 mm or 13 mm away from the weld toe termination below the bulkhead. For interior support diaphragm D2 in Specimen 3, strain gage rosettes r29 and r30 were placed on outer surface of the rib R2, 13 mm away from the termination of the diaphragm plate (see Figure 2.51). The uni-axial strain gages and component 1 of strain gage rosettes placed on ribs were oriented in the vertical direction, component 2 in the longitudinal direction along the rib.

Strain gage rosettes were installed on bulkhead and diaphragm plates to measure the strains near the diaphragm cutout and the bottom corners of the bulkheads. For strain gage rosettes near the diaphragm cutout, component 1 was oriented perpendicular to the rib-to-diaphragm weld, and component 2 parallel to the rib-to-diaphragm weld. At some locations, back-to-back strain gages were placed on both sides of the diaphragm. The strain gages in the bulkhead were positioned 25 mm away from both the bottom edge of the bulkhead plates and the weld toe termination at rib-to-bulkhead welded joint. The

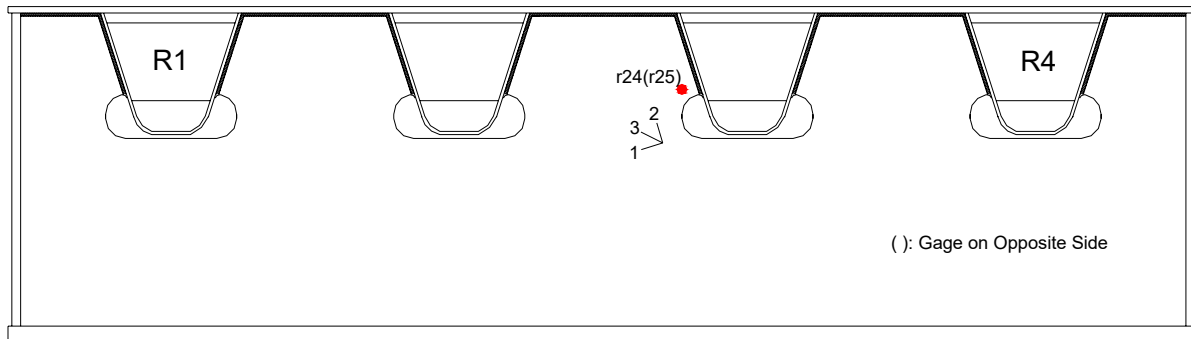
strain gages in the diaphragm were positioned 38 mm away from the rib-to-diaphragm weld toe termination and 25 mm away from the top of the free cutout.



(a) Diaphragm D1 (North Side)

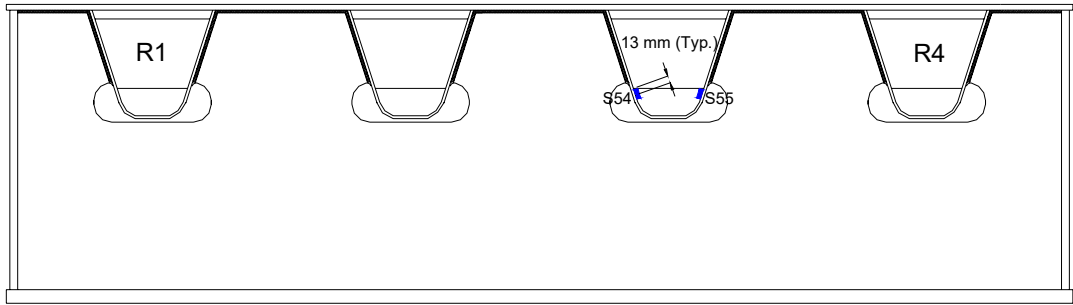


(b) Diaphragm D2 (North Side)

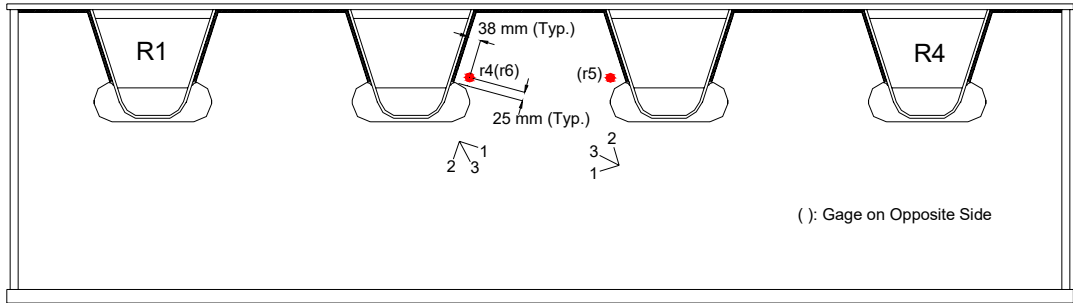


(c) Diaphragm D3 (North Side)

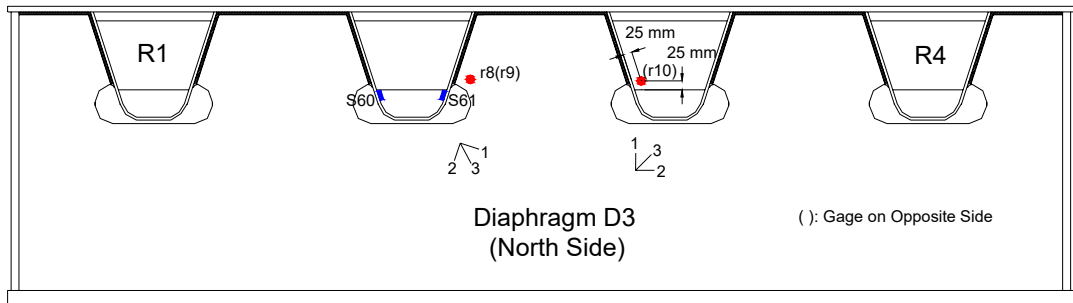
Figure 2.49 Specimen 1: Gages in Bulkheads and Diaphragms at Supports



(a) Diaphragm D1 (North Side)

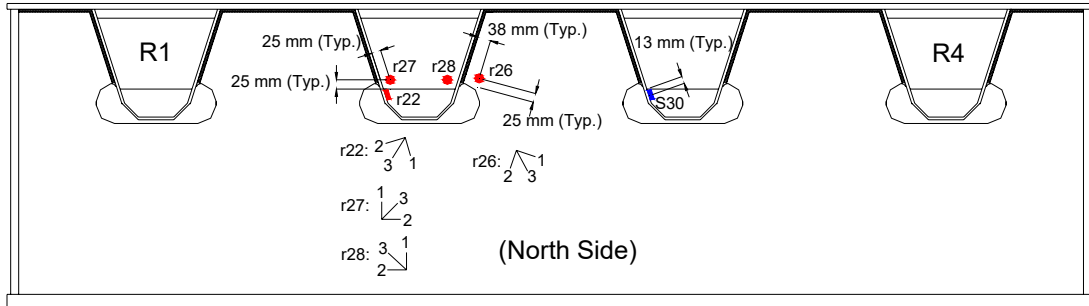


(b) Diaphragm D2 (North Side)

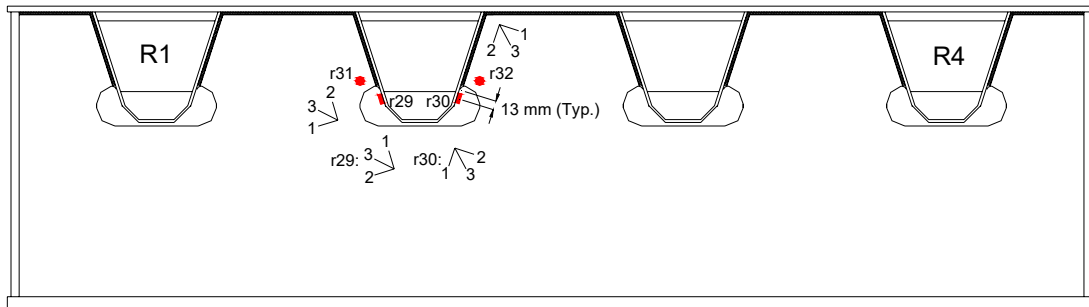


(c) Diaphragm D3 (North Side)

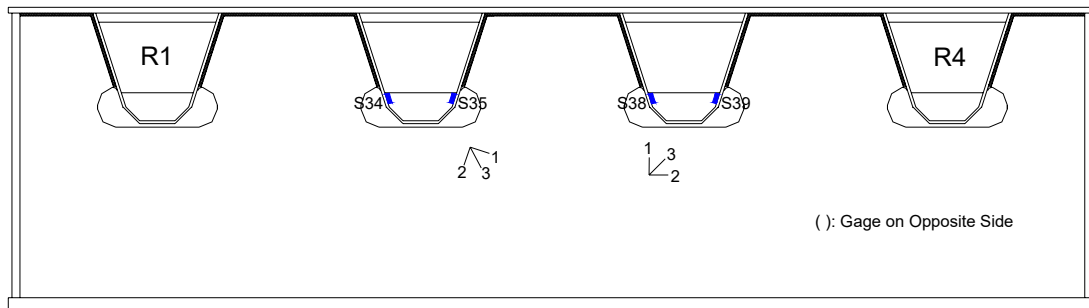
Figure 2.50 Specimen 2: Gages in Ribs, Bulkheads and Diaphragms at Supports



(a) Diaphragm D1 (North Side)

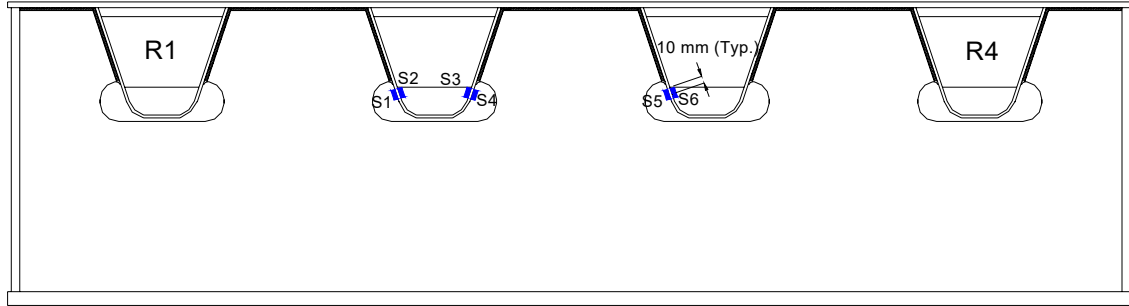


(b) Diaphragm D2 (North Side)

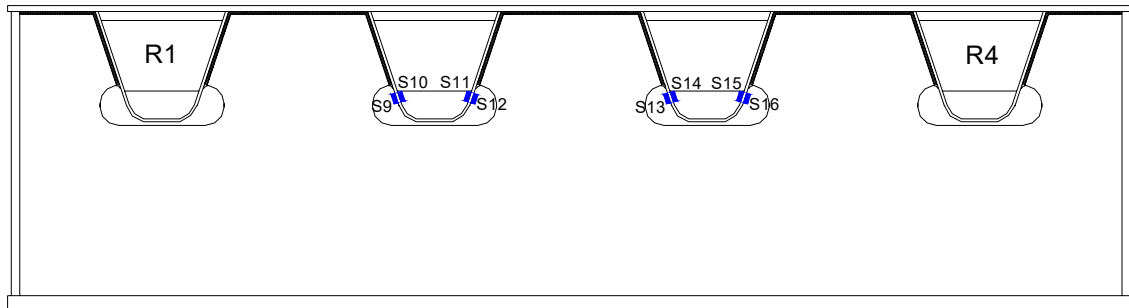


(c) Diaphragm D3 (North Side)

Figure 2.51 Specimen 3: Gages in Ribs, Bulkheads and Diaphragms at Supports

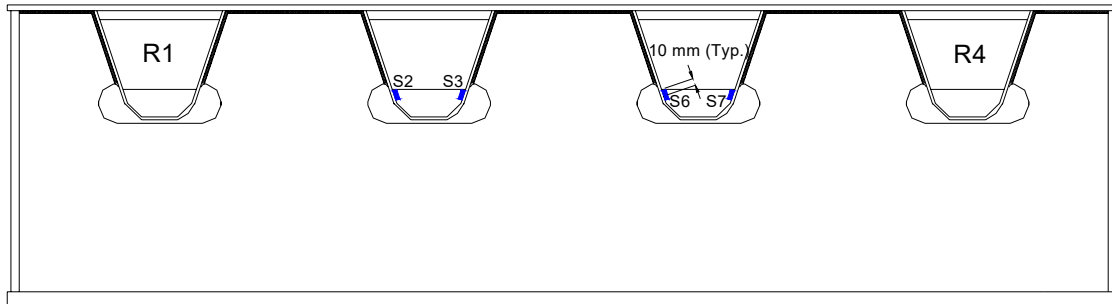


(a) Diaphragm D1 (North Side)

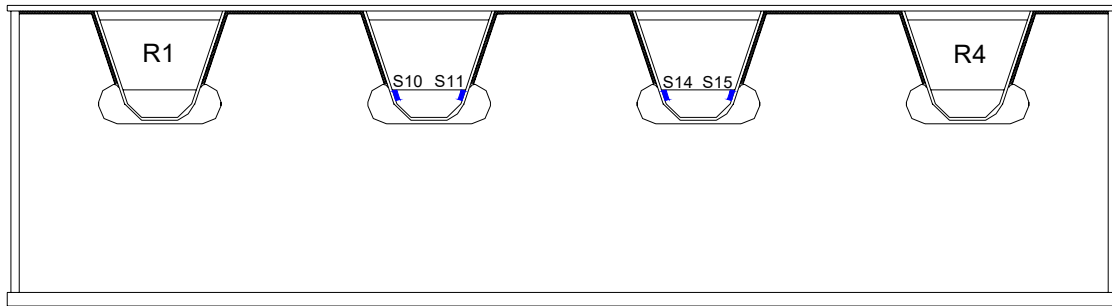


(b) Diaphragm D3 (North Side)

Figure 2.52 Specimen 4: Gages in Ribs at Supports



(a) Diaphragm D1 (North Side)



(b) Diaphragm D3 (North Side)

Figure 2.53 Specimen 5: Gages in Ribs at Supports

3. FINITE ELEMENT ANALYSIS

3.1 Introduction

In order to predict the stress fields prior to testing, finite element models were developed using the structural analysis software ABAQUS (ABAQUS Inc. 2005). Figure 3.1 shows Model 1 for Specimen 1 and Model 2 for Specimens 2 to 6. 3-D shell elements with six degrees of freedom per node were used. For the boundary condition of Model 1, all the nodes at three base plates were restrained for translations. The boundary condition of Model 2 were revised such that the base plate at the middle support diaphragm was restrained for translations, and the base plates at end support diaphragms were allowed to rotate. End stiffener plates at all support diaphragms were removed for Model 2. For the loading condition of Model 1, a pair of wheel axle loads of 190 kN (380 kN total) spaced 1200 mm apart are centered at midspan. The loading condition for Model 2 was revised such that a single wheel axle load of 188 kN are centered at midspan. The loads are uniformly distributed over the contact area through the 250 mm × 510 mm wheel prints,.

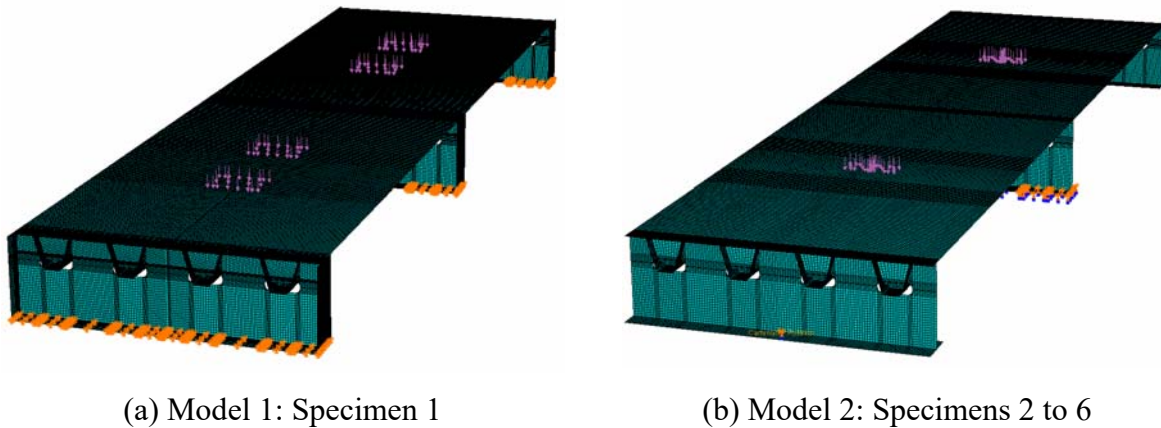
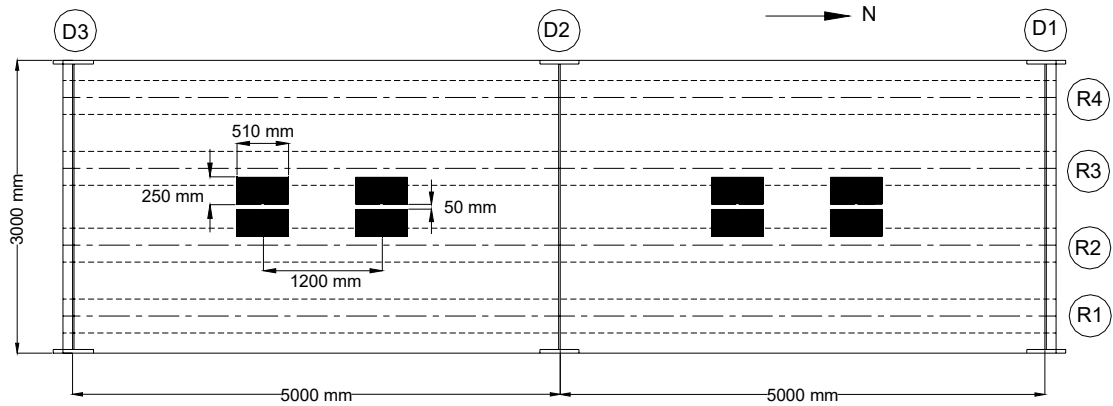


Figure 3.1 ABAQUS Modeling

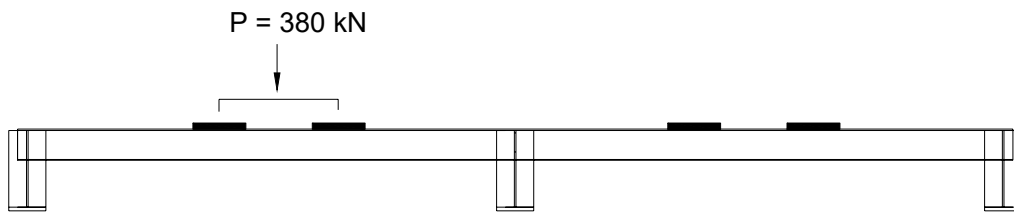
3.2 Predicted Global Behavior

Figures 3.2 and 3.3 show the plan view and load steps for each model. As the actuator loads at midspan are out of phase, the loading can be represented by three load steps. Figures 3.4 and 3.5 show the deformed shape at load steps 1 and 2. The deformed

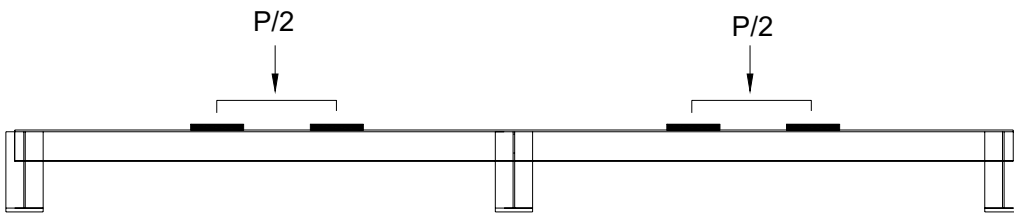
shape at load step 3 is not shown due to symmetry of geometry and loading. Designations of cross sections are also labeled in these figures. Section 1 represents the cross section at midspan, Section 2 for the cross section at end support diaphragm, and Section 3 for the cross section at interior support diaphragm. The maximum vertical displacement of the deck plate at midspan is 7.4 mm for Model 1, and 4.8 mm for Model 2. Deformed shapes of the cross sections at each load step are shown in Figures 3.6 to 3.11. From the deformed shapes in these figures, it can be seen that the loading centered at midspan produce torsion being resisted at the supports, and the torsion twist the ribs at the supports. With this loading distribution mechanism, the out-of-plane transverse bending in the rib wall below the bulkhead and diaphragm plates are produced. The deformed shape of Sections 1 and 2 varies in the transverse direction with the load steps, but the deformed shape of Section 3 (interior support diaphragm) remains the same in the transverse direction through the load steps (see Figures 3.8 to 3.11).



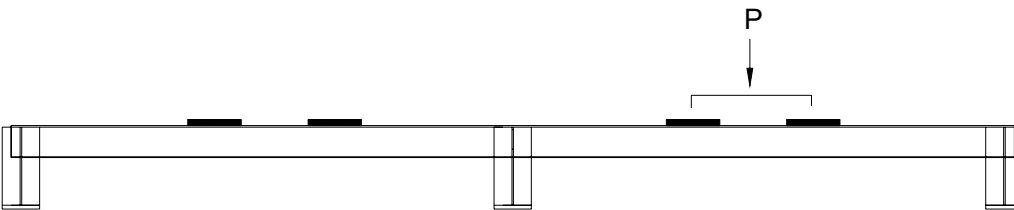
(a) Plan View with Rib and Diaphragm Designations



(b) Load Step 1

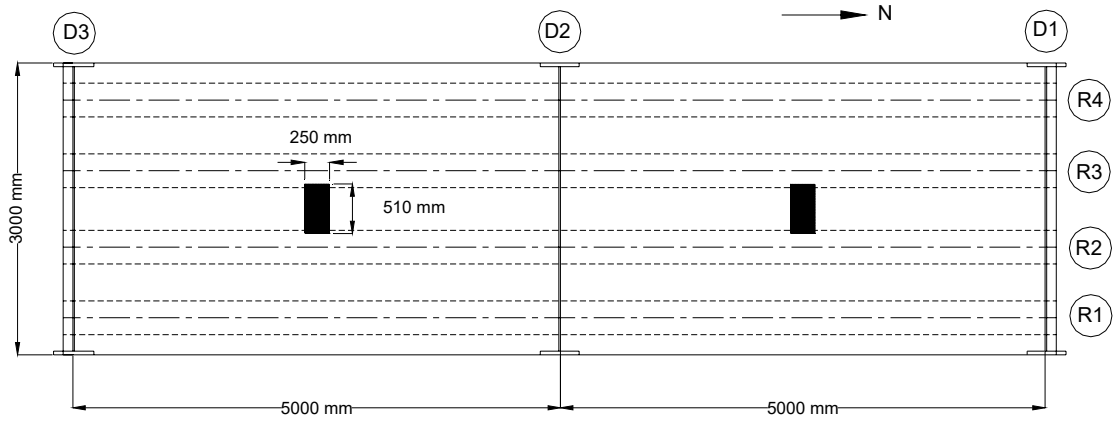


(c) Load Step 2

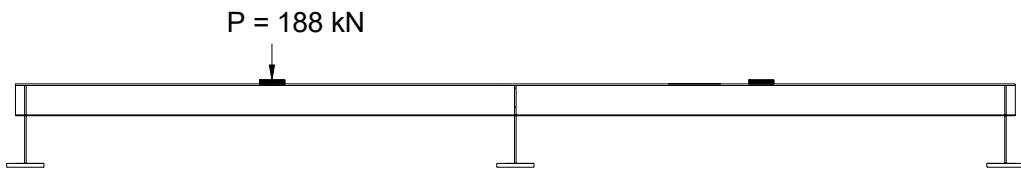


(d) Load Step 3

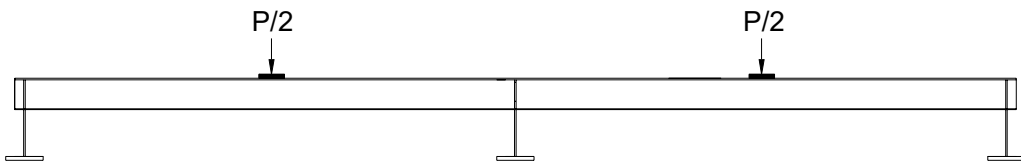
Figure 3.2 Model 1: Plan View and Loading Steps



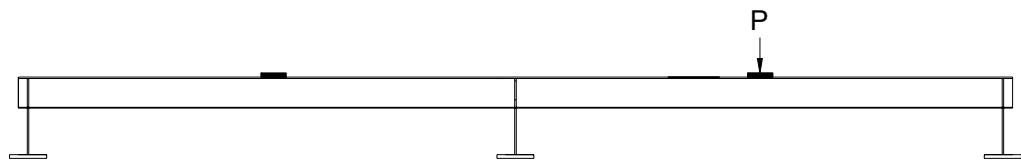
(a) Plan View with Rib and Diaphragm Designations



(b) Load Step 1

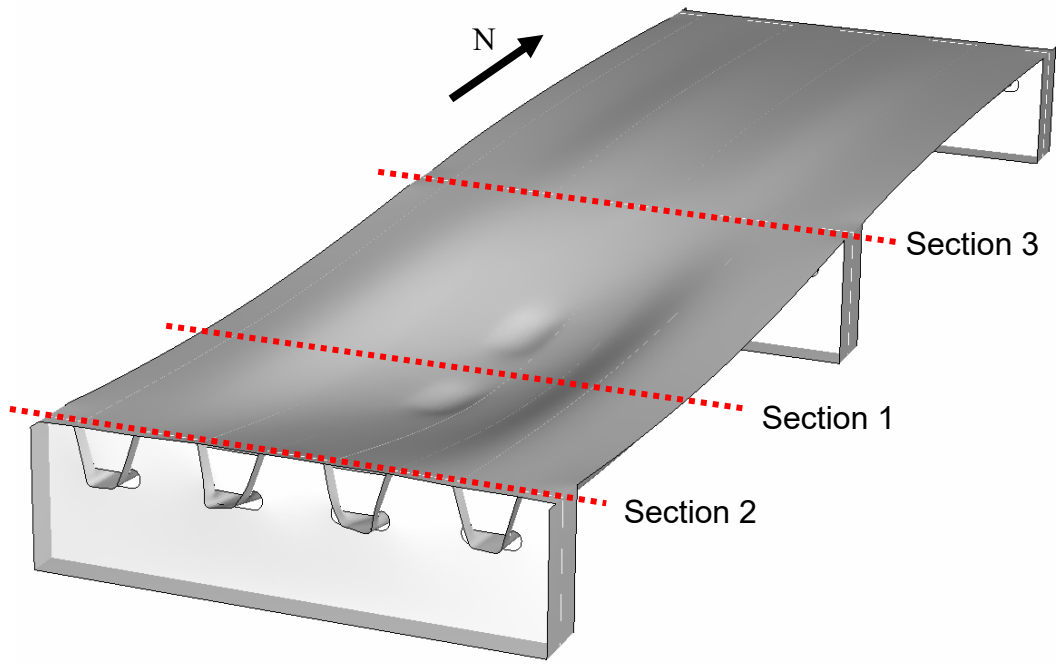


(c) Load Step 2

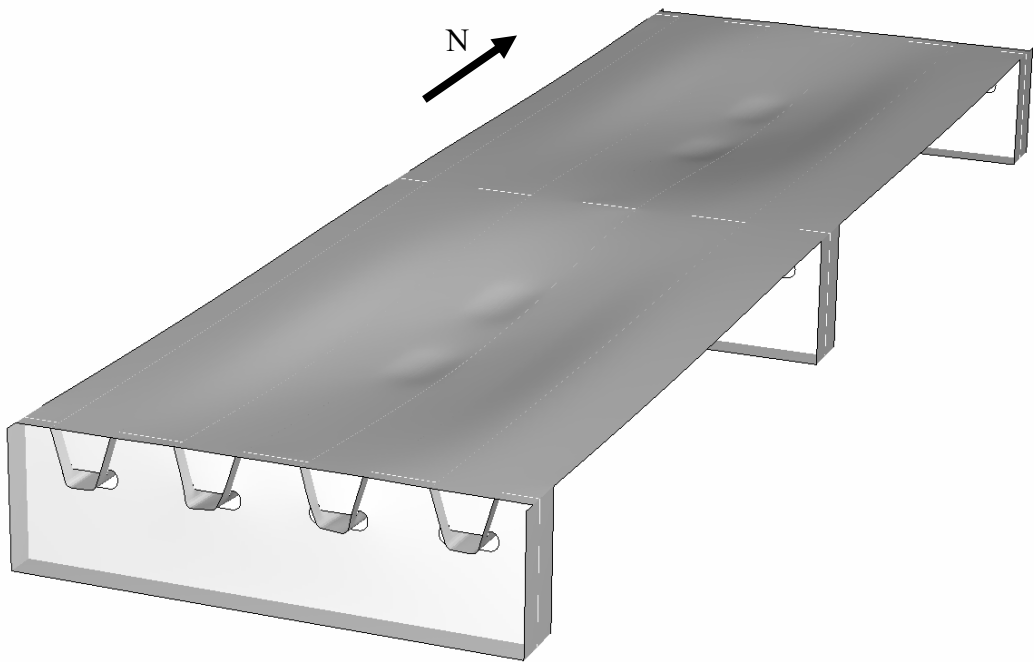


(d) Load Step 3

Figure 3.3 Model 2: Plan View and Loading Steps

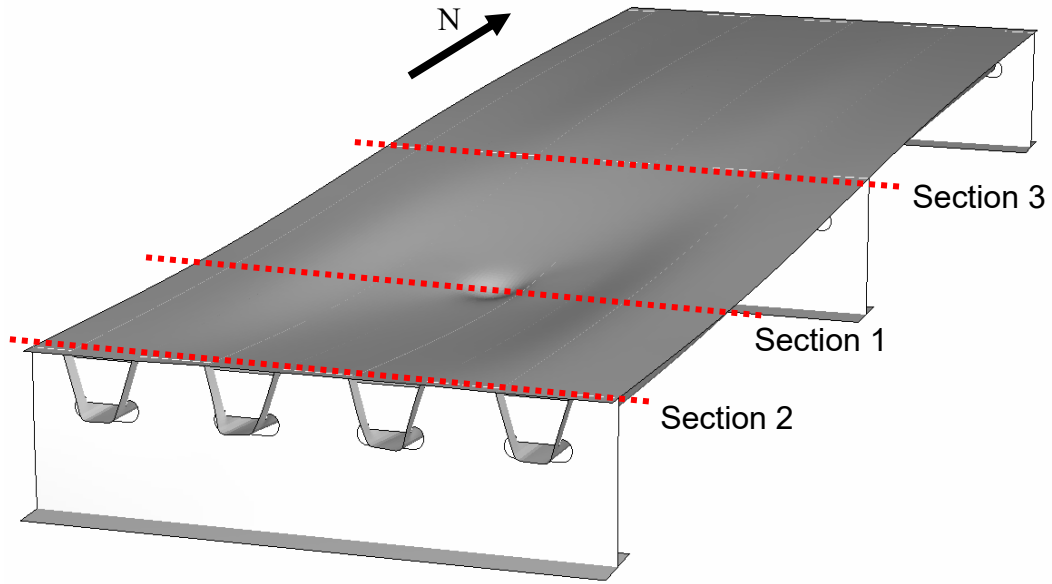


(a) Load Step 1

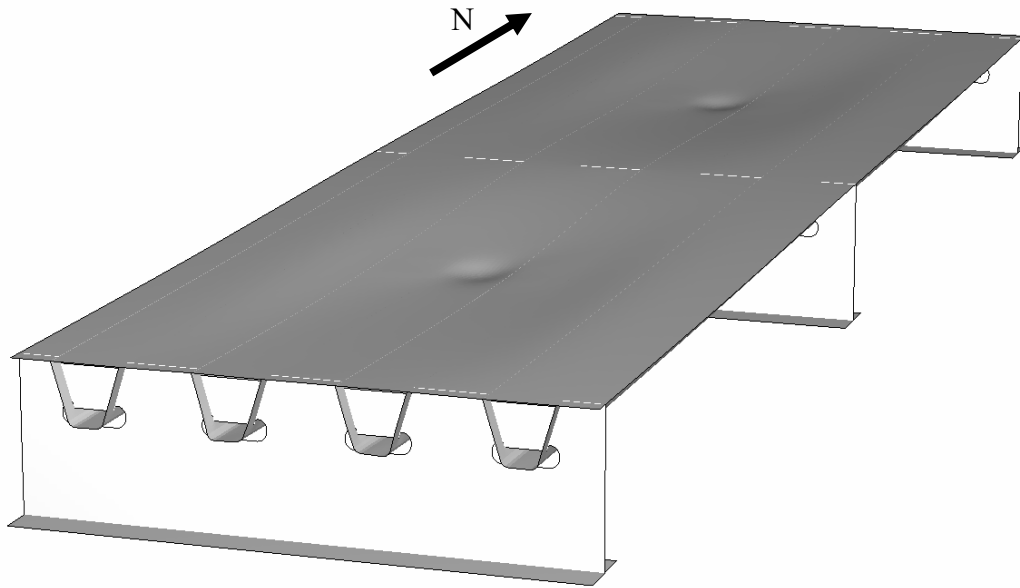


(b) Load Step 2

Figure 3.4 Model 1: Deformed Shape (Amplification Factor = 50)

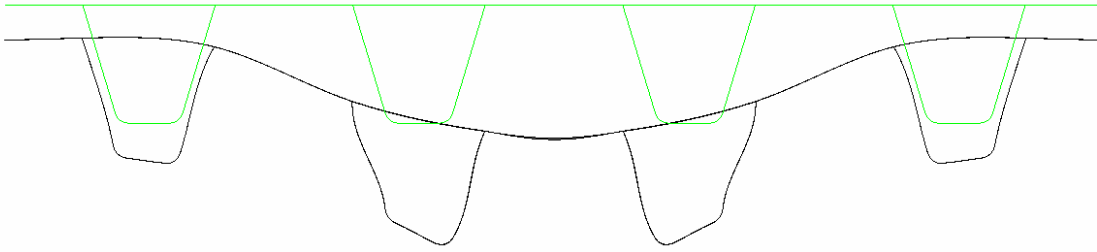


(a) Load Step 1

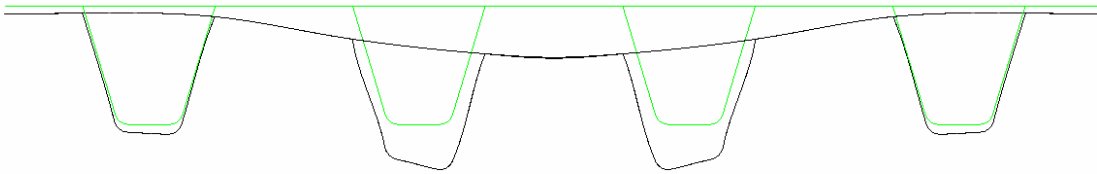


(b) Load Step 2

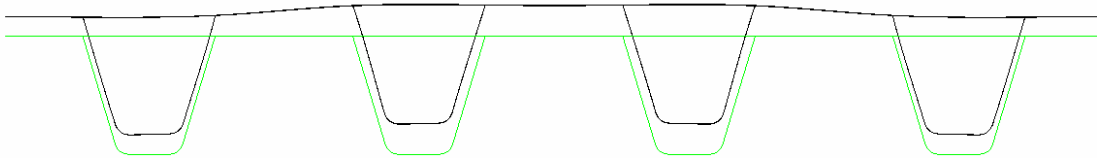
Figure 3.5 Model 2: Deformed Shape (Amplification Factor = 50)



(a) Load Step 1

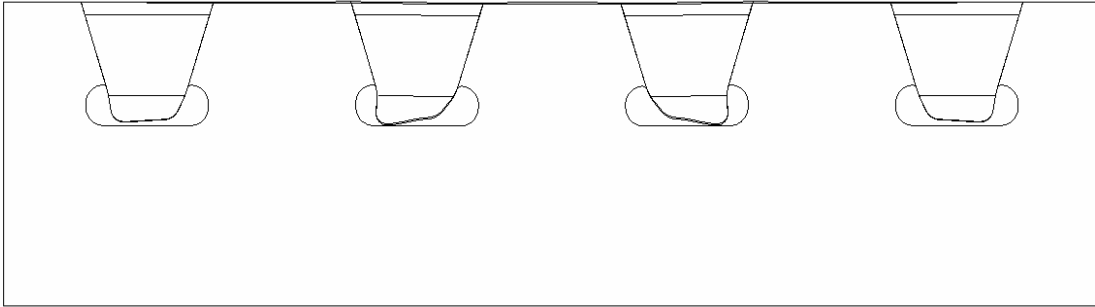


(b) Load Step 2

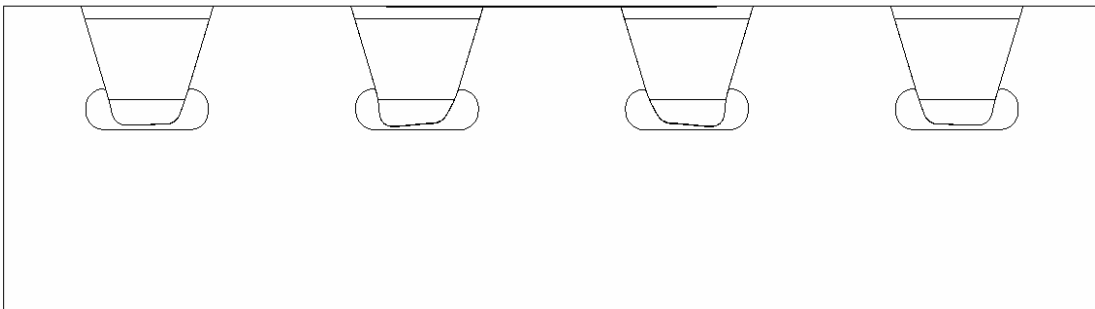


(c) Load Step 3

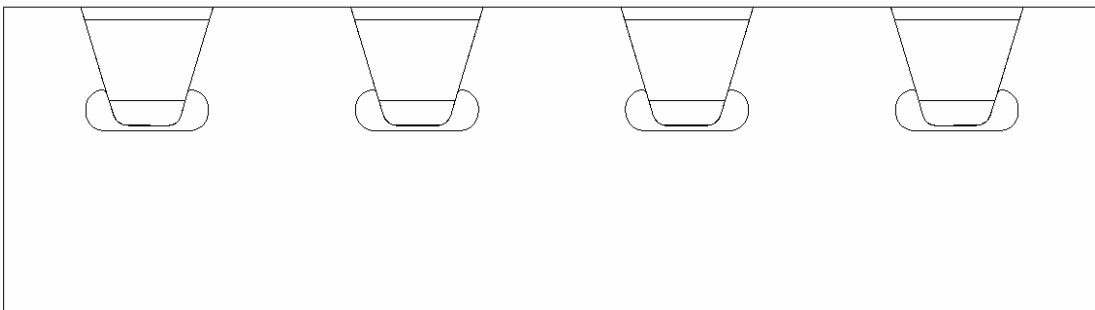
Figure 3.6 Model 1: Deformed Shape at Cross Section 1 (Amplification Factor = 50)



(a) Load Step 1



(b) Load Step 2



(c) Load Step 3

Figure 3.7 Model 1: Deformed Shape at Cross Section 2 (Amplification Factor = 50)

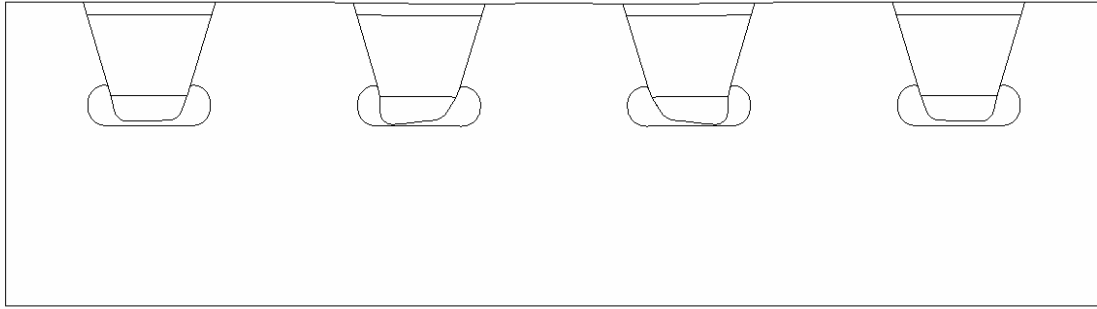
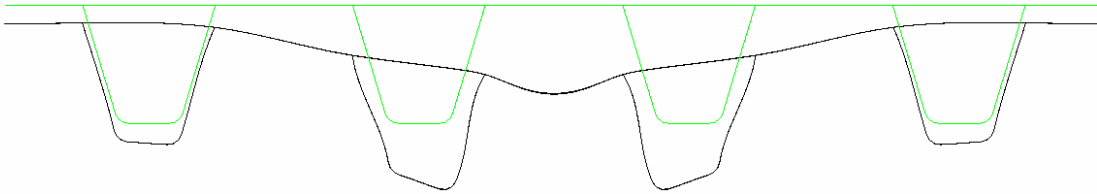
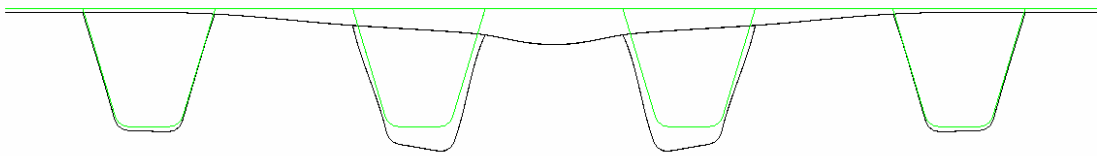


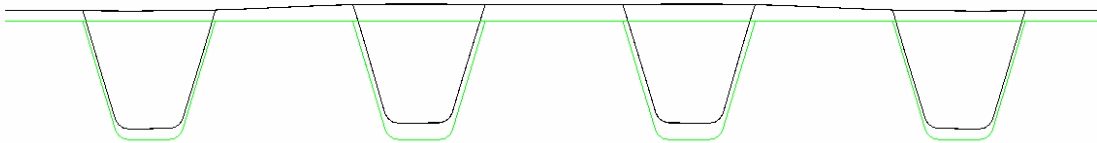
Figure 3.8 Model 1: Deformed Shape at Cross Section 3 through Load Steps 1, 2, and 3 (Amplification Factor = 50)



(a) Load Step 1

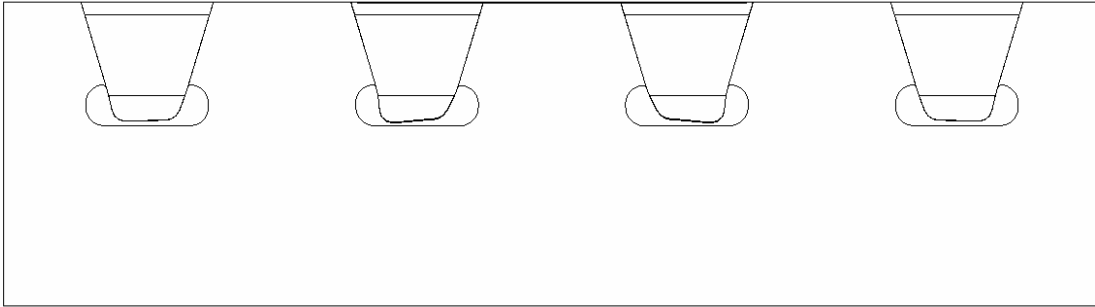


(b) Load Step 2

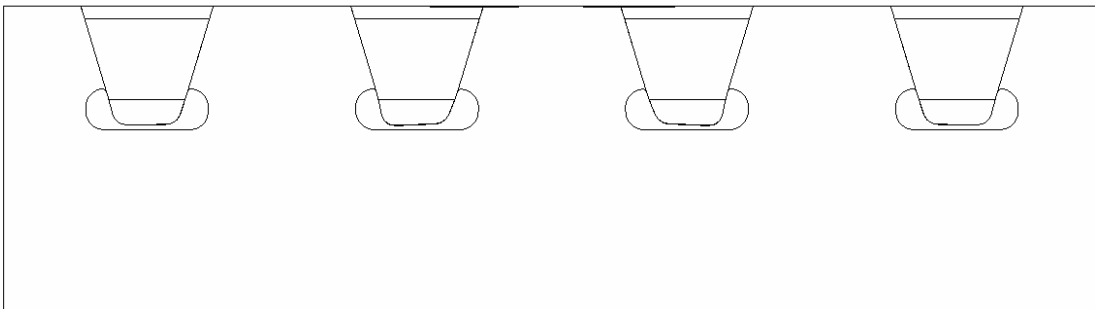


(c) Load Step 3

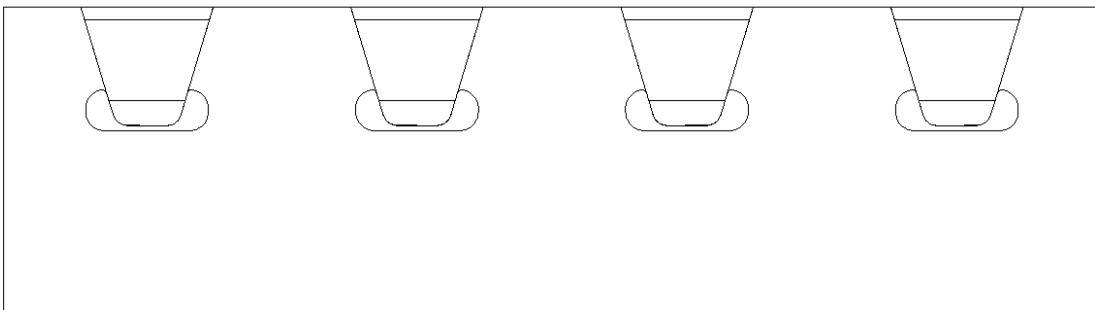
Figure 3.9 Model 2: Deformed Shape at Cross Section 1 (Amplification Factor = 50)



(a) Load Step 1



(b) Load Step 2



(c) Load Step 3

Figure 3.10 Model 2: Deformed Shape at Cross Section 2 (Amplification Factor = 50)

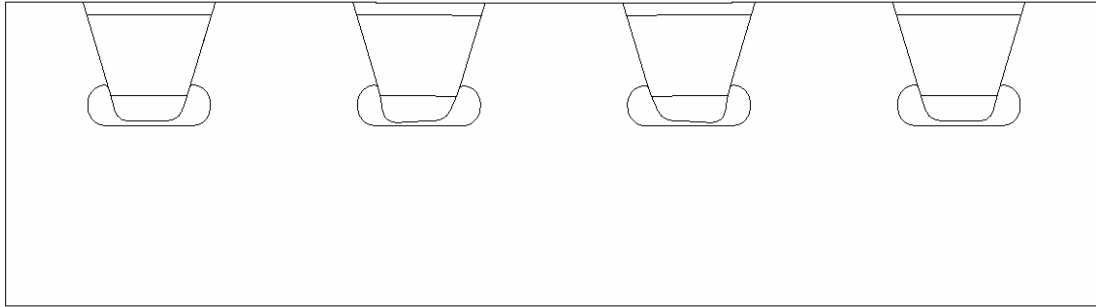


Figure 3.11 Model 2: Deformed Shape at Cross Section 3 through Load Steps 1, 2, and 3 (Amplification Factor = 50)

3.3 Predicted Stresses for Model 1

3.3.1 Stress Contour on Ribs at Support Diaphragms

An interior rib at end support diaphragms, labeled Detail A for Model 1 in Figure 3.12, is identified as a fatigue critical location based on the deformed shape and stress field during the load steps 1, 2, and 3. Figures 3.13 and 3.14 show the predicted stress contours on the rib at the end support diaphragms for Model 1. From the figures, it is shown that the regions below the rib-to-bulkhead connection and the diaphragm cutout are critical. Below the bulkhead, the interior side of the rib is in tension on the west side and in compression on the east side. At the diaphragm cutout, the exterior side of the rib is in compression on the west side and in tension on the east side. The contours of the maximum principal stress in tension and the minimum principal stress in compression for the interior side of the rib below the bulkhead are shown in Figure 3.13(a) and (b), and for the exterior side of the rib near the diaphragm cutout in Figure 3.14(a) and (b). At a location of about 13 mm below the bottom corner of the bulkhead on the west side of the rib, the tensile transverse stress predicted on the rib is approximately 166 MPa, and the compressive transverse stress is 189 MPa. On the east side of the rib at the same location, the compressive transverse stress predicted on the rib is approximately 151 MPa, and the tensile transverse stress is 197 MPa [see Figure 3.13(c) for the transverse stress direction].

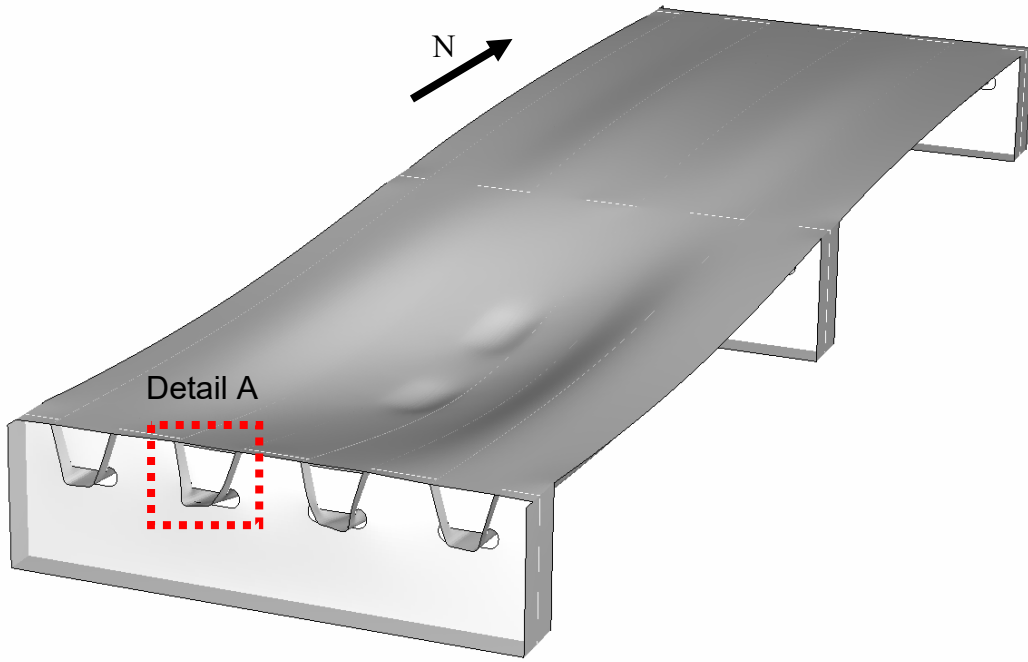
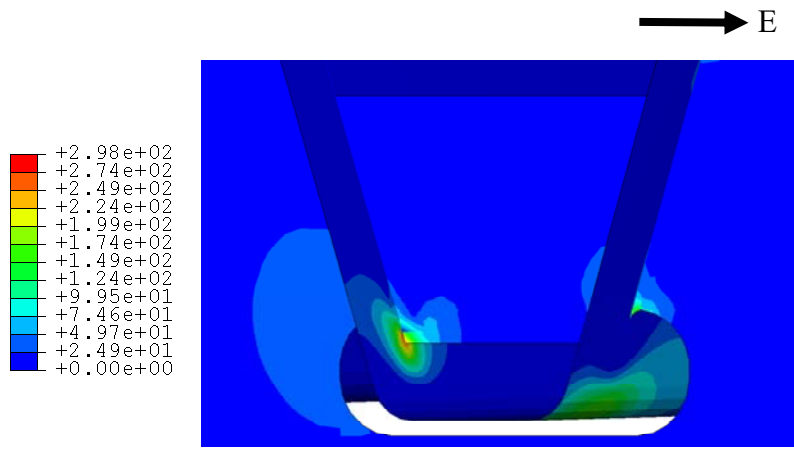
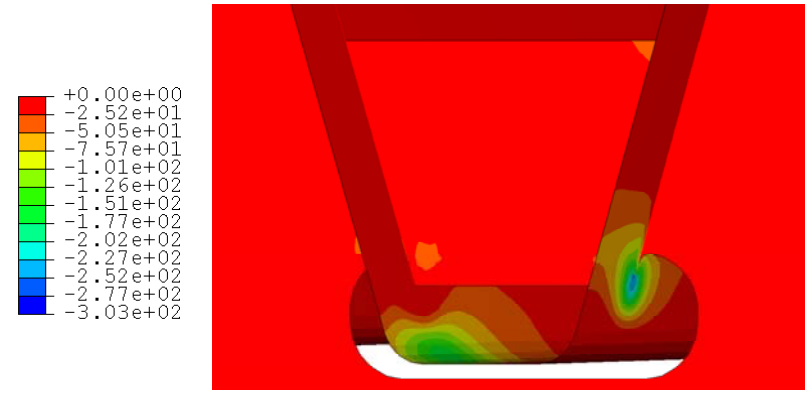


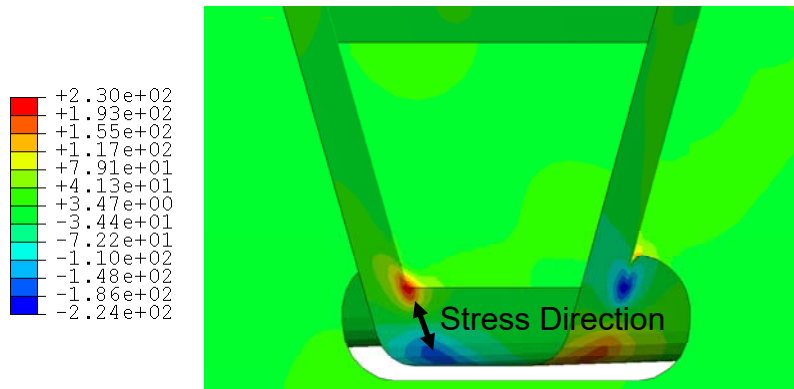
Figure 3.12 Model 1: Location of Detail A



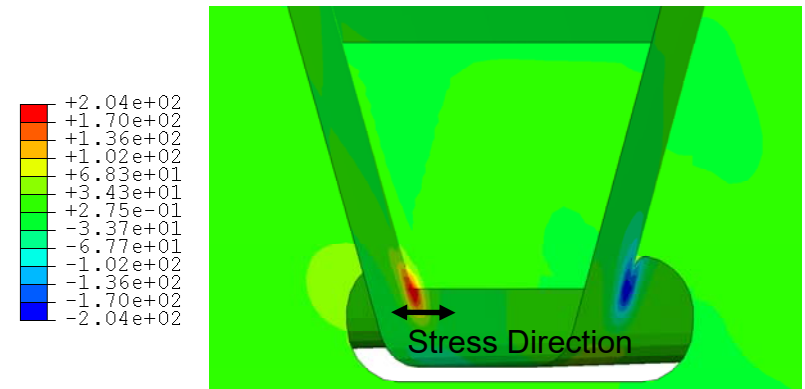
(a) Maximum Principal Stress (in Tension)



(b) Minimum Principal Stress (in Compression)

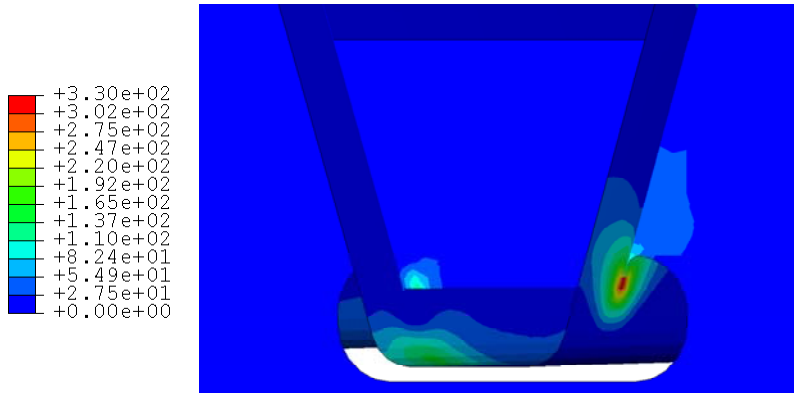


(c) Stress in the Transverse Direction

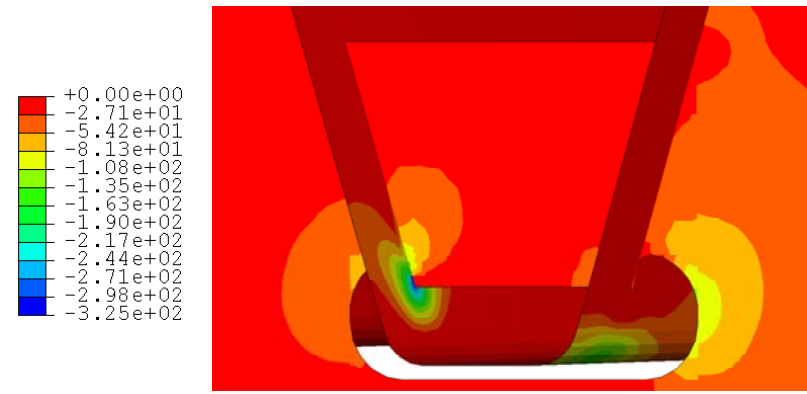


(d) Stress in the Longitudinal Direction

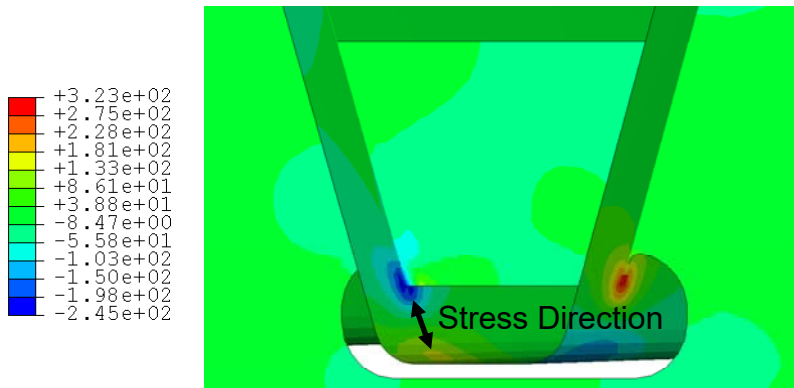
Figure 3.13 Model 1: Stress Contour Inside the Rib of Detail A (MPa)



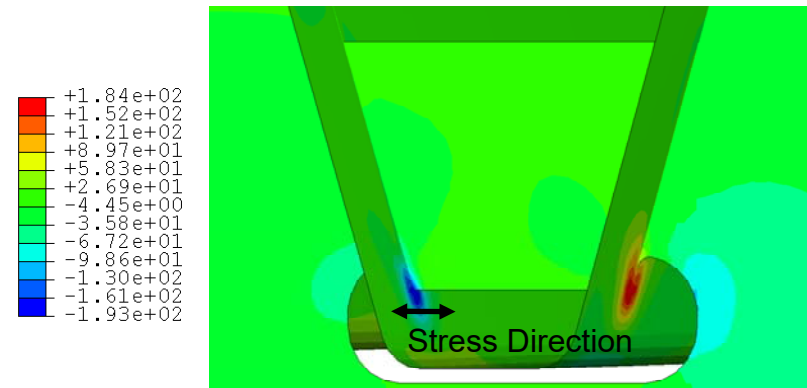
(a) Maximum Principal Stress (in Tension)



(b) Minimum Principal Stress (in Compression)



(c) Stress in the Transverse Direction



(d) Stress in the Longitudinal Direction

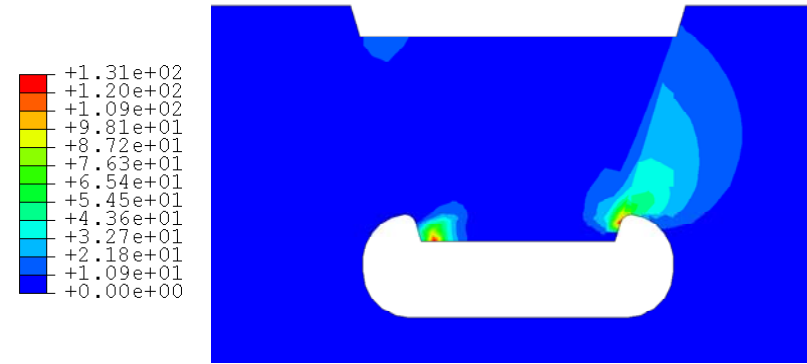
Figure 3.14 Model 1: Stress Contour Outside the Rib of Detail A (MPa)

3.3.2 Principal Stress Distribution on Bulkhead and Diaphragm Plates

Figure 3.15 shows the principal stress contour on both sides (south and north sides) of the bulkhead and diaphragm plate at Detail A on the end diaphragms (see Figure 3.12 for a compass direction and the location of Detail A). As shown from the principal stress contour, the bottom corner of the bulkhead and the diaphragm cutout at rib-to-diaphragm connection are critical. The contour of the maximum principal stress in tension and the minimum principal stress in compression on both sides of the bulkhead and the diaphragm plate are shown in Figure 3.15(a) to (d). The principal stress directions are also shown in Figure 3.15(e) to (h). At a bulkhead location of about 25 mm away from the corners of the bottom and the side of the bulkhead, the predicted maximum principal stress is 60 MPa in tension on the south-west side of Detail A and 49 MPa on the north-west side. The minimum principal stress on the bulkhead is 49 MPa in compression on the south-east side and 61 MPa on the north-east side. At a diaphragm location of about 25 mm away from the top of the free diaphragm cutout and 38 mm apart from the side corner of the bulkhead, the predicted maximum principal stress is 37 MPa in tension on the south-west side and 36 MPa on the north-east side. The minimum principal stress on the diaphragm at the same location is 24 MPa in compression on the south-west side and 61 MPa on the north-east side.



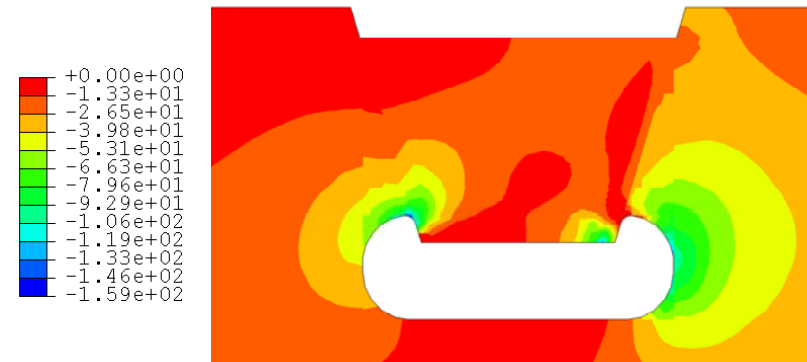
(a) Maximum Principal Stress on South Side (in Tension)



(b) Maximum Principal Stress on North Side (in Tension)

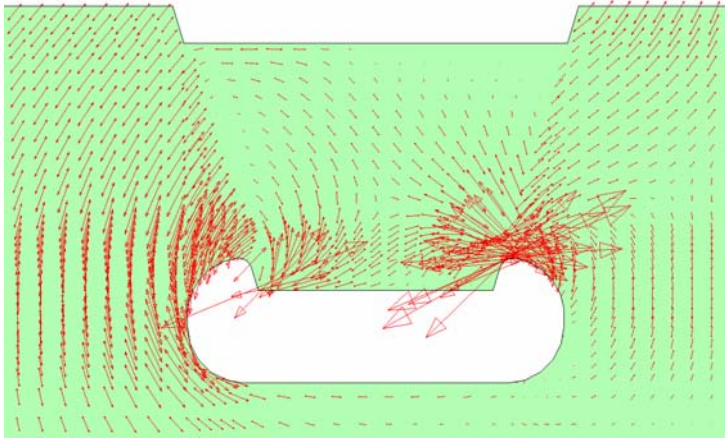


(c) Minimum Principal Stress on South Side (in Compression)

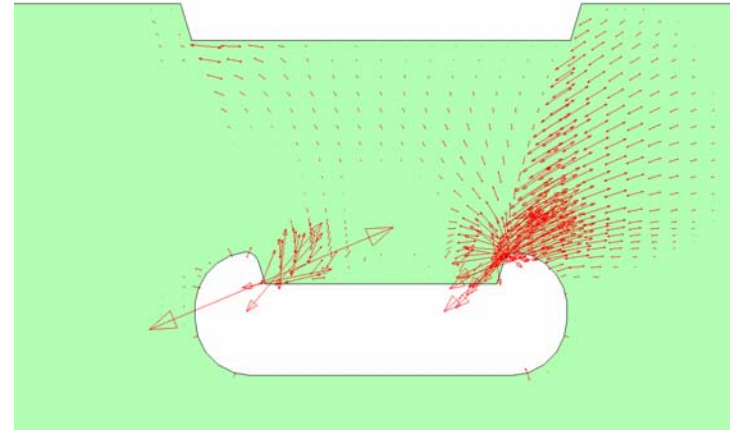


(d) Minimum Principal Stress on North Side (in Compression)

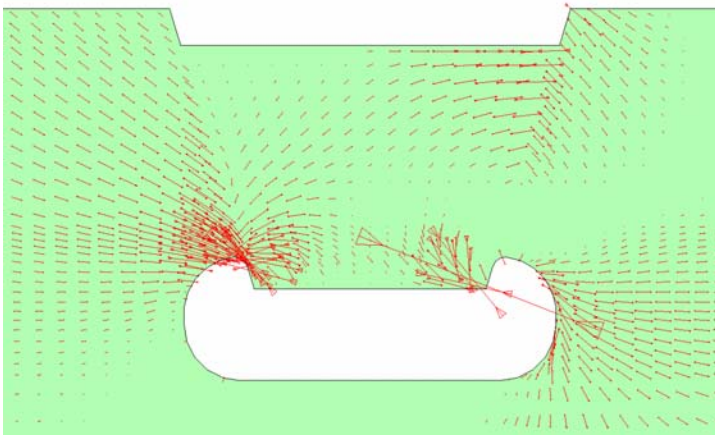
Figure 3.15 Model 1: Principal Stress Contour or Tensor at Detail A (MPa)



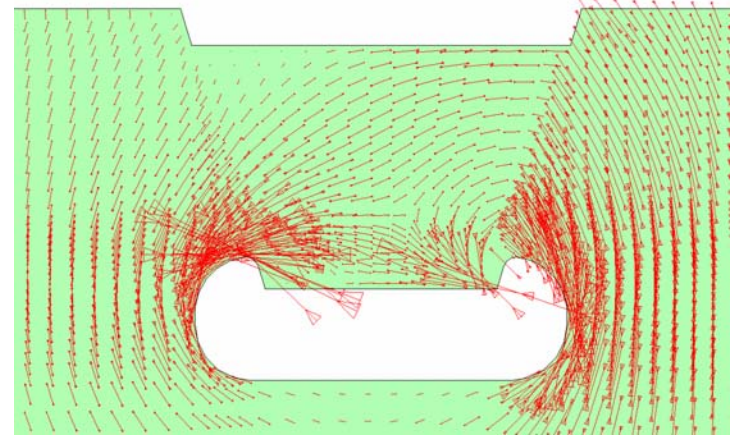
(e) Maximum Principal Stress Tensor on South Side (in Tension)



(f) Maximum Principal Stress Tensor on North Side (in Tension)



(g) Minimum Principal Stress Tensor on South Side (in Compression)



(h) Minimum Principal Stress Tensor on North Side (in Compression)

Figure 3.15 Model 1: Principal Stress Contour or Tensor at Detail A (continued)

3.3.3 Stress Distribution on Ribs near Rib-to-Deck Joints

Figure 3.16 shows the designations of the rib-to-deck joints. Joints 1 and 2 represent the rib-to-deck welded joints on both sides of an interior rib due to the symmetry of geometry of a specimen and the loading pattern. The location and the direction of stresses of interest are shown in Figure 3.17. Plots of the predicted stresses on the deck plate and the rib along a span length 5000 mm, over which the loading is applied, are shown in Figures 3.18 to 3.21. The stresses located approximately 10 mm from the rib-to-deck joints are oriented in the transverse (width) direction.

For Joint 1, the maximum stresses predicted on the deck plate are approximately 58 MPa in compression on the bottom surface and 60 MPa in tension on the top surface. The maximum stresses on the deck plate near Joint 2 are approximately 49 MPa in tension on the bottom surface and 45 MPa in compression on the top surface. The stresses on the deck plate, located 10 mm away from the joints to the inside of the rib, are almost the same as the stresses on the deck plate to the outside of the rib.

For the rib stresses near Joint 1, the maximum predicted stresses are approximately 55 MPa in tension on the inner surface and 100 MPa in compression on the outer surface. For Joint 2, the maximum rib stresses are 92 MPa in compression on the inner surface and 97 MPa in tension on the outer surface.

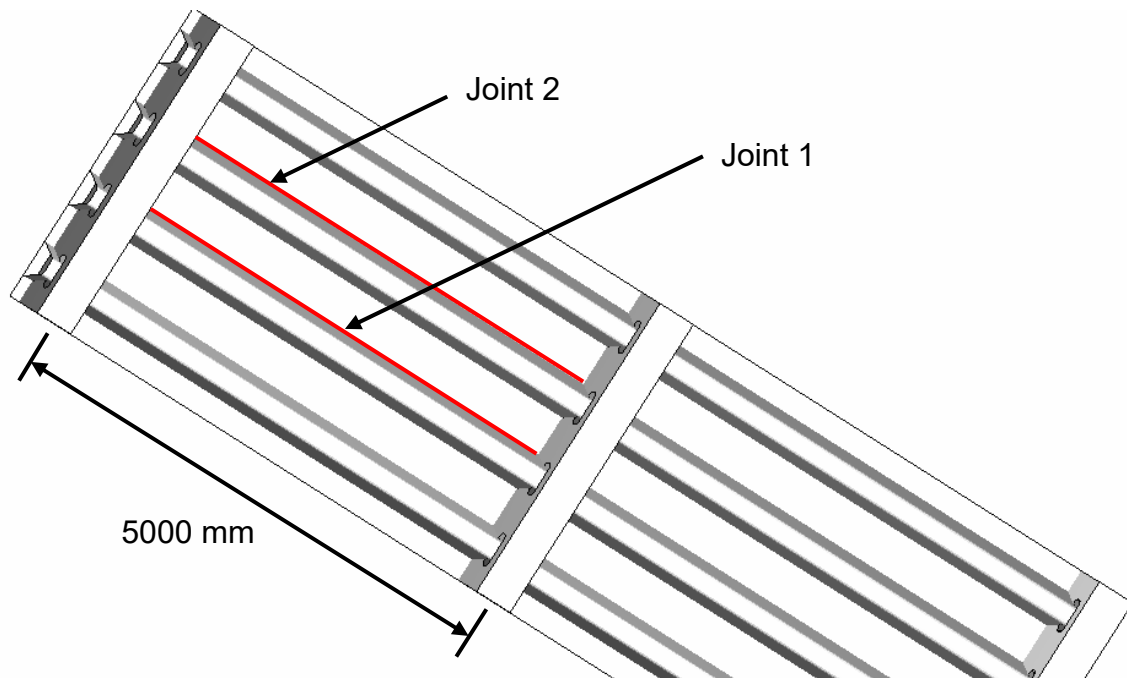


Figure 3.16 Designation of Rib-to-Deck Joints

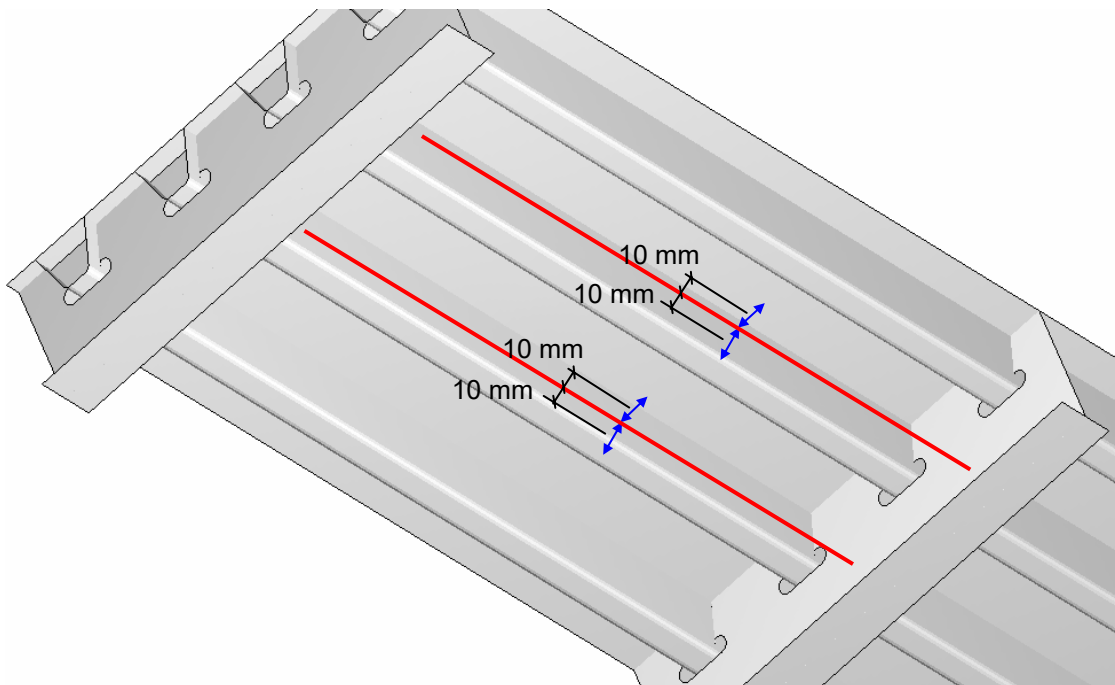


Figure 3.17 Location and Direction of Stresses in Deck Plate and Ribs

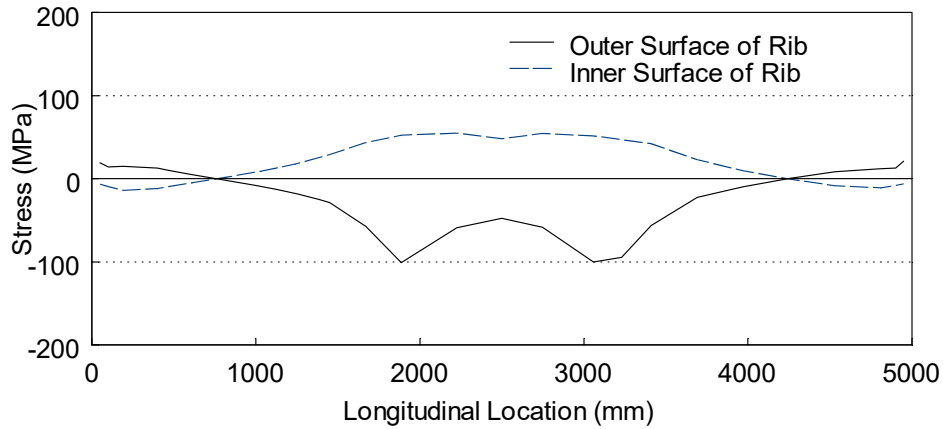


Figure 3.18 Model 1: Predicted Stresses in Ribs at Joint 1

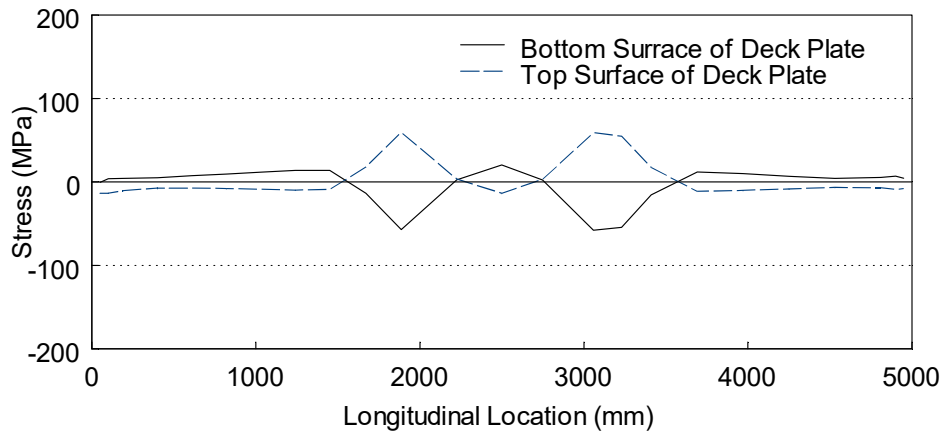


Figure 3.19 Model 1: Predicted Stresses in Deck Plate at Joint 1

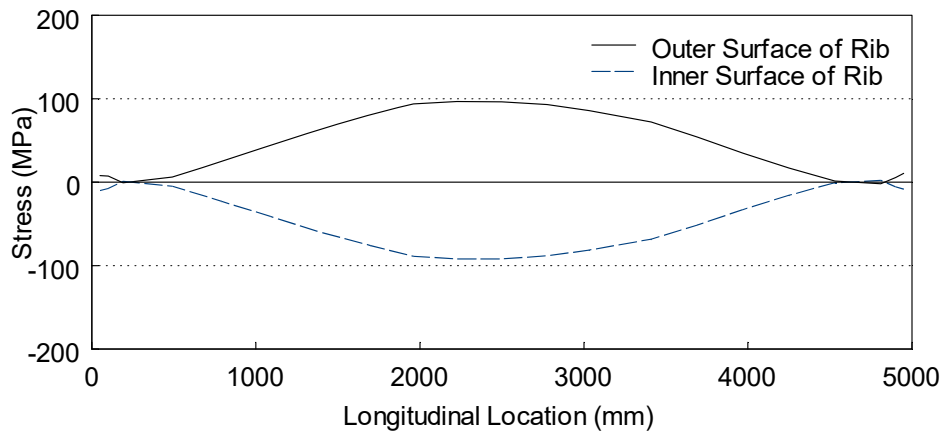


Figure 3.20 Model 1: Predicted Stresses in Ribs at Joint 2

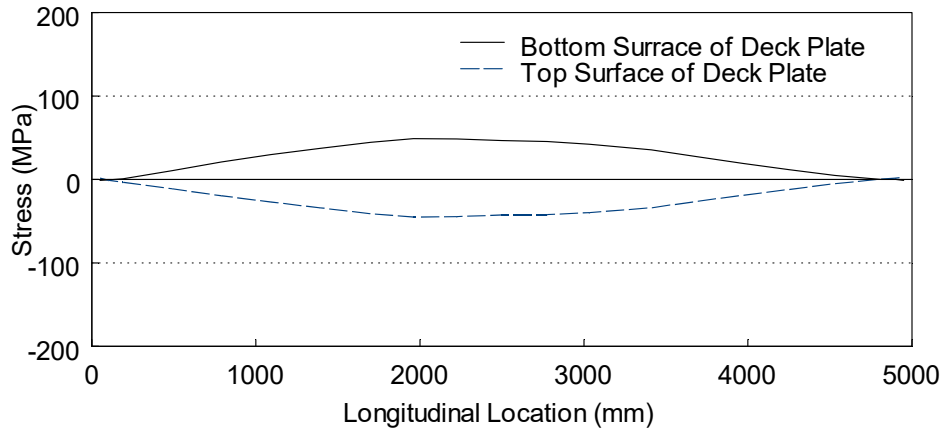


Figure 3.21 Model 1: Predicted Stresses in Deck Plate at Joint 2

3.4 Predicted Stresses for Model 2

3.4.1 Stress Contour on Ribs at Support Diaphragms

Detail B which corresponds to Detail A in Model 1, is shown in Figure 3.22. Figures 3.23 and 3.24 show the predicted stress contours on the rib at the end support diaphragm for Model 2. It is shown that the stress field and the critical region are similar to those of Model 1, but the magnitude of stresses is much lower than that in Model 1. The contours of the maximum principal stress in tension and the minimum principal stress in compression for the interior side of the rib below the bulkhead are shown in Figure 3.23(a) and (b), and for the interior side of the rib near the diaphragm cutout are shown in Figure 3.24(a) and (b). At the same location as in Model 1, about 13 mm below the bottom corner of the bulkhead on the west side of the rib, the predicted tensile stress in the transverse direction is approximately 61 MPa (166 MPa in Model 1) and the compressive stress is 75 MPa (189 MPa in Model 1). On the east side of the rib at the same location, the predicted compressive stress on the rib is approximately 56 MPa (151 MPa in Model 1) and the tensile stress is 77 MPa (197 MPa in Model 1). The significantly reduced magnitude of stresses in Model 2 is mainly due to the reduced load level.

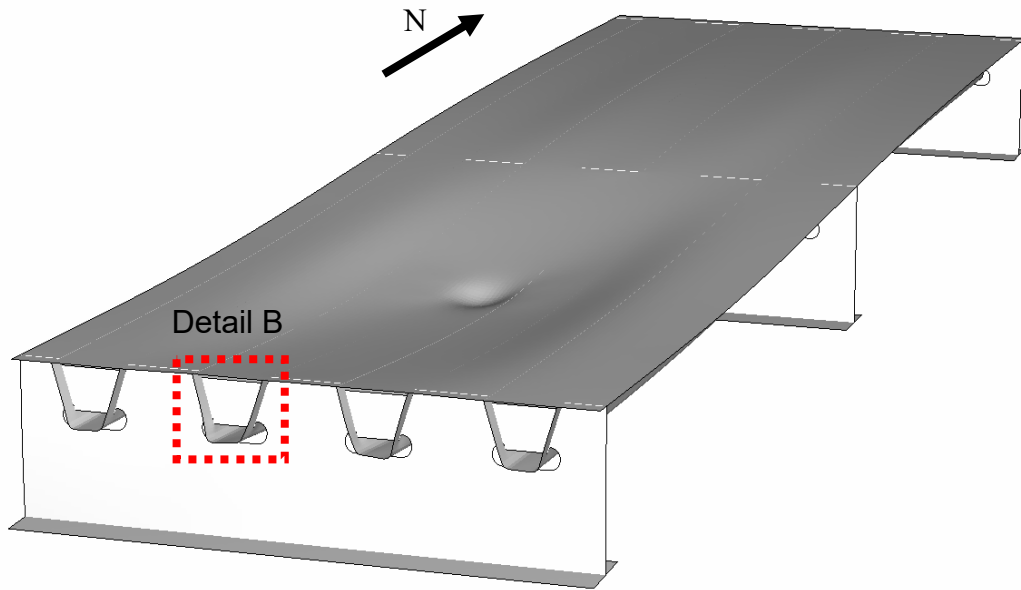
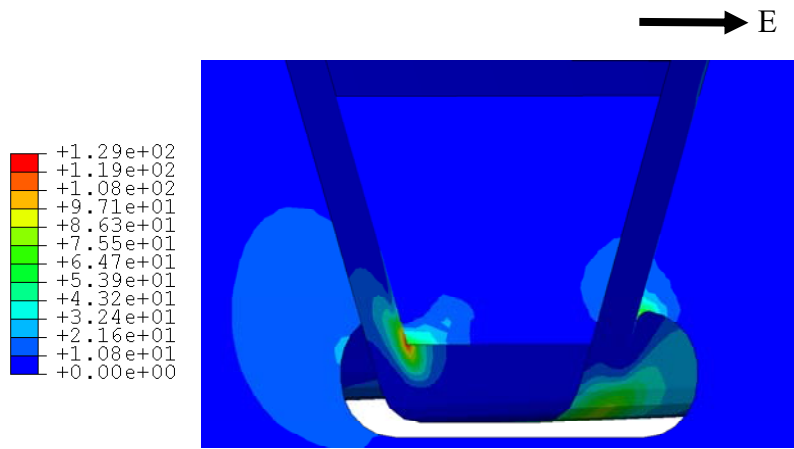
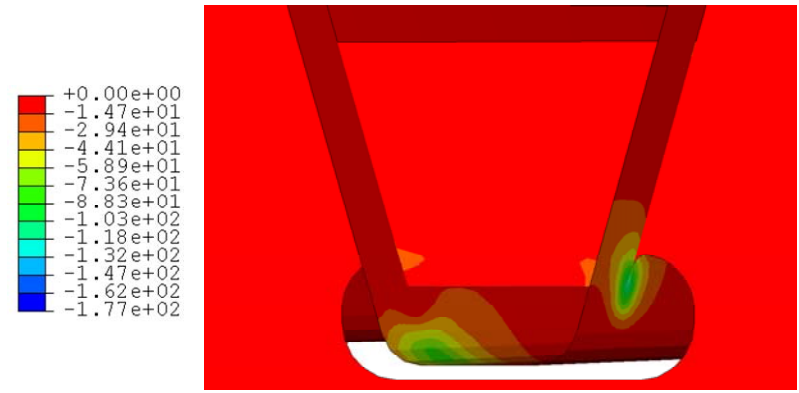


Figure 3.22 Model 2: Location of Detail B



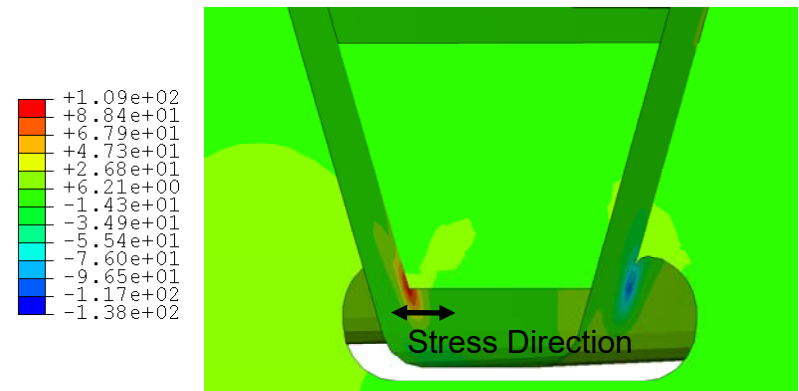
(a) Maximum Principal Stress (in Tension)



(b) Minimum Principal Stress (in Compression)

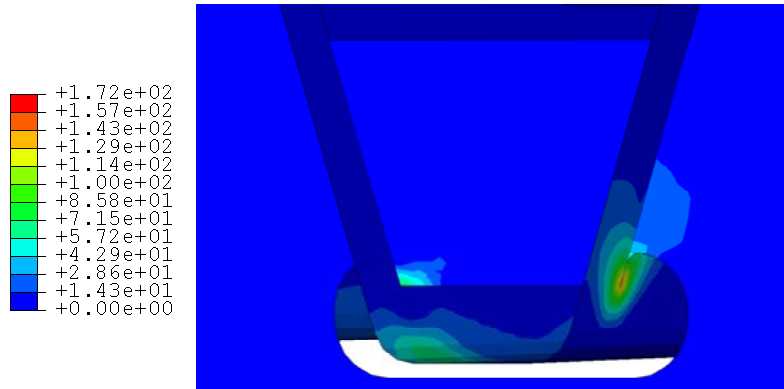


(c) Stress in the Transverse Direction

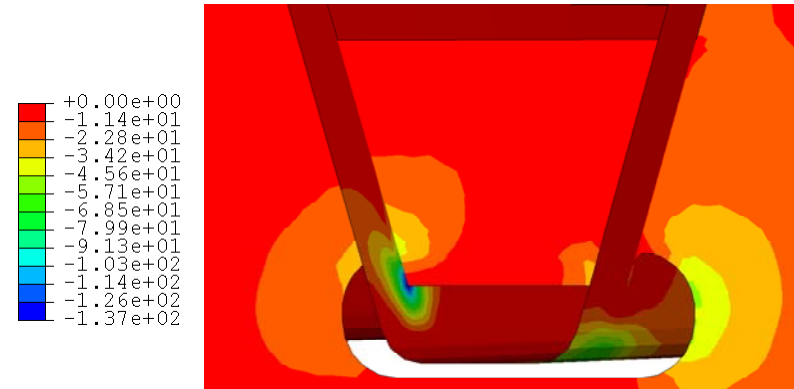


(d) Stress in the Longitudinal Direction

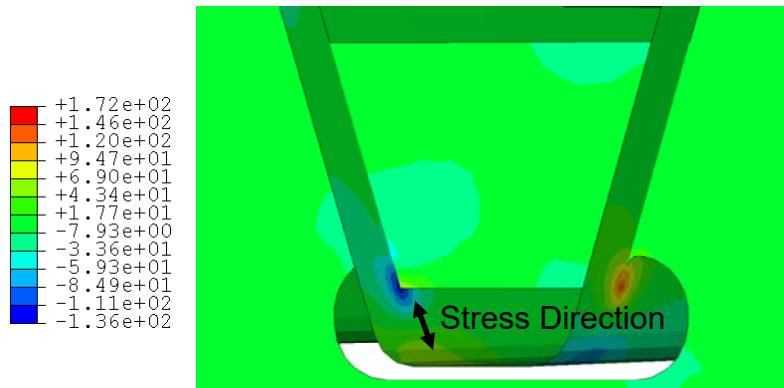
Figure 3.23 Model 2: Stress Contour Inside the Rib of Detail B (MPa)



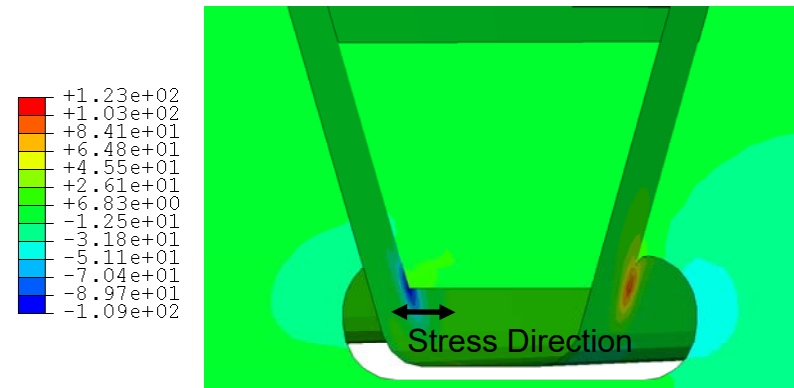
(a) Maximum Principal Stress (in Tension)



(b) Minimum Principal Stress (in Compression)



(c) Stress in the Transverse Direction



(d) Stress in the Longitudinal Direction

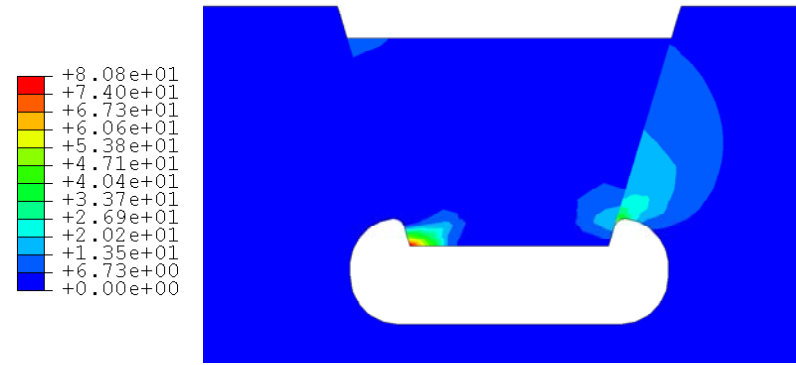
Figure 3.24 Model 2: Stress Contour Outside the Rib of Detail B (MPa)

3.4.2 Principal Stress Distribution on Bulkhead and Diaphragm Plates

Figure 3.25 shows the principal stress contours on both sides (south and north sides) of the bulkhead and diaphragm plate at Detail B (see Figure 3.22). The stress field and the critical region are also similar those of Model 1, but the magnitude of stresses is much lower than that in Model 1. The contours of the maximum principal stress in tension and the minimum principal stress in compression on both sides of the bulkhead and the diaphragm plate are shown in Figure 3.25(a) to (d). The principal stress direction is also shown in Figure 3.25(e) to (h). At the same bulkhead location as in Model 1, about 25 mm away from the corners of the bottom and the side of the bulkhead, the predicted maximum principal stress is 18 MPa (60 MPa in Model 1) in tension on the south-west side and 17 MPa (49 MPa in Model 1) on the north-west side. The minimum principal stress on the bulkhead is 16 MPa (49 MPa in Model 1) in compression on the south-east side and 18 MPa (61 MPa in Model 1) on the north-east side. At the same diaphragm location in Model 1, about 25 mm away from the top of the free diaphragm cutout and 38 mm away from the side corner of the bulkhead, the predicted maximum principal stress is 18 MPa (37 MPa in Model 1) in tension on the south-west side and 18 MPa (36 MPa in Model 1) on the north-east side. The minimum principal stress on the diaphragm at the same location is 12 MPa (24 MPa in Model 1) in compression on the south-west side and 28 MPa (61 MPa in Model 1) on the north-east side.



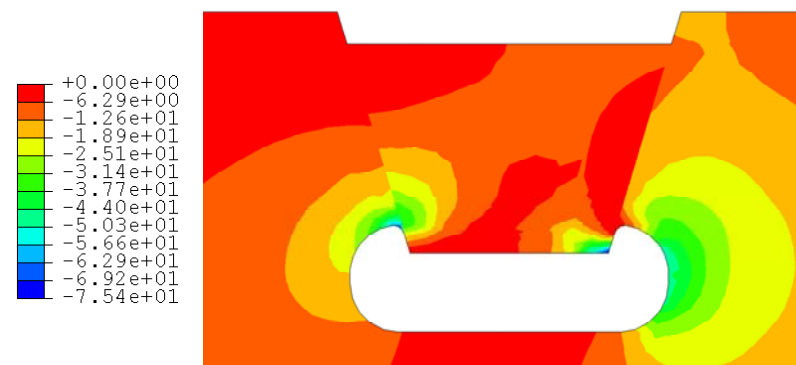
(a) Maximum Principal Stress on South Side (in Tension)



(b) Maximum Principal Stress on North Side (in Tension)

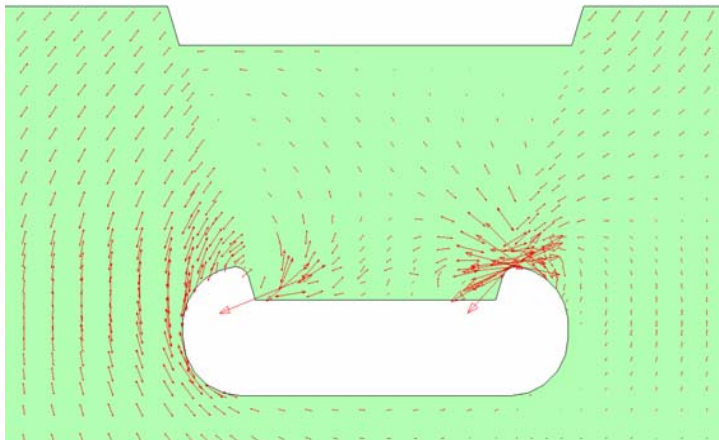


(c) Minimum Principal Stress on South Side (in Compression)

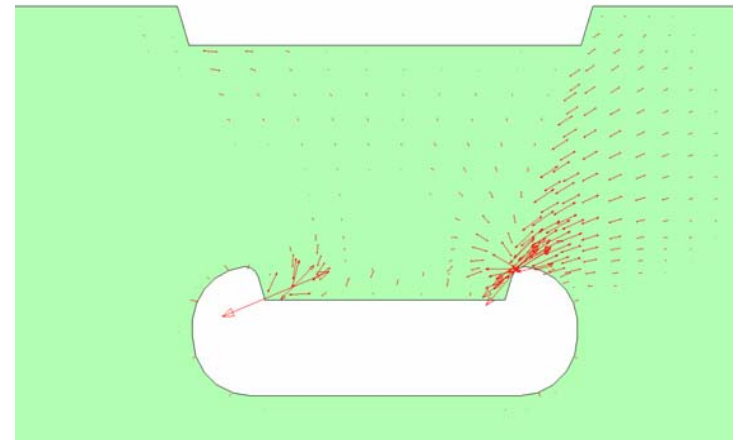


(d) Minimum Principal Stress on North Side (in Compression)

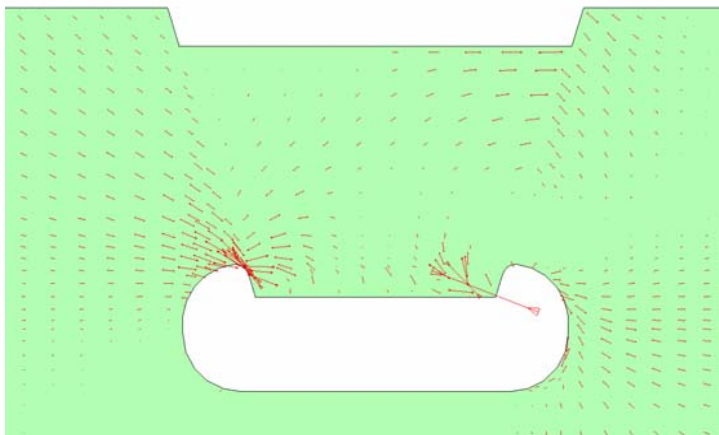
Figure 3.25 Model 2: Principal Stress Contour or Tensor at Detail B (MPa)



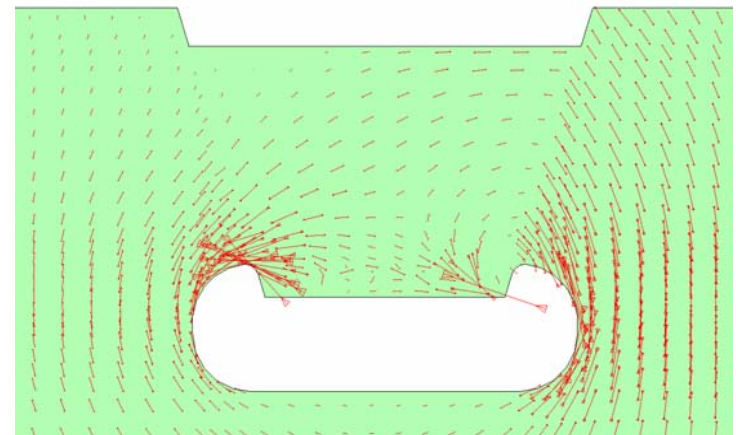
(e) Maximum Principal Stress Tensor on South Side (in Tension)



(f) Maximum Principal Stress Tensor on North Side (in Tension)



(g) Minimum Principal Stress Tensor on South Side (in Compression)



(h) Minimum Principal Stress Tensor on North Side (in Compression)

Figure 3.25 Model 2: Principal Stress Contour or Tensor at Detail B (continued)

3.4.3 Stress Distribution on Ribs near Rib-to-Deck Welded Joints

The same designation for the rib-to-deck joints in Model 1 is used for Model 2 (see Figure 3.16). The location and the direction of stresses of interest are shown in Figure 3.17. Plots of the predicted stresses on the deck plate and the rib along a span length 5000 mm, over which the loading is applied, are shown in Figures 3.26 to 3.29.

For Joint 1, the maximum stresses predicted on the deck plate are approximately 132 MPa (58 MPa in Model 1) in compression on the bottom surface and 130 MPa (60 MPa in Model 1) in tension on the top surface. The maximum stresses on the deck plate near Joint 2 are approximately 30 Mpa (49 MPa in Model 1) in tension on the bottom surface, and 29 MPa (45 MPa in Model 1) in compression on the top surface. The stress on the deck plate, located 10 mm away from the joints to the inside of the rib, is almost the same as the stress on the deck plate outside of the rib.

For the rib stresses near Joint 1, the maximum predicted stresses are approximately 55 MPa (55 MPa in Model 1) in tension on the inner surface, and 138 MPa (100 MPa in Model 1) in compression on the outer surface. For Joint 2, the maximum rib stresses are 58 MPa (92 MPa in Model 1) in compression on the inner surface and 61 MPa (97 MPa in Model 1) in tension on the outer surface.

From the results above, Model 2 for Specimens 2 to 6 produces higher stresses in both the deck plate and the rib near Joint 1, particularly in the deck plate. However, lower stresses are predicted in both the deck plate and the rib near Joint 2. Although the stress field on the bottom of the deck plate near Joint 2 is in tension, the level of stress is low as shown in Figure 3.28.

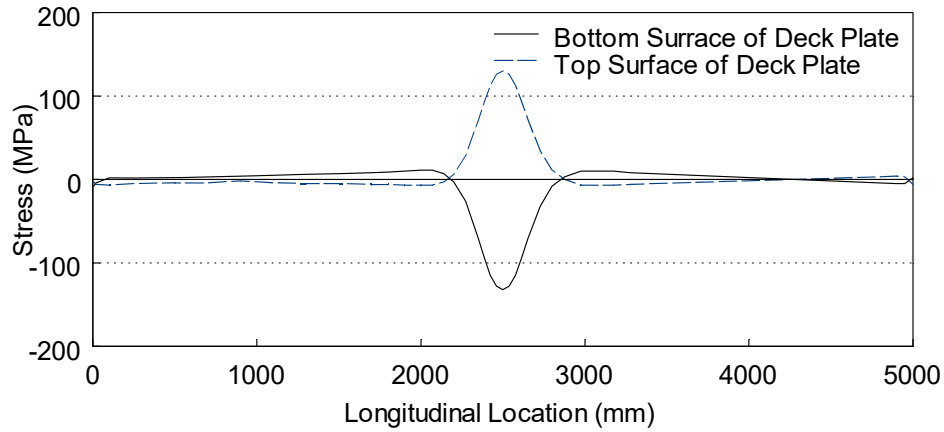


Figure 3.26 Model 2: Predicted Stresses in Deck Plate at Joint 1

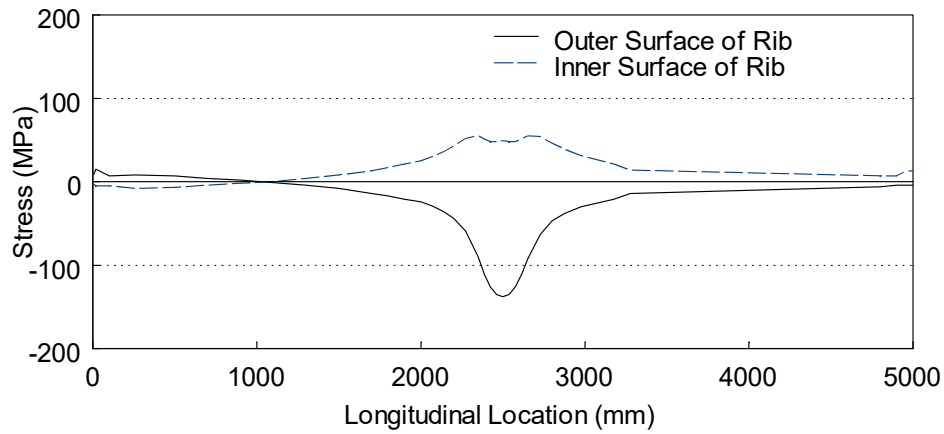


Figure 3.27 Model 2: Predicted Stresses in Ribs at Joint 1

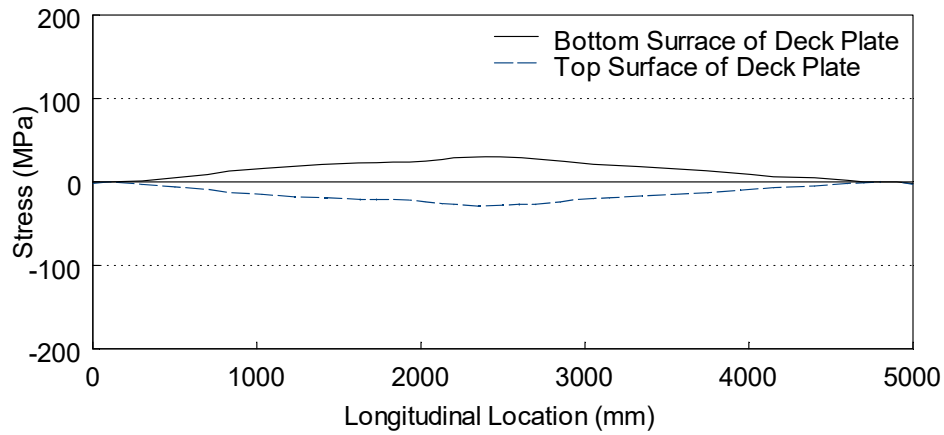


Figure 3.28 Model 2: Predicted Stresses in Deck Plate at Joint 2

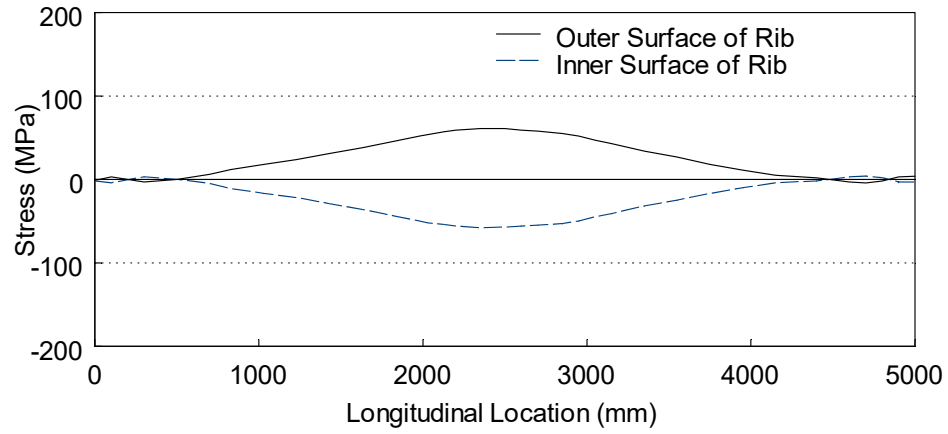


Figure 3.29 Model 2: Predicted Stresses in Ribs at Joint 2

4. SPECIMEN 1 TEST RESULTS

4.1 Testing Program

Specimen 1 was loaded with dual pads (a tandem configuration) centered at midspan (see Figure 4.1). The test setup is shown in Figure 4.2. The measured maximum vertical displacement of the deck plate at midspan was 7.1 mm (7.4 mm from ABAQUS analysis). Prior to fatigue testing, strain measurements were made approximately at every 1 kip actuator loading during 2 slow loading cycles with a frequency of 0.025 Hz. Two slow loading cycles were then conducted every 10,000 loading cycles with a loading frequency of approximately 3 Hz throughout the fatigue testing. Typical applied load and vertical displacement time histories are shown in Figure 4.3.

Large fatigue cracks in the rib walls below the bulkhead and diaphragm plates at the end supports were observed at 1 million cycles. Most of these fatigue cracks initiated from the weld toe below the bulkhead and propagated through the rib wall and were caused by the secondary stresses from the out-of-plane transverse bending of the rib wall at the cutout. No such cracks were observed at the interior support, which was confirmed by cutting out and examining small portions of the ribs at this support. This is expected because the loading scheme was designed to maximize the stress condition on the rib-to-deck welds. The applied loading scheme would not produce large stress range (see Figure 3.8 for the predicted deformation).

Full-axle loads were applied to this specimen. Although “pre-mature” cracks revealed the significant impact that truck overload could have on the orthotropic deck, the objective of this research to investigate the fatigue resistance of rib-to-deck welds was not achieved. Based on the observed crack pattern and subsequent finite element analysis (see Chapter 3), two measures were taken before the remaining five specimens were tested: (1) The magnitude of loading was reduced by 50% to reflect a half axle load. A half axle load is reasonable considering the width (3 m) of the test specimens. (2) The boundary condition at three supports was modified to mitigate the restraining effect imposed on the test specimen (see Section 4.4).

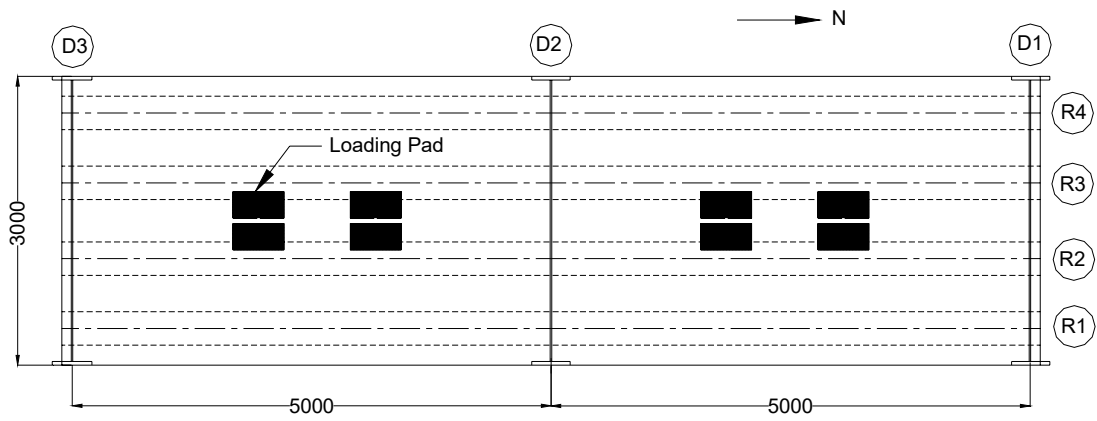


Figure 4.1 Specimen 1: Plan View with Rib and Diaphragm Designs

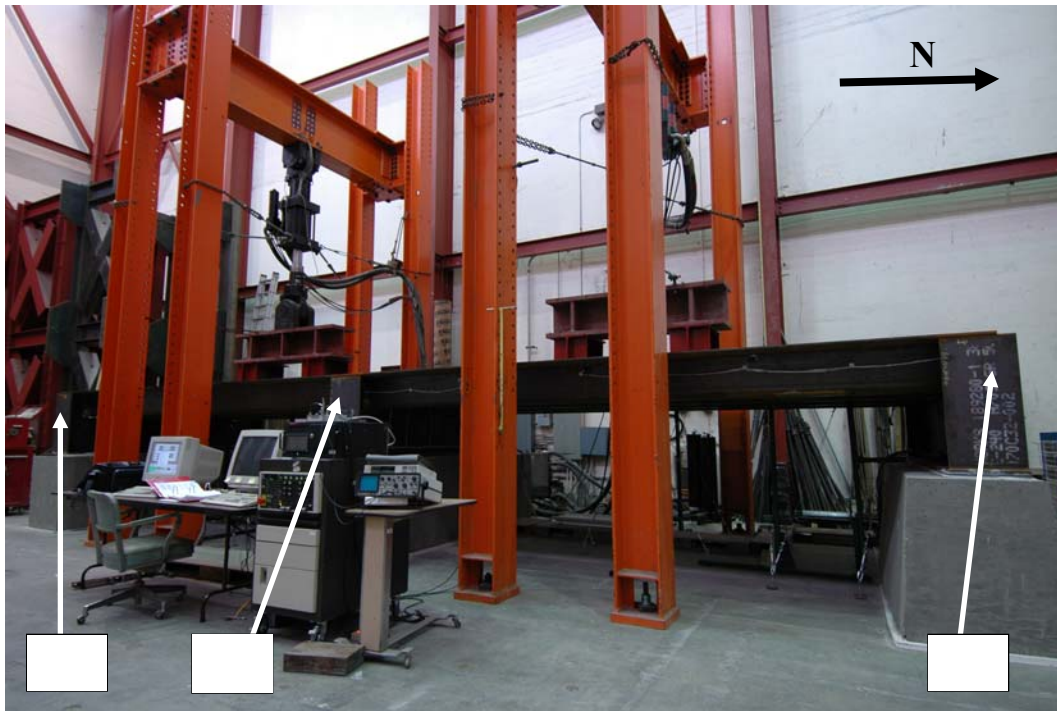


Figure 4.2 Specimen 1: Test Setup and Diaphragm Locations

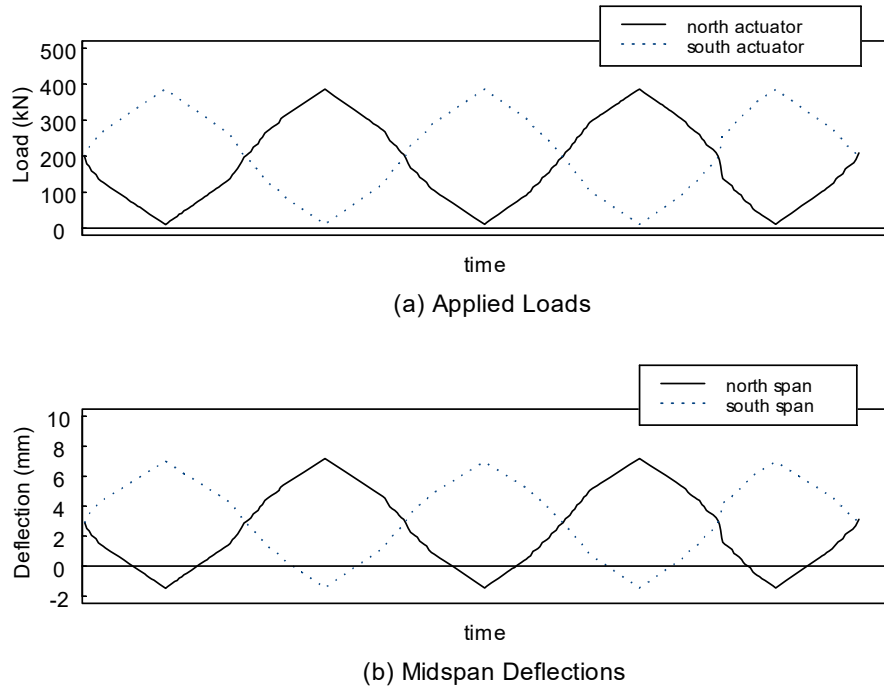
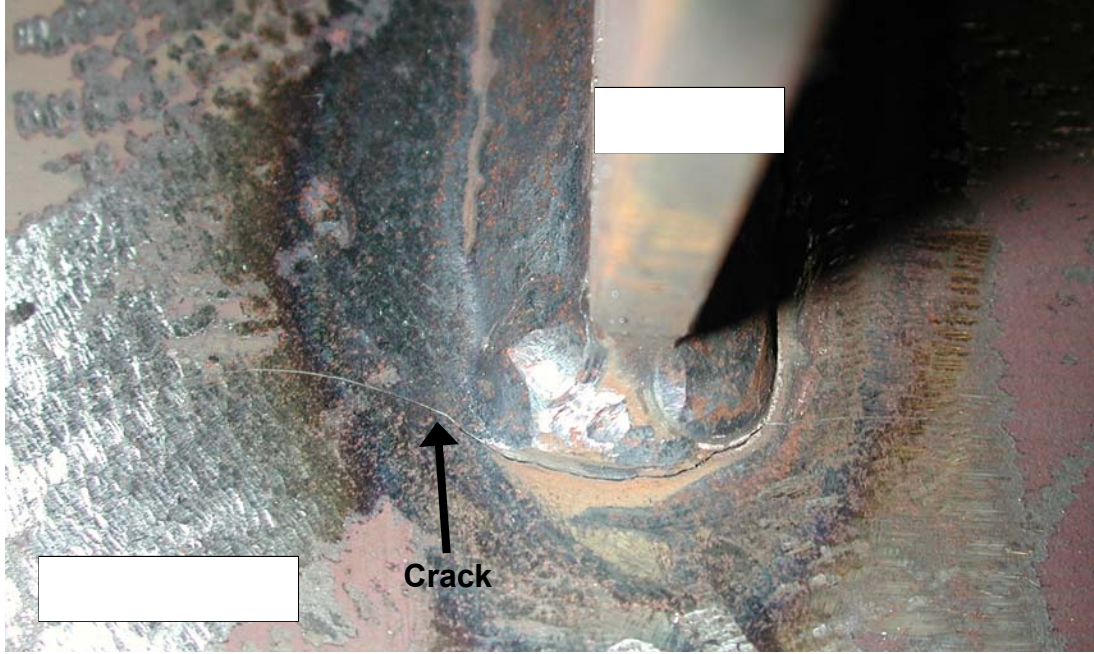


Figure 4.3 Specimen 1: Typical Applied Load and Measured Deflection Time History

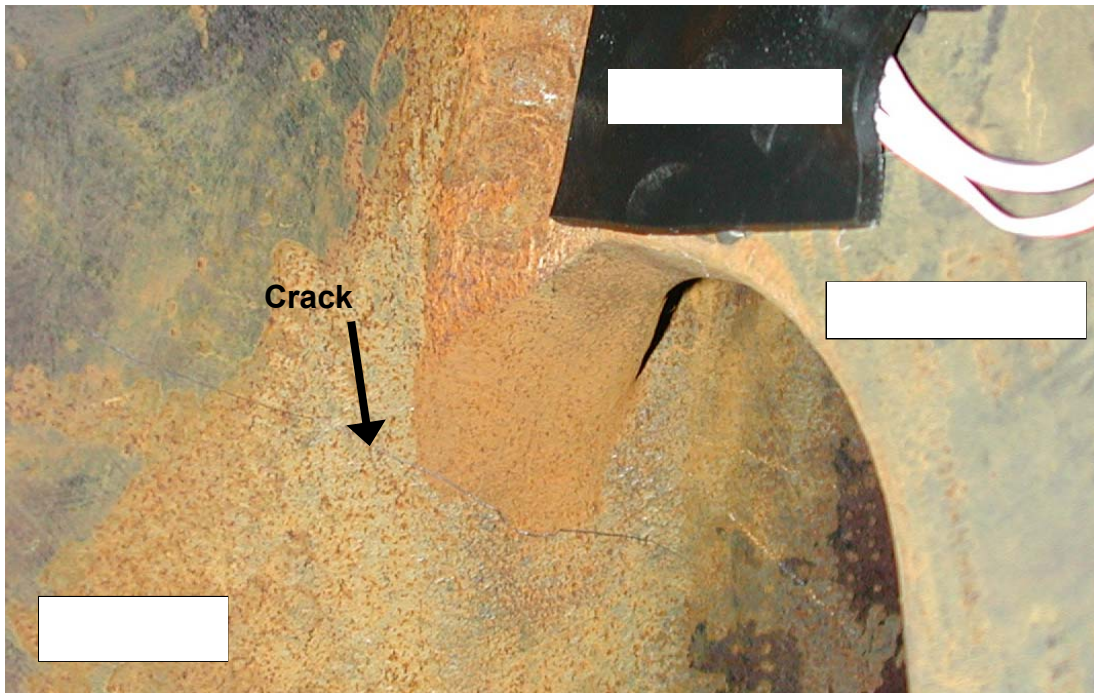
4.2 Fatigue Cracks in Ribs at End Support Diaphragms

Large fatigue cracks were observed at 6 locations at end supports. Figure 4.4 shows typical crack patterns on the rib below the bulkhead, as viewed from inside of the rib, and the diaphragm cutout, as viewed from outside of the rib. These fatigue cracks were produced by out-of-plane distortion due to torsion in the ribs at the end diaphragms.

Magnetic particle test was conducted to inspect the distortion-induced fatigue cracks at the end supports; the mapped cracks and photo views are shown in Figures 4.5 to 4.10. The horizontal length of the cracks measured varies from 25 mm to 106 mm. As verified by cutting the cross section through the cracks in Specimen 2, it shows a tendency that the cracks first initiated at the lower end of bulkhead-to-rib fillet weld. The cracks that initiated at the weld toe then propagated through the rib wall and tended to interconnect with another crack initiated from a location near the end of CJP weld on the outside of the rib (see Figure 5.30 for the cross section of the crack). Considering the large size of the cracks observed at 1 million cycles and the variation of the measured strains near the cracks, the cracks might have initiated much earlier than 1 million cycles.

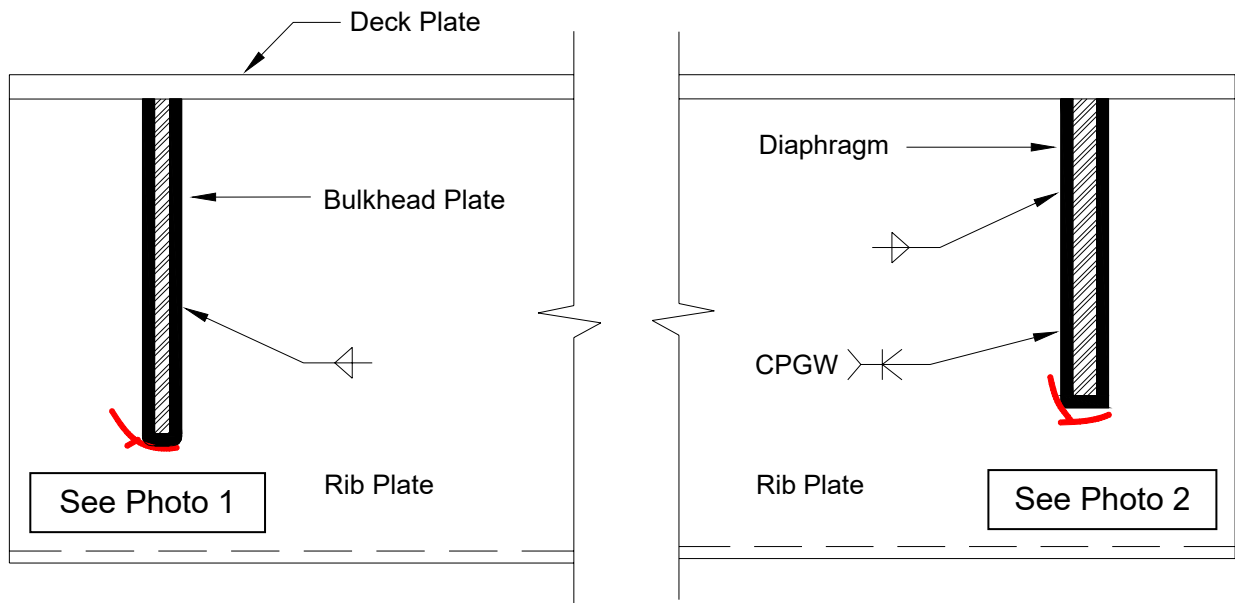


(a) View from Inside of Rib



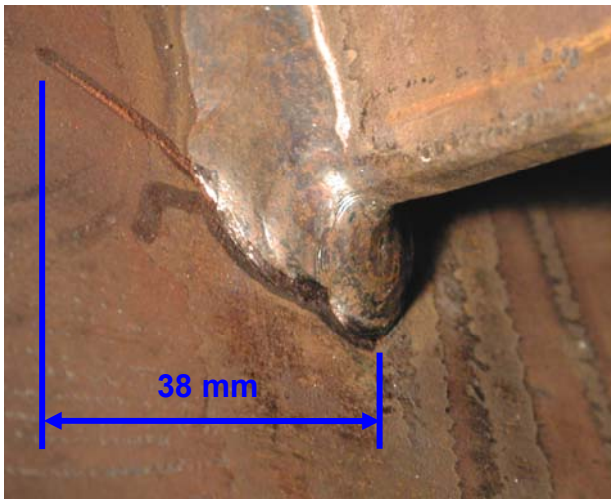
(b) View from Outside of Rib

Figure 4.4 Specimen 1: Crack Pattern on the Rib below bulkhead and diaphragm cutout

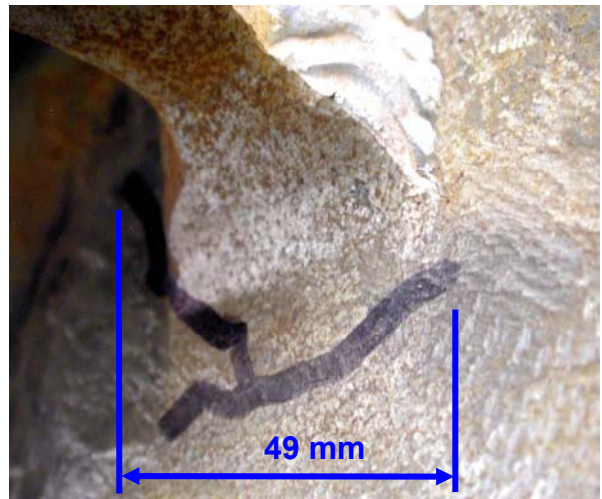


(a) Inner Surface of Rib

(b) Outer Surface of Rib

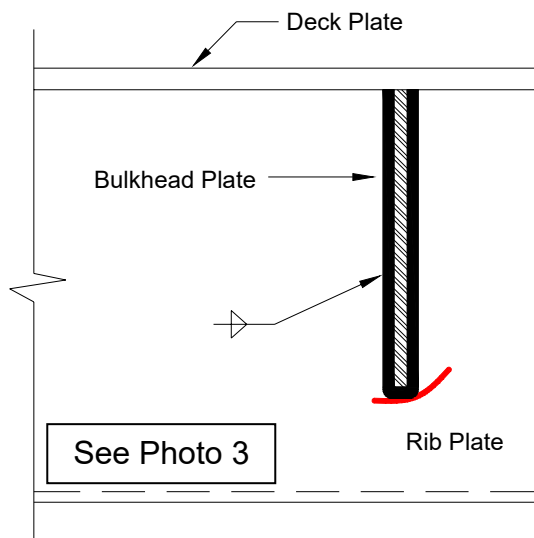


(c) Photo 1

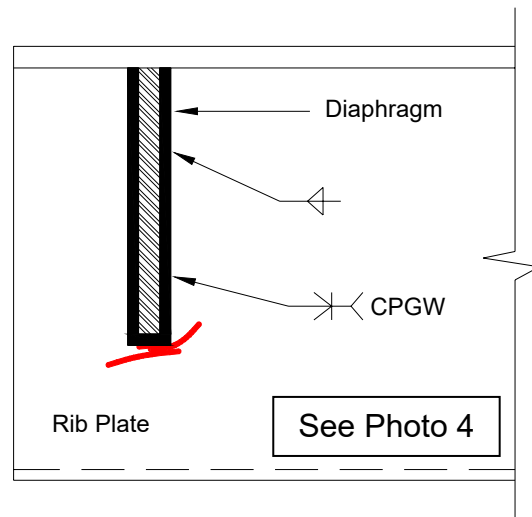


(d) Photo 2

Figure 4.5 Specimen 1: Fatigue Crack at D1-R2-East



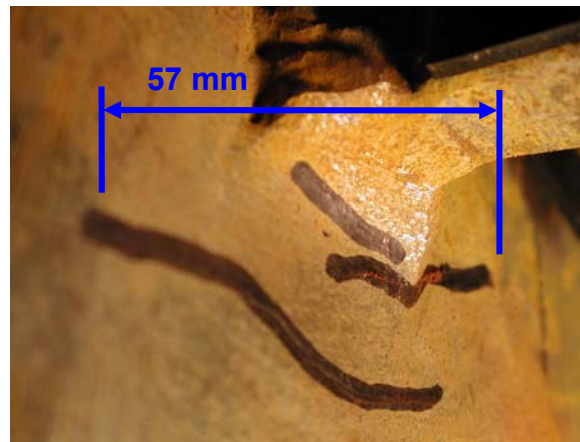
(a) Inner Surface of Rib



(b) Outer Surface of Rib

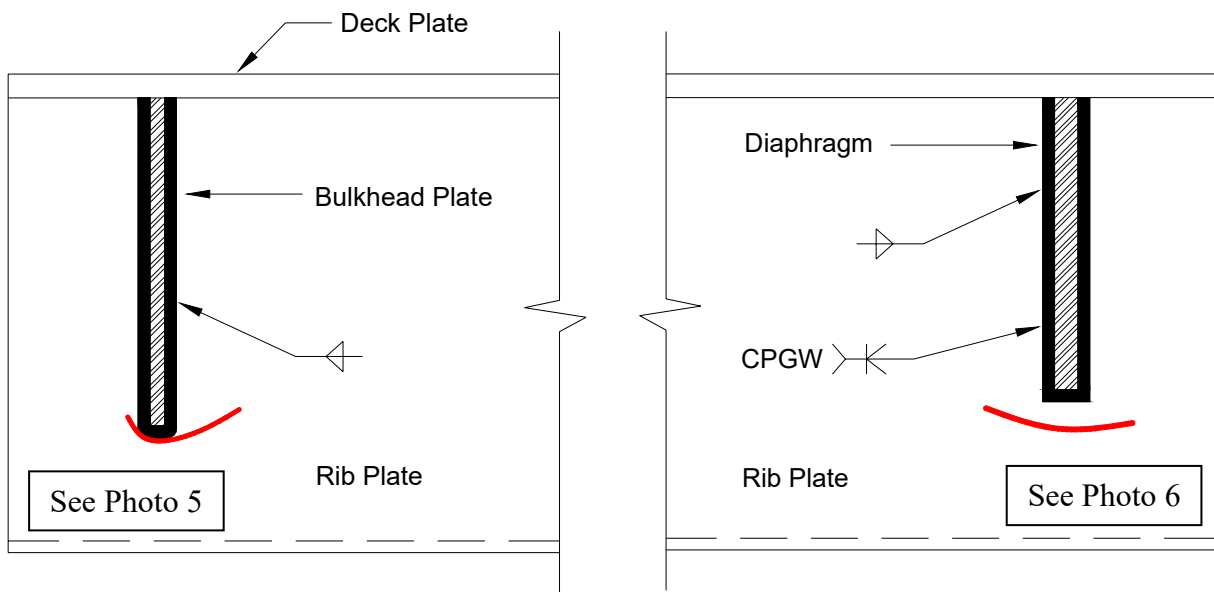


(c) Photo 3



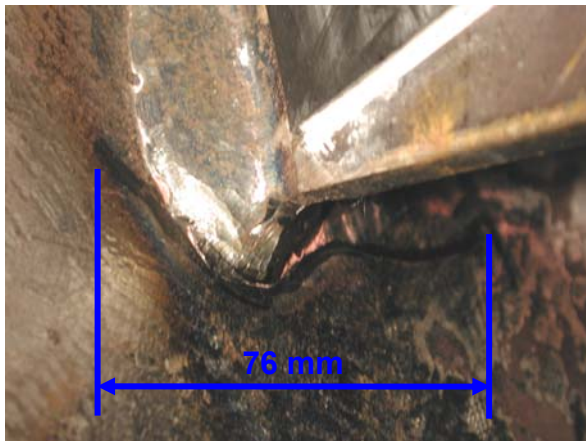
(d) Photo 4

Figure 4.6 Specimen 1: Fatigue Crack at D1-R2-West

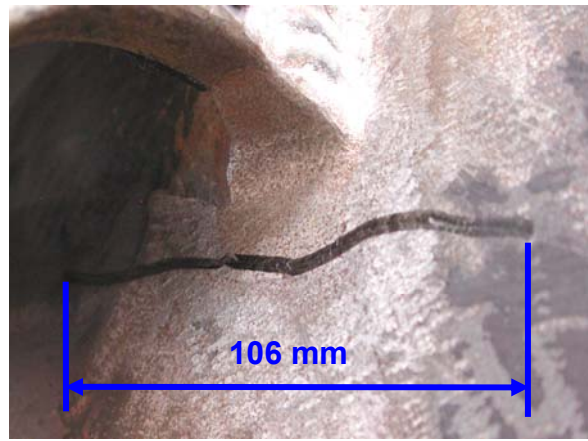


(a) Inner Surface of Rib

(b) Outer Surface of Rib

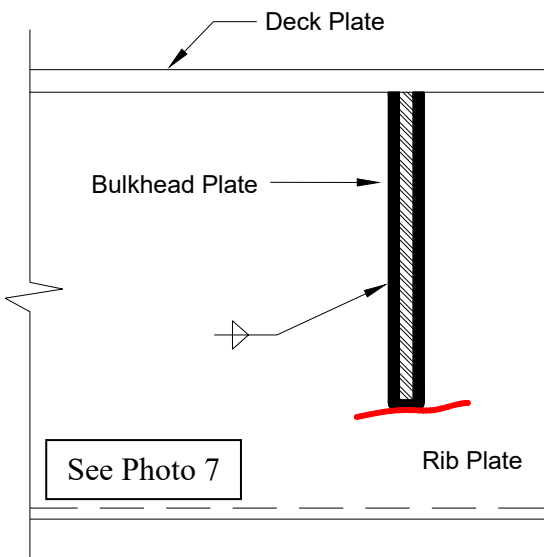


(c) Photo 5

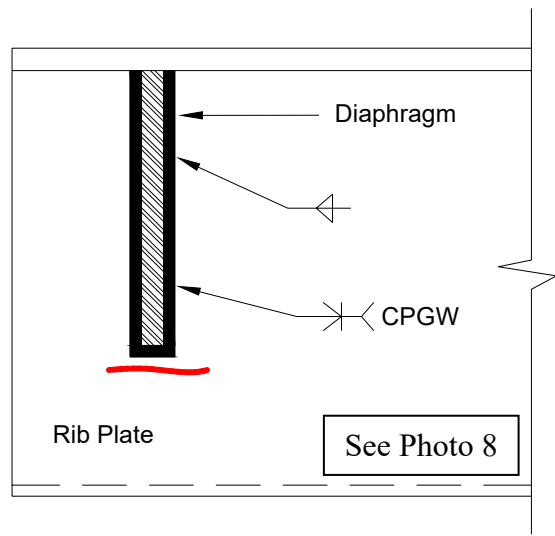


(d) Photo 6

Figure 4.7 Specimen 1: Fatigue Crack at D1-R3-East



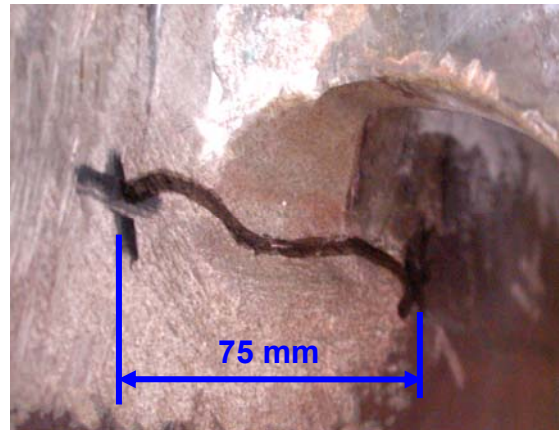
(a) Inner Surface of Rib



(b) Outer Surface of Rib

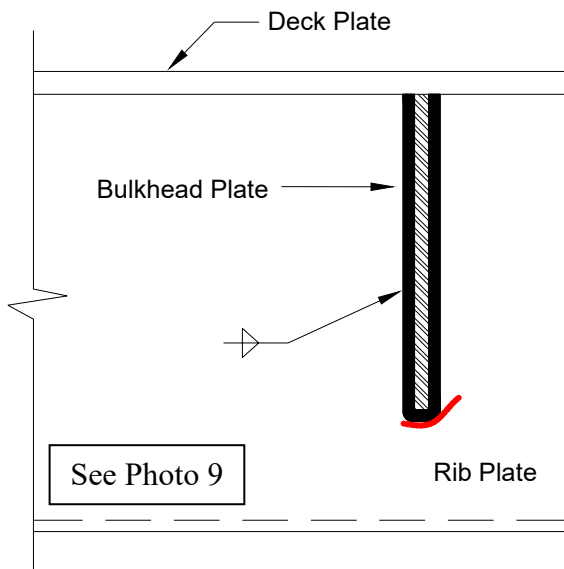


(c) Photo 7

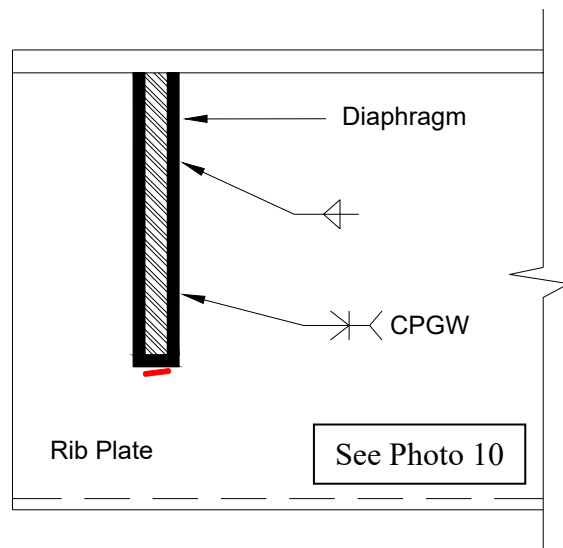


(d) Photo 8

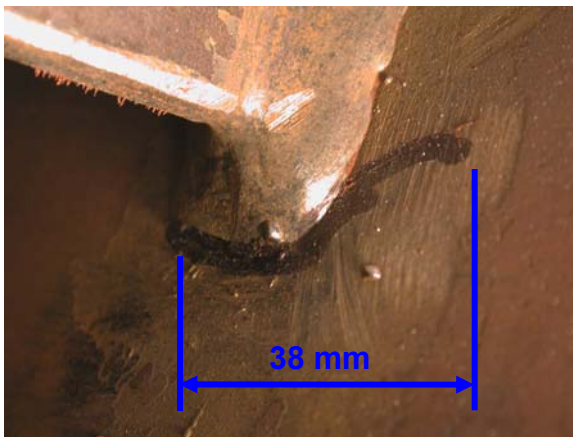
Figure 4.8 Specimen 1: Fatigue Crack at D1-R3-West



(a) Inner Surface of Rib



(b) Outer Surface of Rib

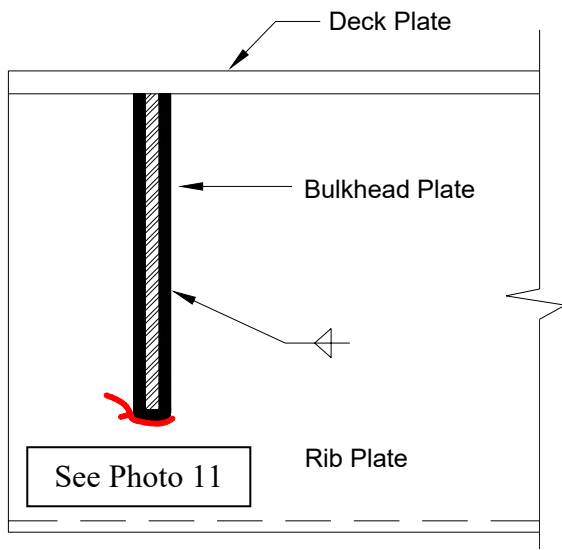


(c) Photo 9

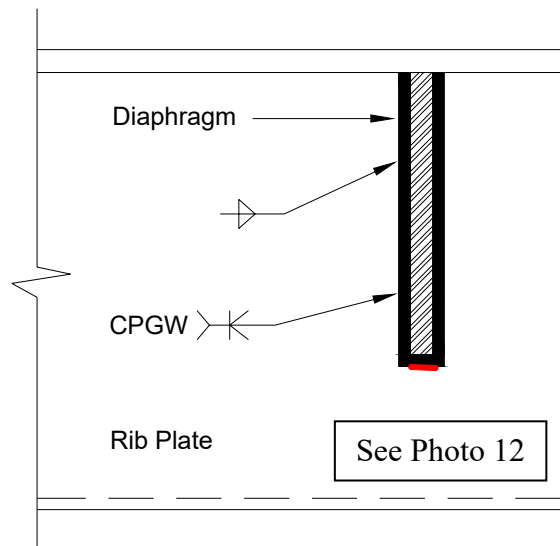


(d) Photo 10

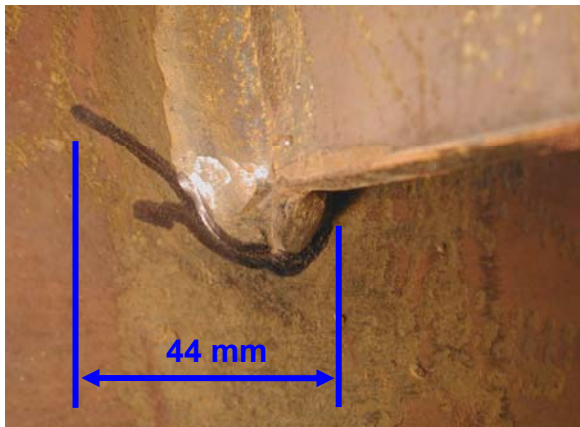
Figure 4.9 Specimen 1: Fatigue Crack at D3-R2-East



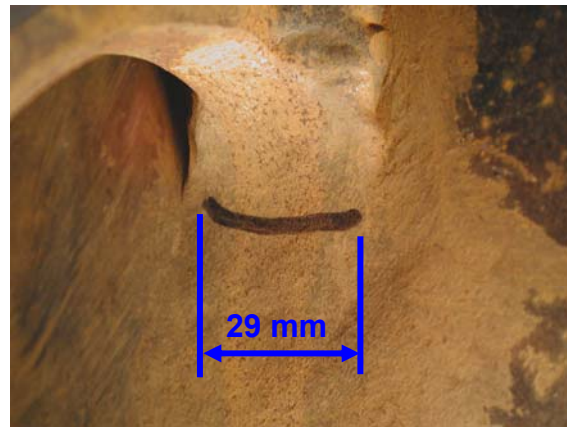
(a) Inner Surface of Rib



(b) Outer Surface of Rib



(c) Photo 11



(d) Photo 12

Figure 4.10 Specimen 1: Fatigue Crack at D3-R3-West

4.3 Measured Response

4.3.1 Rib Stress Distribution near the Rib-to-Deck Welds

Strain gage rosettes were installed on the rib walls to measure the strains near the rib-to-deck welds. From the strain measurements, the stresses were computed by multiplying the strains by the Young's modulus of 200 GPa. Table 4.1 summarizes the stress range (S_r) and the mean stresses (S_m) computed from the measured strains during the fatigue testing. The locations and orientations of the strain gage rosettes instrumented on the ribs near the rib-to-deck welds are shown in Figures 2.34 and 2.35. Plots of the stress range and the mean stresses during the fatigue testing are shown in Figures 4.11 and 4.12. As explained in Section 4.1, the strain measurements were made during 2 slow loading cycles with a frequency of 0.025 Hz, and the 2 slow loading cycles were done every 10,000 loading cycles with a loading frequency of approximately 3 Hz throughout the fatigue testing. For the plots of the stress range and the mean stresses, a total of 17 measurements of the maximum and minimum strains for each gage were selected at even intervals.

For outer surface of the rib walls, the maximum vertical stress range in the transverse direction perpendicular to the longitudinal rib-to-deck welds was 70.9 MPa (mean stress = 26.6 MPa) at gage r47-1 in tension field, and was 23.2 MPa (mean stress = -12.2 MPa) at gage r46-1 in compression field, at the 0.1 million cycle mark. For inner surface of the rib walls, the maximum vertical stress range in the transverse direction perpendicular to the longitudinal rib-to-deck welds was 21.8 MPa (mean stress = 12.1 MPa) at gage r60-1 in tension field, and was 63.9 MPa (mean stress = -30.6 MPa) at gage r61-1 in compression field.

From the strain gage rosettes r47-1 and r61-1 installed back-to-back on both sides of the rib walls on the western side of the rib R3 at midspan, the in-plane (i.e., average) stress was -0.25 MPa, and the out-of-plane (i.e., bending) stress was 62.3 MPa. From the back-to-back strain gage rosettes r46-1 and r60-1 on the eastern side of the rib R3 at midspan, the in-plane stress was -0.4 MPa and the out-of-plane stress was 23.4 MPa. From the back-to-back strain gage rosettes r44-1 and r56-1 on the eastern side of the rib R3 at a quarter point of the span, the in-plane stress was -5.5 MPa and the out-of-plane

stress was 20.1 MPa. From these back-to-back gages on both sides of the rib walls, it was found that the bending stresses are dominant. In the longitudinal direction parallel to the rib-to-deck welds, the stresses were low and were less than 10 MPa (see component 2 of each strain gage rosette in Table 4.1)

From the plots of the stress range and the mean stresses shown in Figures 4.11 and 4.12, it can be found that the stresses at the gages are approximately constant throughout the entire testing up to 1 million cycles. This may be an indication that no significant cracks were developed from the rib-to-deck welds.

Table 4.1 Specimen 1: Stress Range and Mean Stresses in Ribs near Rib-to-Deck Welds

Gage	Component	Stresses or Stress Range (MPa)					
		0.1 million cycles		0.5 million cycles		1 million cycles	
		S_r	S_m	S_r	S_m	S_r	S_m
r38	1	70.7	31.0	67.8	30.2	70.4	30.0
	2	0.5	-0.8	1.0	-0.7	0.9	-1.4
	3	41.4	15.9	38.9	13.8	41.0	10.0
r39	1	10.8	-7.1	14.4	-13.4	14.4	-13.6
	2	6.1	-0.7	6.6	-2.8	6.8	-1.4
	3	7.4	-1.0	8.6	-2.0	8.5	-2.8
r44	1	17.7	-16.8	16.6	-14.0	17.0	-10.7
r56	1	16.2	6.8	15.3	8.1	15.6	5.7
r46	1	23.2	-12.2	22.1	-13.7	23.0	-13.3
	2	9.1	-1.8	6.5	-0.6	8.7	-4.6
r60	1	21.8	12.1	20.6	14.1	22.0	11.4
	2	5.6	5.5	5.4	3.1	5.5	4.0
r47	1	70.9	26.6	68.3	30.7	72.8	30.0
	2	2.5	-1.6	1.5	-1.8	2.1	-2.8
	3	34.7	10.5	35.6	13.5	36.0	9.6
r61	1	63.9	-30.6	62.3	-27.2	65.2	-25.4
	2	1.9	0.7	2.1	1.3	2.1	2.0
	3	31.4	-9.3	31.0	-9.8	32.5	-11.2

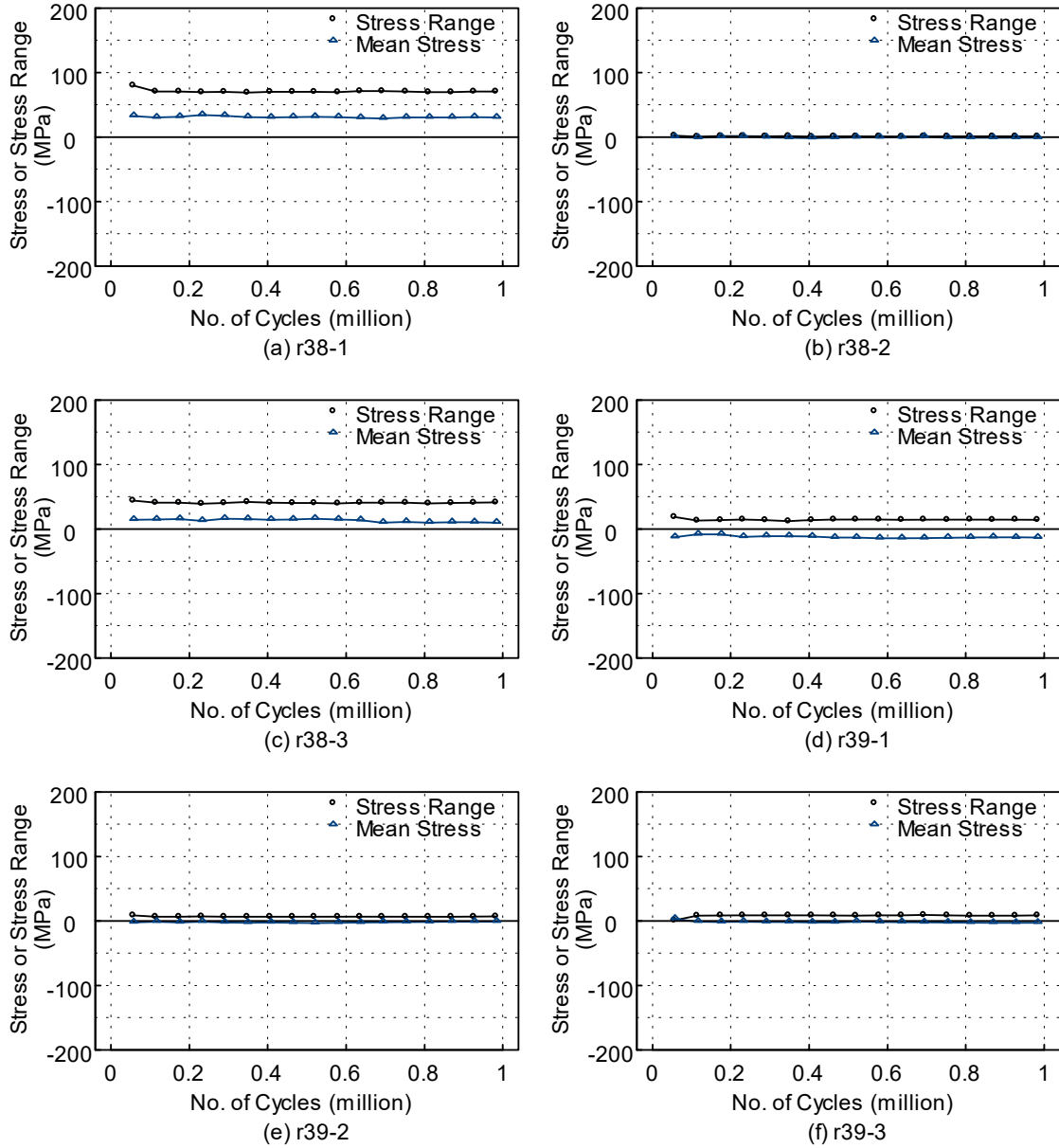


Figure 4.11 Specimen 1: Stress Range and Mean Stresses in Rib R2

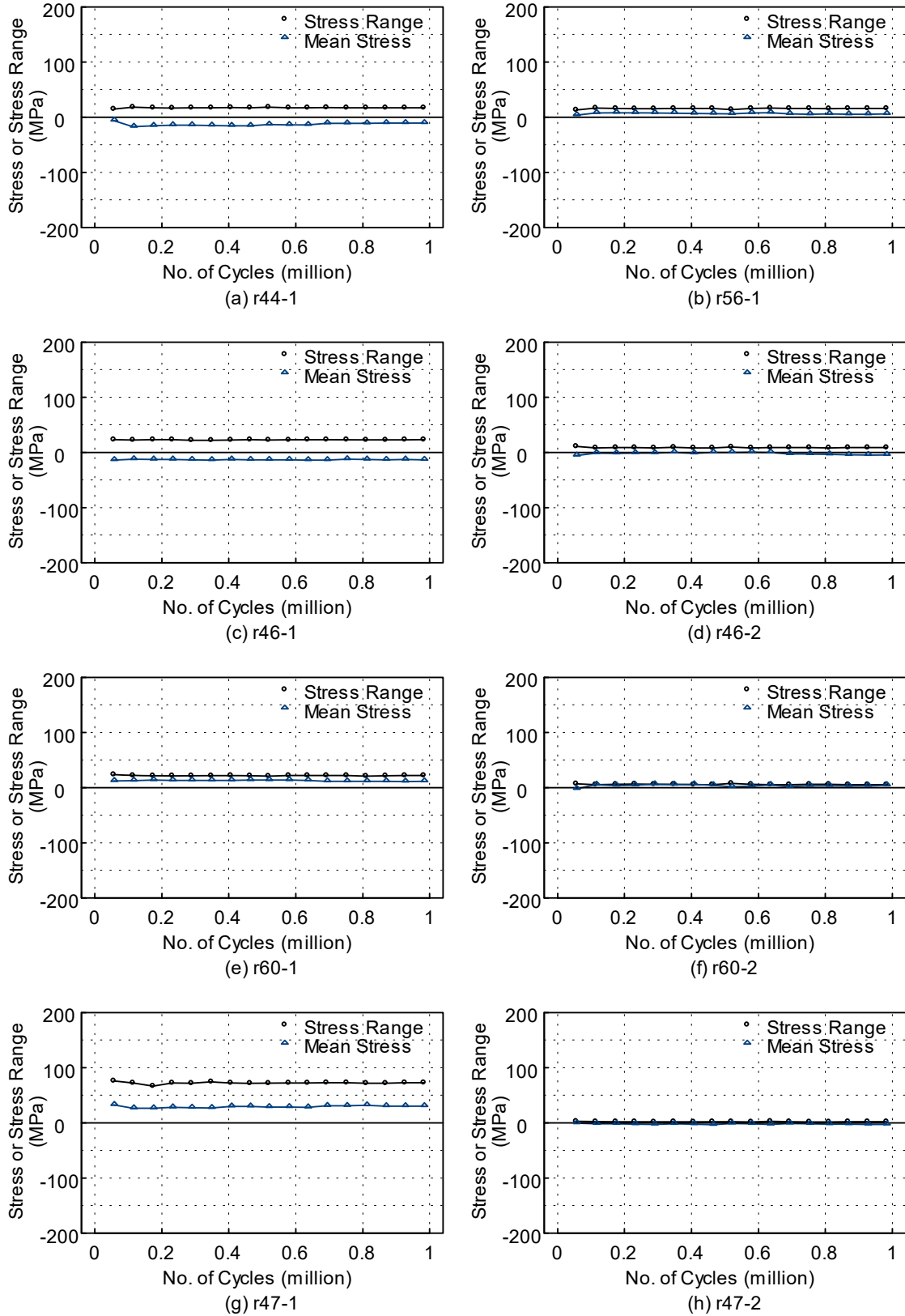


Figure 4.12 Specimen 1: Stress Range and Mean Stresses in Rib R3 near Rib-to-Deck Welds

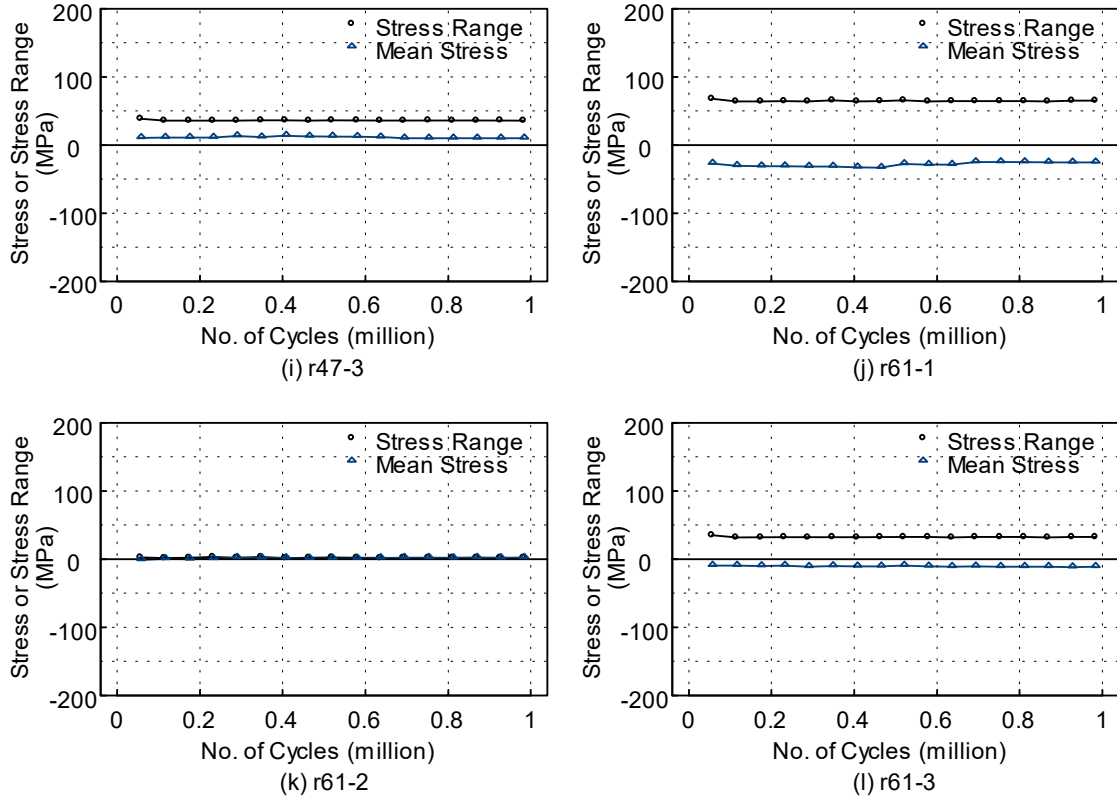


Figure 4.12 Specimen 1: Stress Range and Mean Stress in Rib R3 (continued)

4.3.2 Stress Distribution on Bulkheads and Diaphragms

The locations and orientations of the strain gage rosettes instrumented on the bulkheads and diaphragms are shown in Figure 2.49. The stress range (S_r) and the mean stresses (S_m) computed from the measured rosette strains on the bulkheads and diaphragms are summarized in Table 4.2. Plots of the stress range and the mean stresses are shown in Figure 4.13 for a strain gage rosette placed on the bulkhead and in Figure 4.14 for the strain gage rosettes placed on the diaphragms.

For the strain gage rosette r3 placed on the bottom corner of the bulkhead inside of the rib R3, the maximum stress range was 27.8 MPa (mean stress = 14.4 MPa) at 0.1 million cycle mark. But Figure 4.13 shows a significant variation of the stresses during the latter cycles. This variation of the stresses at the bulkhead was due to stress redistribution caused by a crack initiated from the rib-to-bulkhead weld toe below the bulkhead and propagated into the rib wall (see Figure 4.7 for the crack near strain gage rosette r3).

For the strain gage rosettes placed on the diaphragm plates near the diaphragm cutout at the end supports, Figure 4.14 shows that the maximum stress range in compression field at 0.1 million cycle mark was 84.1 MPa (mean stress = -33.2 MPa) at rosette r4-3, and the maximum stress range in tension field was 57.4 MPa (mean stress = 25.5 MPa) at rosette r5-3. For the strain gage rosettes placed on the diaphragm plates near the diaphragm cutout at the interior support, the stresses were primarily in compression field, with the maximum stress range of 51.5 MPa (mean stress = -45.3 MPa) at 0.1 million cycle mark on rosette r6-3. From the plots of the stress range and the mean stresses of the strain gage rosettes on the diaphragm plate [e.g., Figure 4.14(c)], some variation of the stresses due to crack development was also evident.

Table 4.2 Specimen 1: Stress Range and Mean Stresses on Bulkheads and Diaphragms

Gage	Component	Stress or Stress Range (MPa)					
		0.1 million cycles		0.5 million cycles		1 million cycles	
		S _r	S _m	S _r	S _m	S _r	S _m
r3	1	27.8	14.4	24.4	13.0	18.2	33.6
	2	11.9	-2.8	7.7	-26.7	2.9	-91.5
	3	6.5	19.9	5.1	43.3	2.8	206.3
r1	1	26.7	8.3	24.4	9.0	28.0	21.6
	2	11.2	1.0	10.0	1.0	7.1	-10.1
r5	3	57.4	25.5	57.4	20.4	56.9	-3.0
r2	1	24.3	7.1	22.8	5.4	28.0	12.2
	2	11.1	4.9	10.1	-0.2	8.1	-7.7
	3	15.6	8.6	12.4	1.3	10.8	-1.4
r4	1	18.0	-5.1	17.3	-8.1	22.5	-20.8
	3	84.1	-33.2	81.8	-25.3	85.4	-32.1
r6	1	35.5	-7.3	33.1	-6.6	35.0	-7.6
	2	2.1	1.4	2.1	0.0	2.1	2.1
	3	51.5	-45.3	48.6	-46.3	50.2	-41.7
r21	2	14.8	-12.3	14.4	-11.3	15.0	-13.3
r13	1	23.5	-22.9	23.6	-23.8	24.3	-24.2
r19	2	20.1	-12.0	19.3	-14.9	20.0	-16.7
	3	50.1	-39.6	49.0	-39.4	50.7	-41.4
r24	1	4.0	3.5	2.7	6.6	2.8	2.0
r25	1	17.4	7.7	16.5	6.9	17.3	6.8
	2	10.8	12.9	10.7	18.8	11.7	14.5
	3	17.2	2.1	16.3	-3.1	17.7	1.1

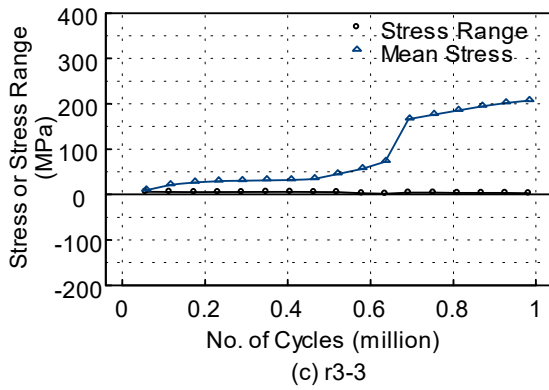
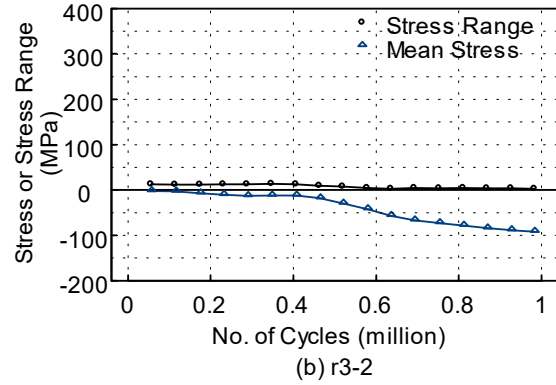
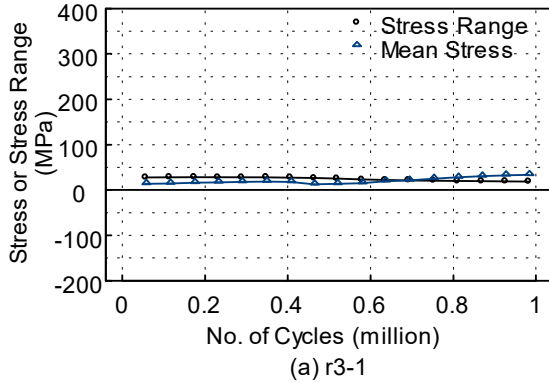


Figure 4.13 Specimen 1: Stress Range and Mean Stresses on Bulkhead

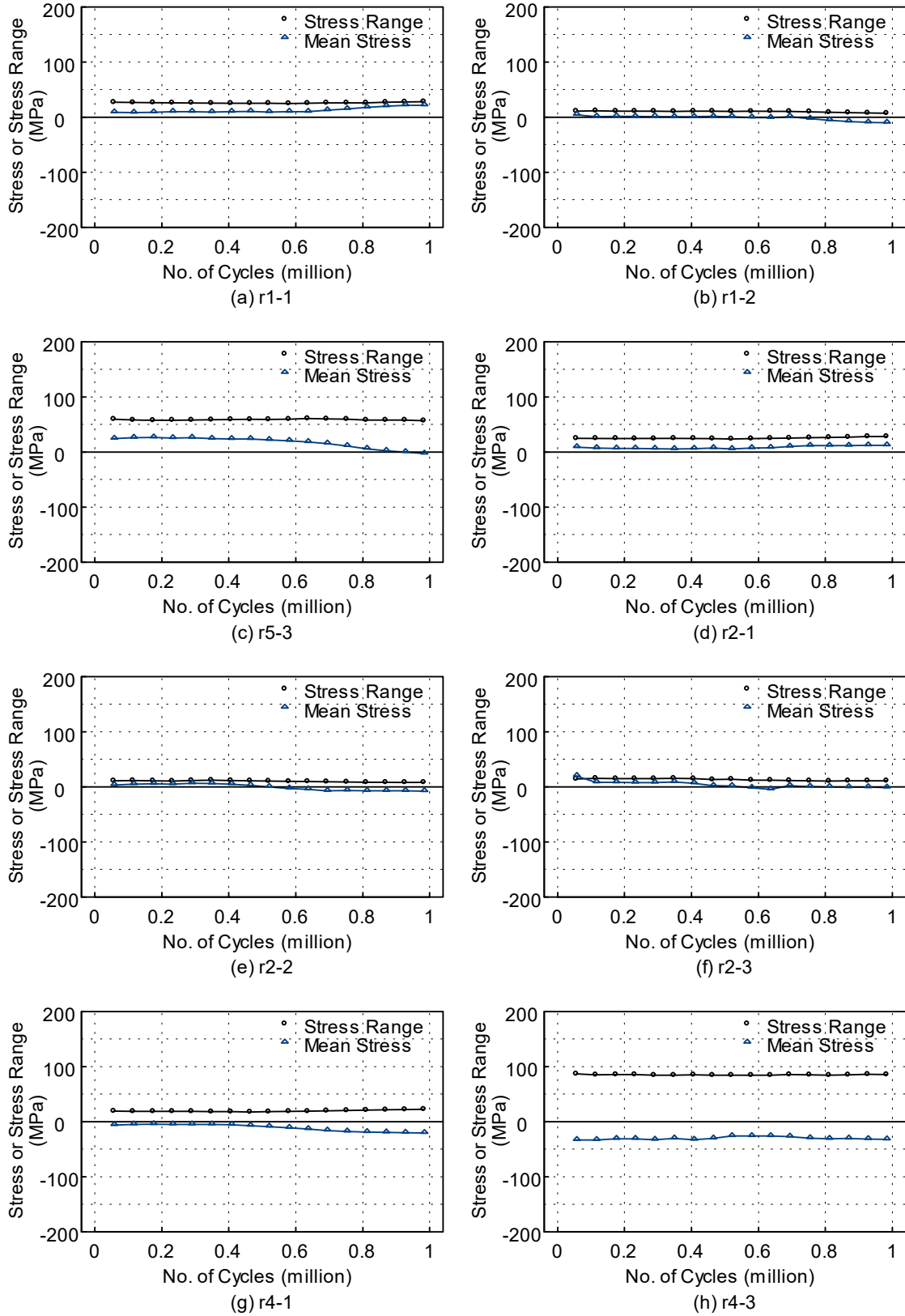


Figure 4.14 Specimen 1: Stress Range and Mean Stresses on Diaphragms

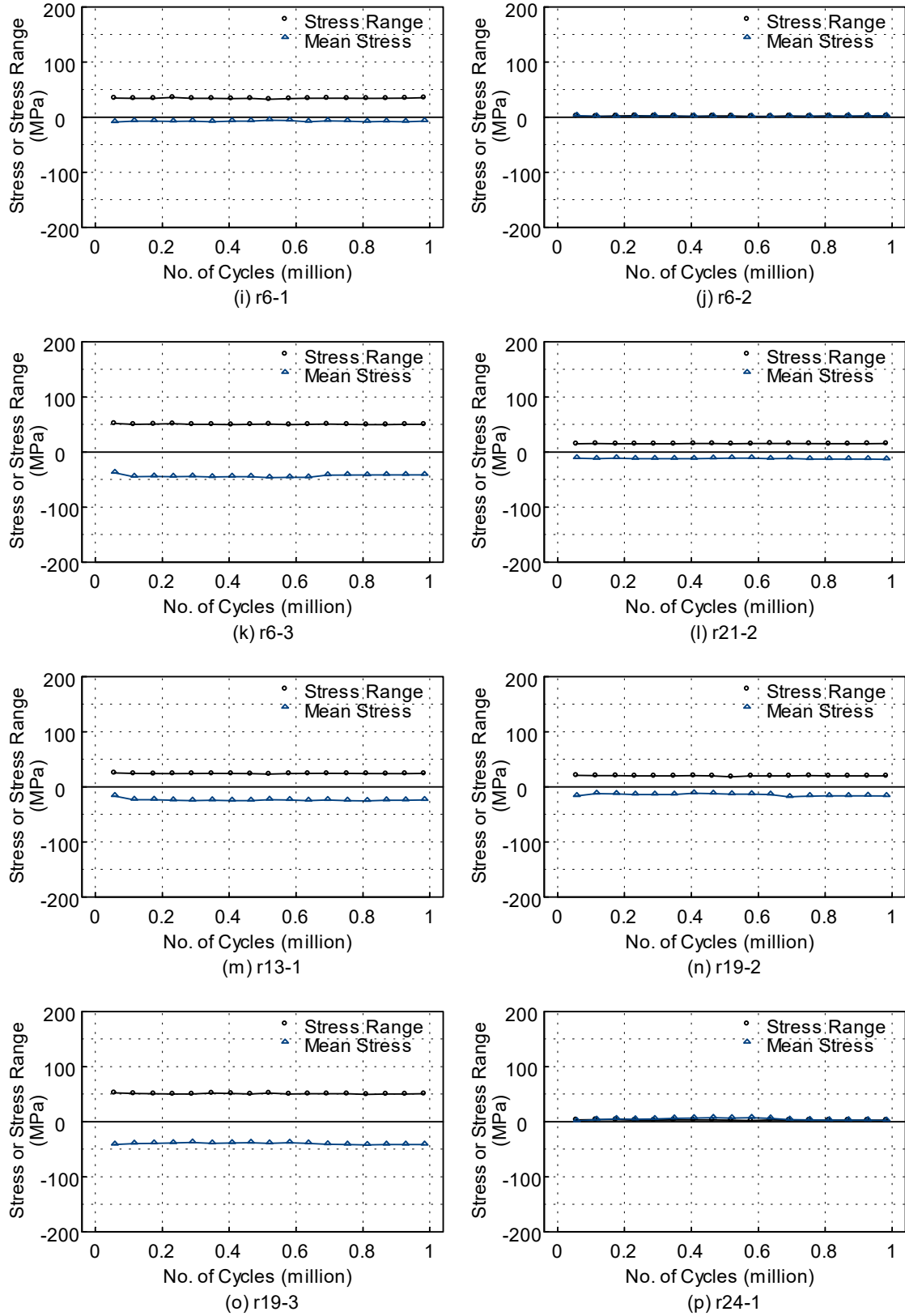


Figure 4.14 Specimen 1: Stress Range and Mean Stress on Diaphragms (continued)

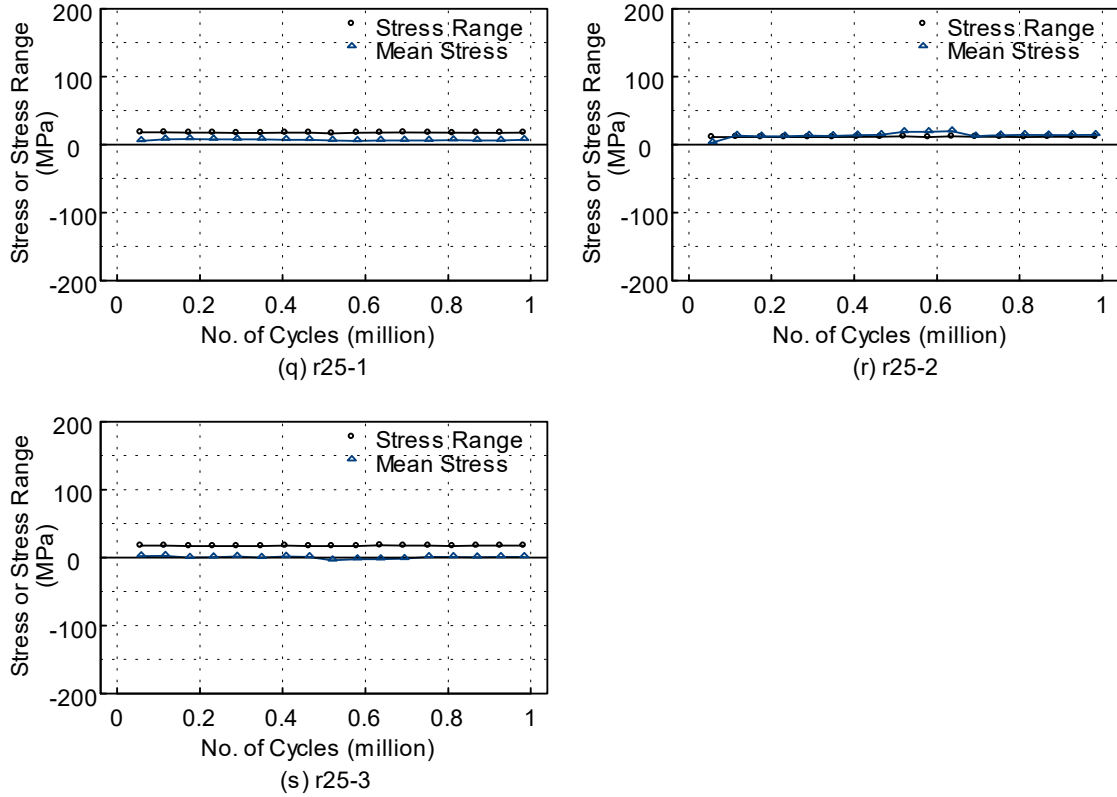


Figure 4.14 Specimen 1: Stress Range and Mean Stresses on Diaphragms—continued

4.3.3 Stress Comparisons between Predicted and Measured Responses

In general, the finite element analysis results by ABAQUS (ABAQUS Inc. 2005) prior to testing showed a good agreement with the measured response of the deck specimen. As shown in Table 4.3, the maximum vertical displacement of the deck plate at midspan was predicted to be 7.1 mm from FEM, and the measured displacement was very close to the predicted one. Figure 4.15 shows the location and orientation of the uni-axial strain gages at midspan; the predicted and the measured responses summarized in Table 4.3 show good agreement.

Table 4.3 Specimen 1: Comparison between predicted and Measured Responses

Midspan	Measured Response	Predicted Response
Vertical Displacement	7.1 mm	7.4 mm
Stress at “a”	120 MPa	126 MPa
Stress at “b”	-27.8 MPa	-31 MPa
Stress at “c”	66 MPa	71 MPa

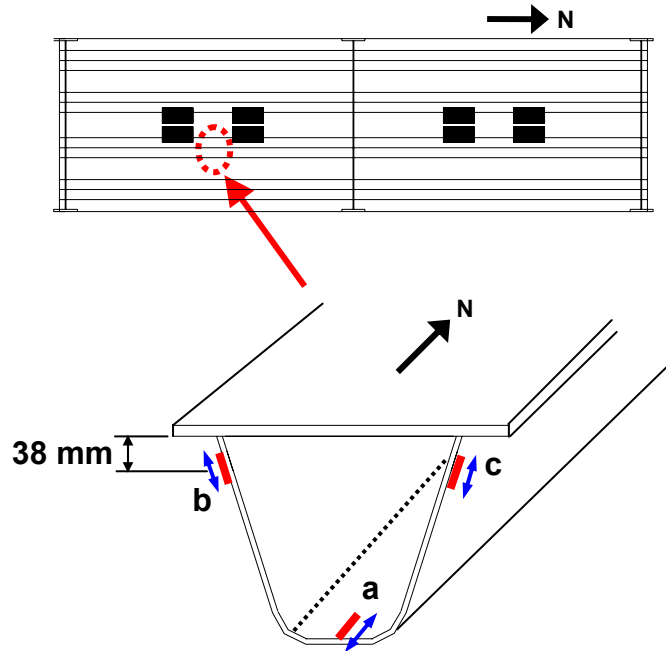


Figure 4.15 Specimen 1: Comparison between Predicted and Measured responses

4.4 Modifications for Testing of Specimens 2 to 6

Since fatigue cracking occurred very early due to high level of loading and the restraining boundary condition, the magnitude of loading was reduced by 50% (i.e., 188 kN) to reflect a half axle of HS-15 truck that the width of specimen can accommodate. The tandem axle configuration with dual pads was also modified to a single axle to be consistent with the truck configuration specified in the AASHTO Specification. Another modification made was the boundary condition at the support diaphragms. In order to create a more flexible boundary condition at the supports, a half-circular rod (diameter = 13 mm) was inserted between the base plate of the end diaphragm and the concrete support block to accommodate a free rotation of the support. The end stiffener plates were also removed from all diaphragms. Figure 4.17 shows the modifications made to the support boundary conditions for testing of each of the remaining specimens. The finite element analysis results verified that the stresses at end diaphragms were significantly reduced with the modification of the loading scheme. The stresses were reduced by approximately 10% with the modified boundary conditions (see Figure 4.16).

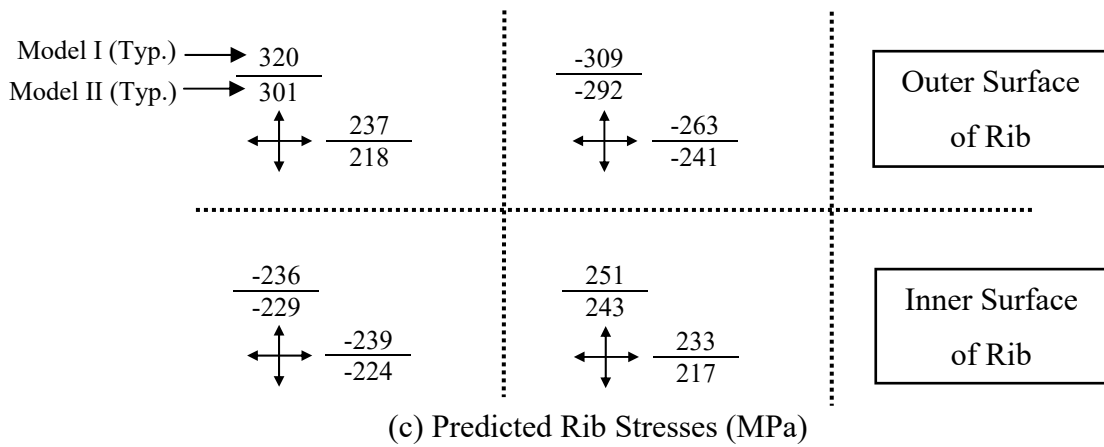
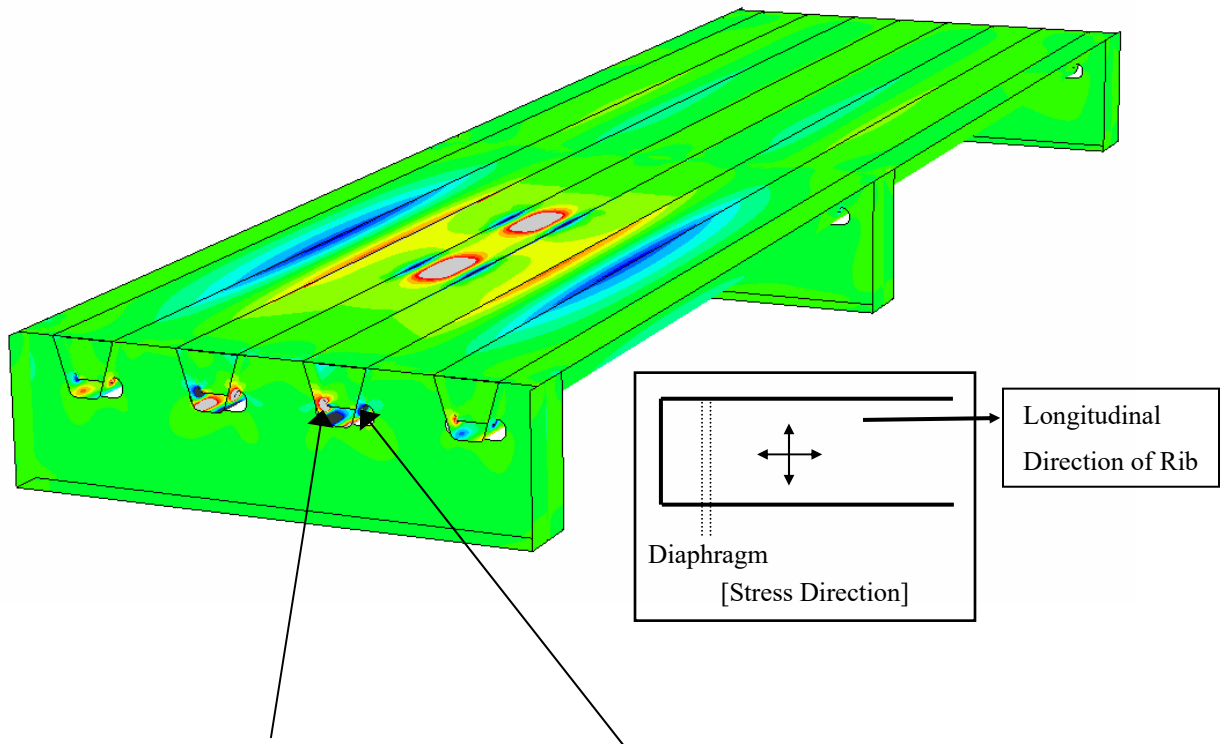
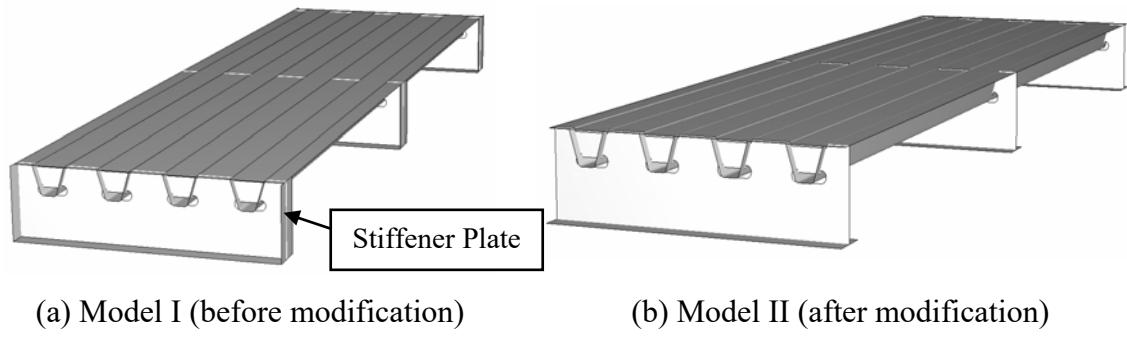


Figure 4.16 Model Configuration and Predicted Rib Stresses at Cutout Location (MPa)



before Modification



after Modification

(a) Removal of End Stiffener Plates



(b) A Half-Circular Rod beneath Base Plate

Figure 4.17 Boundary Condition Modifications

5. SPECIMENS 2 TO 6 TEST RESULTS

5.1 Testing Program

Fatigue testing was conducted for each of the remaining 5 specimens up to 6 million cycles. Each specimen was loaded with a single pad centered at the midspan (see Figure 5.1 for plan view). The measured maximum vertical displacement of the deck plate measured at midspan was approximately between 4 mm and 6 mm (4.8 mm from ABAQUS analysis). See Figure 4.2 for sample load and displacement responses. Strain measurements were made approximately at every 1 kip actuator loading during 2 slow loading cycles with an approximate frequency of 0.025 Hz, and then the 2 slow loading cycles were conducted every 10,000 loading cycles with a frequency ranged between 3.8 Hz and 5.7 Hz throughout the fatigue testing.

Since no significant damage at the rib-to-deck PJP welds was observed, the magnitude of loading (188 kN) was increased by 50% to 282 kN for the next one million cycles, and twice of the original load level (376 kN) was used for the last one million cycles before the test was stopped. The maximum vertical displacement of the deck plate at midspan increased linearly for each of the increased loading level. Regions of rib-to-deck welds under the loading pad were cut out for crack inspection after completion of testing at 8 million cycles. Fatigue cracks at the rib-to-deck welds were observed from 3 specimens (Specimens 2, 3, and 6). Most of the observed cracks at the rib-to-deck welds showed a pattern that the fatigue crack initiated from the weld toe on the bottom of the deck plate, and propagated upward into the deck plate. One crack from Specimen 6 initiated from the weld root, which was not visible from outside of the rib, and propagated into the deck plate. The crack from the weld root started from the region of transition between 80% PJP with no melt-through and 100% PJP with melt-through.

Ultrasonic test (UT) was conducted by a local inspection company to detect cracks at the rib-to-deck welds each time the loading level was increased by 50%. Unfortunately, such effort was no fruitful due to the complicated local geometry at the rib-to-deck welded joints. Therefore, it was not clear when the cracks at these welds were initiated.

With the modified loading scheme and boundary condition, the development of the fatigue cracks that initiated from the rib-to-bulkhead weld toe was delayed significantly. Crack regions at the support diaphragms were cut out for further crack inspection after completion of testing at 8 million cycles. Like Specimen 1, the distortion-induced fatigue cracks at the end supports first initiated at lower end of the bulkhead-to-rib fillet welds. The cracks then propagated into the rib wall, which tended to interconnect with another crack initiated from a location near the end of CJP weld on the outside of rib.

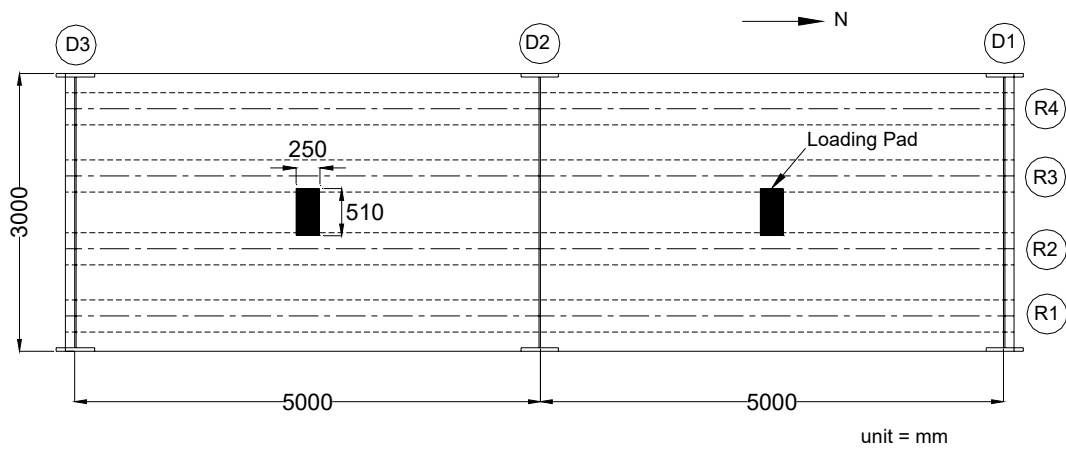


Figure 5.1 Specimens 2 to 6: Plan View with Rib and Diaphragm Designations

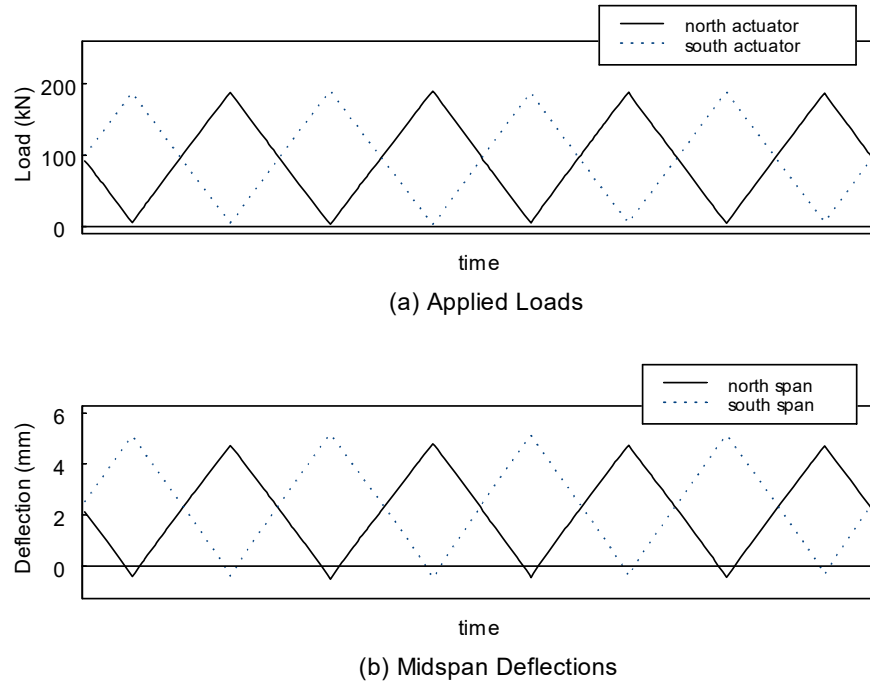


Figure 5.2 Specimens 2 to 6: Typical Applied Load and Measured Deflection Time History

5.2 Measured Response near the Rib-to-Deck PJP Welds

5.2.1 Deck Plate Stress Distribution

Strain gages were installed on the deck plate to measure the strains near the rib-to-deck welds, primarily in the transverse (or width) direction. The stress range (S_r) and the mean stress (S_m) computed from the measured strains are summarized in Tables 5.1 to 5.3 (gage readings for Specimens 2 and 3 were not reliable and are not presented). Figures 5.3 to 5.5 show the plots of the stress range and the mean stress during the entire fatigue testing conducted up to 8 million cycles. For Specimen 5, data beyond 7 million cycles are not presented due to problems with the data acquisition system. The jump of strain readings after 6 million and 7 million cycles was due to the increase of load magnitude.

The location and orientation of the strain gages on the deck plate near the rib-to-deck welds were shown in Figures 2.31 to 2.33. Strain gages on the bottom side of the deck plate were placed either 10 mm or 25 mm away from the weld toe of the rib-to-deck welds. The stresses in the deck plate near the rib-to-deck welds were low during the first

6 million cycles. The maximum stress range of 35.9 MPa (mean stress = 12.6 MPa) in tension field on the bottom of the deck plate, which occurred at 0.1 million cycle, was computed at gage S49 in Specimen 4. This midspan gage was placed 25 mm away from the weld toe on the bottom of the deck plate and oriented in the transverse direction. The maximum stress range of 33.3 MPa (mean stress = -19.5 MPa) in compression field on the bottom of the deck plate was computed from component 1 (transverse direction) of rosette r21 in Specimen 4. This strain gage rosette was placed 10 mm away from the weld toe on the bottom of the deck plate.

In order to compute the in-plane and out-of-plane (bending) stress components from the strain measurements in the transverse direction, a pair of uni-axial strain gages were placed on both sides of the deck plate on the eastern side of the rib R2 and on the western side of the rib R3 in Specimens 5 and 6 (see Figures 2.32 and 2.33). For the S19 and S20 pair in Specimen 5, the in-plane stress was 4.8 MPa and the out-of-plane stress was 16.5 MPa at 0.1 million cycle. For the S31 and S32 pair in Specimen 6, the in-plane stress was 3.7 MPa and the out-of-plane stress was 14.7 MPa at 0.1 million cycle.

Table 5.1 Specimen 4: Stress Range and Mean Stress in Deck Plate near the PJP Welds

Gage	Component	Stress or Stress Range (MPa)									
		0.1 M cycles		3 M cycles		5.9 M cycles		6.5 M cycles		7.5 M cycles	
		S _r	S _m	S _r	S _m	S _r	S _m	S _r	S _m	S _r	S _m
r17	1	1.0	-0.7	0.4	-1.8	2.0	-2.7	7.3	-6.0	8.8	-7.3
	3	24.3	-11.9	30.6	-15.0	32.6	-17.1	53.3	-28.3	69.6	-36.2
r18	1	23.8	-14.7	19.9	-15.3	24.8	-15.5	48.5	-31.8	65.7	-42.1
	2	16.0	-6.9	16.0	-7.5	14.1	-4.6	21.0	-7.8	28.7	-10.7
	3	23.4	-11.7	20.8	-12.5	22.0	-5.3	40.5	-18.9	56.6	-25.7
r19	1	13.2	-8.2	8.7	-7.5	13.1	-8.1	32.5	-22.1	52.0	-33.0
	2	18.8	-7.5	17.0	-5.5	18.3	-6.3	24.6	-9.6	31.3	-11.9
r20	2	24.5	-11.4	24.3	-11.1	24.4	-9.8	37.0	-15.8	49.3	-23.4
r21	1	33.3	-19.5	35.9	-24.1	40.4	-23.6	60.3	-38.2	88.2	-54.0
	2	20.3	-8.8	19.0	-8.8	20.3	-7.7	27.6	-11.4	41.4	-20.2
	3	36.4	-18.2	35.6	-20.0	40.2	-24.2	57.8	-35.9	87.1	-50.8
r22	1	19.6	-9.3	22.4	-13.1	25.6	-13.4	43.9	-26.7	64.3	-35.7
	2	16.5	-6.4	15.9	-5.7	14.6	-4.0	23.0	-8.1	28.8	-10.9
	3	15.1	-7.1	19.3	-9.8	19.9	-10.9	28.5	-14.0	45.0	-22.9
r23	2	21.7	-6.3	20.8	-3.2	19.7	-4.9	29.5	-9.8	38.4	-16.9
r24	2	20.0	-8.3	15.7	-4.8	19.9	-7.4	26.6	-8.3	36.9	-10.9

Table 5.2 Specimen 5: Stress Range and Mean Stress in Deck Plate near the PJP Welds

Gage	Stress or Stress Range (MPa)									
	0.1 M cycles		3 M cycles		5.9 M cycles		6.1 M cycles		6.9 M cycles	
	S _r	S _m	S _r	S _m	S _r	S _m	S _r	S _m	S _r	S _m
S17	27.7	7.8	29.4	9.7	29.6	8.6	46.4	14.3	44.5	14.0
S18	18.0	-3.8	20.0	-5.3	20.8	-6.0	32.4	-9.6	30.3	-9.1
S19	27.6	7.5	30.2	8.0	30.1	8.6	47.9	14.7	45.5	13.4
S20	18.1	-2.7	20.2	-4.0	21.3	-3.9	33.0	-9.0	30.9	-8.1
S21	29.7	8.6	32.4	8.4	32.2	10.0	50.5	14.1	47.9	13.4
S22	18.9	-3.3	19.8	-6.1	21.0	-4.6	31.1	-10.4	29.9	-10.0
S23	3.2	0.7	1.6	-0.3	0.2	-0.5	2.5	-1.4	4.7	-5.8
S24	9.2	2.7	2.8	-1.9	1.9	-2.6	13.6	1.2	5.7	-10.7
S25	9.6	4.2	7.6	1.7	4.2	2.1	18.1	5.3	4.2	-2.8
S26	2.9	-0.5	3.4	-0.3	5.8	-2.3	8.7	-2.0	4.6	-1.3
S27	11.8	-7.3	16.3	-14.1	21.3	-14.6	29.7	-27.6	21.1	-23.9
S28	1.9	-0.7	8.5	-4.7	12.6	-6.4	13.1	-8.0	8.8	-7.7
S29	28.3	8.0	30.3	8.1	30.8	10.1	46.7	12.6	46.8	14.4
S30	15.9	-2.5	18.5	-4.7	19.7	-5.3	27.6	-7.0	28.4	-9.1
S31	26.3	6.4	29.1	8.3	29.4	8.4	44.2	13.5	44.8	14.6
S32	14.9	-2.1	17.7	-3.0	19.1	-4.0	26.1	-6.6	26.9	-6.8
S33	28.5	7.0	31.1	7.8	31.3	8.1	46.6	12.6	47.2	13.6
S34	17.3	-2.7	19.2	-4.5	19.9	-5.2	28.1	-7.4	28.7	-8.3
S35	32.4	9.5	35.3	8.6	37.1	10.0	52.6	12.3	49.4	11.0
S36	21.0	-5.5	24.9	-8.7	25.3	-7.0	36.7	-10.9	33.6	-10.3
S37	31.0	10.5	34.7	10.9	36.7	12.4	51.8	17.8	47.7	15.2
S38	20.2	-5.3	24.8	-9.0	25.7	-8.3	36.9	-12.7	32.0	-10.9
S39	31.3	10.6	34.7	11.3	36.1	12.0	51.4	17.5	47.8	15.8
S40	20.5	-5.9	24.4	-8.4	25.2	-8.4	36.1	-12.2	31.9	-11.0
S41	5.6	2.7	0.2	-3.1	2.0	-2.1	2.1	-6.0	7.8	-9.6
S42	2.1	-1.7	2.9	-8.4	4.8	-5.4	3.5	-8.6	16.6	-17.3
S43	3.6	-0.2	1.3	-4.2	2.2	-2.8	5.2	-6.8	7.6	-9.6
S47	34.0	12.0	35.3	9.4	36.7	11.6	51.6	12.6	50.7	12.6
S48	24.9	-8.2	26.6	-8.7	26.9	-7.3	37.8	-14.1	37.0	-13.5
S49	35.9	12.6	37.1	10.8	38.8	12.9	54.1	14.8	53.3	15.5
S51	33.9	11.9	35.1	12.0	36.3	12.5	51.4	17.5	50.8	17.3
S52	26.3	-9.8	27.7	-7.3	28.4	-9.8	39.2	-10.2	38.8	-11.6

Table 5.3 Specimen 6: Stress Range and Mean Stress in Deck Plate near the PJP Welds

Gage	Stress or Stress Range (MPa)									
	0.1 M cycles		3 M cycles		5.9 M cycles		6.5 M cycles		7.5 M cycles	
	S _r	S _m	S _r	S _m	S _r	S _m	S _r	S _m	S _r	S _m
S18	20.1	-4.5	21.1	-4.2	21.2	-4.5	32.5	-7.9	44.0	-11.8
S19	27.8	8.2	28.7	9.9	28.1	9.9	42.0	14.3	58.9	17.7
S20	20.0	-3.7	21.0	-3.9	21.5	-5.1	32.3	-7.7	43.6	-9.8
S22	21.3	-4.8	21.7	-5.3	22.0	-5.8	33.3	-8.9	43.8	-11.6
S29	15.8	-2.2	15.9	-2.6	16.4	-2.7	25.6	-5.5	37.2	-10.9
S30	28.1	7.2	28.6	7.6	28.4	10.7	44.7	12.7	62.2	15.5
S31	25.8	5.4	26.2	5.7	26.3	6.6	42.3	10.5	59.4	16.4
S32	16.6	-2.7	17.1	-3.2	17.6	-2.9	27.6	-5.8	38.9	-12.4
S33	26.7	5.4	27.1	6.1	27.3	6.4	43.1	10.2	59.3	16.2
S34	18.8	-4.0	19.4	-3.9	19.5	-4.0	30.1	-7.0	40.6	-10.5
S35	29.9	6.1	29.8	7.6	29.4	8.7	46.1	11.5	60.3	14.1
S36	20.6	-5.0	21.2	-4.8	21.0	-5.3	31.1	-8.2	42.5	-11.6
S38	21.1	-5.7	20.6	-4.4	20.7	-4.5	31.0	-6.9	40.3	-8.4
S40	19.9	-10.6	21.6	-5.7	21.7	-5.8	26.7	-11.4	41.6	-16.6
S43	9.4	7.1	4.5	2.5	3.6	-0.3	10.8	6.1	14.2	10.3
S46	13.9	5.3	11.9	6.7	11.2	6.1	17.5	6.4	22.4	10.3
S47	28.0	5.2	29.2	11.6	28.8	10.8	46.8	15.1	60.5	18.3
S48	19.7	-4.3	20.1	-3.7	20.0	-4.1	33.2	-6.7	41.5	-9.2
S49	28.9	7.8	29.5	8.9	29.3	8.8	46.5	13.8	61.0	19.8
S51	30.1	9.7	30.6	10.4	30.9	10.7	47.8	15.3	62.6	18.9
S52	17.7	-7.6	20.2	-4.8	20.6	-5.0	32.8	-8.5	42.4	-12.8

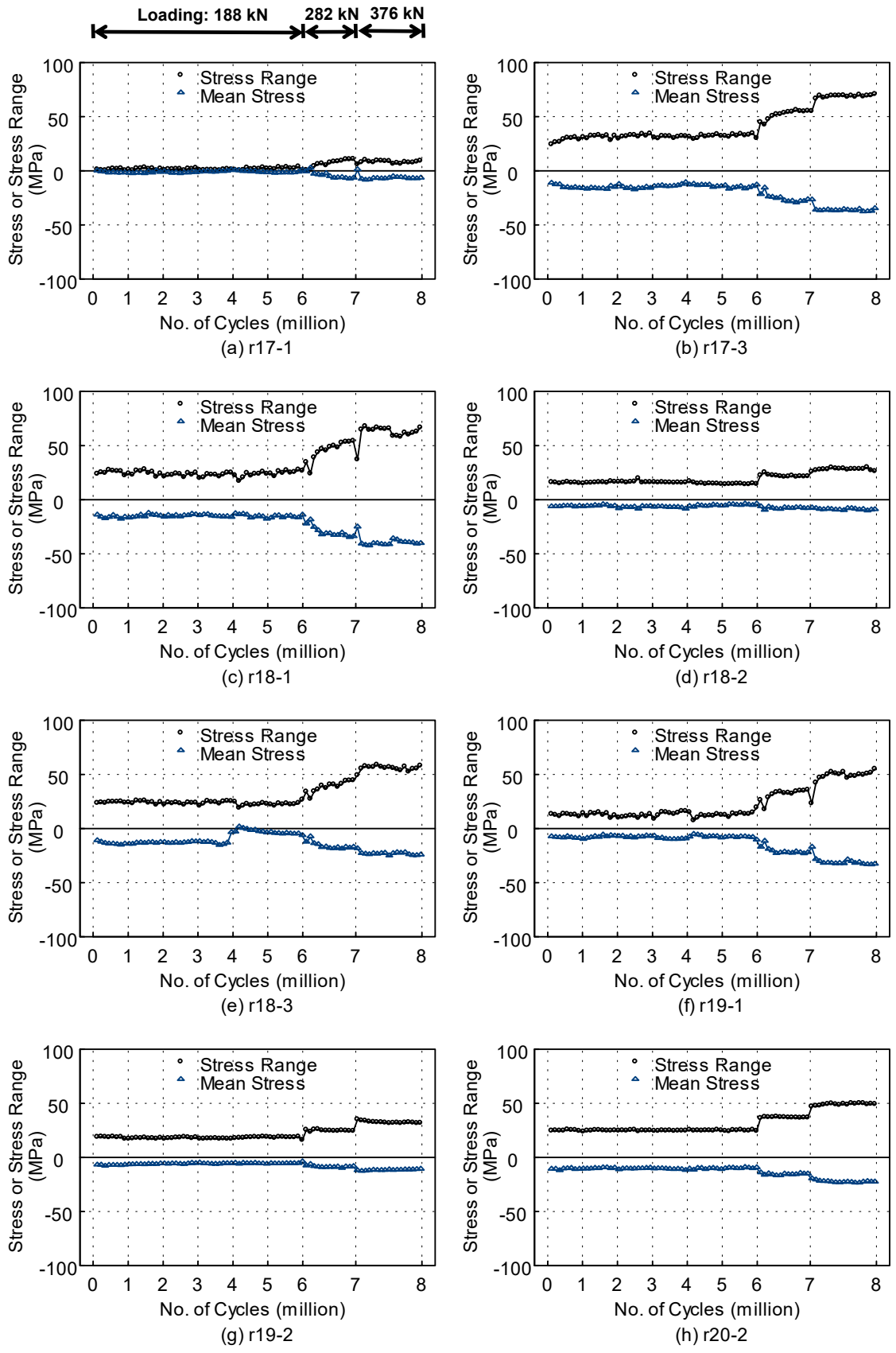


Figure 5.3 Specimen 4: Stress Range and Mean Stress in Deck Plate near the PJP Welds

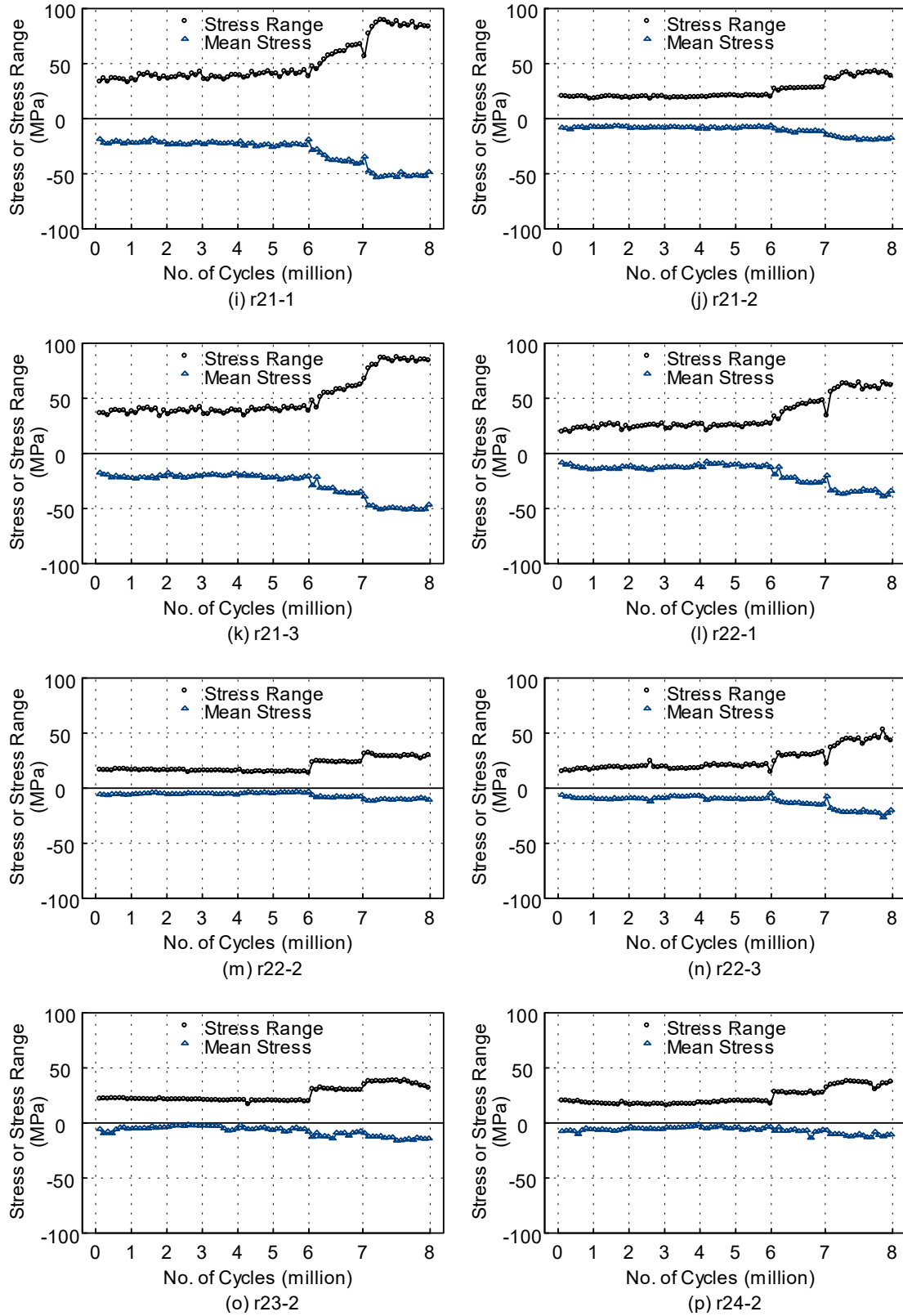


Figure 5.3 Specimen 4: Stress Range and Mean Stress in Deck Plate near the PJP Welds (continued)

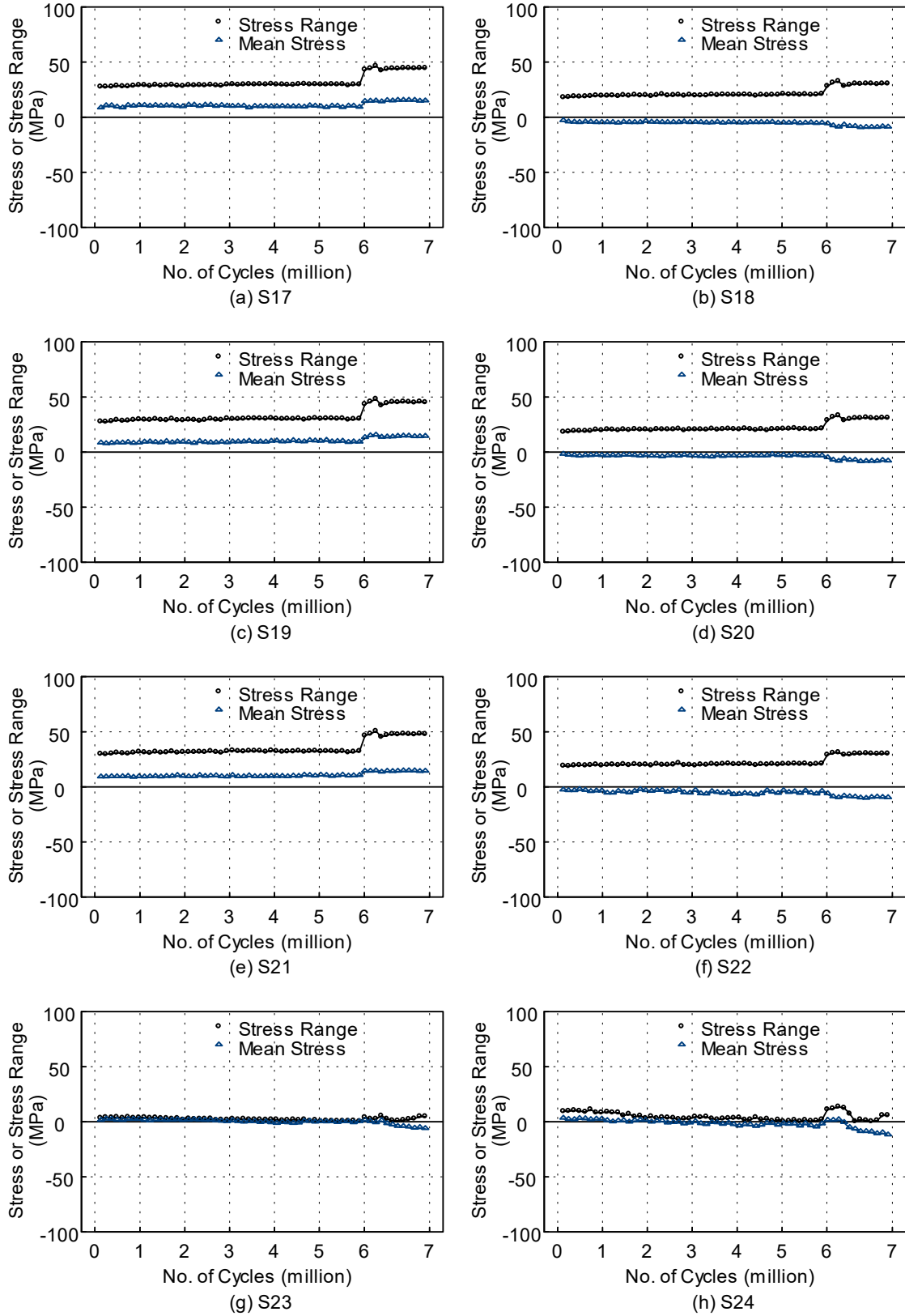


Figure 5.4 Specimen 5: Stress Range and Mean Stress in Deck Plate near the PJP Welds

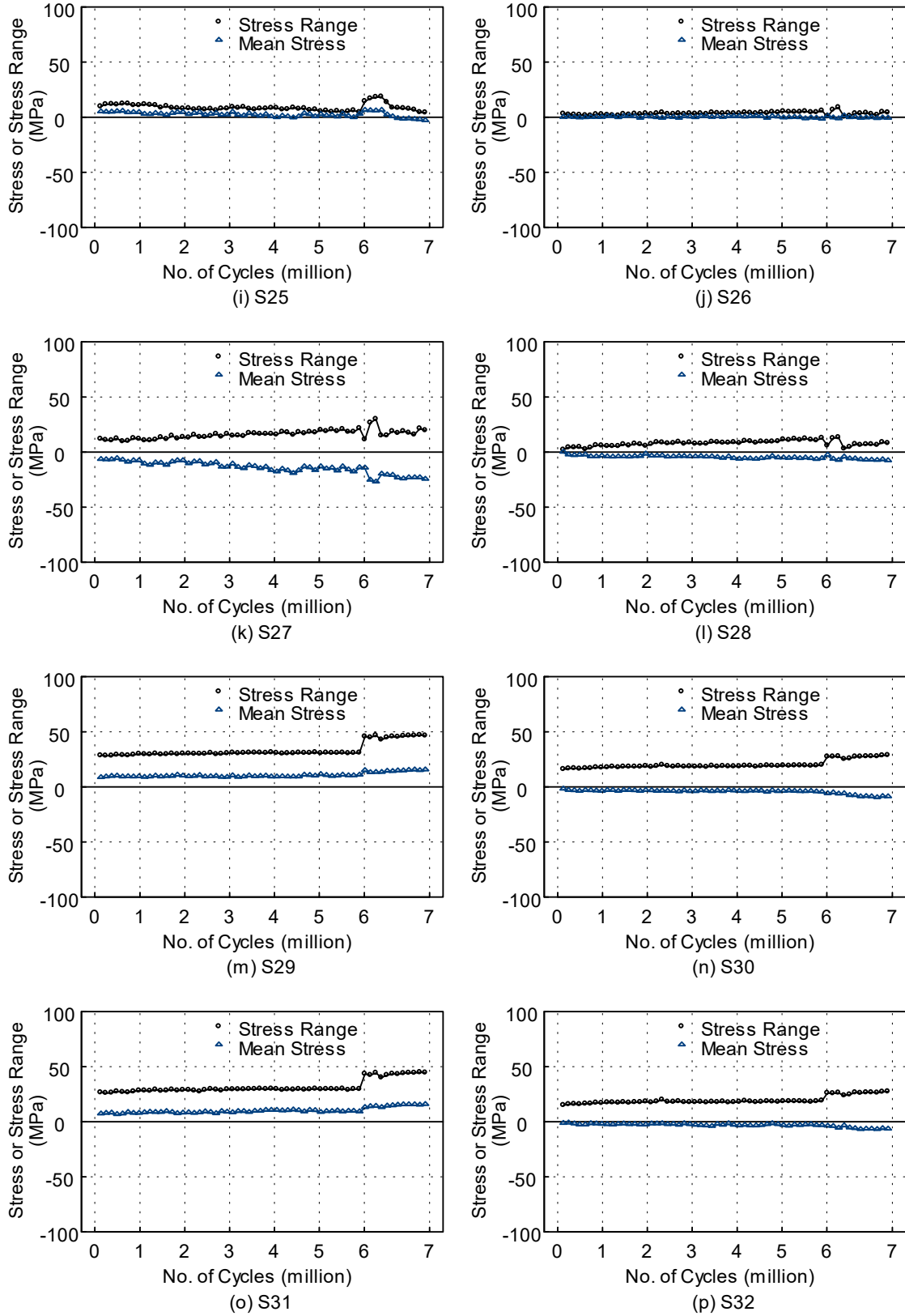


Figure 5.4 Specimen 5: Stress Range and Mean Stress in Deck Plate near the PJP Welds (continued)

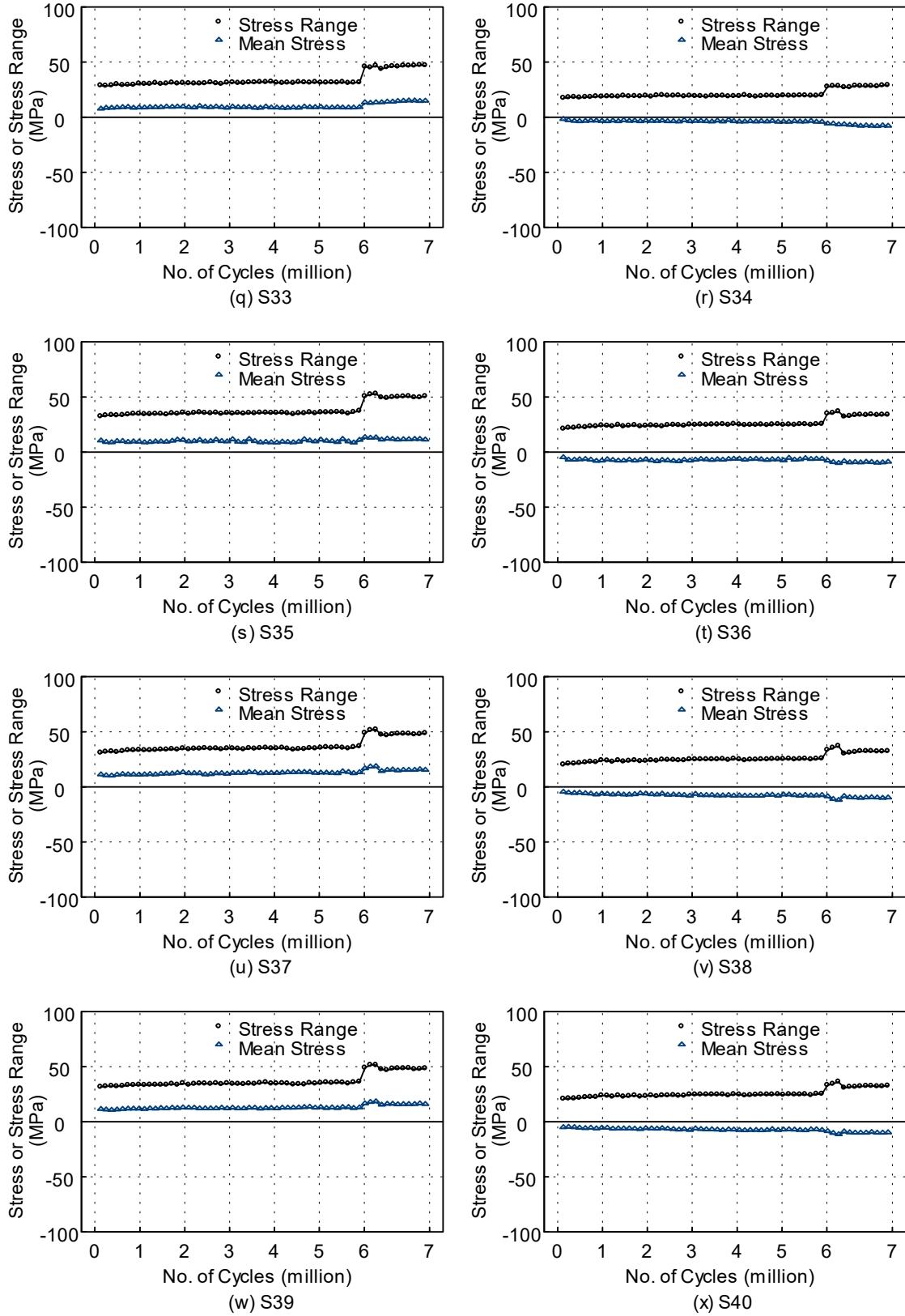


Figure 5.4 Specimen 5: Stress Range and Mean Stress in Deck Plate near the PJP Welds (continued)

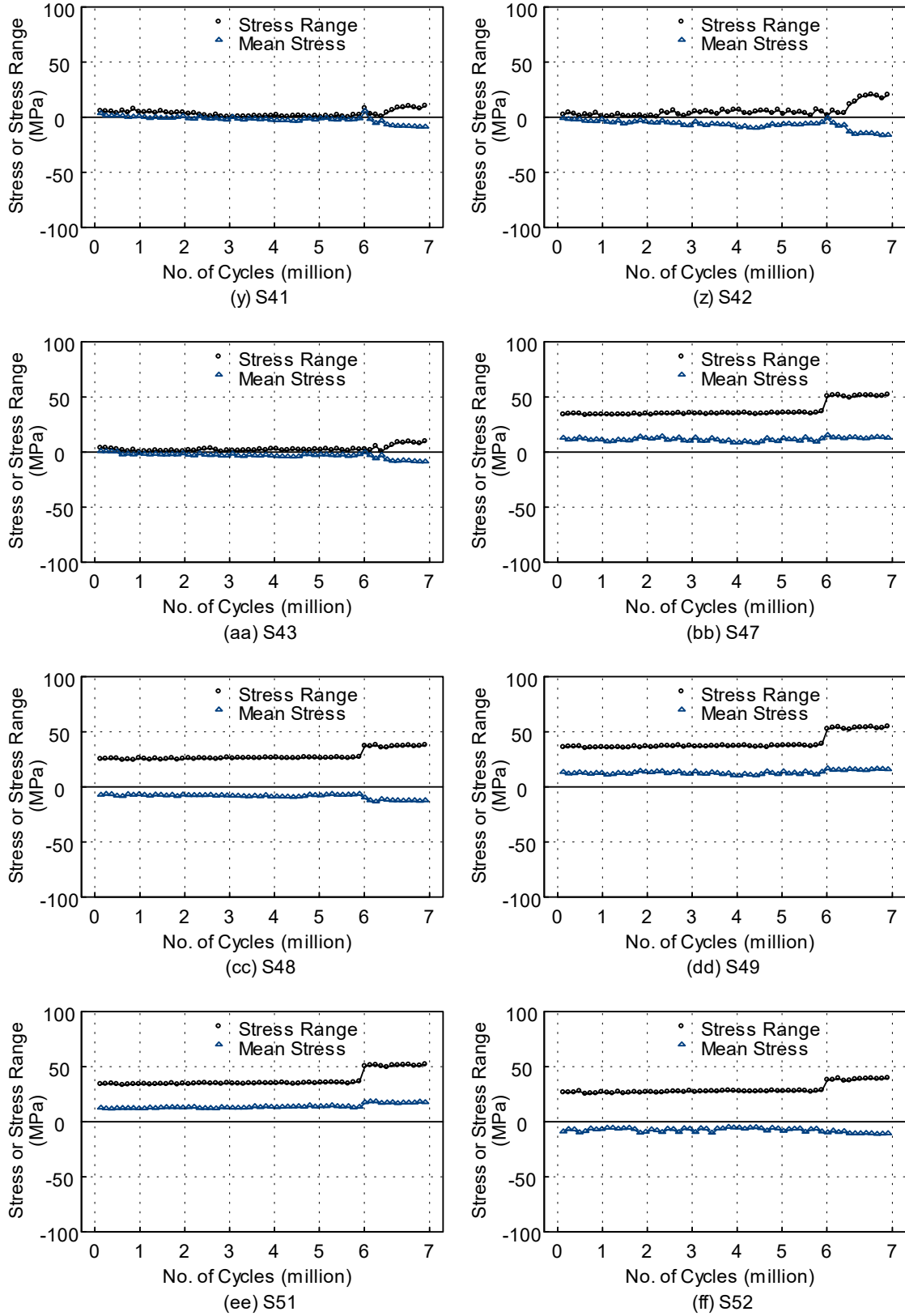


Figure 5.4 Specimen 5: Stress Range and Mean Stress in Deck Plate near the PJP Welds (continued)

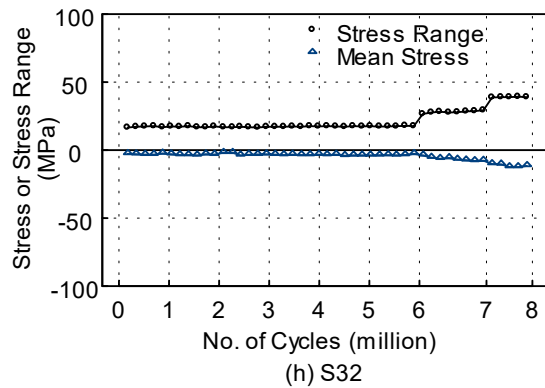
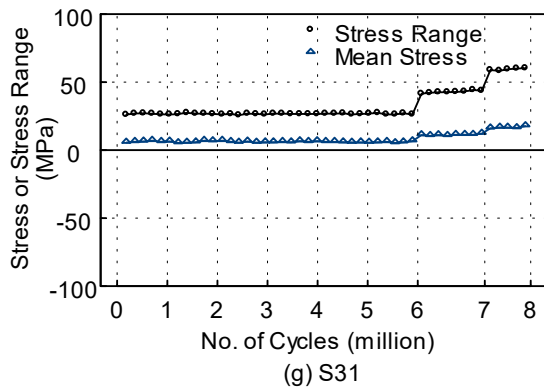
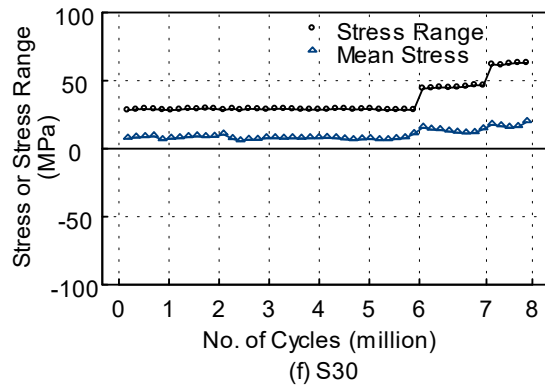
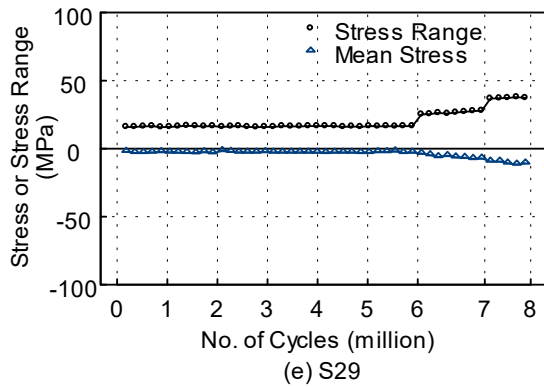
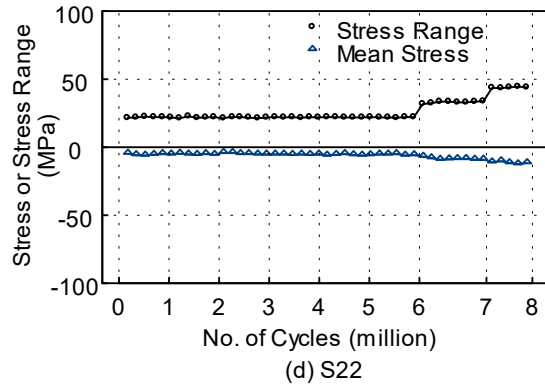
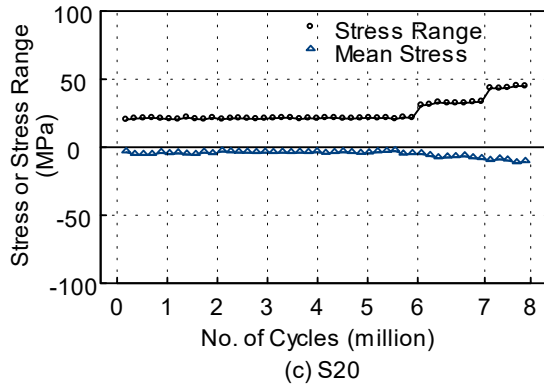
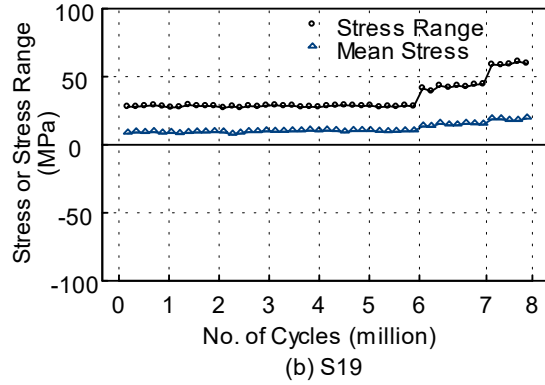
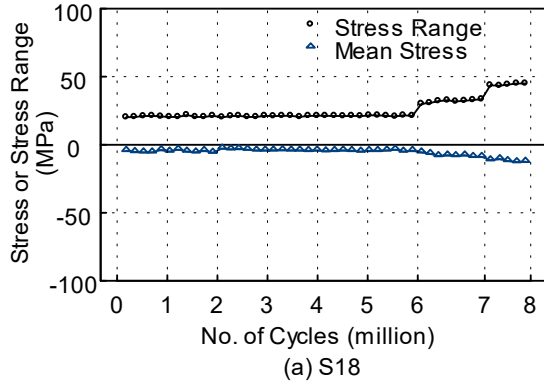


Figure 5.5 Specimen 6: Stress Range and Mean Stress in Deck Plate near the PJP Welds

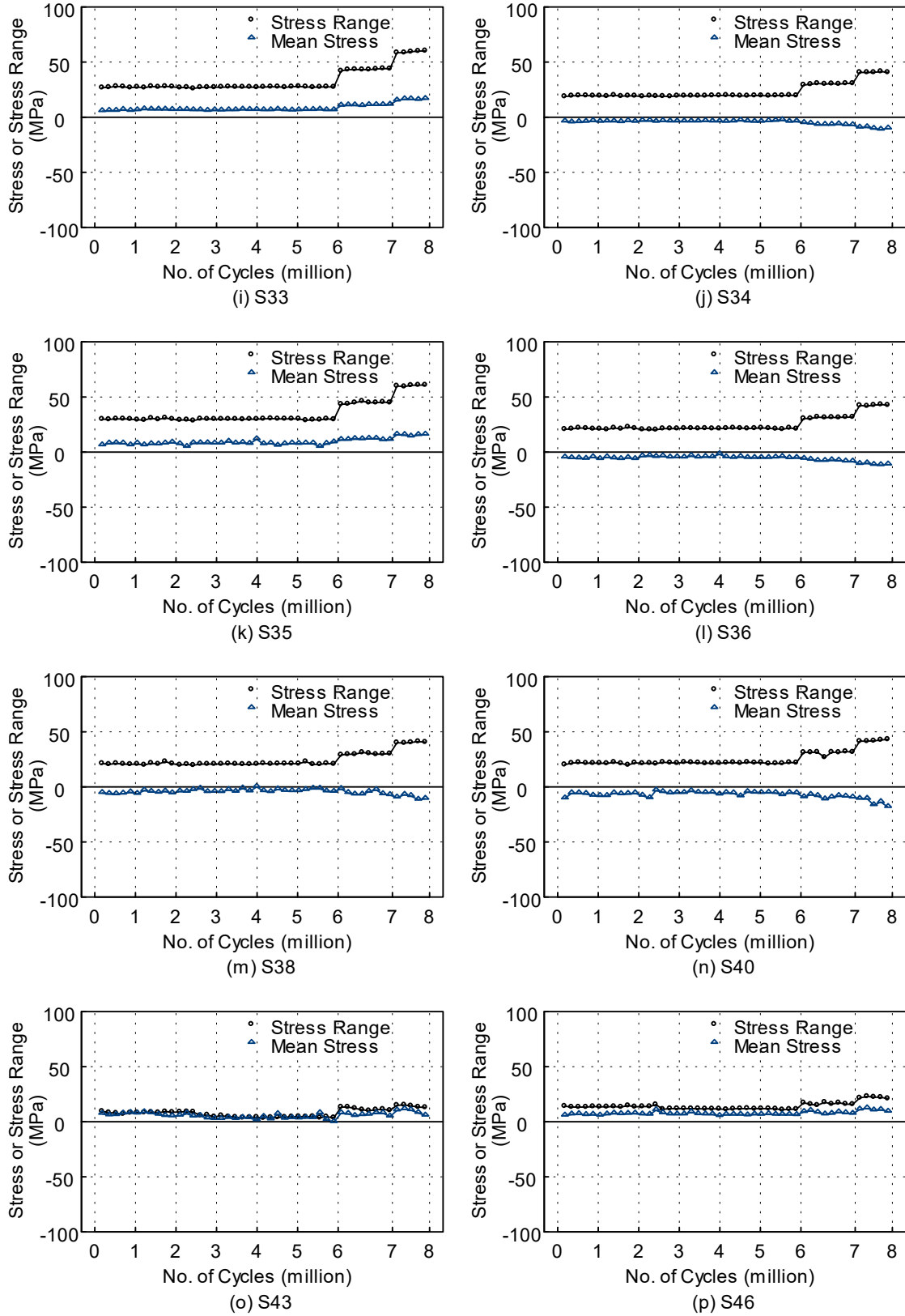


Figure 5.5 Specimen 6: Stress Range and Mean Stress in Deck Plate near the PJP Welds (continued)

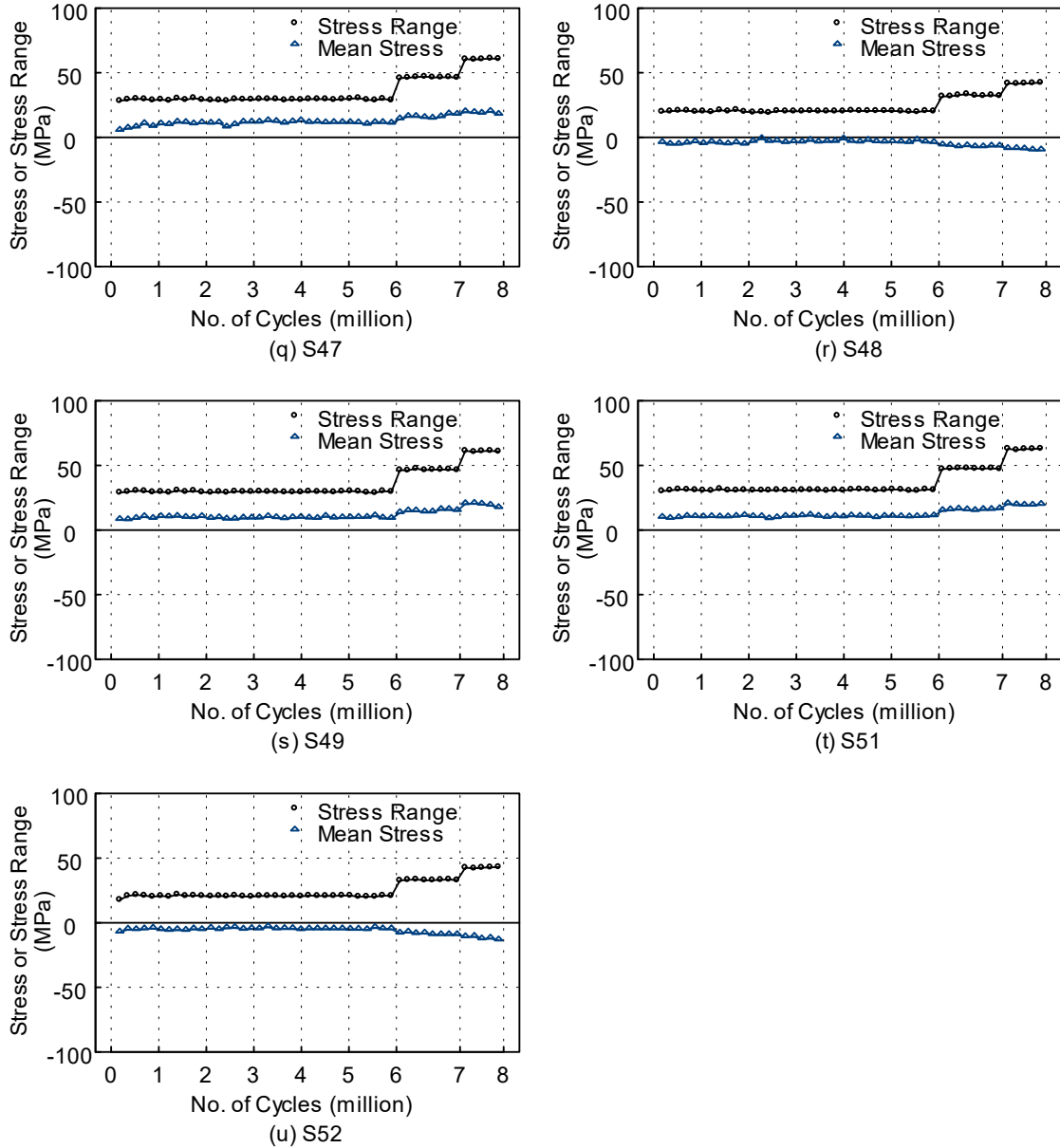


Figure 5.5 Specimen 6: Stress Range and Mean Stress in Deck Plate near the PJP Welds (continued)

5.2.2 Rib Stress Distribution near Rib-to-Deck Welds

The location and orientation of the strain gages on the ribs near the rib-to-deck welds were shown in Figures 2.36 and 2.47. Tables 5.4 to 5.8 summarize the stress range (S_r) and the mean stress (S_m). Plots of stress range and mean stress up to 8 million cycles are shown in Figures 5.6 to 5.15.

For the outer surface of the rib walls, the maximum stress range in the direction perpendicular to the longitudinal rib-to-deck welds was 62.8 MPa (mean stress = 31.6

MPa) in tension field at midspan gage r16-1 of Specimen 3, and 92.2 MPa (mean stress = -50.3 MPa) in compression field at gage r10-1 of Specimen 3 during the first 0.1 million cycles. Similar stress range for the inner surface of the rib walls was 49.9 MPa (mean stress = -21.9 MPa) in compression field at gage r27-1 in Specimen 5 during the first 0.1 million cycles. But the maximum stress range in tension field was low (less than 10 MPa) within the first 6 million cycles.

For Specimens 4 and 5, several pairs of gages were placed on both sides of the rib walls to compute the in-plane and out-of-plane stress components in the direction perpendicular to the longitudinal rib-to-deck welds. From the pair of r7-1 and r10-1 on the eastern side of rib R3 in Specimen 4, the in-plane stress was -40.25 MPa, and the out-of-plane stress was 33.6 MPa during the first 0.1 million cycles. From the pair of r2-1 and r28-1 on the eastern side of rib R2 in Specimen 5, the in-plane stress was -20.2 MPa and the out-of-plane stress was 26.3 MPa.

Table 5.4 Specimen 2: Stress Range and Mean Stress in Ribs near the PJP Welds

Gage	Stress or Stress Range (MPa)									
	0.1 M cycles		3 M cycles		5.9 M cycles		6.5 M cycles		7.5 M cycles	
	S _r	S _m	S _r	S _m	S _r	S _m	S _r	S _m	S _r	S _m
r19-1	34.7	18.1	37.9	17.9	39.5	17.1	57.5	25.2	76.0	32.1
r24-1	10.6	-7.6	10.0	-6.5	9.8	-1.8	16.4	-8.3	20.4	-11.3
r24-3	15.6	9.2	18.3	5.5	20.2	8.6	27.9	2.6	36.1	11.8
S32	12.3	-8.6	12.1	-10.3	12.2	-12.7	18.3	-13.5	24.0	-18.5
S33	42.1	19.9	47.3	26.3	46.4	28.1	72.7	37.4	98.2	48.2
S34	67.2	-39.6	72.9	-43.0	73.4	-39.2	106.3	-56.0	150.3	-81.6
S39	64.8	-51.7	85.5	-49.7	87.2	-58.1	112.6	-72.5	153.6	-99.8
S40	45.1	23.9	45.6	21.3	44.1	27.6	71.9	43.6	93.5	52.8
S41	12.4	-9.1	15.2	-10.3	17.0	-10.3	24.0	-13.7	30.7	-19.8
S42	33.8	14.7	34.8	14.3	34.7	7.0	55.3	16.9	71.3	20.8
S45	19.8	-10.7	21.0	-7.5	20.9	-9.1	32.9	-14.1	43.0	-18.4
S47	22.9	-9.2	24.6	-8.7	24.5	-8.5	37.8	-15.4	49.0	-17.3
S49	20.5	-8.8	21.4	-8.6	21.6	-10.6	33.8	-14.7	44.4	-15.5

Table 5.5 Specimen 3: Stress Range and Mean Stress in Ribs near the PJP Welds

Gage	Component	Stress or Stress Range (MPa)									
		0.1 M cycles		3 M cycles		5.9 M cycles		6.5 M cycles		7.5 M cycles	
		S _r	S _m	S _r	S _m	S _r	S _m	S _r	S _m	S _r	S _m
r1	1	61.8	31.7	61.8	29.1	63.2	30.4	91.0	43.2	116.7	52.7
r2	1	59.6	34.5	63.8	37.7	67.0	38.4	92.6	53.5	119.9	63.6
r5	1	46.1	-22.3	40.8	-22.8	43.7	-21.6	107.1	-61.1	154.7	-84.5
r6	1	49.2	-26.1	55.4	-29.5	58.8	-26.3	83.1	-44.0	110.0	-57.2
	3	55.2	-29.4	62.4	-32.6	64.8	-31.8	92.0	-48.1	122.7	-65.9
r7	1	81.2	-39.8	83.8	-39.0	88.7	-41.4	128.5	-64.0	175.8	-88.1
r8	1	53.3	-26.2	46.5	-20.8	49.8	-22.4	81.1	-44.2	122.0	-63.1
r10	1	92.2	-50.3	95.9	-44.5	100.1	-59.6	141.9	-92.2	179.3	-110.3
r11	1	62.3	-31.6	59.2	-29.9	63.5	-29.0	119.6	-65.7	177.0	-91.5
r12	1	39.0	-18.4	56.0	-27.6	60.6	-23.0	85.2	-39.6	107.4	-52.1
r13	1	67.9	-32.5	77.8	-37.6	84.3	-39.4	123.7	-61.5	170.1	-86.0
	3	29.8	-12.6	43.5	-21.7	47.5	-22.8	66.5	-33.4	84.5	-42.5
r14	1	43.2	-13.7	48.1	-16.4	52.0	-16.1	75.4	-29.8	114.3	-50.1
	3	56.6	-25.3	59.1	-27.0	61.5	-23.0	90.6	-41.4	129.3	-64.0
r15	1	50.4	20.6	51.0	13.4	51.2	22.4	76.8	25.3	101.4	35.9
	3	20.5	11.4	20.6	12.7	20.5	11.6	30.7	20.9	40.4	25.3
r16	1	62.8	31.6	58.1	28.3	58.7	29.4	88.4	42.5	116.4	52.8
	3	34.0	17.4	31.6	12.2	32.1	14.3	48.9	20.4	64.6	24.0

Table 5.6 Specimen 4: Stress Range and Mean Stress in Ribs near the PJP Welds

Gage	Component	Stress or Stress Range (MPa)									
		0.1 M cycles		3 M cycles		5.9 M cycles		6.5 M cycles		7.5 M cycles	
		S _r	S _m	S _r	S _m	S _r	S _m	S _r	S _m	S _r	S _m
r1	1	32.5	-17.8	37.1	-23.0	38.4	-22.0	60.4	-33.7	80.5	-48.0
	2	19.6	-8.1	19.3	-7.6	19.5	-8.3	28.6	-12.3	37.4	-15.1
	3	53.3	-25.6	57.3	-29.7	58.0	-28.5	88.6	-45.7	117.4	-60.9
r2	1	79.8	-42.1	85.5	-48.9	90.9	-50.5	136.7	-82.3	178.5	-120.6
	2	9.0	-3.7	10.7	-4.2	9.7	-2.7	14.0	-5.6	19.1	-7.0
	3	54.3	-26.1	55.9	-28.8	58.5	-29.1	88.9	-49.3	120.0	-72.7
r3	1	61.7	-32.3	69.0	-37.2	67.8	-37.0	113.4	-64.6	155.5	-93.9
	3	8.9	-2.2	12.2	-4.4	11.8	-3.9	29.9	-15.6	41.4	-23.4
r5	1	33.8	-17.9	36.5	-22.0	38.0	-20.5	59.6	-34.2	86.8	-51.7
r6	1	71.8	-37.6	72.9	-40.2	77.6	-43.2	114.8	-66.8	164.4	-97.6
	2	8.6	-3.4	9.0	2.6	8.5	6.7	14.7	3.2	18.2	1.2
	3	33.4	-18.2	35.7	-22.4	37.7	-21.3	58.5	-34.5	86.6	-55.8
r7	1	72.7	-37.4	73.2	-39.0	77.6	-41.6	116.2	-62.7	166.5	-85.6
	2	1.9	0.6	1.2	0.2	1.4	1.9	0.4	1.4	1.8	0.4
	3	25.2	-13.9	26.7	-16.7	28.4	-16.2	45.2	-25.6	68.5	-37.2
r8	1	66.3	-34.7	69.5	-38.9	69.9	-38.6	115.0	-66.9	146.2	-88.5
	2	11.4	-4.4	10.6	-4.0	11.3	-3.7	16.3	-6.0	24.0	-10.0
	3	66.4	-34.6	67.7	-34.9	66.9	-35.5	100.4	-55.7	138.7	-77.9
r10	1	6.0	-3.7	2.8	0.2	1.4	4.4	7.2	9.5	11.9	11.2
	2	3.7	2.2	3.5	1.4	4.1	2.0	4.7	0.8	9.0	1.2
	3	5.3	-1.5	3.6	-0.2	2.4	1.5	1.9	4.4	8.2	6.5
r11	2	4.0	-1.3	3.7	-1.6	4.0	0.5	5.2	-0.9	7.0	-1.5
	3	26.0	-14.7	25.2	-15.4	25.1	-12.2	37.3	-20.7	49.0	-28.5
r12	1	2.7	0.5	2.9	0.1	2.8	2.6	4.0	2.7	5.7	3.2
	2	3.1	-0.9	2.5	-0.9	2.9	1.8	3.9	0.0	5.2	-0.7
	3	22.0	12.1	22.2	12.6	22.1	13.7	33.7	19.5	45.0	26.8

Table 5.7 Specimen 5: Stress Range and Mean Stress in Ribs near the PJP Welds

Gage	Component	Stress or Stress Range (MPa)									
		0.1 M cycles		3 M cycles		5.9 M cycles		6.1 M cycles		6.9 M cycles	
		S _r	S _m	S _r	S _m	S _r	S _m	S _r	S _m	S _r	S _m
r1	2	0.5	-0.4	0.1	0.5	0.4	0.2	0.6	2.5	0.8	2.8
	3	27.0	9.2	27.4	7.6	27.6	10.8	40.5	13.1	40.0	16.0
r2	1	49.8	21.6	50.1	20.5	50.0	21.3	73.4	30.1	72.6	30.1
	2	0.4	-0.3	0.6	-0.5	0.0	1.2	0.0	0.2	0.2	1.4
	3	27.2	9.1	27.5	9.2	27.5	9.3	40.2	14.3	40.0	15.1
r3	1	50.8	21.6	51.1	19.7	51.0	19.8	75.1	28.5	74.4	28.8
	2	0.4	-0.1	0.6	-1.0	0.2	0.6	0.2	-0.7	0.2	-0.1
	3	28.1	8.1	28.8	10.2	28.7	7.4	42.2	16.8	41.8	15.7
r4	2	0.7	0.2	0.1	0.6	0.1	-0.8	0.0	0.1	0.4	0.4
	3	26.9	13.8	24.8	14.3	25.0	11.4	36.4	19.5	38.0	20.4
r5	1	53.7	22.6	51.1	20.0	51.3	20.5	74.9	29.6	77.4	31.7
	2	0.8	0.1	0.4	0.5	0.1	1.5	0.0	0.0	0.7	0.8
	3	27.3	14.0	25.2	12.7	25.6	10.8	36.9	17.9	38.8	19.0
r6	1	51.5	23.0	49.2	20.7	49.5	20.6	72.2	31.1	74.7	32.5
	2	0.5	0.8	0.1	0.7	0.1	-1.0	0.6	0.4	1.1	1.0
	3	25.1	14.3	23.6	11.1	23.9	13.0	34.6	15.0	35.9	16.6
r7	1	35.2	-19.2	39.3	-19.8	41.3	-21.5	70.0	-34.6	66.9	-35.4
	2	5.7	-3.0	5.9	-3.4	5.8	-6.5	7.6	-21.2	7.7	-20.2
	3	48.5	-24.0	51.6	-25.2	53.1	-20.7	83.7	-34.1	80.0	-33.9
r8	1	75.8	-39.9	84.5	-42.3	86.6	-43.2	134.5	-67.9	126.4	-65.4
	2	6.5	3.0	4.8	1.7	4.5	2.0	4.4	1.4	4.4	1.4
r9	1	50.2	-26.9	62.6	-34.9	64.2	-34.1	99.6	-54.1	95.1	-52.8
	2	0.1	0.4	0.6	-0.8	0.3	1.7	1.6	-1.4	1.6	0.2
r10	2	2.5	0.4	2.6	-2.8	2.1	-3.1	3.4	-4.4	3.9	-4.5
	3	64.2	-36.5	71.4	-35.2	73.6	-38.0	104.3	-50.6	96.8	-51.1
r11	1	71.9	-41.7	90.8	-49.4	96.0	-50.7	136.2	-72.6	126.2	-69.1
	2	2.5	-0.8	2.0	5.7	2.1	0.4	4.0	6.7	6.7	8.2
	3	27.4	-17.7	40.5	-23.7	44.0	-25.8	61.7	-37.3	58.6	-37.1
r12	1	39.5	-24.7	51.0	-22.4	54.1	-26.1	75.9	-32.5	70.1	-31.3
	2	4.2	-2.6	5.1	-2.8	4.8	-3.5	7.5	-2.9	6.5	-2.3
	3	7.9	0.8	3.3	-1.0	3.1	-6.2	3.6	-1.9	7.1	-3.2
r26	1	1.8	0.2	1.9	0.9	2.0	-0.1	4.0	2.0	4.1	1.7
	3	21.3	-12.5	22.6	-12.5	22.3	-15.0	33.6	-17.8	32.8	-18.2
r27	1	49.9	-21.9	49.2	-21.6	49.0	-21.1	71.3	-34.0	71.2	-34.2
	2	4.2	-1.6	4.3	-2.7	3.7	-4.3	5.7	-6.7	5.7	-7.4

Table 5.7 Specimen 5: Stress Range and Mean Stress in Ribs near PJP Weld (continued)

Gage	Component	Stress or Stress Range (MPa)									
		0.1 M cycles		3 M cycles		5.9 M cycles		6.1 M cycles		6.9 M cycles	
		S _r	S _m	S _r	S _m	S _r	S _m	S _r	S _m	S _r	S _m
r27	3	29.3	-10.0	28.6	-9.3	28.4	-9.4	41.6	-16.1	41.8	-16.4
r28	1	6.7	-2.8	1.4	-0.3	3.3	-0.7	13.4	6.9	10.5	6.7
	2	3.7	2.2	4.0	1.7	4.4	-0.2	6.3	3.8	5.2	3.4
r29	1	1.7	1.1	1.2	1.4	1.6	6.2	2.7	11.8	3.1	11.0
	3	19.1	8.6	19.4	8.6	19.8	12.5	29.6	12.0	29.1	11.5

Table 5.8 Specimen 6: Stress Range and Mean Stress in Ribs near the PJP Welds

Gage	Component	Stress or Stress Range (MPa)									
		0.1 M cycles		3 M cycles		5.9 M cycles		6.5 M cycles		7.5 M cycles	
		S _r	S _m	S _r	S _m	S _r	S _m	S _r	S _m	S _r	S _m
r1	1	54.5	23.9	53.7	20.7	53.7	21.6	82.0	33.2	106.1	41.1
r2	1	56.5	23.8	55.7	24.0	55.6	23.8	83.9	35.3	110.2	45.2
r3	1	59.1	25.0	57.7	23.2	57.7	24.3	88.3	36.5	114.5	47.6
	3	32.9	12.3	32.1	15.0	32.3	20.4	49.3	25.3	64.3	31.1
r7	1	28.6	-14.4	35.5	-34.8	37.0	-46.8	54.8	-60.8	80.3	-76.8
	2	14.8	-6.3	15.0	-6.3	15.1	-6.2	23.5	-9.8	29.8	-13.8
	3	49.1	-23.0	55.2	-27.4	55.0	-28.9	82.9	-41.9	113.5	-54.5
r8	1	69.4	-35.4	75.9	-38.7	75.9	-41.3	113.9	-62.3	154.9	-85.0
	2	5.2	-1.7	6.1	-0.7	5.7	0.0	8.5	-1.0	11.4	-7.1
	3	52.5	-25.1	51.1	-26.0	51.3	-27.3	76.3	-40.1	109.7	-60.5
r9	1	59.8	-29.9	57.7	-28.1	58.4	-30.8	88.9	-48.2	128.9	-66.9
	2	9.6	-3.8	11.5	-5.0	11.2	-6.7	16.5	-9.0	22.2	-10.6
r10	1	79.8	-40.5	73.4	-34.2	73.4	-35.6	117.7	-57.9	153.8	-75.0
r13	1	27.8	-12.7	35.2	-16.5	35.4	-17.1	56.2	-27.6	89.5	-45.2
	2	12.1	-4.6	11.2	-2.0	13.5	-3.9	19.2	-6.2	27.2	-6.6
	3	4.3	1.2	1.3	-0.8	1.4	-1.1	3.4	-1.0	3.3	-1.9
r14	1	65.1	-32.3	72.9	-36.3	74.5	-38.7	115.8	-60.0	155.1	-94.8
r15	1	53.5	-27.0	46.4	-23.0	47.3	-23.6	80.9	-40.5	118.3	-60.1
	3	53.4	-29.9	53.9	-50.8	54.7	-64.3	86.8	-83.1	122.8	-102.3
r16	1	78.1	-42.7	71.1	-36.7	72.0	-37.3	114.4	-61.1	152.9	-80.2
r19	1	54.3	24.2	53.8	26.9	53.3	32.6	81.8	43.3	107.2	51.3
	3	23.7	11.9	23.7	14.2	23.2	13.9	35.7	19.7	46.5	24.1
r20	1	59.1	25.6	58.2	24.6	57.3	24.1	88.1	36.8	114.6	46.8
	3	27.4	15.1	27.0	15.4	26.3	14.6	40.6	22.1	52.1	28.5

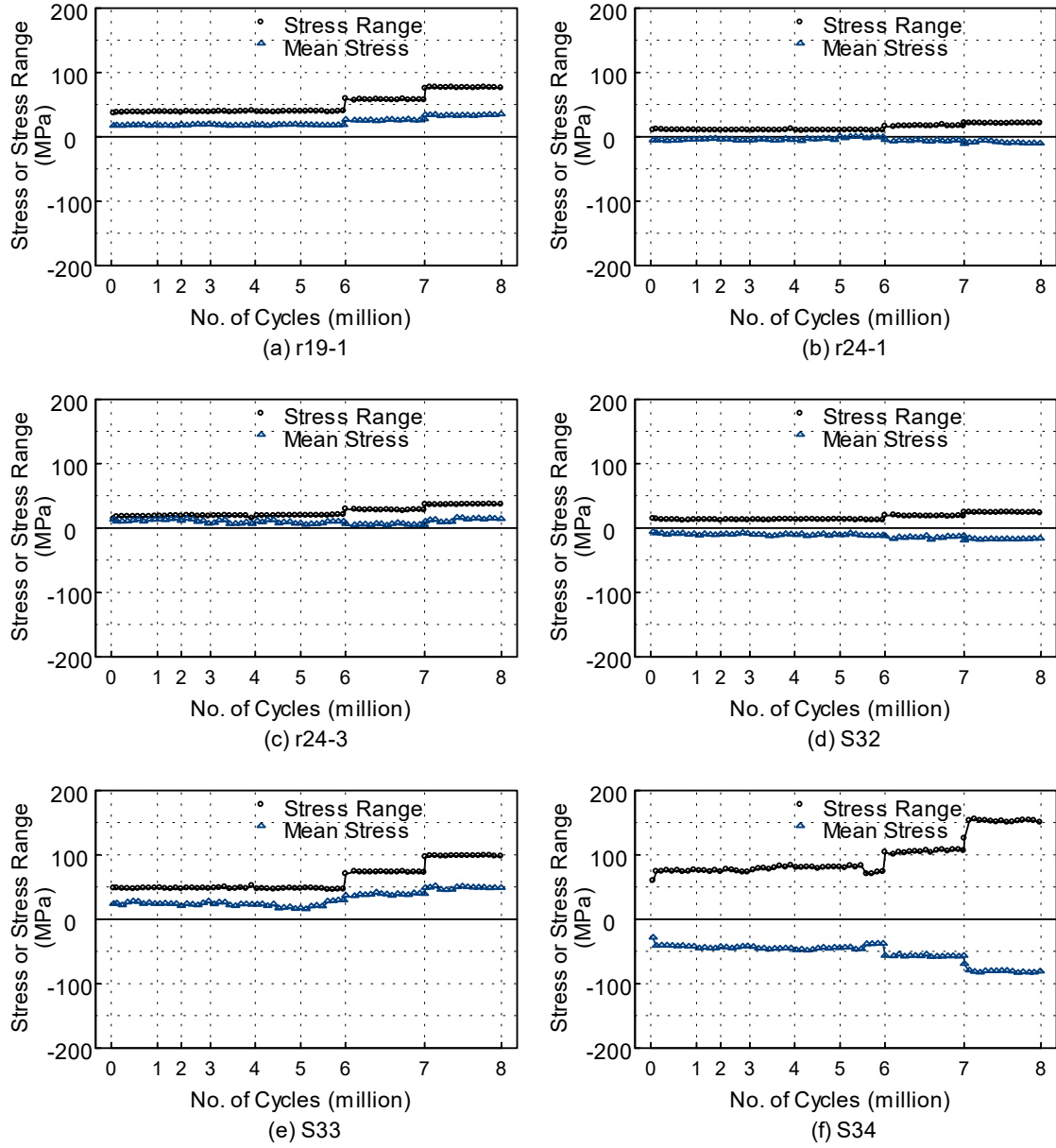


Figure 5.6 Specimen 2: Stress Range and Mean Stress in Rib R2 near the PJP Welds

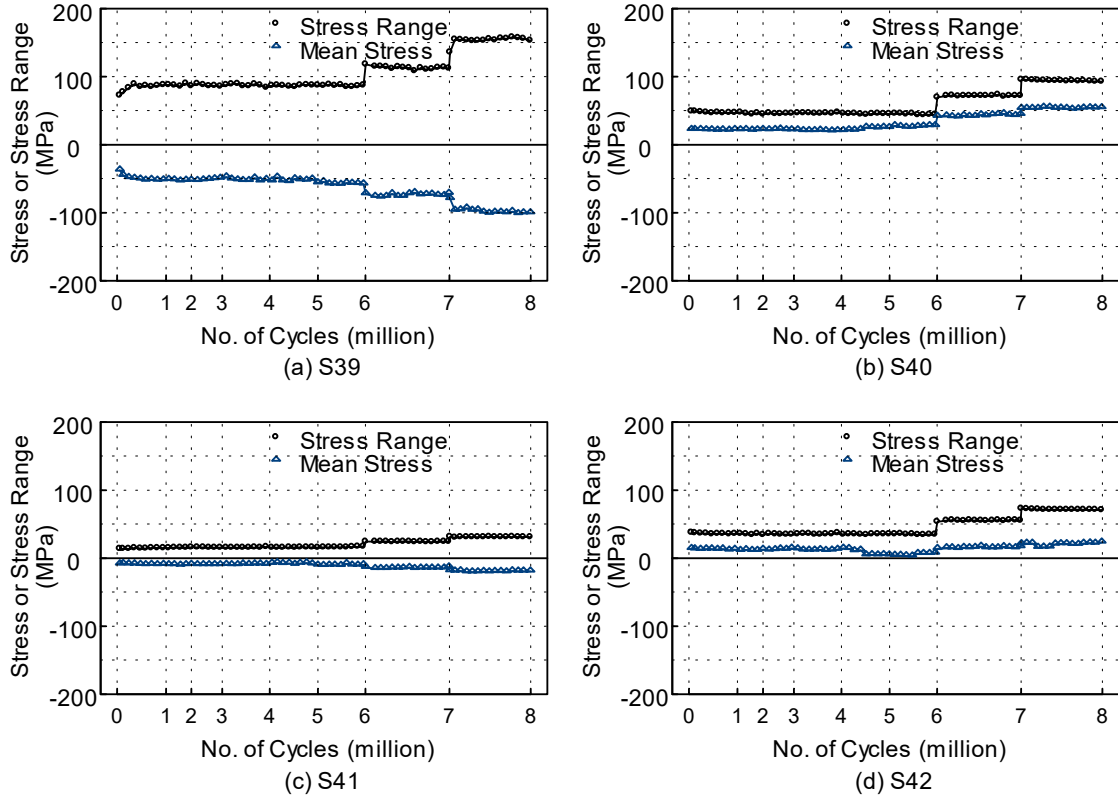


Figure 5.7 Specimen 2: Stress Range and Mean Stress in Rib R3 near the PJP Welds

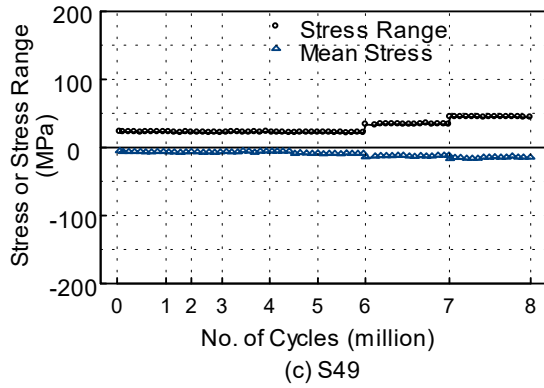
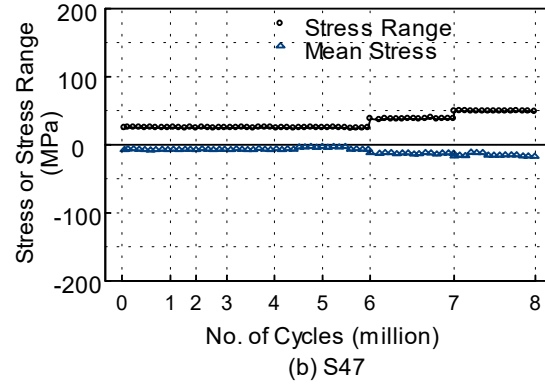
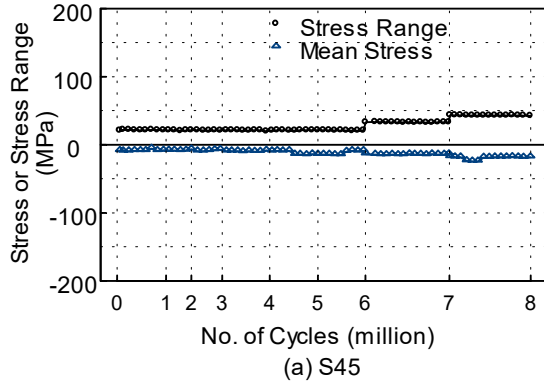


Figure 5.8 Specimen 2: Stress Range and Mean Stress in Rib R4 near the PJP Welds

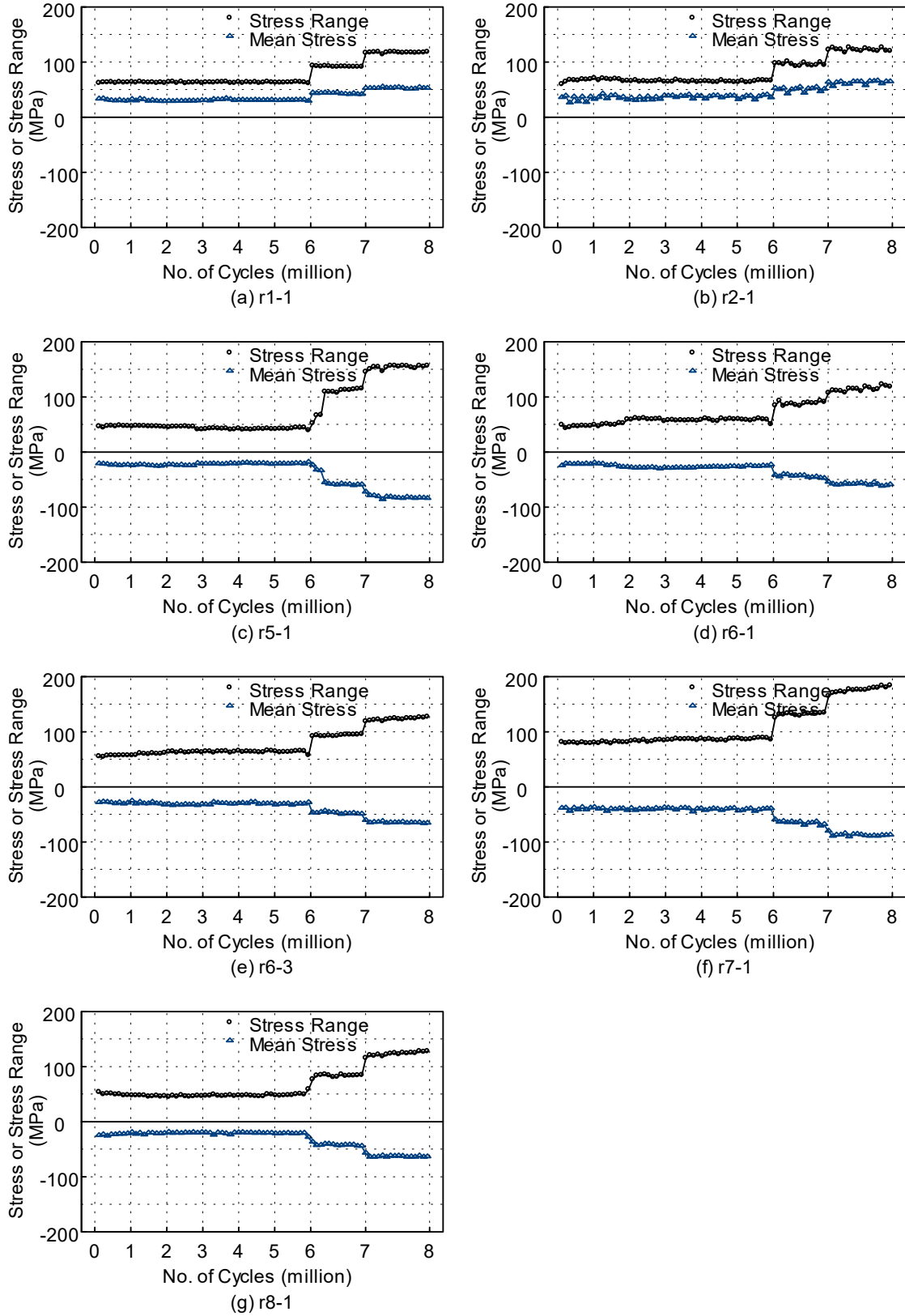


Figure 5.9 Specimen 3: Stress Range and Mean Stress in Rib R2 near the PJP Welds

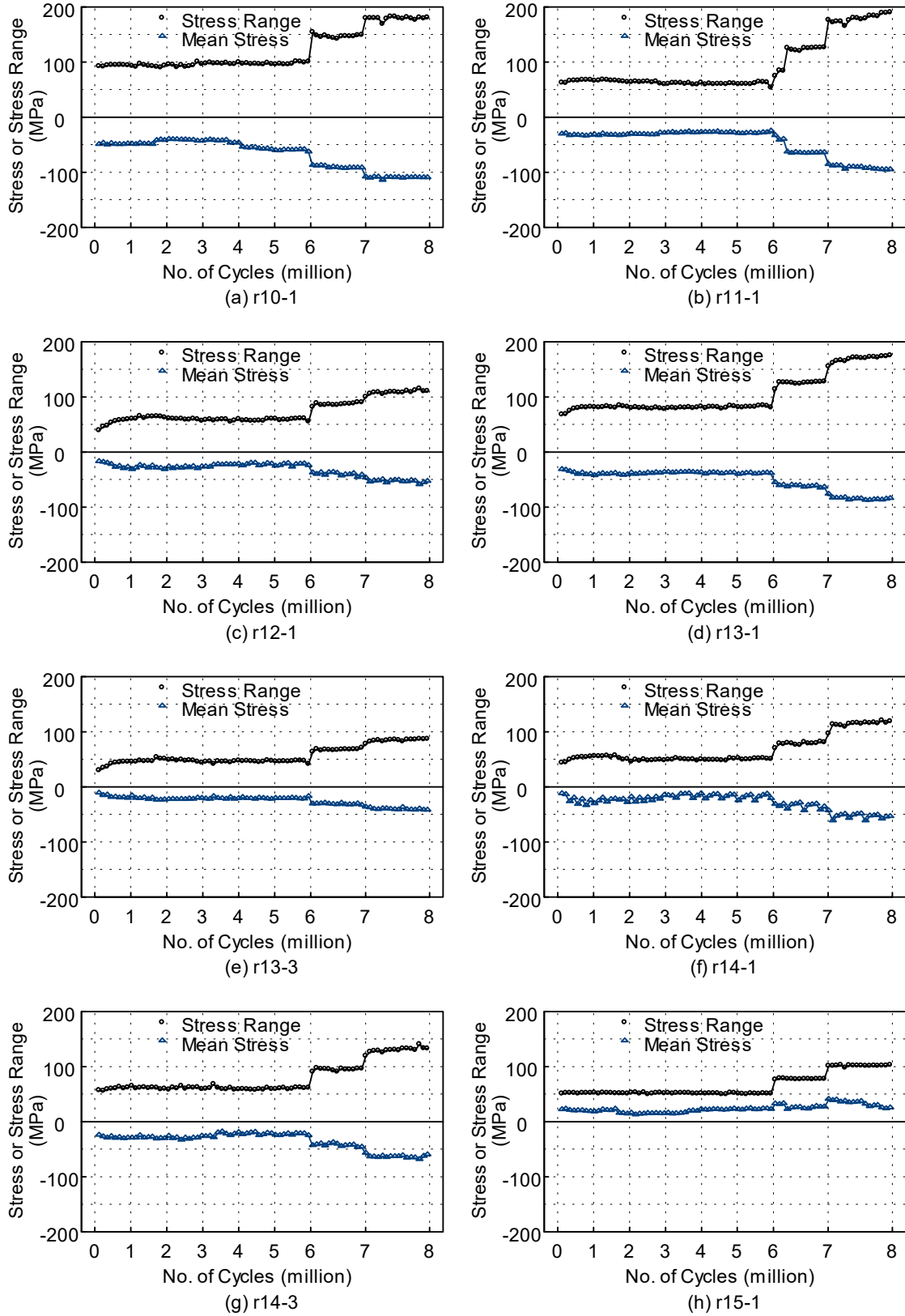


Figure 5.10 Specimen 3: Stress Range and Mean Stress in Rib R3 near the PJP Welds

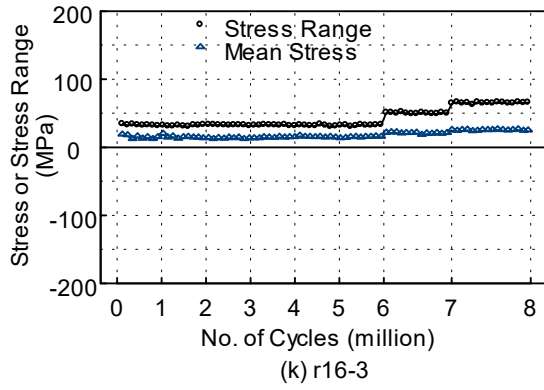
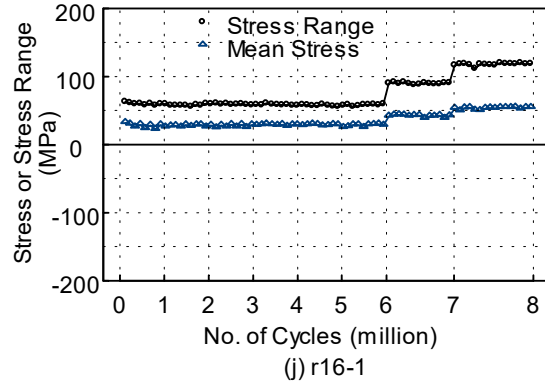
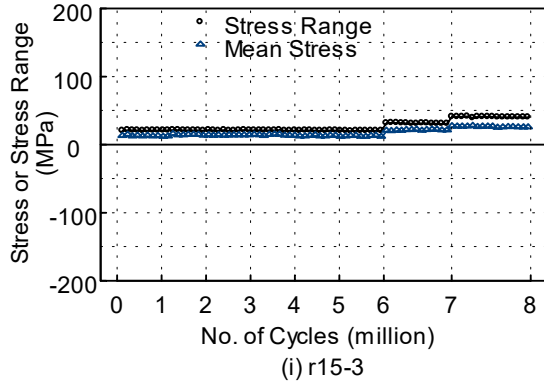


Figure 5.10 Specimen 3: Stress Range and Mean Stress in Rib R3 near the PJP Welds
(continued)

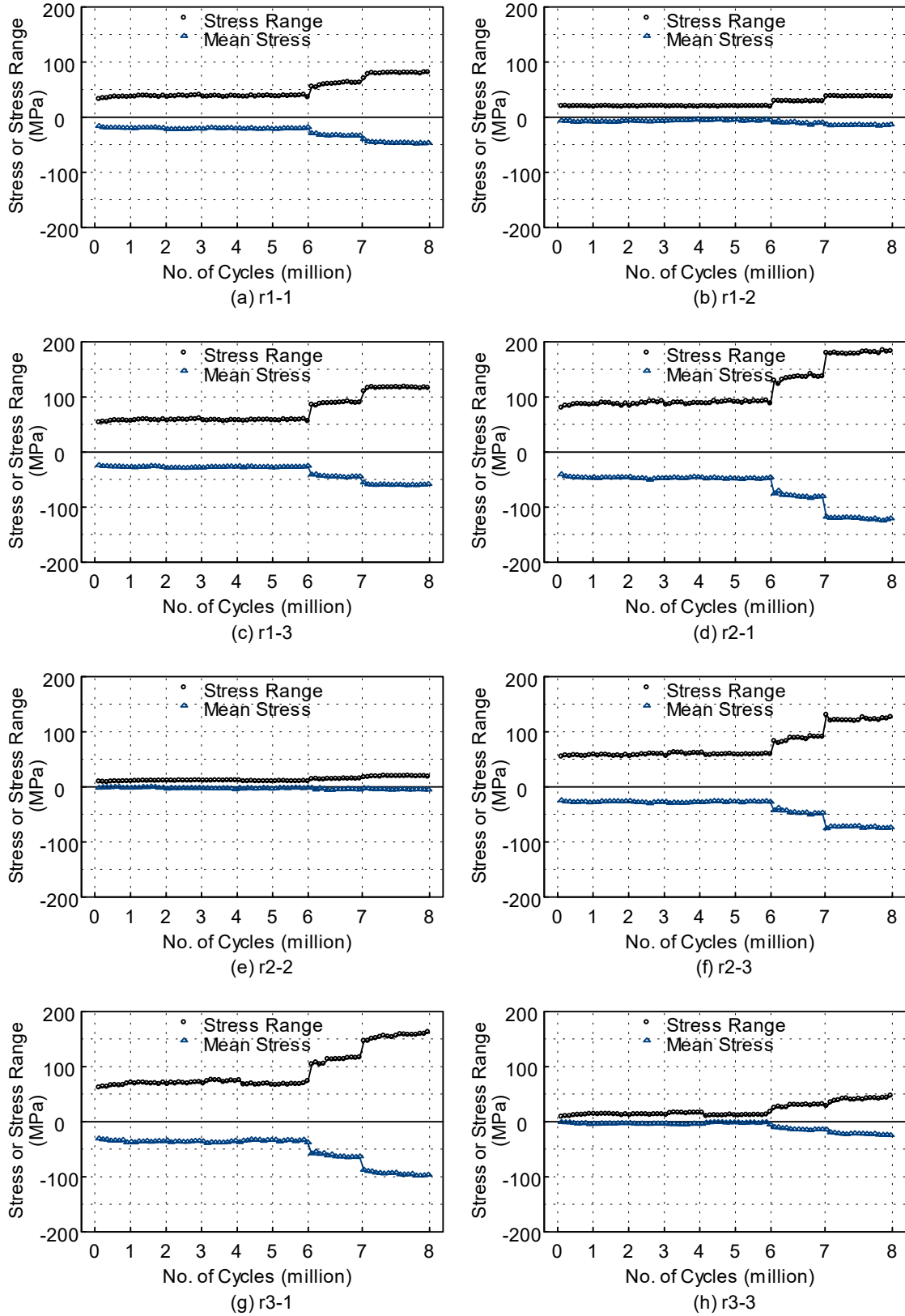


Figure 5.11 Specimen 4: Stress Range and Mean Stress in Rib R2 near the PJP Welds

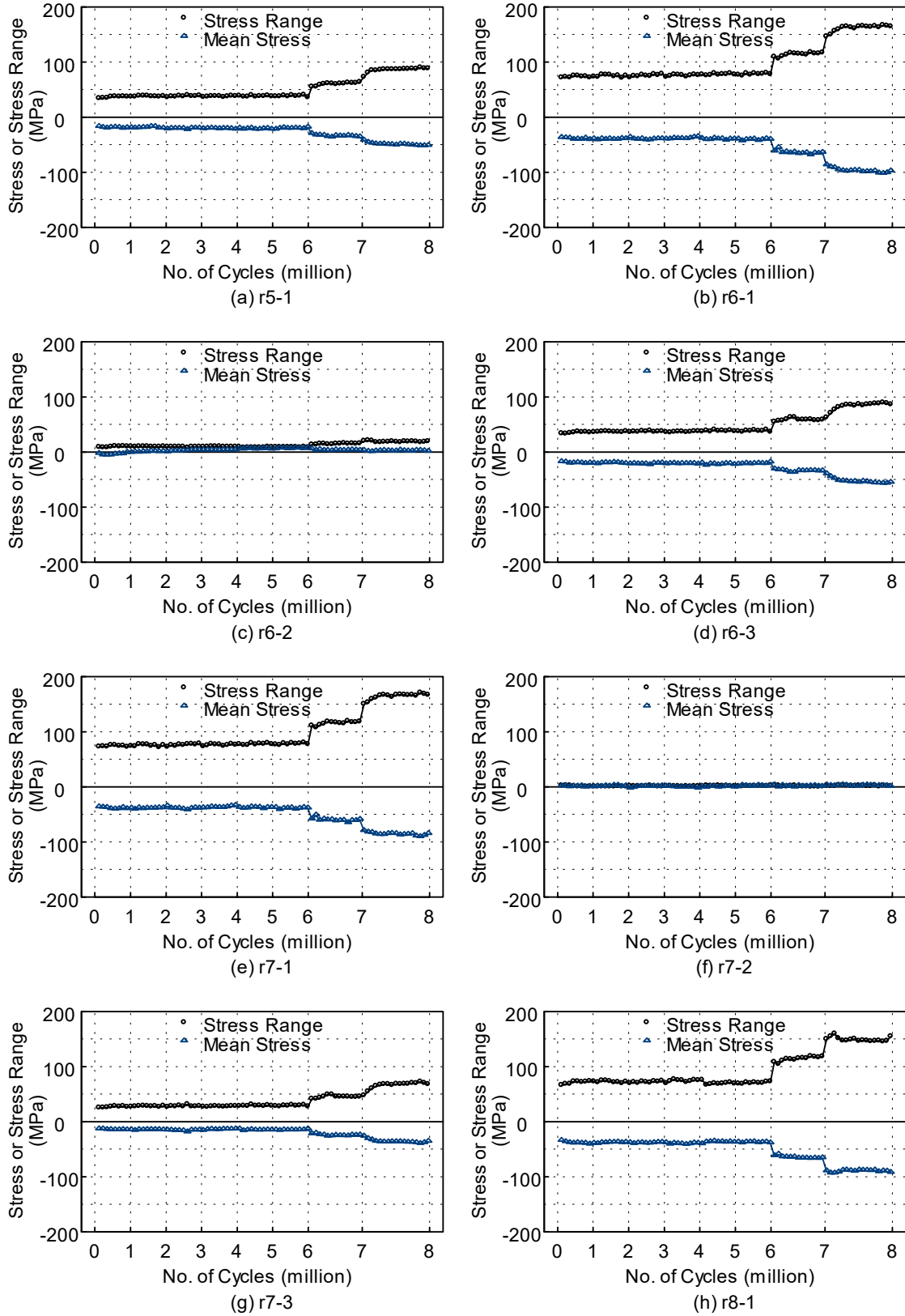


Figure 5.12 Specimen 4: Stress Range and Mean Stress in Rib R3 near the PJP Welds

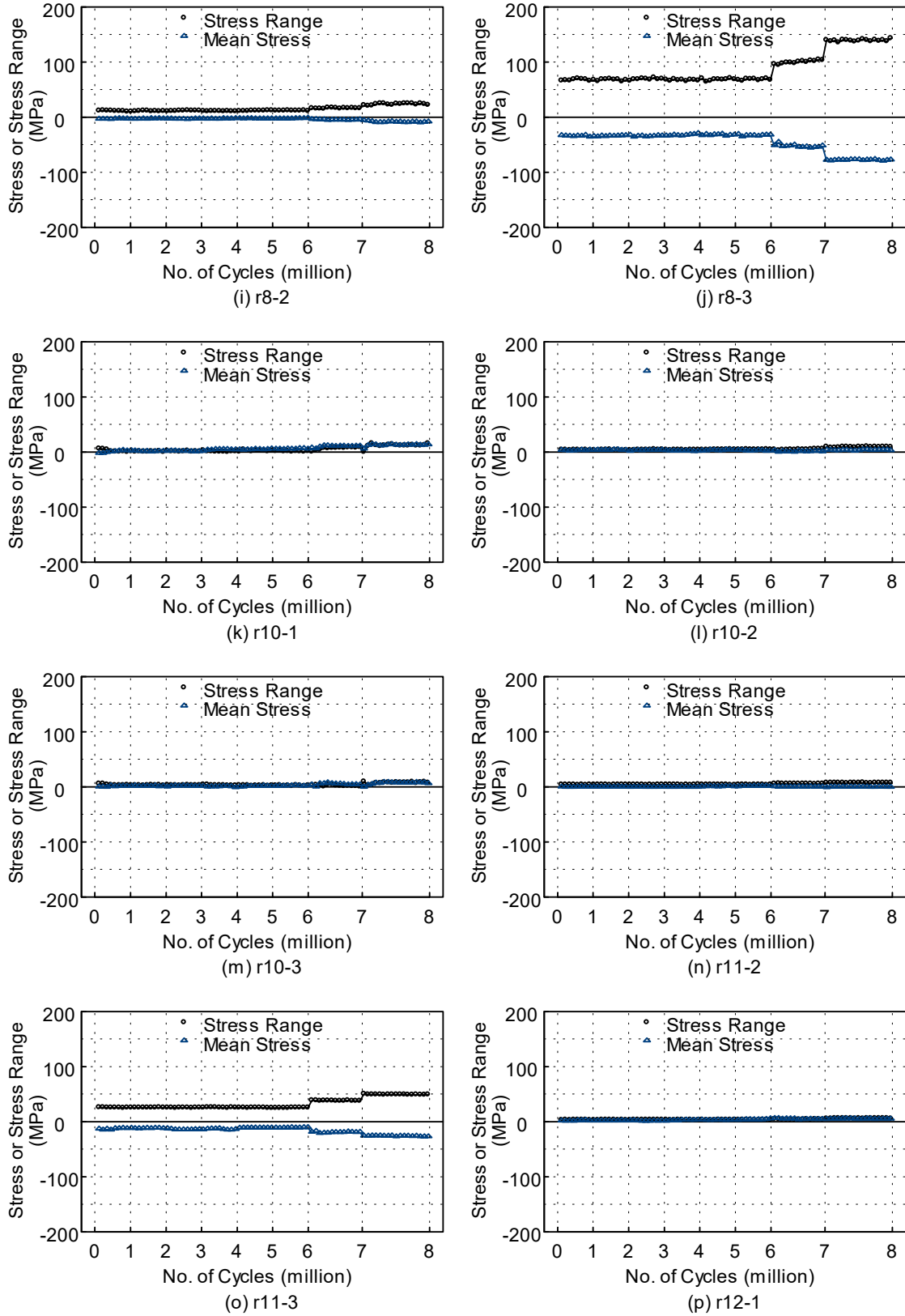


Figure 5.12 Specimen 4: Stress Range and Mean Stress in Rib R3 near the PJP Welds (continued)

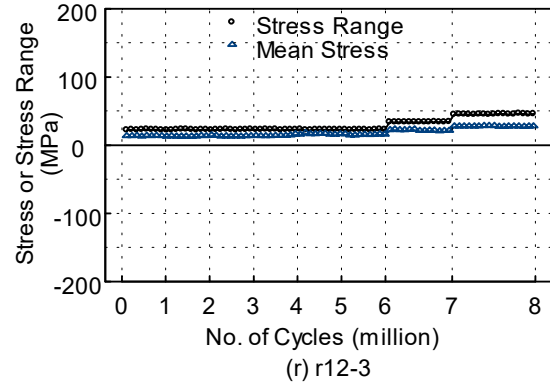
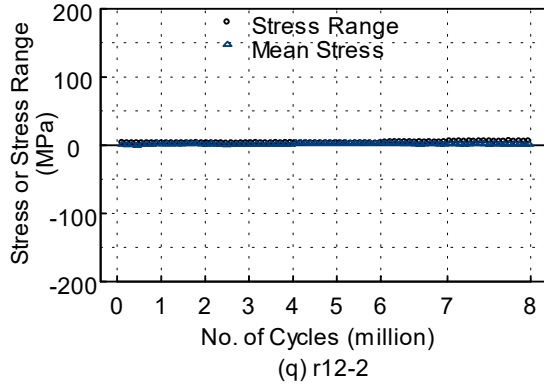


Figure 5.12 Specimen 4: Stress Range and Mean Stress in Rib R3 near the PJP Welds (continued)

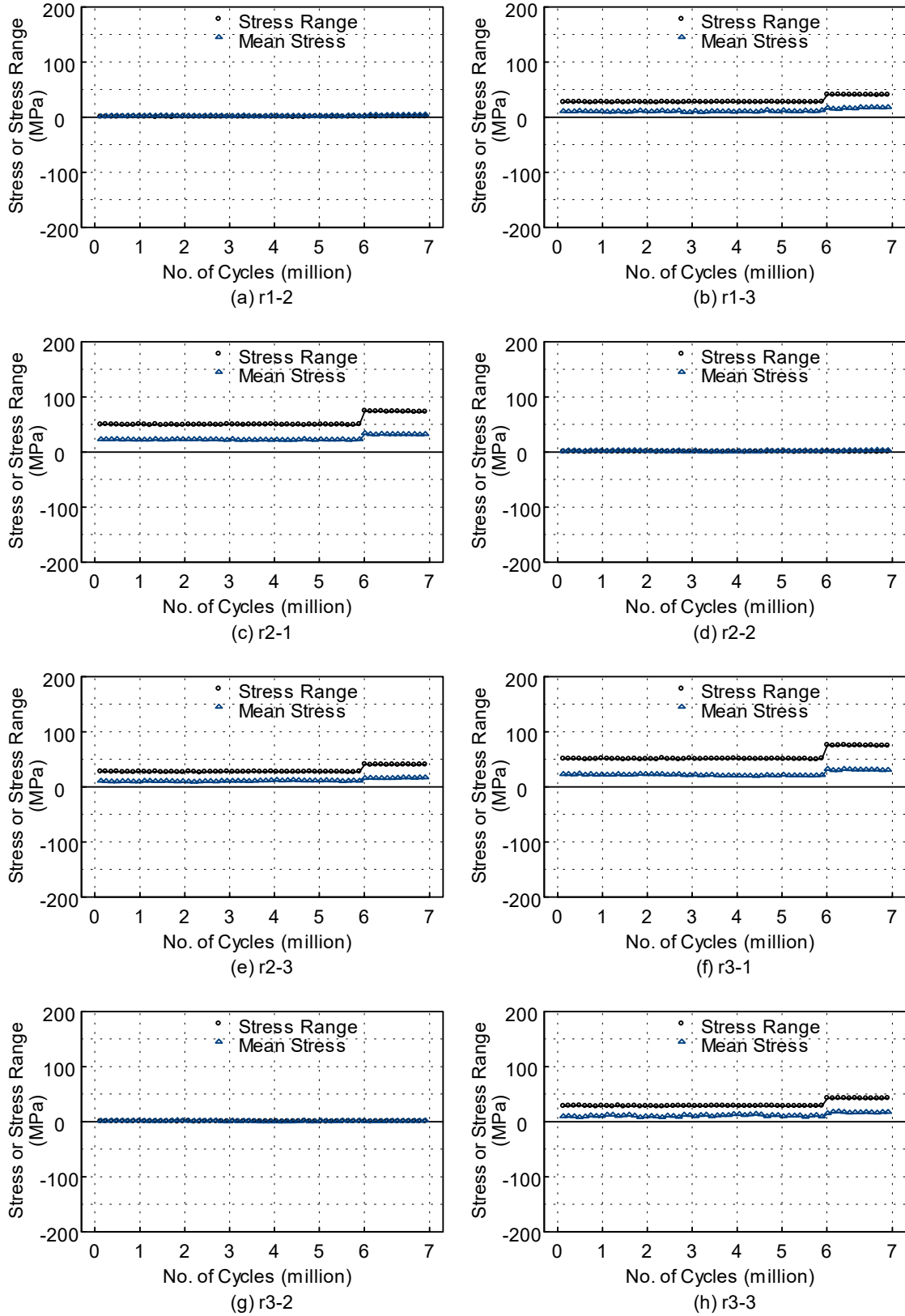


Figure 5.13 Specimen 5: Stress Range and Mean Stress in Rib R2 near the PJP Welds

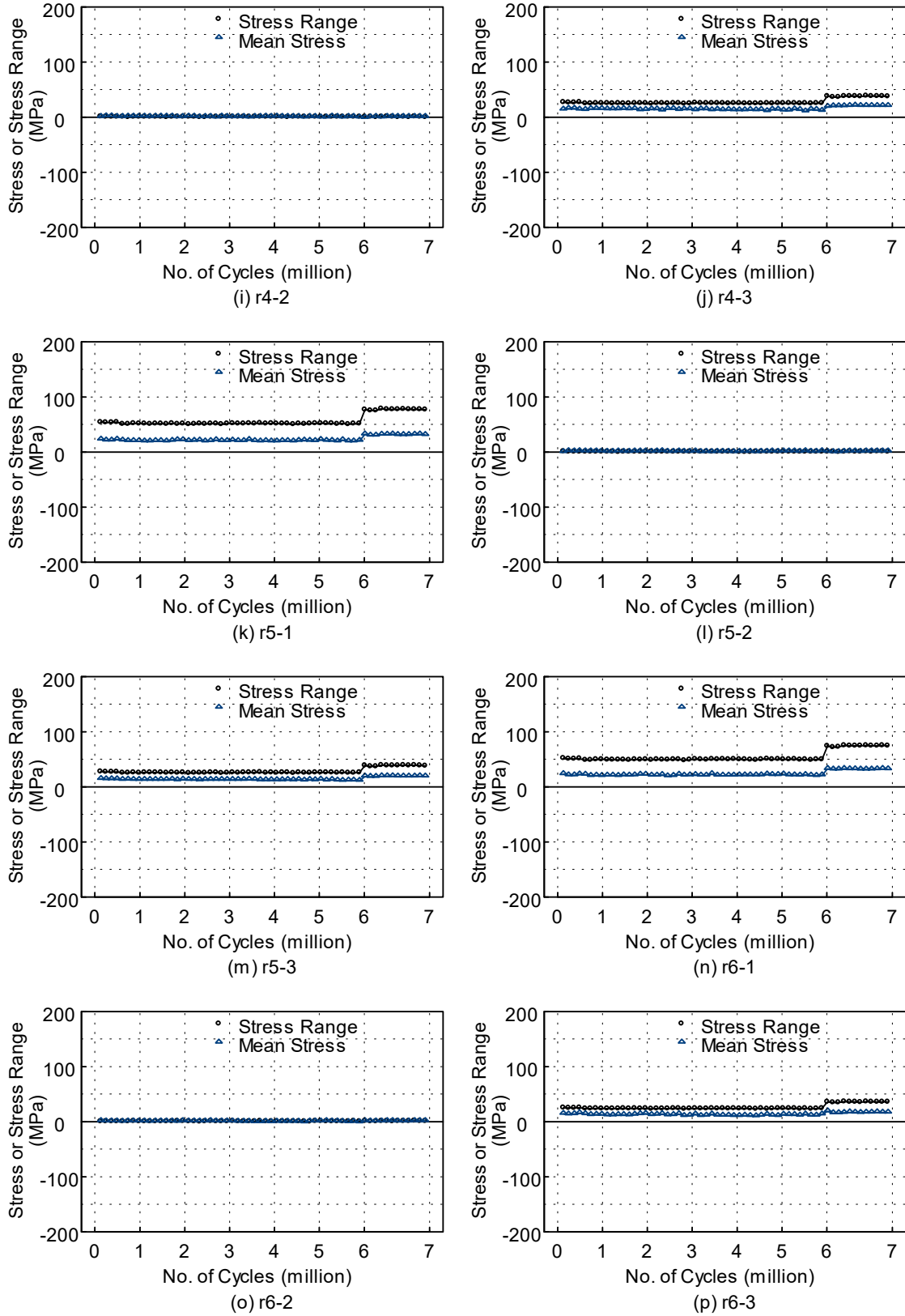


Figure 5.13 Specimen 5: Stress Range and Mean Stress in Rib R2 near the PJP Welds (continued)

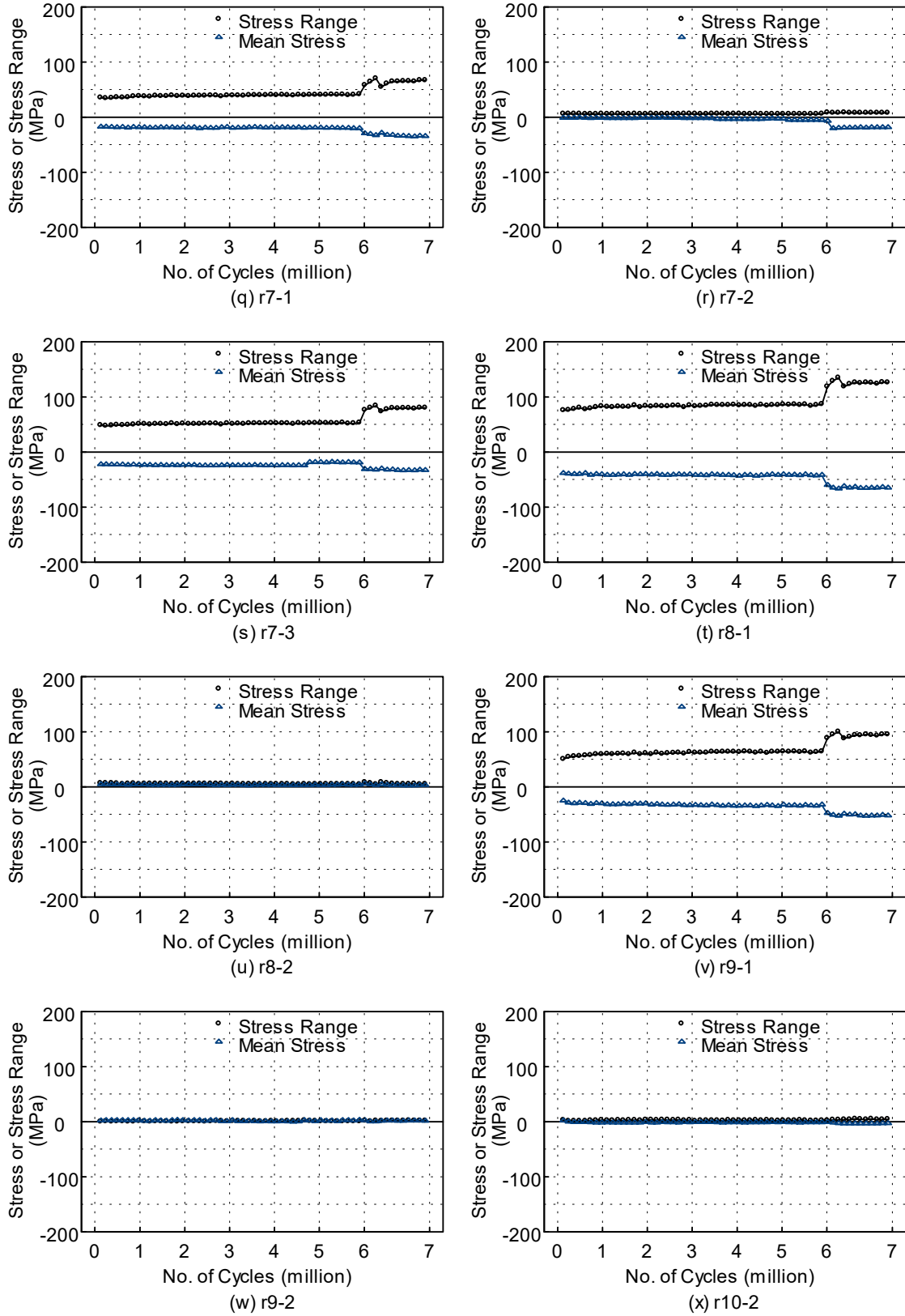


Figure 5.13 Specimen 5: Stress Range and Mean Stress in Rib R2 near the PJP Welds (continued)

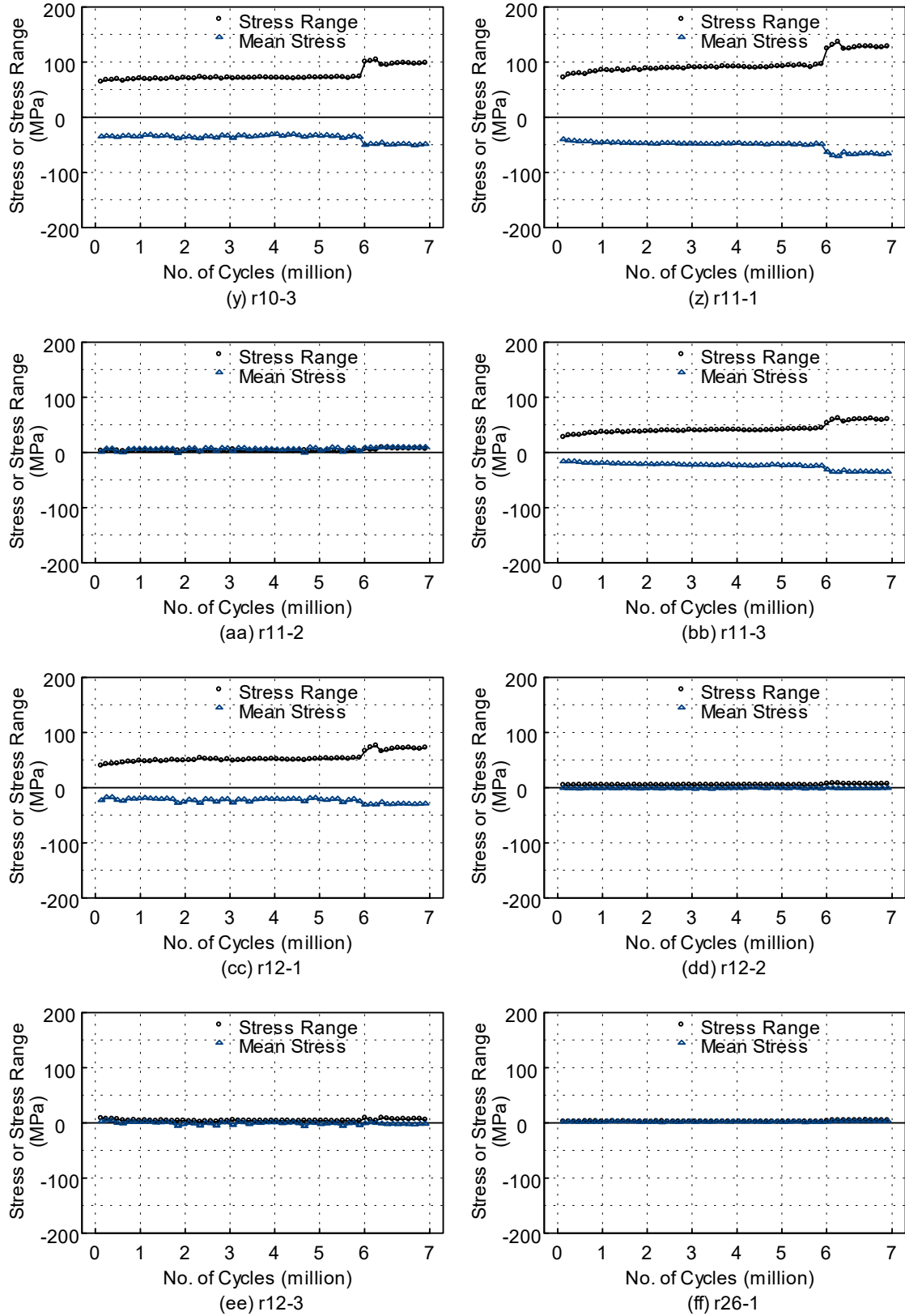


Figure 5.13 Specimen 5: Stress Range and Mean Stress in Rib R2 near the PJP Welds (continued)

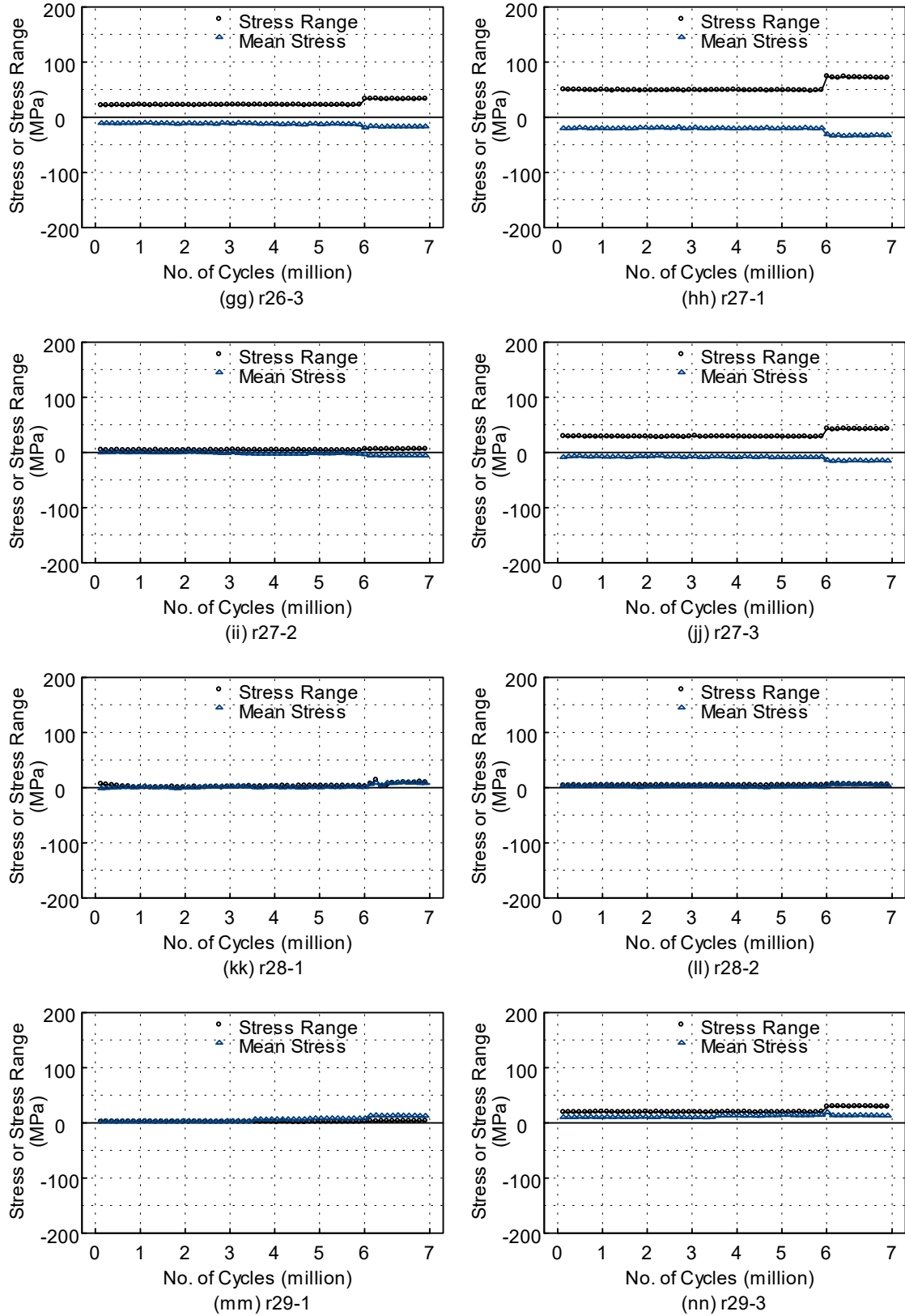


Figure 5.13 Specimen 5: Stress Range and Mean Stress in Rib R2 near the PJP Welds (continued)

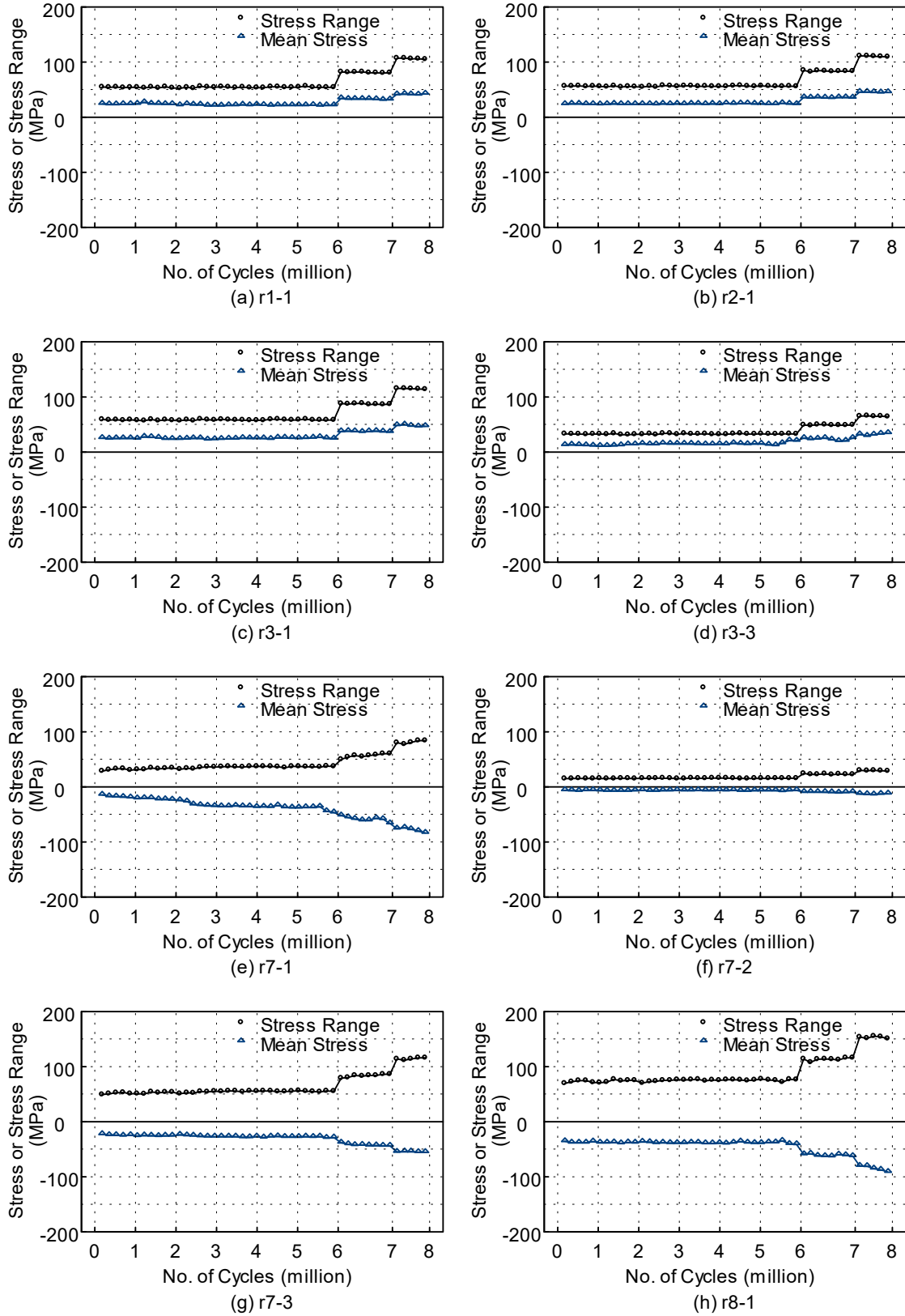


Figure 5.14 Specimen 6: Stress Range and Mean Stress in Rib R2 near the PJP Welds

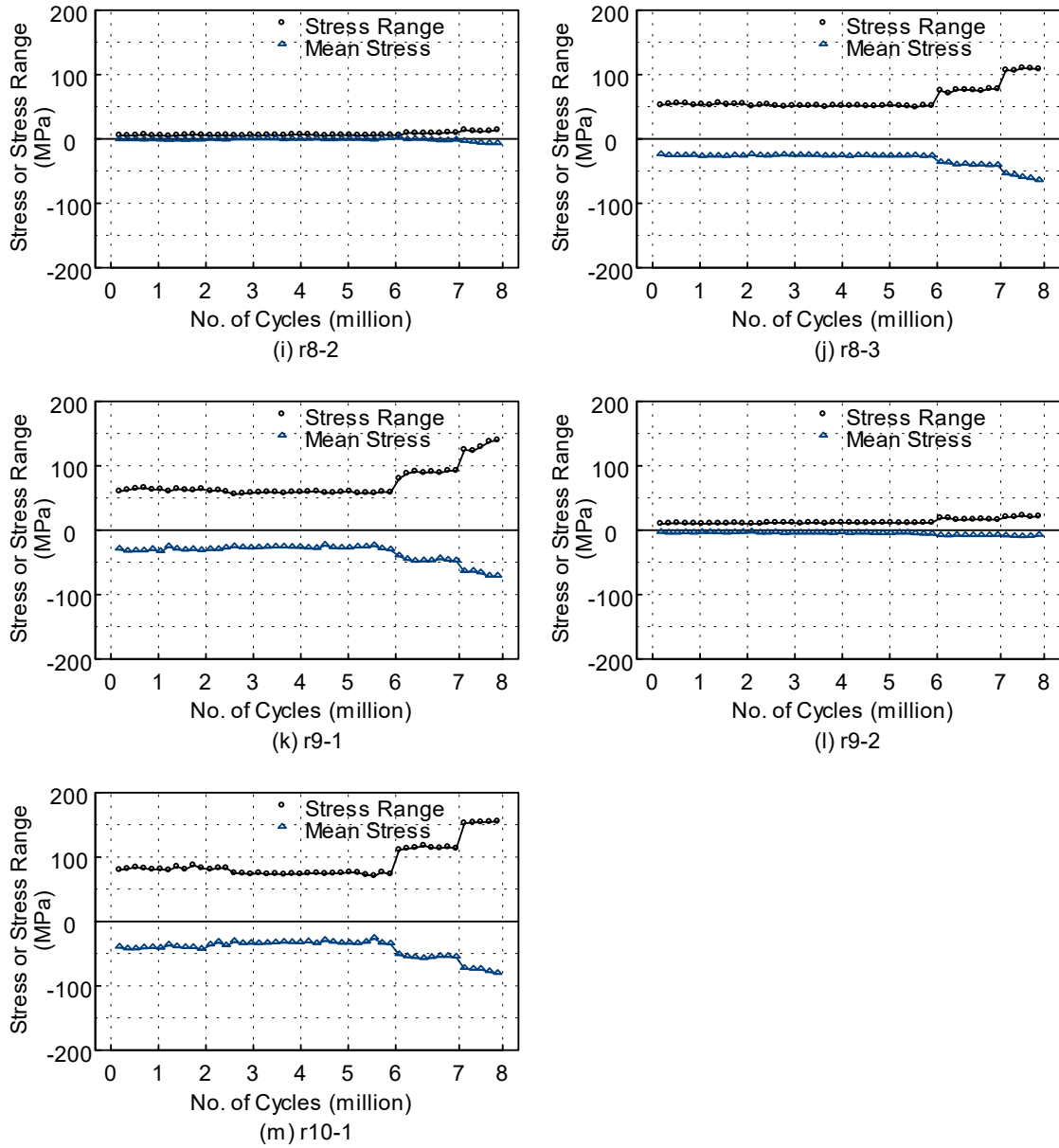


Figure 5.14 Specimen 6: Stress Range and Mean Stress in Rib R2 near the PJP Welds
(continued)

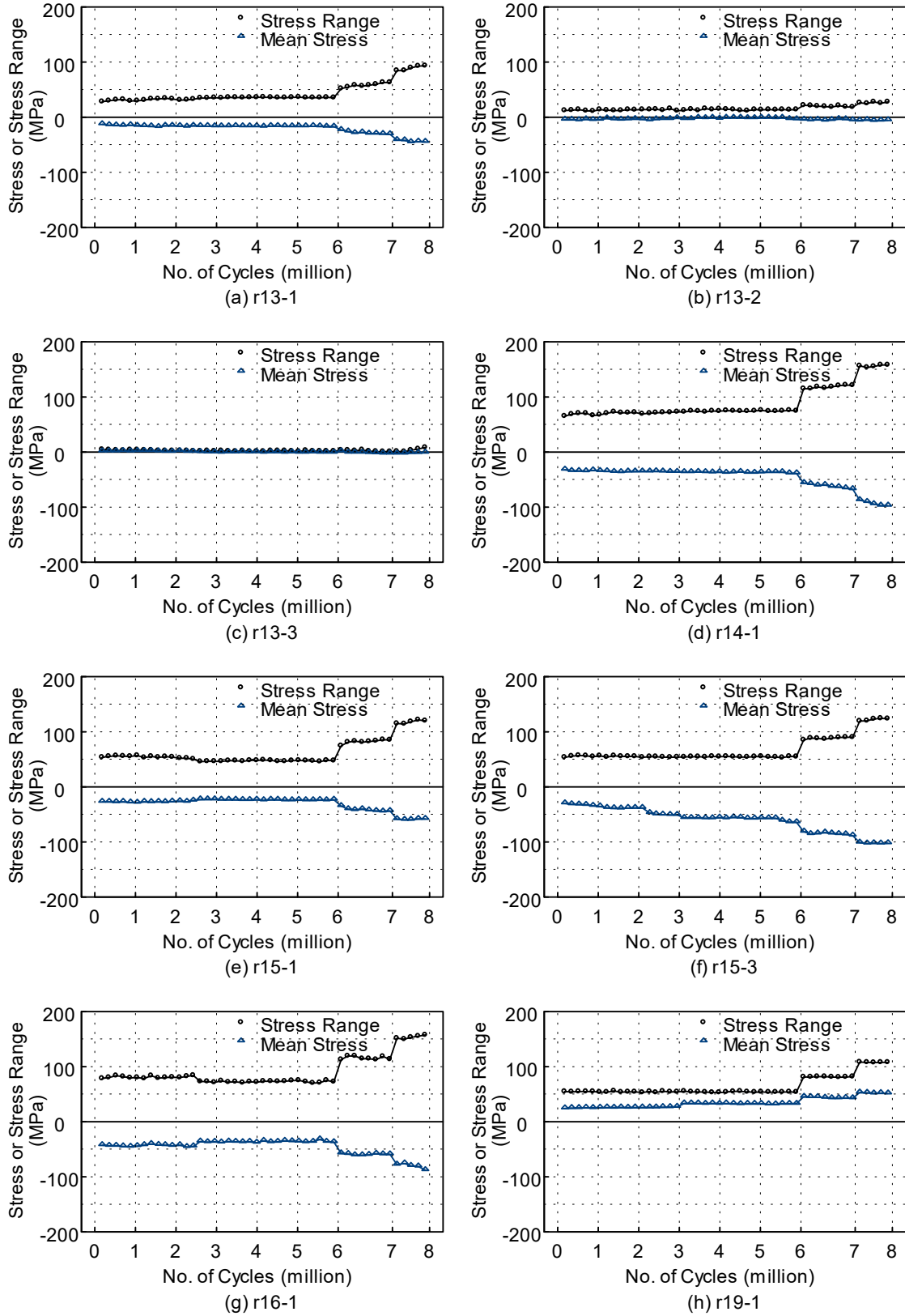


Figure 5.15 Specimen 6: Stress Range and Mean Stress in Rib R3 near the PJP Welds

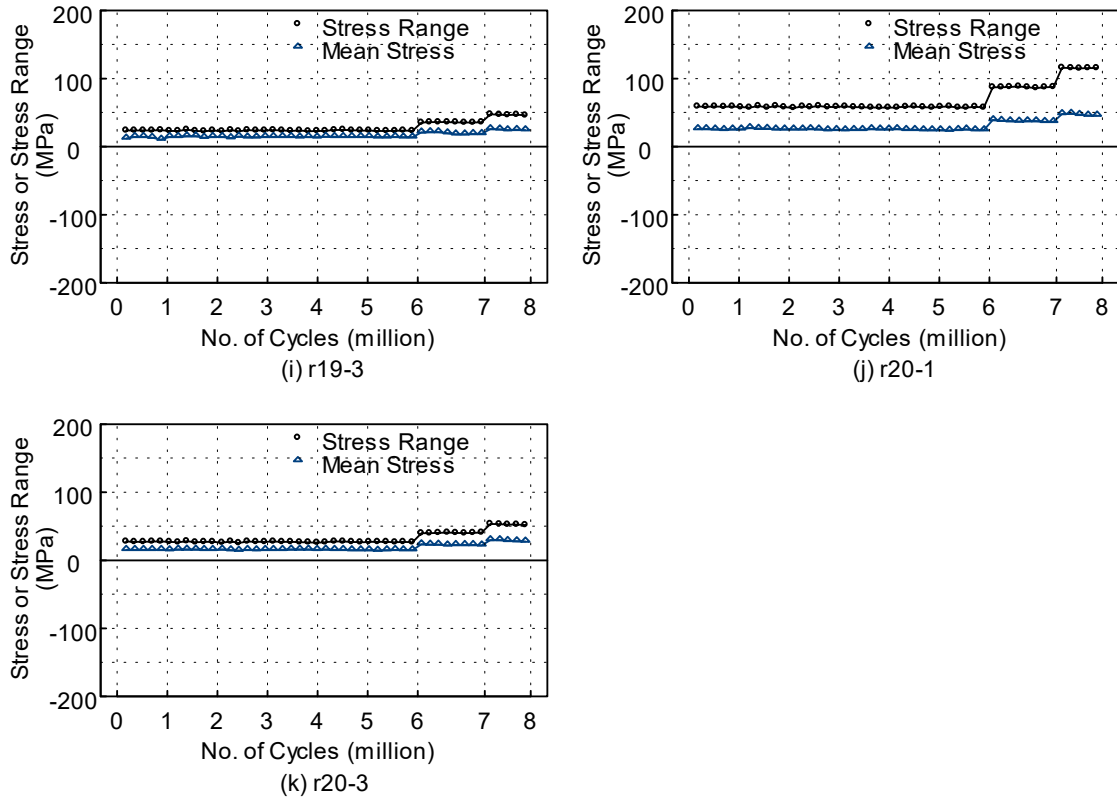


Figure 5.15 Specimen 6: Stress Range and Mean Stress in Rib R3 near the PJP Welds (continued)

5.2.3 Fatigue Cracks near Rib-to-Deck Welds

Regions of rib-to-deck welds directly beneath the loading pads were cut out for further crack inspection after completion of testing at 8 million cycles for each of the specimens. Figure 5.16 show the cutting locations with their designation (C1 to C4). Once pieces were removed from the specimen, each piece was sliced in strips as shown in Figure 5.17. Magnetic particle test (MT) was conducted on the strips to identify cracks at the rib-to-deck welded joints. MT inspection revealed fatigue cracks in three specimens (Specimens 2, 3, and 6). No cracks were observed in Specimens 4 and 5. Figure 5.18 shows typical cracks identified by MT. Most of the identified cracks showed a pattern that initiated from the weld toe on the bottom side of the deck plate, and propagated into the deck plate. One crack initiated from the weld root, and also propagated into the deck plate. The crack from the weld root initiated from transition region between 80% PJP and 100% PJP welds. No deck plate crack penetrated completely through the deck plate,

but was observed to arrest after it grew out of the residual tensile stress field of the partial penetration weld toe or weld root.

Cracks from the weld toe on the bottom of the deck plate were identified in Specimen 2 at three locations (C1, C2, and C3). Figure 5.19 shows the crack depth at location C2 and C3, measured vertically from the bottom side of the deck plate. A cross section through the crack in C1 of Specimen 2 was cut, and it verified the linear crack indication as shown in Figure 5.20. One crack was identified at the location of C1 in Specimen 3, and the plot of the crack depth is shown in Figure 5.21. Cracks were identified at three locations (C1, C2, and C3) in Specimen 6, among which the cracks initiated from the weld toe at C1 and C2 and the crack initiated from the weld root at C3. The plots of the crack depth at these locations are shown in Figure 5.22.

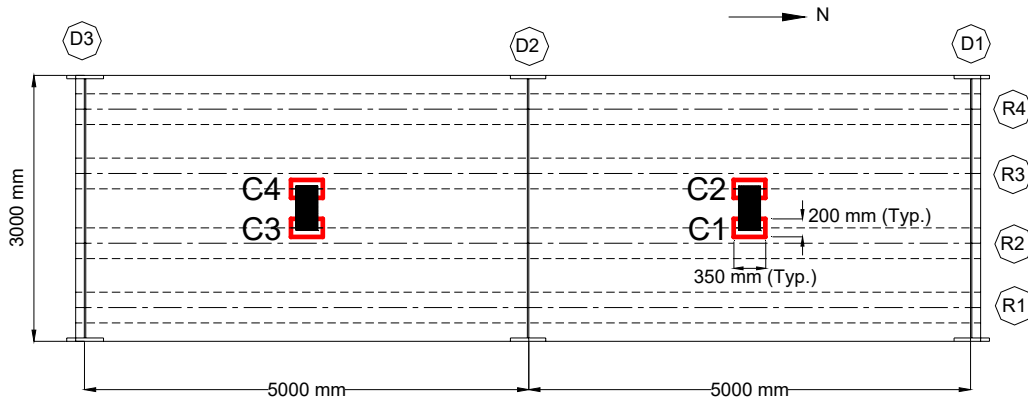


Figure 5.16 Four Cutting Locations with Designations (C1 to C4)

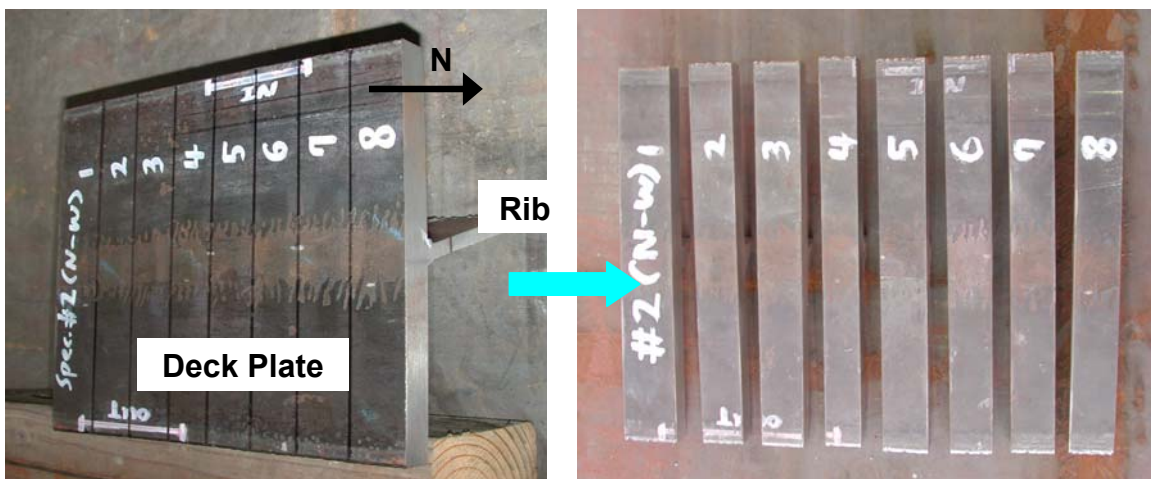


Figure 5.17 Sliced Pieces

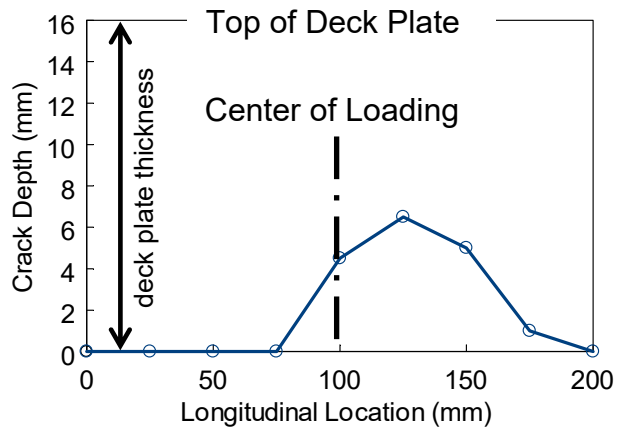


(a) Crack from Weld Toe

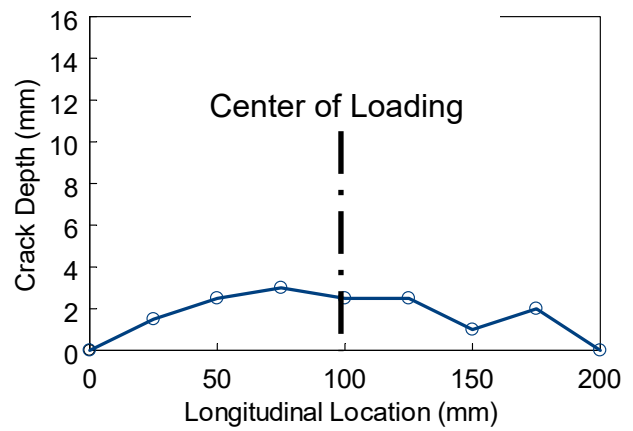


(b) Crack from Weld Root

Figure 5.18 Typical Crack Pattern at Rib-to-Deck PJP Welds



(a) Location C2



(b) Location C3

Figure 5.19 Specimen 2: Depth of Crack Initiating from Rib-to-Deck PJP Welds

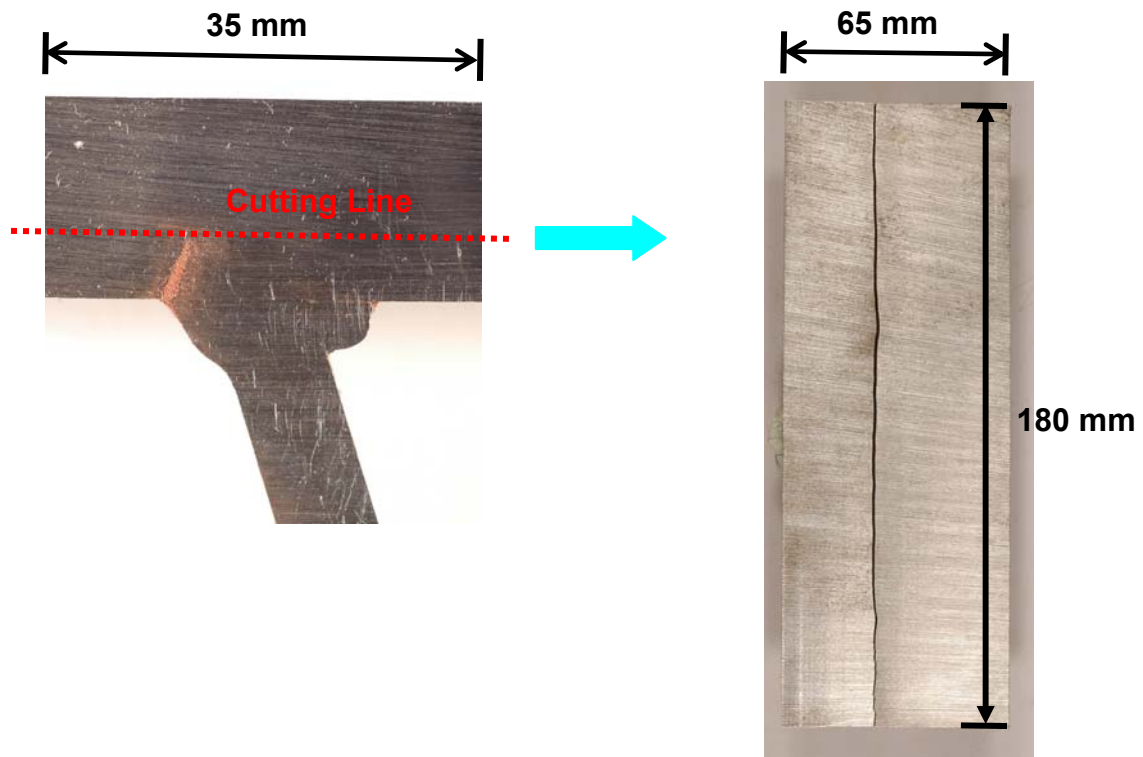


Figure 5.20 Specimen 2: Indication of Linear Crack at Rib-to-Deck PJP Weld (Piece Location C1)

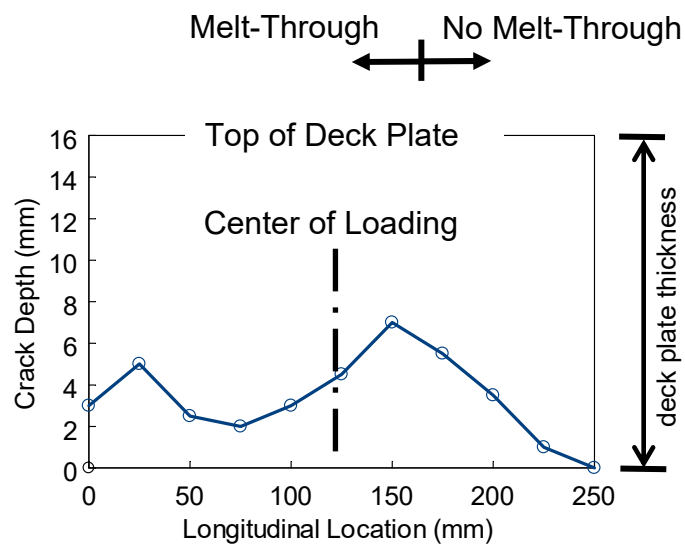
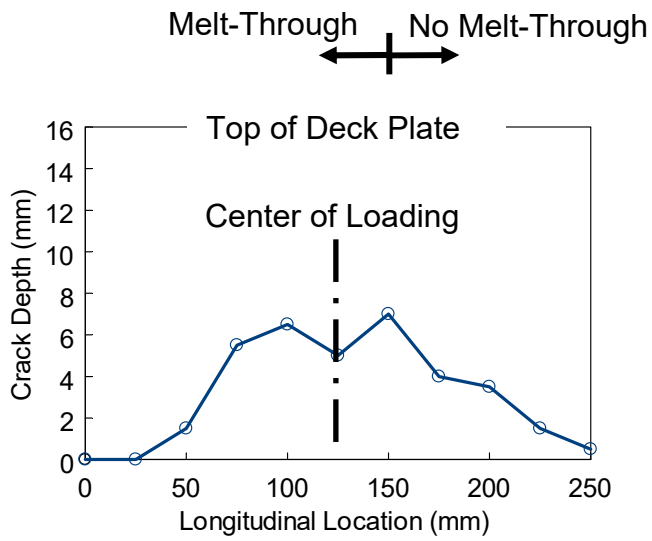
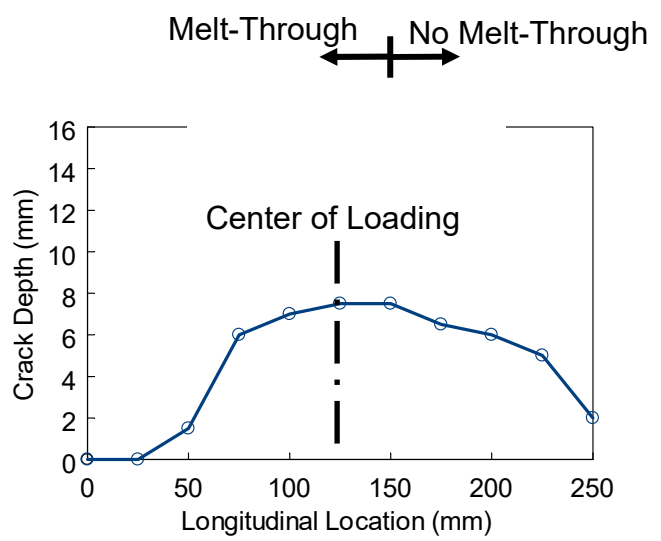


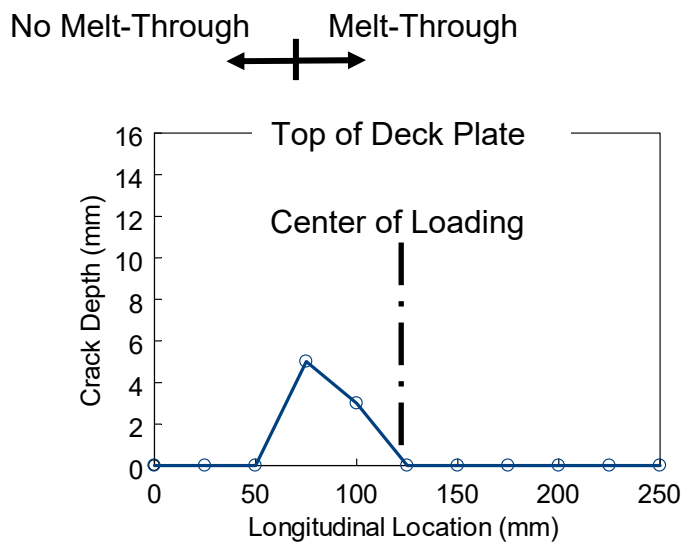
Figure 5.21 Specimen 3: Crack Depth at Rib-to-Deck PJP Welds (Location C1)



(a) Location C1



(b) Location C2



(c) Location C3

Figure 5.22 Specimen 6: Crack Depth at Rib-to-Deck PJP Welds

5.3 Measured Response at Support Diaphragms

5.3.1 Stress Distribution in Ribs, Diaphragms, and Bulkheads

The stress range (S_r) and the mean stress (S_m) computed from the measured strains on ribs, bulkheads, and diaphragms at the supports are summarized in Tables 5.9 to 5.12. Plots of the stress range and the mean stress up to 8 million cycles are shown in Figures 5.23 to 5.28.

For example, up to the first 100,000 cycles before cracks were initiated, the S15 and S16 pair would give a maximum in-plane stress of -7.5 MPa and a maximum out-of-plane (or bending) stress of 48.5 MPa. The stress range on the inner surface of the rib wall was 40.6 MPa (mean stress = 20.7 MPa), and the stress range on the outer surface was 54.5 MPa (mean stress = -28.8 MPa). These plots show a significant variation of the stresses during the entire loading cycles. Such variation was caused by a redistribution of the stresses once the cracks developed.

The stress range in the bulkheads and diaphragms was low in general. During the first 100,000 cycles, gage r32-3 of Specimen 3 showed a maximum stress range of 32.9 MPa (mean stress = -19.1 MPa) in compression field, and gage r6-3 of Specimen 2 showed a maximum stress range of 9.2 MPa (mean stress = 8.9 MPa) in tension field. Based on the strain gage rosettes placed at the bottom corners of the bulkheads of an exterior support, r28-3 of Specimen 3 gave a maximum stress range of 13.4 MPa (mean stress = -8.2 MPa) in compression field, and r27-2 of Specimen 2 gave a maximum stress range of 7.4 MPa (mean stress = 4.0 MPa) in tension field.

Table 5.9 Specimen 2: Stress Range and Mean Stress at Support Diaphragms

Gage	Component	Stress or Stress Range (MPa)									
		0.1 M cycles		3 M cycles		5.9 M cycles		6.5 M cycles		7.5 M cycles	
		S _r	S _m	S _r	S _m	S _r	S _m	S _r	S _m	S _r	S _m
r4	1	8.4	3.2	9.3	3.5	9.3	2.5	13.9	5.5	19.1	9.2
	2	7.8	-9.5	9.1	-10.5	9.4	-27.4	13.7	-26.5	18.5	-27.5
	3	25.0	-22.7	28.2	-17.6	29.0	-20.9	44.3	-33.2	58.1	-40.6
r5	1	9.8	-2.6	10.9	-1.5	10.9	-10.0	16.7	-6.7	21.5	-4.5
	3	26.9	-18.8	28.9	-20.4	29.4	-19.5	45.8	-26.8	60.7	-39.9
r6	2	12.9	-7.6	13.9	-6.3	13.6	-9.3	21.5	-11.5	29.7	-16.8
	3	9.2	8.9	9.5	9.8	9.6	0.0	15.3	5.8	21.2	10.7
r8	2	9.7	-2.6	10.1	-2.4	10.7	-8.4	16.2	-8.8	23.3	-18.7
r9	1	9.8	0.7	9.6	-0.7	9.6	-2.0	13.8	-0.4	21.5	2.9
r10	1	6.4	-3.3	5.7	-15.9	4.2	-22.5	6.1	-25.9	5.2	-20.2
	3	10.1	-1.6	11.2	-8.9	11.9	-13.3	17.8	-8.2	18.4	-7.1
S54	-	61.8	-30.3	73.9	-46.5	78.4	-33.6	116.8	-54.7	17.7	-302.7
S55	-	52.1	34.7	0.7	-227.0	9.3	-250.9	16.7	-259.9	35.0	-238.6
S60	-	59.2	26.0	9.2	-354.0	19.1	-398.2	26.4	-388.2	35.7	-371.4
S61	-	50.5	-14.1	2.2	-334.0	19.0	-357.7	33.3	-361.2	85.3	-327.5

Table 5.10 Specimen 3: Stress Range and Mean Stress at Support Diaphragms

Gage	Component	Stress or Stress Range (MPa)									
		0.1 M cycles		3 M cycles		5.9 M cycles		6.5 M cycles		7.5 M cycles	
		S _r	S _m	S _r	S _m	S _r	S _m	S _r	S _m	S _r	S _m
r26	1	21.0	9.4	21.2	8.7	22.0	10.9	29.2	13.4	37.6	13.0
r27	2	7.4	4.0	5.5	0.3	4.7	3.5	6.7	3.7	5.3	11.2
r28	2	10.6	-6.6	11.2	-8.1	12.0	-8.7	17.3	-16.9	18.2	-29.5
	3	13.4	-8.2	14.6	-12.4	15.8	-13.0	24.4	-20.8	20.0	-35.3
r31	1	27.5	-6.8	27.0	-5.8	28.3	-2.0	44.1	-11.4	58.8	-17.7
r32	3	32.9	-19.1	32.2	-17.8	33.3	-16.8	53.7	-33.7	71.2	-38.3
S30	-	33.2	-14.8	37.7	-27.9	40.7	-28.7	60.4	-32.5	7.6	-103.9
r22	1	37.0	19.7	10.9	-243.7	19.9	-287.0	33.7	-307.3	46.7	-320.5
	3	38.4	22.9	21.4	-66.3	17.1	-88.0	24.3	-85.7	0.5	-93.2
S34	-	34.5	16.3	18.3	-295.7	31.3	-313.7	42.1	-328.7	64.6	-371.6
S35	-	21.7	-6.1	23.4	-13.2	26.4	-8.7	27.7	-29.4	72.2	-206.7
S38	-	25.1	-7.6	27.9	-15.3	30.6	-14.8	36.8	-38.3	36.8	-250.2
S39	-	35.4	21.6	14.4	-262.0	22.4	-299.4	35.6	-318.3	47.4	-319.4

Table 5.11 Specimen 4: Stress Range and Mean Stress at Support Diaphragms

Gage	Stress or Stress Range (MPa)									
	0.1 M cycles		3 M cycles		5.9 M cycles		6.5 M cycles		7.5 M cycles	
	S _r	S _m	S _r	S _m	S _r	S _m	S _r	S _m	S _r	S _m
S1	67.1	-32.3	31.2	-21.2	24.1	-37.5	7.4	-184.9	39.8	-309.9
S2	63.0	30.5	2.6	-326.6	9.7	-354.1	18.3	-351.1	33.9	-331.1
S3	41.2	-20.0	44.9	-34.0	46.9	-34.4	70.9	-39.8	53.9	-218.3
S4	89.7	42.2	95.0	66.3	98.8	72.5	151.3	96.8	50.6	-215.6
S5	58.0	28.4	60.3	44.3	62.7	49.6	95.8	55.8	132.7	61.0
S6	34.8	-16.2	37.1	-28.4	39.0	-32.6	59.5	-38.5	80.1	-54.4
S9	60.2	-28.1	43.2	45.9	25.2	49.2	31.8	27.8	7.9	-145.2
S10	45.0	22.3	16.8	-121.3	8.9	-275.6	19.3	-312.0	34.0	-330.2
S11	32.7	-14.4	33.3	-20.9	35.6	-28.7	49.2	-21.8	59.8	-201.6
S12	61.7	29.0	51.3	28.8	51.3	27.5	74.8	3.4	74.6	37.2
S13	51.5	28.7	51.3	28.8	51.3	27.5	74.8	3.4	74.6	37.2
S14	33.4	-18.6	33.6	-19.5	33.4	-19.5	46.3	-12.8	4.1	-176.8
S15	40.6	20.7	40.6	22.5	39.7	24.6	59.1	10.4	66.3	-17.5
S16	54.5	-28.8	54.0	-27.8	54.2	-29.3	79.3	-22.2	100.9	-21.4

Table 5.12 Specimen 5: Stress Range and Mean Stress at Support Diaphragms

Gage	Stress or Stress Range (MPa)									
	0.1 M cycles		3 M cycles		5.9 M cycles		6.1 M cycles		6.9 M cycles	
	S _r	S _m	S _r	S _m	S _r	S _m	S _r	S _m	S _r	S _m
S2	21.9	-12.3	24.1	-17.0	26.6	-22.2	40.4	-24.8	16.1	-143.4
S3	53.9	27.4	10.0	-223.7	16.2	-342.2	26.9	-353.9	23.5	-349.9
S6	23.7	-7.1	27.0	-14.4	28.6	-15.9	42.0	-4.1	44.0	9.5
S7	46.7	20.8	8.4	-318.6	16.8	-366.9	25.9	-378.2	26.5	-383.0
S10	20.5	6.0	7.2	-164.1	20.1	-243.1	32.1	-254.4	36.5	-279.2
S11	27.9	-13.0	30.5	-19.2	32.2	-24.0	48.4	-20.6	43.9	-4.6
S14	23.5	-12.4	24.5	-12.8	24.6	-11.5	35.4	-14.2	28.2	-45.0
S15	41.2	20.4	41.9	20.7	41.9	21.5	62.7	27.9	1.0	-182.6

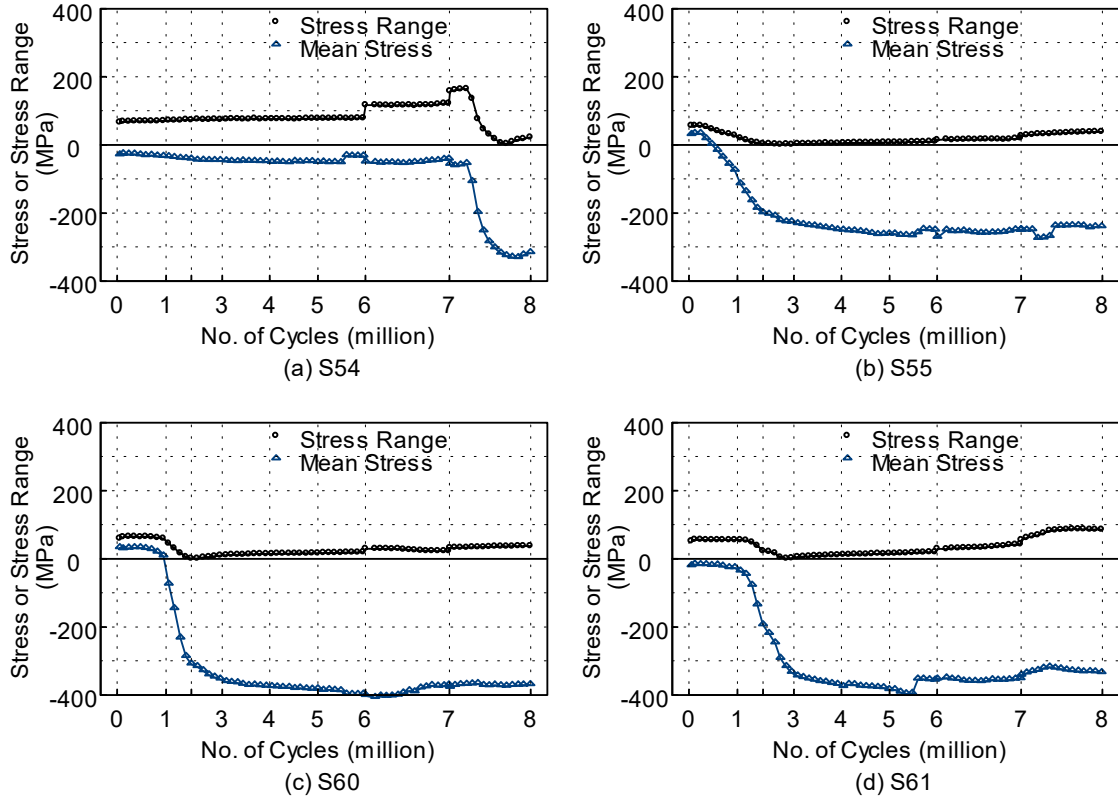


Figure 5.23 Specimen 2: Stress Range and Mean Stress in Ribs at Supports

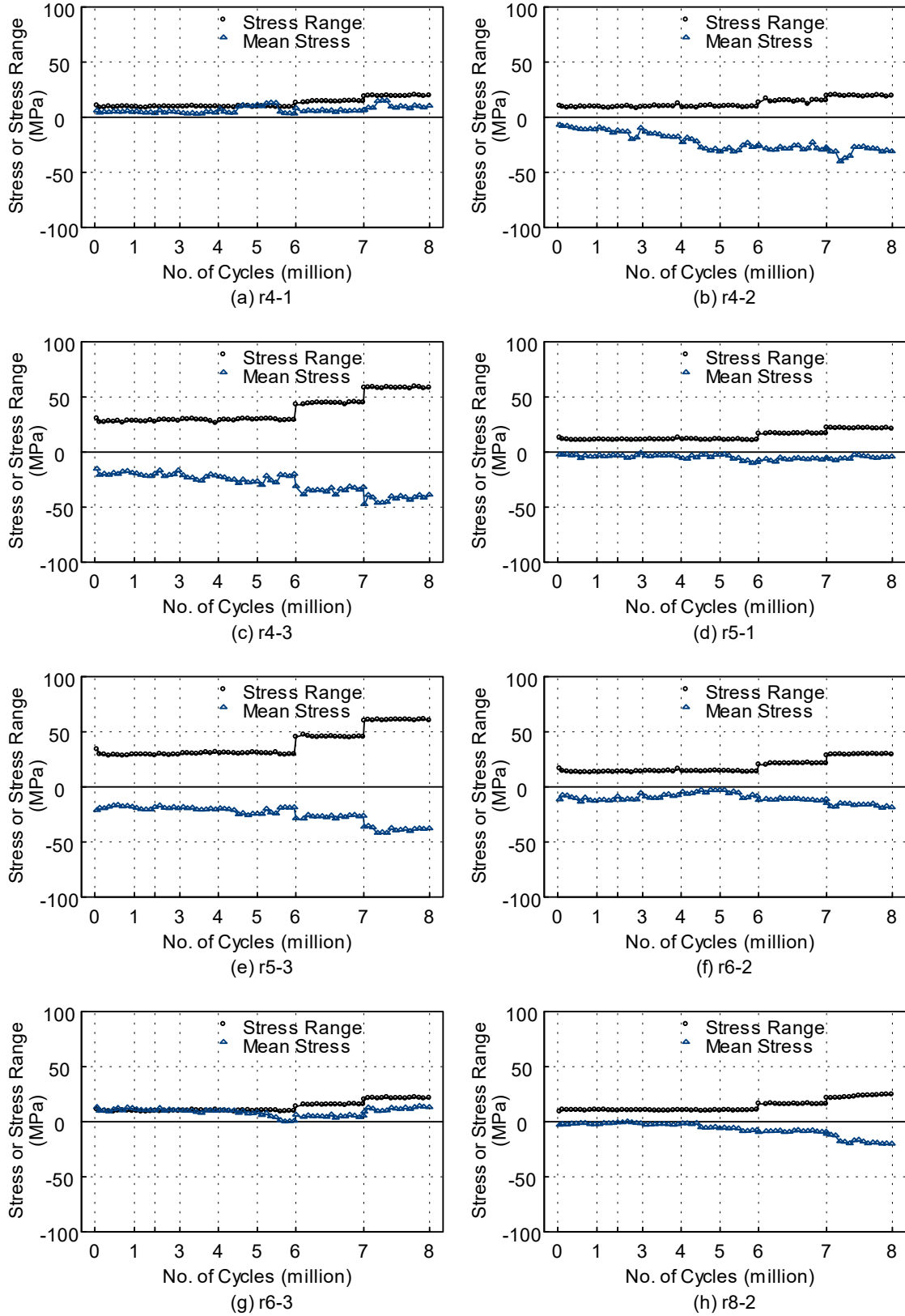


Figure 5.24 Specimen 2: Stress Range and Mean Stress in Bulkheads and Diaphragms

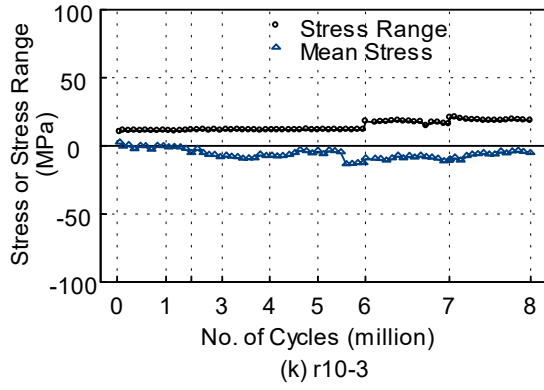
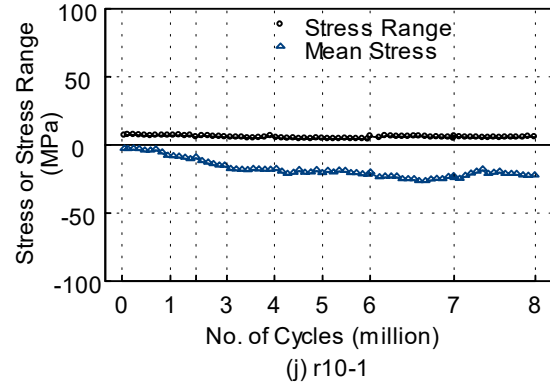
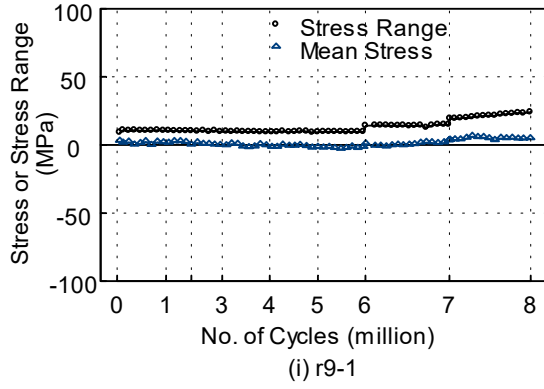


Figure 5.24 Specimen 2: Stress Range and Mean Stress in Bulkheads and Diaphragms (continued)

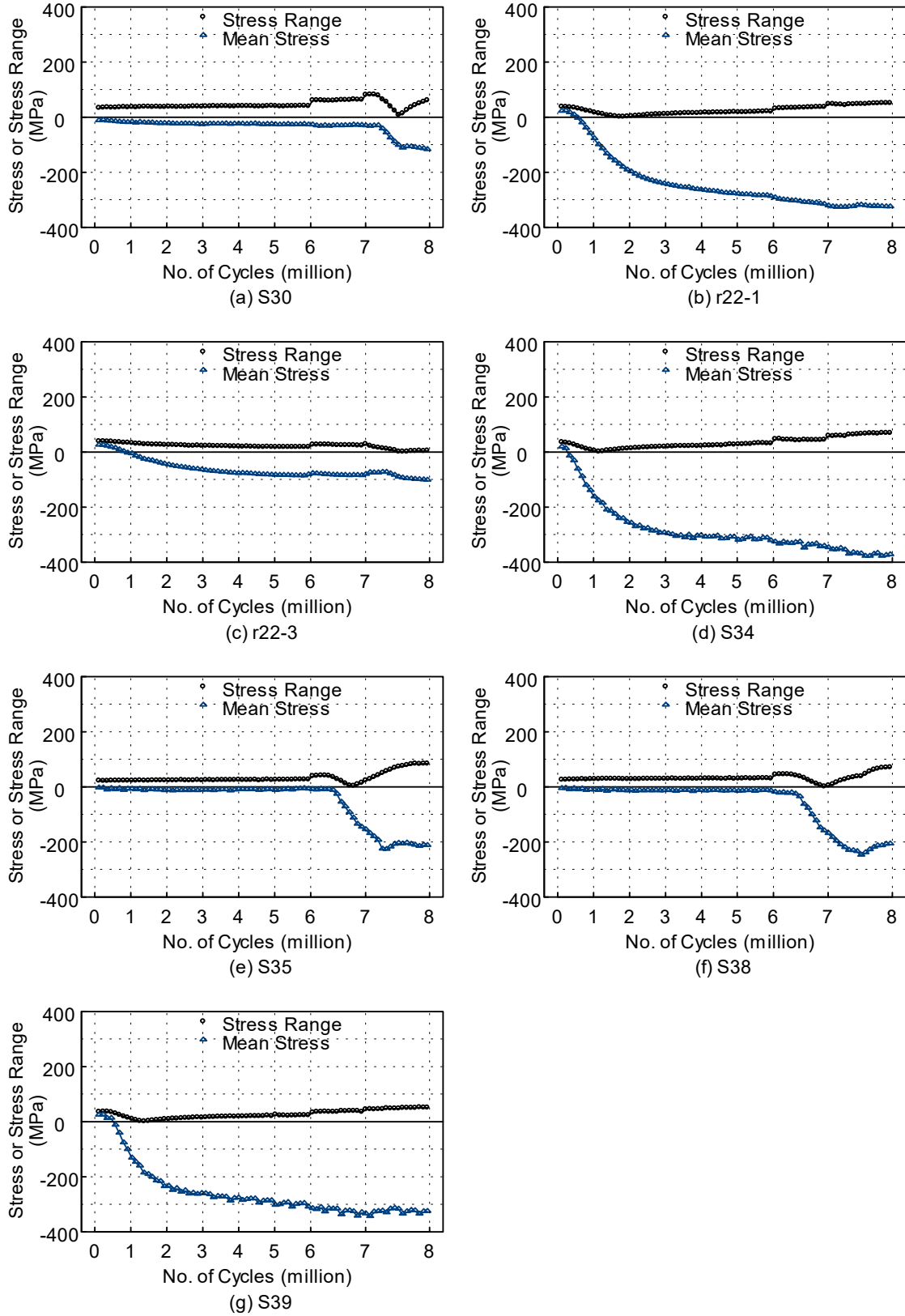


Figure 5.25 Specimen 3: Stress Range and Mean Stress in Ribs at Supports

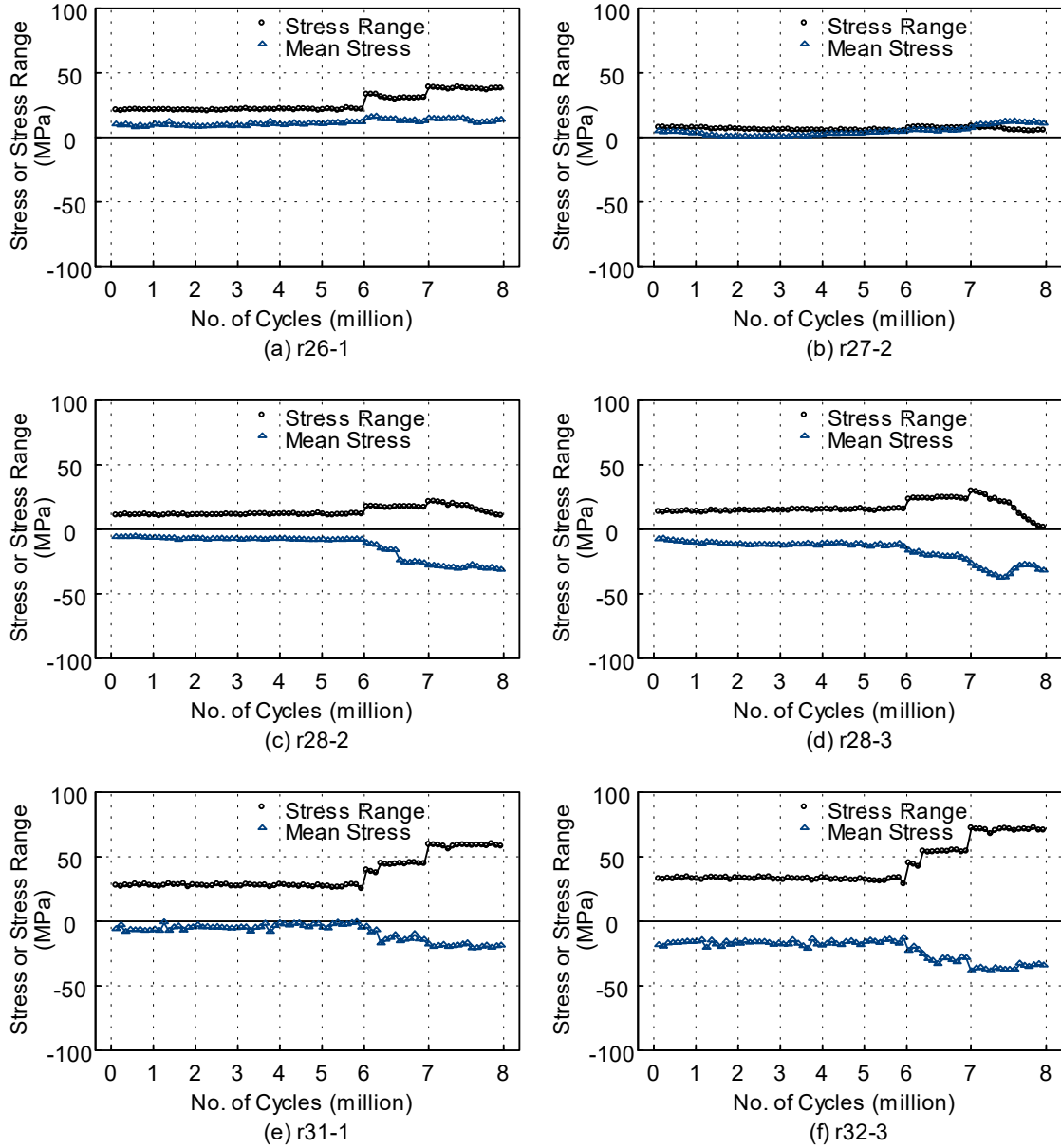


Figure 5.26 Specimen 3: Stress Range and Mean Stress in Bulkheads and Diaphragms

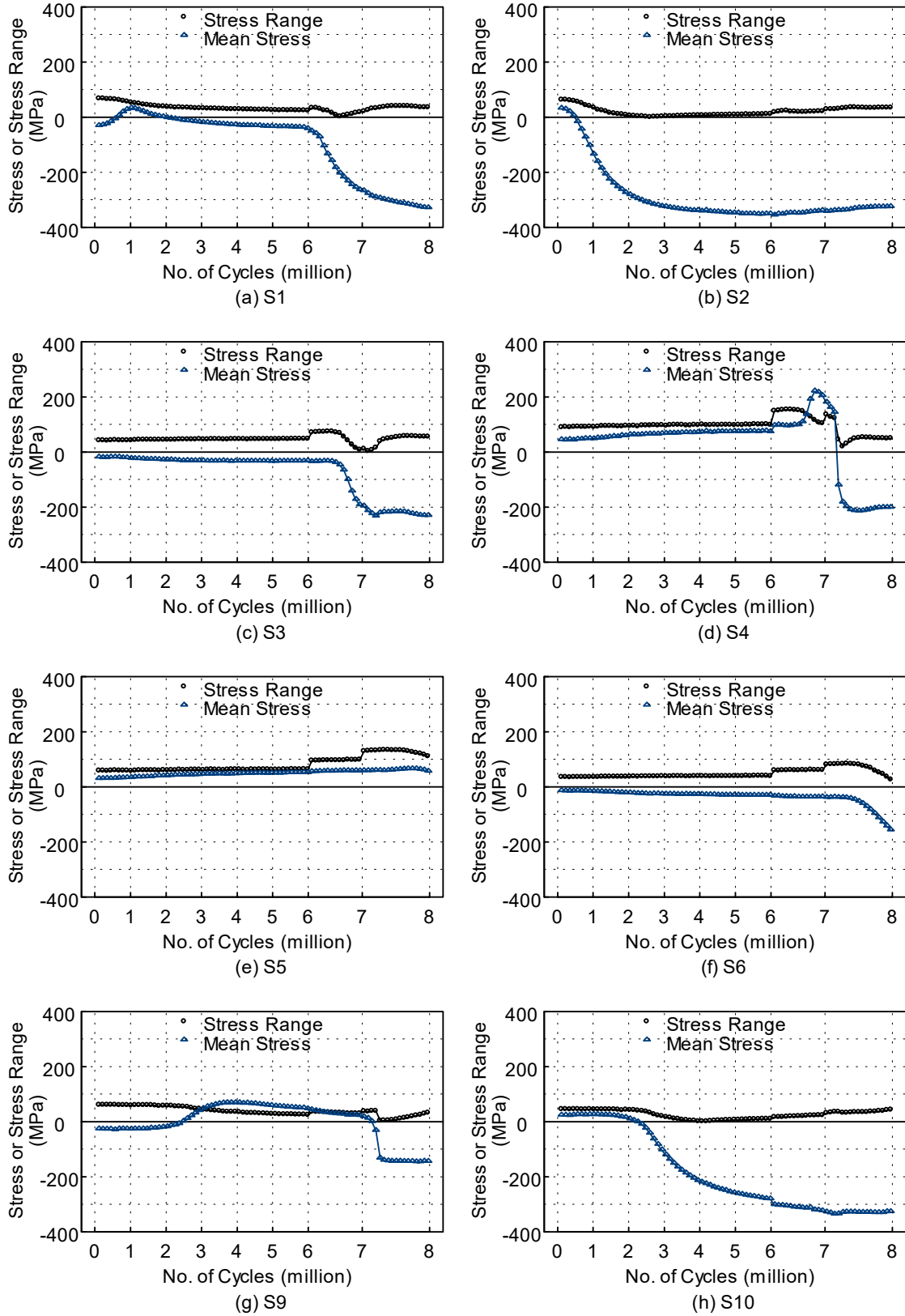


Figure 5.27 Specimen 4: Stress Range and Mean Stress in Ribs at Supports

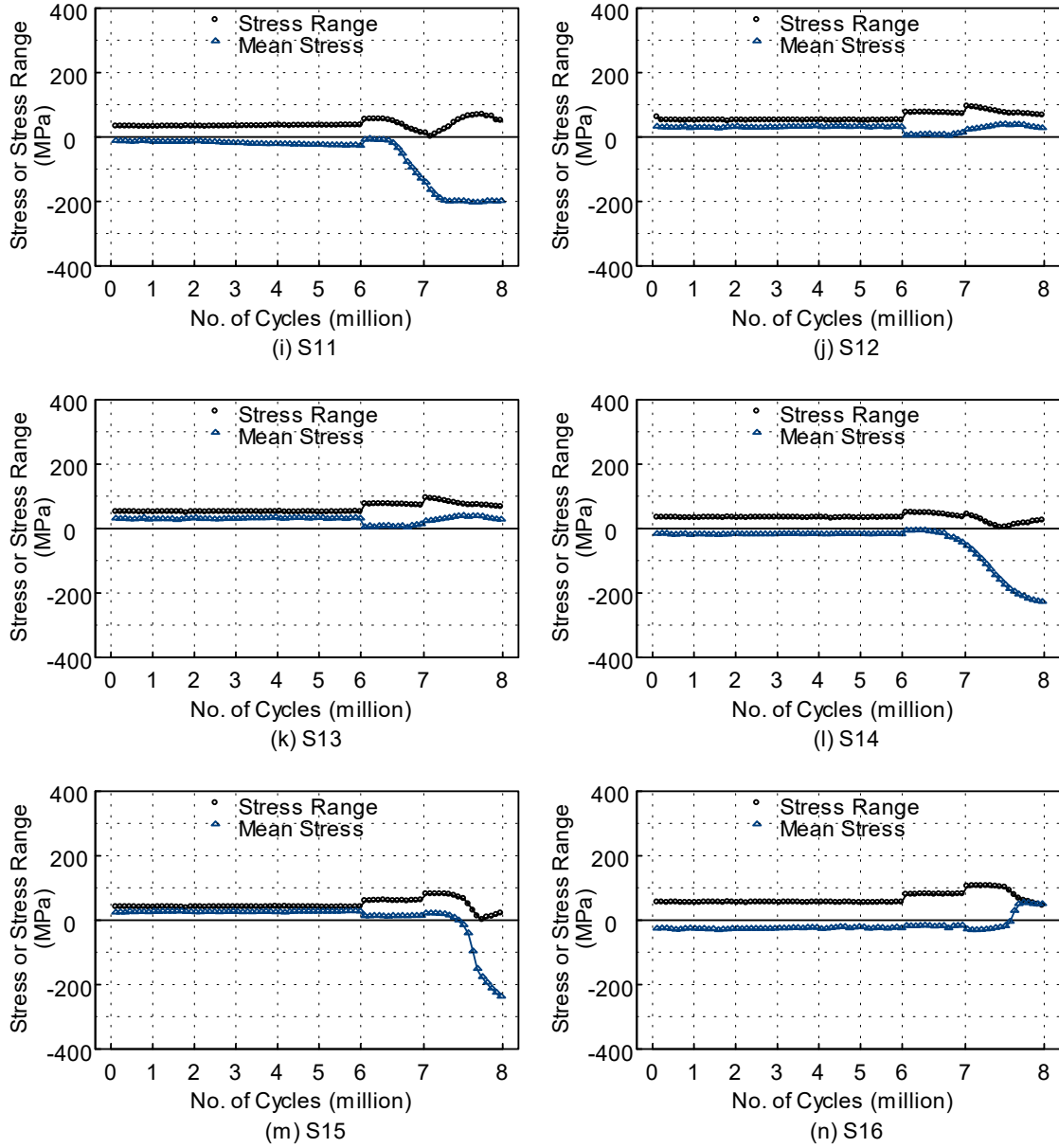


Figure 5.27 Specimen 4: Stress Range and Mean Stress in Ribs at Supports (continued)

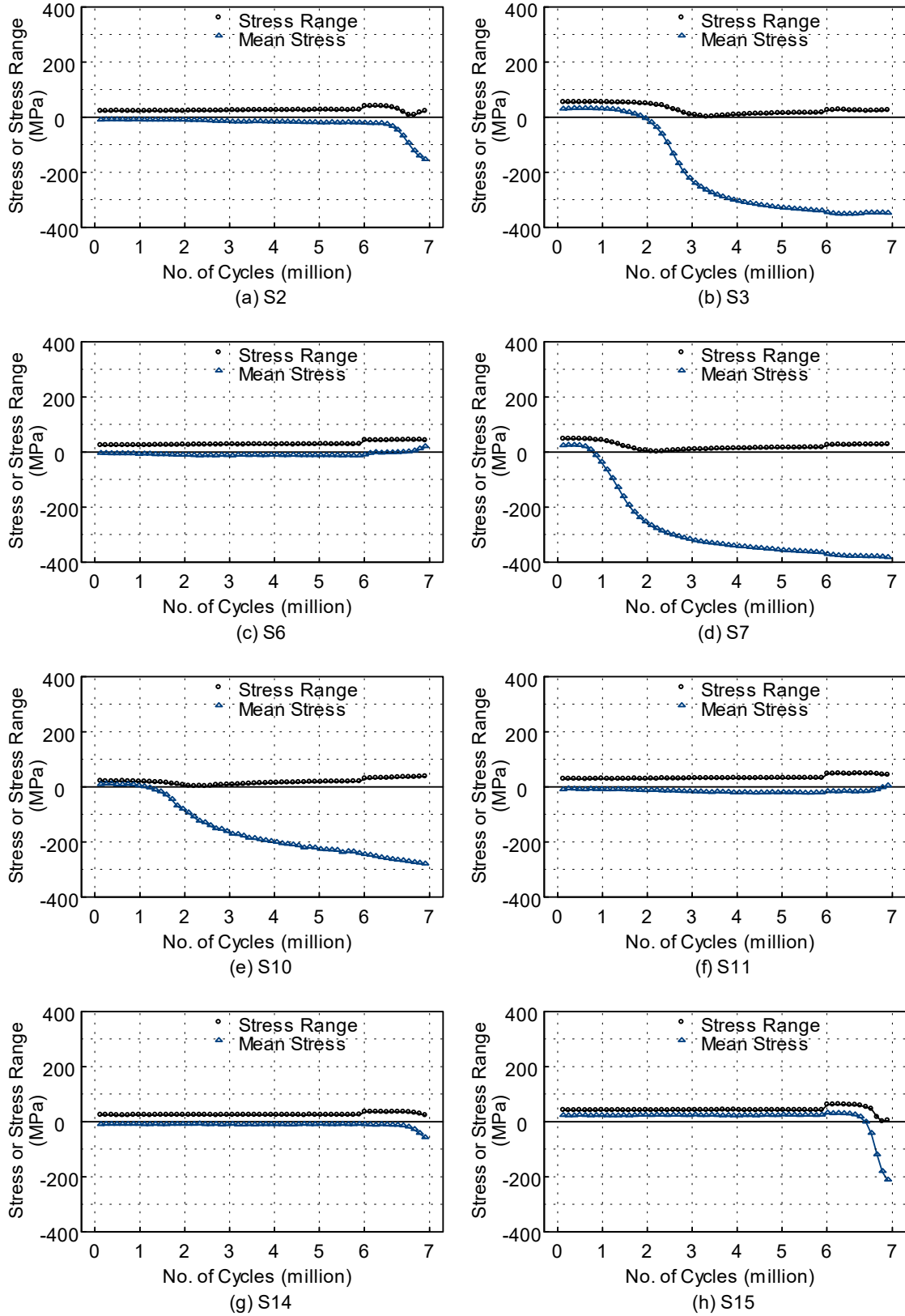


Figure 5.28 Specimen 5: Stress Range and Mean Stress in Ribs at Supports

5.3.2 Fatigue Cracks Observed in Ribs below Bulkhead and Diaphragm Cutout

Figure 5.29 shows an observed crack pattern on the rib walls below the bulkhead and the diaphragm cutout at the end supports. A cross section through the crack is shown in Figure 5.30. Most of the cracks on the rib walls initiated at the weld toe below the bulkhead in tension cycles. Cracks that initiated at the weld toe below the bulkhead in compression cycles did not propagate as quickly as those initiated in tension cycles. Table 5.13 summarizes the length of the rib wall cracks, measured horizontally in the longitudinal direction at each million cycles. No cracks were identified at the interior support.

Table 5.13 Specimen 4: Crack Length Below Rib-to-Bulkhead Connection (mm)

No. of Cycles (million)	Diaphragm D1				Diaphragm D3			
	Rib R2		Rib R3		Rib R2		Rib R3	
	East	West	East	West	East	West	East	West
1	15, 6	-	11	9, 12	-	-	-	-
2	22, 12	14	15	12, 17	24	5	8	-
3	36	20	17	16, 20	30	9	13	12
4	48	23	18	37	32	25	15	16
5	55	25	19	39	35	27	18	19
6	70	28	27	49	47	33	25	30

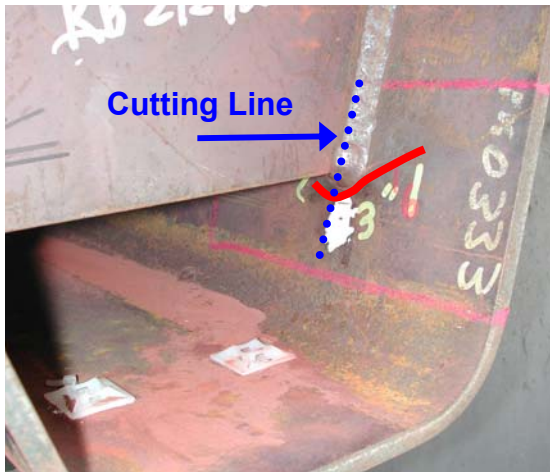


(a) View from Inside of Rib

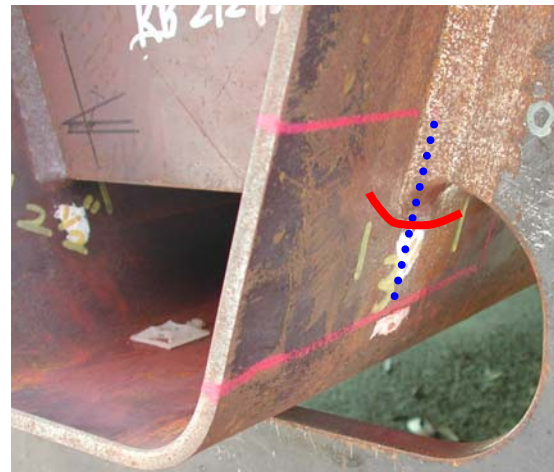


(b) View from Outside of Rib

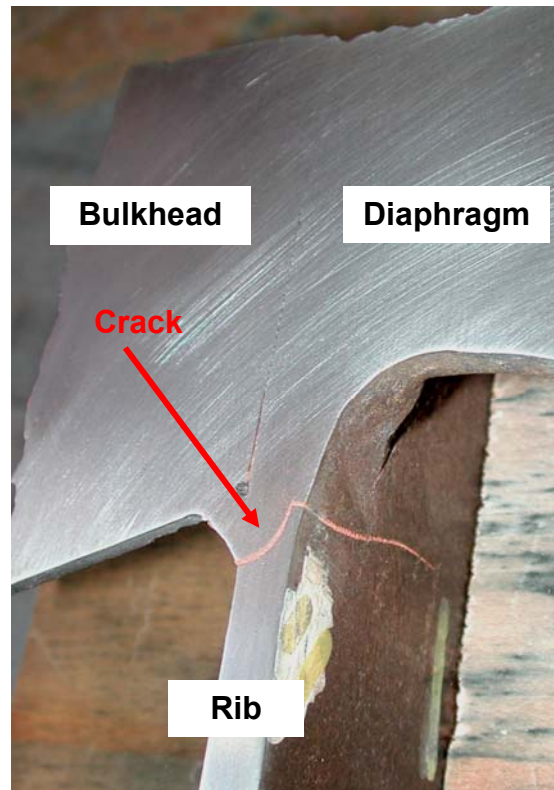
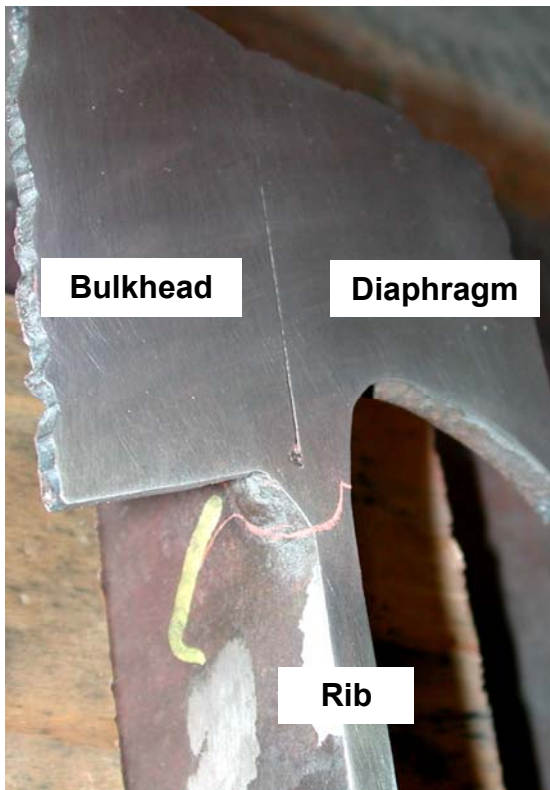
Figure 5.29 Specimen 5: Observed Crack Pattern at End Supports (at 8 M cycles)



(a) View from Inside of rib wall



(b) View from Outside of rib wall



(c) Cross Section

Figure 5.30 Cross Section through the Crack at End Support



(a) 1 million cycles



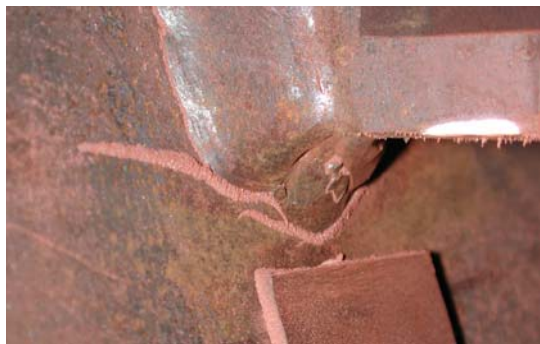
(b) 2 million cycles



(c) 3 million cycles



(d) 4 million cycles



(e) 5 million cycles



(f) 5 million cycles (different view)



(g) 6 million cycles



(h) 6 million cycles (different view)

Figure 5.31 Specimen 4: Cracks at Rib-to-Bulkhead Welded Joint (D1-R2-East)

5.4 Comparison of Test Results

5.4.1 Effect of Heat Straightening on Fatigue Resistance of Rib-to-Deck Welds

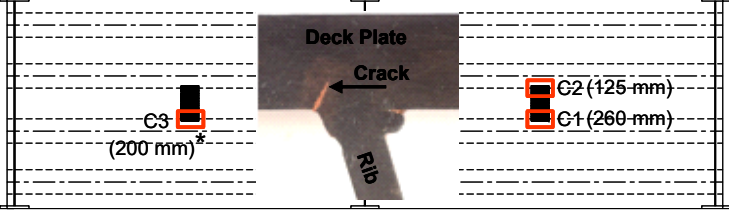
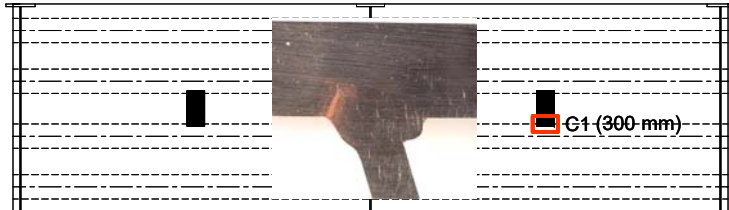
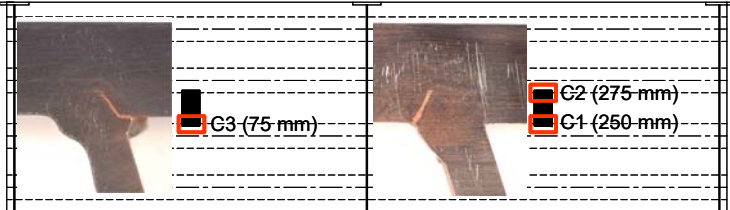
As was stated in Section 2.1.3, Specimen 6 was the first one that was pre-cambered. Since the measured distortion was not that different from its counterpart (Specimen 3) without pre-cambering, additional shims were used for Specimens 4 and 5, a measure that was shown from measurement to be effective. As a result, no heating on the ribs was required.

Table 5.14 shows the number of cracks and crack types at four loading location of all test specimens. Rib-to-deck weld cracks were identified in three specimens (Specimens 2, 3, and 6); these specimens required significant heat straightening. (Specimen 1 also required significant heat straightening. Unfortunately, it was the first specimen that was tested with a much higher load, although the contact stress was lower. Furthermore, the test result of this specimen cannot be compared with the others because the boundary condition was also different and the test was stopped at 1 million cycles.) On the other hand, the two effectively pre-cambered specimens (Specimens 4 and 5) did not show any cracks. Based on this limited database, it is prudent to conclude that effective pre-cambering is beneficial to mitigate the potential for rib-to-deck cracking.

5.4.2 Effect of Weld Melt-Through on Fatigue Resistance of Rib-to-Deck Welds

Of the seven cracks listed in Table 5.14, six cracks were initiated from outside of the rib at weld toe. Only one location (C3) in Specimen 6 had a crack that initiated from inside the rib at the weld root. The crack length was the shortest among all seven identified cracks, but the crack initiated from the transition from 80% PJP to 100% PJP welds (see Figure 5.22). No such crack was identified in another specimen (Specimen 3) with similar weld condition. Nor were Specimens 2 and 5 that had continuous weld melt-through. Since no other specimens showed weld root cracking, this limited database would suggest that discontinuous weld melt-through is not desirable.

Table 5.14 Number of Cracks and Crack Types at Loading Locations

Weld Condition	without Pre-Camber	with Pre-Camber
I (80 % PJP without Weld Melt-Through)	Specimen 1: none	Specimen 4: none
II (100 % PJP with Evident Continuous Weld Melt-Through)	<p>Specimen 2: 3 cracks at C1, C2, and C3</p> 	Specimen 5: none
III (Alternating Weld Conditions I and II Every 1 m)	<p>Specimen 3: 1 crack at C1</p> 	<p>Specimen 6: 3 cracks at C1, C2, and C3</p> 

*: Length of crack

6. SUMMARY AND CONCLUSIONS

6.1 Summary

A common US practice for the fabrication of orthotropic bridge deck with closed ribs is to use 80% partial-joint-penetration groove welds (PJP) between the deck plate and the rib. For fatigue considerations, AASHTO Specification limits the thickness of the rib in order to minimize local out-of-plane flexural stress at the welded joint. To avoid weld melt-through a tight fit is essential during welding. It is challenging to avoid weld melt-through along the entire length when welding such thin ribs. When it occurs, unfortunately, weld melt-through cannot be inspected easily inside the closed rib. It is not clear how the fatigue resistance of PJP welds will be affected by weld melt-through, which usually produces a geometric discontinuity or even a notch-like condition near the weld root.

The second issue for fabrication is related to the straightening procedure after welding in order to satisfy the flatness requirement of the orthotropic deck. This includes heating along the PJP weld lines from the top of the deck plate in order to correct the weld distortion in the transverse direction and heating the ribs at selected locations to correct the longitudinal distortion. In addition to heat straightening, pre-cambering before welding is also used from time to time. When pre-cambering is not used, however, it is not clear whether repetitive heat straightening will affect the fatigue resistance of PJP welds.

Six full-scale orthotropic steel deck specimens (10 m long by 3 m wide) were fabricated and tested in order to study the effects of both weld melt-through and distortion control measures on the fatigue resistance of the deck-to-rib PJP welded joint. Three of the specimens were only heat straightened, and the other three were pre-cambered to minimize the need for subsequent heat straightening. For the two distortion control schemes one of the three weld conditions [80% PJP weld as shown in Figure 1.5(b), 100% PJP weld with evident continuous weld melt-through as shown in Figure 1.5(a)], and alternating the above two weld conditions every 1 m} was used for each specimen.

Each specimen was composed of two spans with diaphragms at three support locations. Cyclic loading with an amplitude of 188 kN was applied at the mid-length of each span and was out of phase to simulate the effect of a moving truck. The testing plan called for 6 million cycles first, followed by an increase of the initial load level of 50% to 282 kN for the next one million cycles, and another 50% increase of the initial load to 376 kN for the last one million cycles, for a total of 8 million cycles. Prior to testing, finite element analysis was also conducted to predict the response and to provide information for instrumentation.

A tandem loading pattern was used for testing the first specimen (see Figure 2.26). Testing was stopped after 1 million cycles when significant cracking initiating from the bottom ends of the welds connecting the ribs to both the diaphragm plate and bulkheads at the cutouts was observed (see Figure 4.4). Such “premature” cracking, which was caused by out-of-plane twisting of the cross section (see Figure 3.7), was associated with two factors: (i) the load level was high considering that the width of the test specimen would only accommodate one half an axle, and (ii) transverse stiffeners installed on the diaphragm would not allow the supports to rotate freely. These stiffeners were then removed (see Figure 4.17) and a half-axle loading scheme was used (see Figure 2.27) for the remaining specimens.

Such modifications were effective to delay the development of cracks in end diaphragms, and all the remaining five specimens were tested to 8 million cycles. While diaphragm cracks were easy to identify, this was not the case for cracks in the rib-to-deck PJP welds under the loading points, especially when these cracks propagated upward into the deck plate, even though UT inspection was attempted. For each specimen, pieces were cut from four locations after testing for further examination. Table 5.14 summarizes the findings.

6.2 Conclusions

Based on the loading scheme applied and the limited database in Table 5.14, the following conclusions can be made on the fatigue resistance of rib-to-deck PJP welded joints.

- (1) Initially, weld melt-through which creates a geometric discontinuity at the weld root, was one concern that initiated this research. Table 5.14 shows that cracks were observed in three specimens at seven locations in the deck plate. But only one crack initiated from weld root inside the closed rib (location C3 of Specimen 6), and all the other six cracks initiated from weld toe outside the closed rib. Based on the loading pattern applied, it appears that these welds are more vulnerable to cracks initiating from the weld toe, not weld root. All deck plate cracks developed where a single axle wheel load of 188 kN was applied. All cracks appeared to arrest after they had extended out of the residual tensile stress field from welding.
- (2) Of the only one that developed at the weld root in Specimen 6, the crack initiated from a location transitioning from 80% PJP weld to 100% PJP weld. The geometric discontinuity that existed in not only transverse but also longitudinal directions appears detrimental. This type of discontinuity may be representative of the effect of weld melt-through in actual production of orthotropic steel decks.
- (3) Specimen 6 was the first specimen that was pre-cambered. The deck panel was insufficiently pre-cambered (see Figures 2.18 and 2.19) and the resulting distortion and heat straightening were the same as required for the un-cambered specimens. The figure also shows that the other two specimens (Specimens 4 and 5) were effectively pre-cambered by using the revised cambering scheme (see Figure 2.10 and Table 2.2). Excluding Specimen 1, which was tested up to 1 million cycles only due to “premature” cracking in the end diaphragms resulting from the extreme full axle load of 188 kN that was applied to simulate two half axles and unanticipated end restraint, Table 5.14 shows that only these two effectively pre-cambered specimens did not experience cracking in the PJP welds. Therefore, effective pre-cambering is beneficial to mitigate the crack potential in rib-to-deck PJP welds.

REFERENCES

- (1) AASHTO. (2007). *LRFD Bridge Design Specifications*, American Association of State Highway and Transportation Officials, Washington, D.C.
- (2) Bocchieri, W. J., Fisher, J. W. (1998). “Williamsburg Bridge Replacement Orthotropic Deck As-Built Fatigue Test.” *ATLSS Report No. 98-04*, Advanced Technology for Large Structural Systems, Lehigh University, Bethlehem, PA
- (3) Chen, W. F., Duan, L. (1999), editors. *Bridge Engineering*, Handbook, CRC Press, Washington, D.C.
- (4) Connor, R. J., Fisher, J. W. (2006a). “Consistent Approach to Calculating Stresses for Fatigue Design of Welded Rib-to-Web Connections in Steel Orthotropic Bridge Decks.” *Journal of Bridge Engineering*, ASCE, Vol. 11, No. 5, pp. 517-525.
- (5) Connor, R. J., Fisher, J. W. (2006b). “Identifying Effective and Ineffective Retrofits for Distortion Fatigue Cracking in Steel Bridges Using Field Instrumentation.” *Journal of Bridge Engineering*, ASCE, Vol. 11, No. 6, pp. 745-752.
- (6) Fisher, J. W., Kulak, G. L., Smith, Ian F. C. (1997). “A Fatigue Primer for Structural Engineers.” *ATLSS Report No. 97-11*, Advanced Technology for Large Structural Systems, Lehigh University, Bethlehem, PA
- (7) Fisher, J. W. (2005). *Personal Communication*.
- (8) Gurney, T. (1992). *Fatigue of Steel Bridge Decks: State-of-the-Art Review 8*, Transportation Research Laboratory, Department of Transport, HMSO, London

- (9) Kaczinski, M. R., Stokes, F. E., Lugger, P., Fisher, J. W. (1997). "Williamsburg Bridge Orthotropic Deck Fatigue Test." *ATLSS Report No. 97-04*, Advanced Technology for Large Structural Systems, Lehigh University, Bethlehem, PA
- (10) Machida, F., Miki, C., Hirabayashi, Y., Tokida, H., Shimozato, T. (2003). "Fatigue of Weld Connections to Trough Stiffeners in Orthotropic Steel Bridge Decks." Doc. XIII-1972-03, 2003 Annual Assembly of International Institute of Welding, , Bucharest
- (11) Masahiro, Y., Akihiro, K., Mitsuhiro, Y., Takeshi, N., Shinji, M. (2006). "Fabrication and Transportation of Orthotropic Box Girder for New Carquinez Bridge." *IHI Engineering Review*, Vol. 39, No. 2.
- (12) Miki, C. (2006). "Fatigue Damage in Orthotropic Steel Bridge Decks and Retrofit Works." *International Journal of Steel Structures*, KSSC, Vol. 6, No. 4, pp. 255-267.
- (13) Troitsky, M. S. (1987). *Orthotropic Bridges, Theory and Design*, 2nd Edition, The James F. Lincoln Arc Welding Foundation, Cleveland, OH
- (14) Tsakopoulos, P. A., Fisher, J. W. (1999). "Williamsburg Bridge Replacement Orthotropic Deck As-Built Full-Scale Fatigue Test." *ATLSS Report No. 99-02*, Advanced Technology for Large Structural Systems, Lehigh University, Bethlehem, PA
- (15) Tsakopoulos, P. A., Fisher, J. W. (2006). "Full-Scale Fatigue Tests of Steel Orthotropic Decks for the Williamsburg Bridge." *Journal of Bridge Engineering*, ASCE, Vol. 8, No. 5, pp. 323-333.
- (16) Wolchuk, W. (2004). "*Orthotropic Deck Bridges*." Roman Wolchuk Consulting Engineers, ASCE Seminar, Sacramento, CA

- (17) Xiao, Z. G., Yamada, K., Inoue, J., Yamaguchi, K. (2005). "Fatigue Cracks in Longitudinal Ribs of Steel Orthotropic Deck." *International Journal of Fatigue*, Vol. 28, pp. 409-416.
- (18) Ya, S., Yamada, K., Ojio, T., Biehn, B. (2007). "Fatigue Tests of Welded Joint of Trough Rib to Orthotropic Steel Deck Plate." *Journal of Structural Engineering*, JSCE, Vol. 53A. (in Japanese)
- (19) Yamada, K. (2006). "Some New Approaches to Fatigue Evaluation of Steel Bridges." *International Journal of Steel Structures*, KSSC, Vol. 6, No. 4, pp. 319-326.